

Distribution Agreement

In presenting this thesis or dissertation as a partial fulfillment of the requirements for an advanced degree from Emory University, I hereby grant to Emory University and its agents the non-exclusive license to archive, make accessible, and display my thesis or dissertation in whole or in part in all forms of media, now or hereafter known, including display on the world wide web. I understand that I may select some access restrictions as part of the online submission of this thesis or dissertation. I retain all ownership rights to the copyright of the thesis or dissertation. I also retain the right to use in future works (such as articles or books) all or part of this thesis or dissertation.

Signature:

Yao Jing

Date

Structure-Activity Relationship and Quantitative Structure-Activity Relationship of
GluN2C/D Subunit Selective Antagonists of the *N*-Methyl-D-Aspartate Receptor

By

Yao Jing
Doctor of Philosophy

Chemistry

Dennis C. Liotta, PhD
Advisor

Frank E. McDonald, PhD
Committee Member

Stephen F. Traynelis, PhD
Committee Member

Emily Weinert, PhD
Committee Member

Accepted:

Lisa A. Tedesco, Ph.D.
Dean of the James T. Laney School of Graduate Studies

Date

Structure-Activity Relationship and Quantitative Structure-Activity Relationship of
GluN2C/D Subunit Selective Antagonists of the *N*-Methyl-D-Aspartate Receptor

By

Yao Jing

B.S., New Mexico State University, 2012

B.S., Sichuan University, 2012

Advisor: Dennis C. Liotta, PhD

An abstract of

A dissertation submitted to the Faculty of the
James T. Laney School of Graduate Studies of Emory University
in partial fulfillment of the requirements for the degree of

Doctor of Philosophy in Chemistry

2018

Abstract

Structure-Activity Relationship and Quantitative Structure-Activity Relationship of GluN2C/D Subunit Selective Antagonists of the *N*-Methyl-D-Aspartate Receptor

By Yao Jing

The *N*-methyl-D-aspartate (NMDA) receptors belong to the ionotropic glutamate receptor (iGluR) family and contribute to synaptic plasticity and excitatory neuronal transmission in the central nervous system. The functional NMDA receptors are heterotetramers, and they are assembled from two GluN1 subunits with two GluN2 (A-D) subunits. GluN2D subunits regulate synaptic transmission in basal ganglia, which controls movement disorders such as Parkinson's disease. Our goal is to develop potent GluN2C/D subunit-selective antagonists of the NMDA receptor with a dihydroquinoline-pyrazoline (DQP) scaffold, which can be used as potential therapies for neuropathological diseases.

This dissertation consists of two projects. In the first project, 997 series compounds with DQP scaffold are synthesized and their structure-activity relationship (SAR) are explored in depth. Results indicate that compound (S)-997-74 is the most active candidate with an IC_{50} value of 46 nM at the GluN2D subunit. Although compound 997-110 is less potent than 997-74, it is more selective (625-fold) at GluN2D subunit over GluN2B subunit. Then, 2D- and 3D-quantitative SAR (QSAR) models are implemented to analyze the favorable and unfavorable moieties of 997-series that contribute to the inhibition activity at the GluN2D subunit and to make predictions of future compounds. The 2D QSAR models show that the halogen substitution on the phenyl ring and the difluoro substitution on the acyl chain play crucial roles on this series, while the phenyl ring on the quinolone moiety is unfavorable to improve the activity at GluN2D subunit. The 3D QSAR model based on the NAMFIS-1a conformer can be used in combination with the 2D QSAR models to guide prediction of future medicinal efforts of the 997-series. The second project develops another novel series of GluN2C/D subunits selective antagonists of the NMDA receptor with piperazine scaffold. Compound 1121-35 with thiophene substitution on the A-ring provides the best results with IC_{50} values of 13 μ M and 11 μ M at GluN2C and GluN2D subunits, respectively, and shows no inhibition at GluN2A and GluN2B subunits. The SAR of this series is relatively flat, allowing only limited advancing progress over the initial screening hit.

Structure-Activity Relationship and Quantitative Structure-Activity Relationship of
GluN2C/D Subunit Selective Antagonists of the *N*-Methyl-D-Aspartate Receptor

By

Yao Jing

B.S., New Mexico State University, 2012

B.S., Sichuan University, 2012

Advisor: Dennis C. Liotta, PhD

A dissertation submitted to the Faculty of the
James T. Laney School of Graduate Studies of Emory University
in partial fulfillment of the requirements for the degree of
Doctor of Philosophy in Chemistry
2018

Acknowledgements

I would like to thank my dissertation advisors, Dr. Dennis C. Liotta and Dr. Stephen Traynelis for their valuable guidance and continuous support throughout the course of my PhD. I am grateful for their encouragement and help through difficult times in my last years of graduate study. Working with them has been a pleasant and memorable experience.

Thanks also to Dr. Frank McDonald and Dr. Emily Weinert for agreeing to serve on my committee and providing helpful comments on my work.

Thanks to Dr. Timothy M. Acker, Dr. Katie L. Strong, Dr. Eric Miller, Dr. Spandan Chennamadhavuni, Dr. David S. Menaldino, Matthew Epplin, Samantha Summer, and Peipei Ma for their help during my Ph.D. study. Special thanks to Dr. Pieter Burger, Dr. Tom Kaiser and Stephen Kell for their help of building QSAR models. I am grateful for the funding sponsored by the NIH.

I would also like to thank the whole Liotta group and the Traynelis group, both current and past members and staffs, for an energetic and pleasing environment. I am especially thankful to Mr. Steve Krebs in the stockroom for helping order and send chemicals.

My deepest appreciation goes to my parents, Chenggui Jing and Xiuying Shi, for all their loves and supports, and to my husband, Dr. Xingjian Wang, for his constant love and support.

Finally, I remain grateful for the people who I have not mentioned for their support and guidance.

Table of Contents

Chapter 1. Introduction	1
1.1 NMDA topology	1
1.2 NMDA receptor pharmacology	6
1.2.1 NMDA receptor agonists	6
1.2.2 NMDA competitive antagonists	6
1.2.3 NMDA uncompetitive antagonists	7
1.2.4 NMDA noncompetitive modulators	8
1.3 Therapeutic rationale for GluN2D-selective NMDA antagonists	11
1.4 DQP-1105 properties	13
Chapter 2. SAR study of 997-series	18
2.1 Background of 997 project:	18
2.2 SAR results of 997-series with DQP-1105 scaffold	19
2.2.1 Acyl chain modification	19
2.2.2 A-phenyl ring modification	28
2.2.3 B-phenyl ring modification	32
2.2.4 Quinolone ring modification	35
2.3 SAR results of 997-series with 997-95 scaffold	38
2.3.1 Development of 997-95 scaffold	38
2.3.2 A-phenyl ring modification	40
2.3.3 B-phenyl ring modification	42
2.4 Chemistry Experimental	44
2.4.1 Synthetic procedures	44
2.4.2 Evaluation of Enantiomers	100
2.4.3 X-ray	101
2.4.4 Two-electrode voltage-clamp recording	102
2.4.5 Data Analysis	103
Chapter 3. QSAR study of 997-series	104
3.1 Introduction	104
3.2 2D-QSAR study of 997-series	105
3.2.1 Introduction of 2D-QSAR	105
3.2.2 AutoQSAR study of 997-series	107
3.2.2.a Introduction of autoQSAR	107
3.2.2.b Data preparation and autoQSAR model creation	108

3.2.2.c	AutoQSAR model analysis	108
3.2.2.d	Analyzing predictions and identifying outliers.	110
3.2.3	KPLS model	115
3.2.3.a	Introduction of KPLS	115
3.2.3.b	KPLS model creation	115
3.2.3.c	Results and discussion:	116
3.3	Field-based 3D-QSAR study of 997-series	121
3.3.1	Introduction of 3D-QSAR	121
3.3.2	Field-based QSAR	122
3.3.2.a	Background	122
3.3.2.b	Field-based QSAR experimental section	125
3.3.2.c	Field-based QSAR results	130
3.3.2.d	Field-based QSAR discussion	141
Chapter 4.	1121 series	143
4.1	Introduction	143
4.2	A-ring modification	143
4.3	Linker modification	148
4.4	Piperazine ring modification	153
4.5	B-ring modification	155
Chapter 5.	Conclusion and Outlook	185
Appendix A:	Crystal data and structure refinement for (R)-(+)-997-74	204
Appendix B:	The report for the best AutoQSAR model kpls_dendritic_1	205
Appendix C:	Concentration-response data for 997-series at ionotropic glutamate receptors.	210
Appendix D:	Concentration-response data for 997-enantiomers at ionotropic glutamate receptors.	212
Appendix E:	Concentration-response data for 1121-series at ionotropic glutamate receptors.	213
References		215

List of Illustrations

List of Tables

Table 1. Acyl chain modifications.....	16
Table 2. Acyl chain modifications.....	25
Table 3. Stereoselectivity for the purified enantiomers.	27
Table 4. A-ring modifications.	31
Table 5. B-ring modifications.	34
Table 6. Quinolone ring modifications (1).....	36
Table 7. Quinolone ring modifications (2).....	37
Table 8. SAR study of 997-95 and 997-99.....	39
Table 9. SAR study of compounds with right ring modification.	41
Table 10. SAR study of compounds with B-ring modification.....	43
Table 11. Ten top-ranked QSAR models.....	109
Table 12. QSAR statistics of KPLS model.	116
Table 13. Visualized structures of least active and most active compounds.....	118
Table 14. Field-based QSAR model of (S)-997-23 NAMFIS-1a with QSAR statistics.	130
Table 15. The default colors for field contours.	132
Table 16. Five field contours of the most active compound 997-74 and the least active compound 2063 with NAMFIS-1a structure.	134
Table 17. Field-based QSAR model of (S)-997-23 NAMFIS-2a with QSAR statistics.	135
Table 18. Five field contours of the most active compound 997-74 and the least active compound 2063 with NAMFIS-2a structure.	137
Table 19. Field-based QSAR model of (S)-997-23-min with QSAR statistics.....	138
Table 20. Five field contours of the most active compound 997-74 and the least active compound 2063 with (S)-997-23 conformation.	140
Table 21. Field-Based QSAR statistics.	141
Table 22. SAR of purchased compound 1121, 2030, and 2032.	144
Table 23. A-ring modification.....	146
Table 24. SAR of purchased compounds 2035, 2101, and 2103.	148
Table 25. Linker 1 modification.....	149
Table 26. Linker 2 modification.....	152
Table 27. SAR study of purchased compounds 1121, 2106, and 2109.....	153
Table 28. Piperazine ring modification.	154
Table 29. SAR study of compounds with different B ring substitutions.....	155
Table 30. B-ring modification.....	157
Table 31. Future compounds with predicted GluN2D IC50 values from the KPLS model.....	191
Table 32. Statistics for KPLS model with 3 factors.	194
Table 33. Statistics for KPLS model with 4 factors.....	195

List of Figures

Figure 1. Glutamate mimics that selectively bind to receptors from iGluR family.....	1
Figure 2. The various populations of di- and tri-heteromeric NMDARs that are thought to exist in the CNS.....	2
Figure 3. Architecture and domain organization of the iGluR family.....	2
Figure 4. Linear representation of the subunit polypeptide chain and schematic illustration of the subunit topology.....	4
Figure 5. Distribution of NMDA receptor subunit mRNAs in the rat brain..	6
Figure 6. NMDA receptor channel blockers [34].	8
Figure 7. Subunit-selective antagonists [34].....	10
Figure 8. Homology Model of an NMDA receptor highlighting known binding sites Ribbon diagram depicting the NMDA receptor.....	11
Figure 9. Models of basal ganglia circuits in the healthy brain and Parkinson's brain.	13
Figure 10. Subunit selectivity of DQP-1105.....	14
Figure 11. Structure of previously reported representative compound DQP-1105 and optimized scaffold [79].....	18
Figure 12. Crystallographic data for R configuration of 997-74.	28
Figure 13. Flowchart of a general QSAR study.	105
Figure 14. Observed and predicted GluN2D pIC50 values of training (blue) and test (red) sets.....	110
Figure 15. Observed and predicted GluN2D pIC50 values with domain alert of outliers.....	111
Figure 16. Outliers 1248 and 997-78.	112
Figure 17. Outliers with structure related.	113
Figure 18. Observed and predicted GluN2D pIC50 values with domain alert of outliers without compound 1248 and 997-78.....	114
Figure 19. Predicted and observed GluN2D pIC50 for training set (blue) and test set (magenta) compounds using KPLS models constructed from dendritic fingerprints.	117
Figure 20. A 2D representation of compound 997-23.....	127
Figure 21. Signal was observed between the protons of the B and C rings.....	128
Figure 22. Alignments of A, NAMFIS-1a; B, NAMFIS-2a; and C, (S)-997-23-min.	129
Figure 23. The plot of NAMFIS-1a training (in blue) and test (in red) sets results.....	131
Figure 24. The plot of NAMFIS-2a training (in blue) and test (in red) sets results.....	136
Figure 25. The plot of (S)-997-23-min training (in blue) and test (in red) results.....	138
Figure 26. The Craig plot for various substituents with hydrophobic and electrostatic properties.	142
Figure 27. Structure of ifenprodil and 1121, and optimized scaffold of 1121.	143
Figure 28. Composite concentration-effect curves for DQP-1105 against recombinant NMDA receptors. Data were analyzed using prism.....	186
Figure 29. The proposed pharmacophore features that contribute to the GluN2D inhibition.....	187
Figure 30. The ratios of test errors between two KPLS models using dendritic fingerprints and linear fingerprints.....	192
Figure 31. The ratios of test errors between the KPLS model with four factors and the model with three factors.....	193
Figure 32. Identification of structural determinants of GluN2D-selective DQP-1105 using chimeric GluN2A-GluN2D receptors..	199
Figure 33. Amino acid sequence alignment of the S2a-c segment from GluN2A-D.....	200
Figure 34. Visualized structures of 997-74 of the models built for GluN2C and GluN2D.....	201

List of Schemes

Scheme 1. Synthesis of dihydroquinolone pyrazoline amines.....	20
Scheme 2. Synthesis of acyl chains.	20
Scheme 3. Synthesis of acylated quinolone pyrazoline products.	22
Scheme 4. Synthesis of 997-101.....	23
Scheme 5. Synthesis of amides 997-96 and 997-115.....	23
Scheme 6. Enantiomer separation.....	26
Scheme 7. Synthesis of 997-series with different A-ring modifications.....	29
Scheme 8. Synthesis of 997-76 and 997-77.....	32
Scheme 9. Synthesis of 997-series with B-phenyl ring modifications.....	33
Scheme 10. Synthesis of 997-90, 997-91, and 997-102.....	36
Scheme 11. Synthesis of thioamide-containing compound 997-97 and 997-98.....	37
Scheme 12. Synthesis of 997-95 and its analogue.....	39
Scheme 13. Synthesis of 997-95 analogues with A-ring modifications.....	40
Scheme 14. Synthesis of 997-95 analogues with B-ring modifications.....	42
Scheme 15. Synthesis of 1121 analogues with A-ring modifications.....	145
Scheme 16. Synthesis of 1121-7.....	149
Scheme 17. Synthesis of 1121-16.....	150
Scheme 18. Synthesis of 1121 analogues with linker modifications.....	151
Scheme 19. Synthesis of thioamide compound 1121-32.....	152
Scheme 20. Synthesis of 1121 analogues with piperazine ring modifications.....	154
Scheme 21. Synthesis of 1121 analogues with different B ring substitutions.....	156
Scheme 22. Purposed enantioselective synthesis of (S)-pyrazoline amines.....	189
Scheme 23. Strategies of synthesizing prodrugs of 997-74.....	202
Scheme 24. The strategy of making 997-74-SynB1.....	203

List of Abbreviations

ACN	Acetonitrile
AMPA	α -amino-3-hydroxy-5-methyl-4-isoxazolepropionic acid
ANN	Artificial neural networks
ATD	Amino terminal domain
BBB	Blood-brain barrier
CDCl ₃	Deuterated chloroform
CIQ	(3-Chlorophenyl)(6,7-dimethoxy-1-((4-methoxyphenoxy)methyl)-3,4-dihydroisoquinolin-2(1 <i>H</i>)-yl)methanone
CNS	Central nervous system
CoMFA	Comparative molecular field analysis
CoMSIA	Comparative molecular similarity indices analysis
CTD	Carboxyl terminal domain
DCM	Dichloromethane (CH ₂ Cl ₂)
DMF	Dimethylformamide
DMSO	Dimethyl sulfoxide
DQP	Dihydro-quinolone pyrazoline
EC ₅₀	Half-maximal effective concentration
EDTA	Ethylenediaminetetraacetic acid
EtOAc/EA	Ethyl acetate
EtOH	Ethanol
FDA	Federal Drug Administration
FMNR	Full matrix Newton-Rhapson
GA	Genetic algorithm
GPe	External globus pallidus
Gpi	Internal globus pallidus
HEPES	(4-(2-hydroxyethyl)-1-piperazineethanesulfonic acid
HRMS	High-resolution mass spectrometry
HTS	High throughput screening
IC ₅₀	Half-maximal inhibitory concentration
iGluR	The ionotropic glutamate receptor
i-ProAc	Isopropyl acetate
<i>k</i> NN	<i>k</i> -Nearest neighbors
KPLS	Kernel-based partial least squares
LBD	Ligand binding domain
LCMS	Liquid chromatography-mass spectrometry
L-DOPA	L-dihydroxyphenylalanine
logP	Octanol/water partition
MCMM	Monte Carlo Macro Model
MDR1-MDCK	Madin-Darby canine kidney cells transfected with the human MDR1 gene
Me	Methyl
MeOH	Methanol
MHz	Megahertz
MK-801	(5 <i>R</i> ,10 <i>S</i>)-5-methyl-10,11-dihydro-5 <i>H</i> -dibenzo[<i>a,d</i>]cycloheptene-5,10-imine

MLR	Multiple linear regression
mRNA	Messenger ribonucleic acid
MSDS	Material Safety Data Sheets
MTLM	Mixed torsional/Low-Mode
MW	Microwave
NAMFIS	NMR analysis of molecular flexibility in solution
NaOH	Sodium hydroxide
NMDA	<i>N</i> -methyl <i>D</i> -aspartate
NMR	Nuclear magnetic resonance
NOE	The nuclear overhauser effect
PCA/PCR	Principal component analysis/regression
PCP	Phencyclidine
PD	Parkinson's disease
PLS	Partial least squares
PRCG	Polak-Ribier conjugate gradient
PYD	Pyrrolidinone
QNZ	Qunazilinone-4-one
QNZ46	€4-(6-methoxy-2-(3-nitrostyryl)-4-oxoquinazolin-3(4H)-yl)-benzoic acid
QSAR	Quantitative structure activity relationship
RMSE	Root-mean-square deviation
Ro 25-6981	[R-(R*,S*)]- α -(4-hydroxyphenyl)- β -methyl-4-(phenylmethyl)-1-piperidinepropanol hydrochloride
SAR	Structure activity relationship
SBDD	Structure-based drug discovery
SD	Standard deviation
SNc	Substantia nigra pars compacta
SNr	Substantia nigra pars reticulata
SSD	Sum of Squared Distances
STN	Subthalamic nucleus
SVM	Support vector machine
TCN-201	3-Chloro-4-fluoro-N-[4-[[2-(phenylcarbonyl)hydrazine]carbonyl]benzyl]benzenesulfonamide
TLC	Thin-layer chromatography
TEVC	Two-electrode voltage-clamp
TFA	Trifluoro acetic acid
TFAA	Trifluoroacetic anhydride
Thal	Thalamus
THF	Tetrahydrofuran
TMD	Transmembrane domain
TPSA	Topological polar surface area

Chapter 1. Introduction

1.1 NMDA topology

In the past decades, scientists have explored the physiological and pathophysiological properties of the ionotropic glutamate receptor (iGluR) family, which includes the *N*-methyl-D-aspartate (NMDA) receptors, the α -Amino-3-hydroxy-5-methyl-4-isoxazolepropionic acid (AMPA) receptors, and the kainate receptors (*Figure 1*) [1]. Because of its high permeability of Ca^{2+} , Na^{+} , K^{+} and sensitivity to voltage-dependent Mg^{2+} block, the NMDA receptor contributes to synaptic plasticity and excitatory neuronal transmission in the central nervous system (CNS) [2, 3]. It does this by serving as a coincident detector, responding when glutamate is released coincident with neuronal depolarization. The influx of Ca^{2+} can alter synaptic function through its interaction with signaling systems [4, 5].

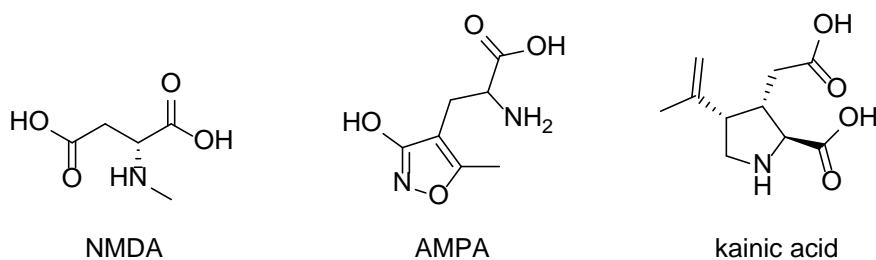


Figure 1. Glutamate mimics that selectively bind to receptors from iGluR family.

The NMDA receptors consist of three different subunits GluN1, GluN2, and GluN3 [6]. There are four GluN2 subtypes and two GluN3 gene products: GluN2A, GluN2B, GluN2C, GluN2D, GluN3A, and GluN3B [1, 3]. The functional NMDA receptors are heterotetramers and are assembled from two glycine-binding GluN1 subunits with either two glutamate-binding GluN2 (A-D) subunits (*Figure 2*) [3, 7-9]. The role of GluN3 is poorly understood.



Figure 2. The various populations of di- and tri-heteromeric NMDARs that are thought to exist in the CNS [3].

Each subunit folds into four semiautonomous domains, including the amino-terminal domain (ATD), the ligand-binding domain (LBD), the transmembrane domain (TMD) and the intracellular carboxyl-terminal domain (CTD) (Figure 3) [1, 10].

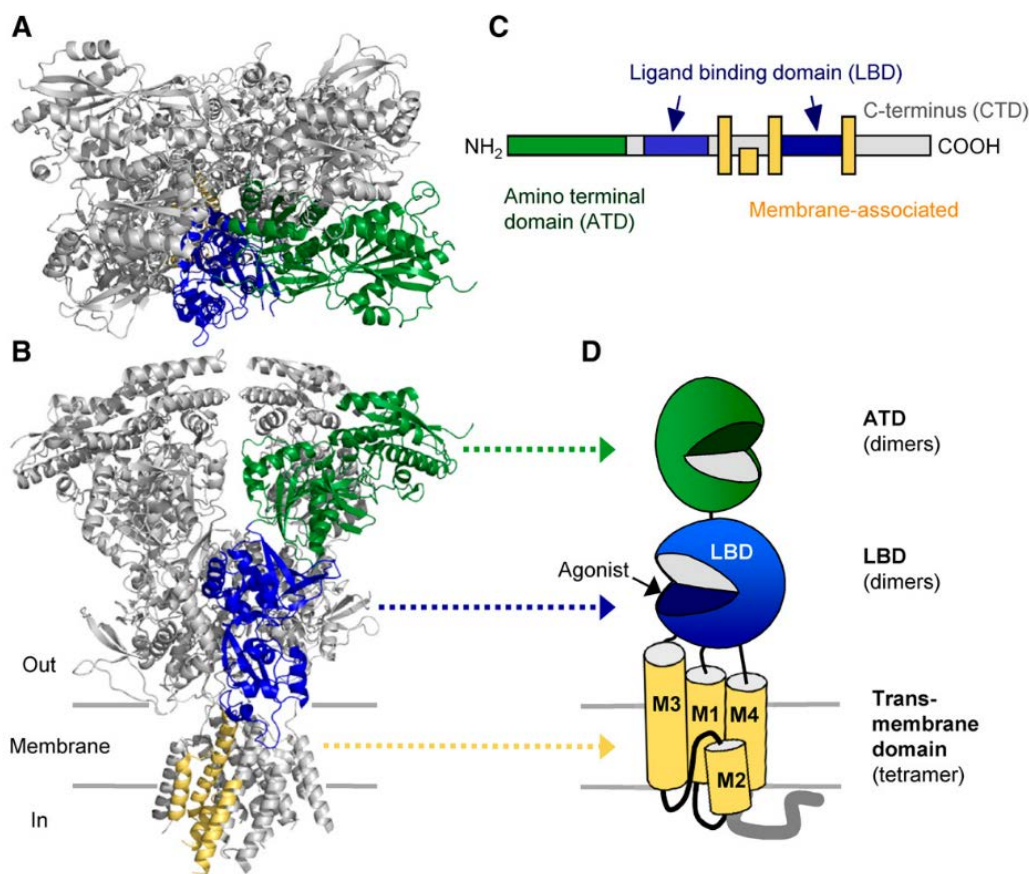


Figure 3. Architecture and domain organization of the iGluR family. A, top-down view of an NMDA receptor (PDB ID: 4PE5); B, side view of an NMDA receptor; C, linear representation of modular amino-terminal domain (green), ligand-binding domain (blue), TMD (yellow), and C-terminal domain (gray) within a subunit polypeptide chain; D, Schematic illustration of a glutamate receptor subunit topology with the extracellular domain (blue and green) and membrane-associated elements (yellow). Short peptide linkers between domains are shown in black lines [10, 11].

The extracellular ATD domain is a heterodimer between GluN1 and GluN2 which harbor multiple binding sites for allosteric modulators, which affect different subunits. The X-ray crystal structure of GluN1-GluN2B ATD has been resolved, which revealed the ATD for each subunit to be a clamshell-like structure with two parts R1 and R2 [11-13]. The ATD of the NMDA receptor has lower sequence homology compared to non-NMDA glutamate receptors than the LBD pore-forming region. Thus, the ATD of the NMDA receptor controls significant pharmacological properties, such as channel opening probability, deactivation time course, and agonist EC₅₀ [1, 14-16]. Zn²⁺ binds within the GluN2B ATD clamshell and partially inhibits both GluN2A and GluN2B subunits at physiological concentrations [1, 17, 18]. The GluN2B-selective inhibitor ifenprodil binds within the interface between the GluN1 and GluN2B ATD heterodimer, which is a different binding site than Zn²⁺ ions (*Figure 8*) [13].

The extracellular LBD, which consists of two stretches of amino acids (S1 and S2), has a clamshell-like conformation [15]. One half of the clamshell is largely (but not exclusively) formed by S1 which is located on the amino-terminal side of membrane helix M1, while the other half of the clamshell mostly comes from S2, which is located between the membrane helices M3 and M4 (*Figure 4*) [1]. Between these two lobes is a cleft in which the co-agonists glycine and glutamate bind; glycine binds to GluN1 and glutamate binds to GluN2. Once agonist binds, the LBD undergoes a conformational change, and transfers this signal to the TMD. Although LBD of the NMDA receptor and LBD of non-NMDA glutamate receptors have high sequence homology, the NMDA and AMPA receptor have different channel opening pattern because of the respective conformational changes of the receptor protein complex [15, 19].

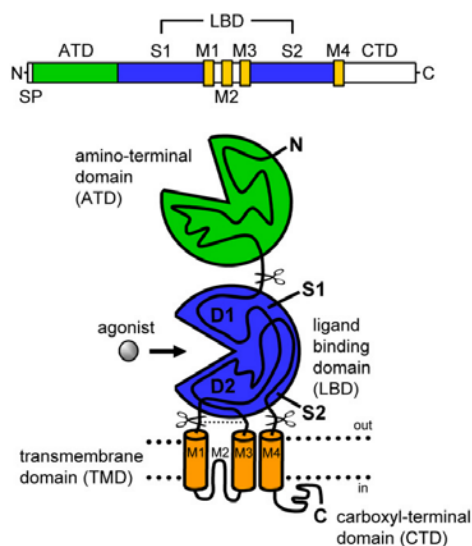


Figure 4. Linear representation of the subunit polypeptide chain and schematic illustration of the subunit topology. The LBD is defined by two segments of amino acids termed S1 and S2. The TMD contains three membrane-spanning helices (M1, M3, and M4) and a membrane re-entrant loop (M2) [1].

The glutamate receptor TMD, which is linked to the LBD, forms the pore that is configured like a potassium channel interface. TMD has three transmembrane helices, M1, M3 and M4, and a re-entrant M2 loop connecting M1 and M3 in the pore (*Figure 4*) [1, 11]. Voltage-dependent Mg^{2+} blockage of the NMDA receptor and uncompetitive antagonists bind within the channel pore [20]. The linker region between the LBD and TMD impact the ligand binding, which further modulates receptor function [21].

The glutamate receptor CTDs are different in sequence and length. The CTD affects stabilization, membrane targeting, and post-translational modifications [1, 21]. However, a lack of CTD for glutamate receptor subunits could change regulation of membrane trafficking and receptor function because of deletion of phosphorylation sites and binding sites for intracellular proteins [1].

The four GluN2 subunits possess different properties, such as channel opening probability, deactivation time course, and agonist sensitivity. Compared to other GluN2-

containing receptors, GluN2A-containing NMDA receptors are less sensitive to both glycine and glutamate and have 10-fold higher open probability and faster deactivation time course following rapid removal of glutamate. GluN2 subunits specify the channel properties, such as Mg^{2+} blockade, Ca^{2+} permeability, and single-channel conductance, which are determined by the residue at a single GluN2 subunit in the M3 transmembrane region [1]. The GluN2 subunits have different developmental expression levels and locations in the brain, which lead to the GluN2 subunits are critical in determining biophysical and pharmacological properties of the NMDA receptor.

Multiple lines of investigation have described the expression pattern of functional NMDA receptors in rat brain, which vary throughout development both spatially and temporally[22]. The intensity of the expression of the GluN1 mRNA gradually increases in all neuronal cells in rat brain. GluN2B and GluN2D are observed at low levels in the forebrain (cortex and hippocampus) and lower brain-stem region (thalamus, hypothalamus, and brain stem), respectively. The expressions of GluN2B and GluN2D mRNAs are markedly decreased after the second week of birth. GluN2A and GluN2C mRNAs appear later than the other subunit mRNAs, and continue to express in forebrain and the cerebellum through adulthood, respectively (*Figure 5*) [22, 23].

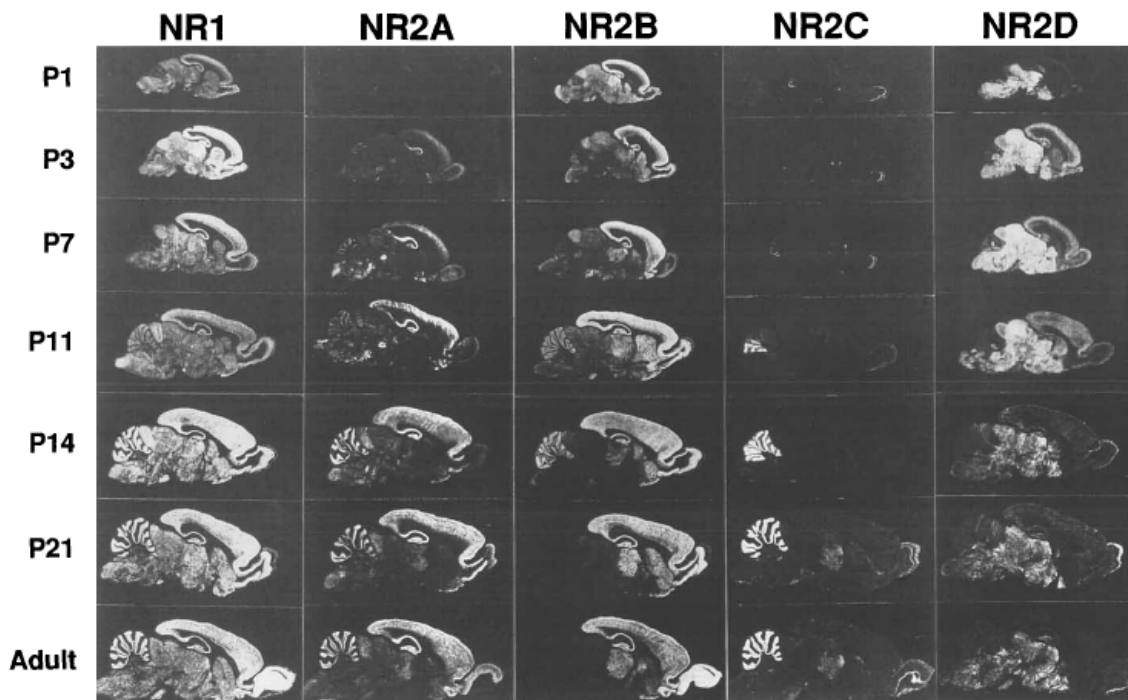


Figure 5. Distribution of NMDA receptor subunit mRNAs in the rat brain. *In situ* hybridizations, postnatal developmental change in the expression of GluN1 and GluN2A-D mRNAs. Scale bar = 10 mm [22].

1.2 NMDA receptor pharmacology

1.2.1 NMDA receptor agonists

The crystal structure of agonist-bound GluN1/GluN2 LBD heterodimers shows that the agonists bind at the cleft between the D1 and D2 regions of LBD (Figure 4). Agonists such as glycine, L/D-serine, and L/D-alanine bind to the GluN1 subunit of the NMDA receptor, while endogenous agonists including glutamate, D/L-aspartate, homocysteate, and cysteinesulfinate bind to the GluN2 subunit [1, 24-26]. Although GluN3 binds glycine like GluN1, the affinity of glycine that binds to GluN3 is 600-fold higher than that for GluN1 [27].

1.2.2 NMDA competitive antagonists

Competitive antagonists bind at the agonist binding site but do not activate the

NMDA receptor. NMDA competitive antagonists were pursued as a therapeutic approach in the early 1990s. Numerous competitive antagonists of the GluN1 and GluN2 subunits have been identified. For example, 7-chlorokynurenic acid and its analog 5,7-dichlorokynurenic acid (5,7-DCKA) are competitive antagonists of the GluN1 subunit [28, 29], while (R)-2-amino-5-phosphonopentanoate and its analogs are used as competitive antagonists of the GluN2 subunit. These antagonists are often used to distinguish the activity of NMDA receptor from the other glutamate non-NMDA receptors [1]. Due to high homology among GluN2 LBDs, the GluN2 competitive antagonists are not selective among the four different GluN2 subunits [30].

1.2.3 NMDA uncompetitive antagonists

Compounds that bind deep in the ion channel pore, such as adamantine and memantine, act as uncompetitive antagonists [31, 32]. Uncompetitive antagonists, also known as channel blockers, require activation of the NMDA receptor before binding because the blockade of the channel pore is voltage- and use-dependent [33]. Due to this fact, the channel blockers show slow inhibition, and increased binding rapidly with increases in channel opening probability. The channel blockers show low subunit selectivity because of the highly conserved ion channel region across GluN2 subunits [34]. Memantine and adamantine have been approved by the FDA for the treatment of Alzheimer's disease and Parkinson's disease, respectively [35]. Other channel blockers including ketamine, MK-801, phencyclidine (PCP), dextromethorphan, and dextrorphan, share similar binding sites within the pore [33, 36-41] (*Figure 6*).

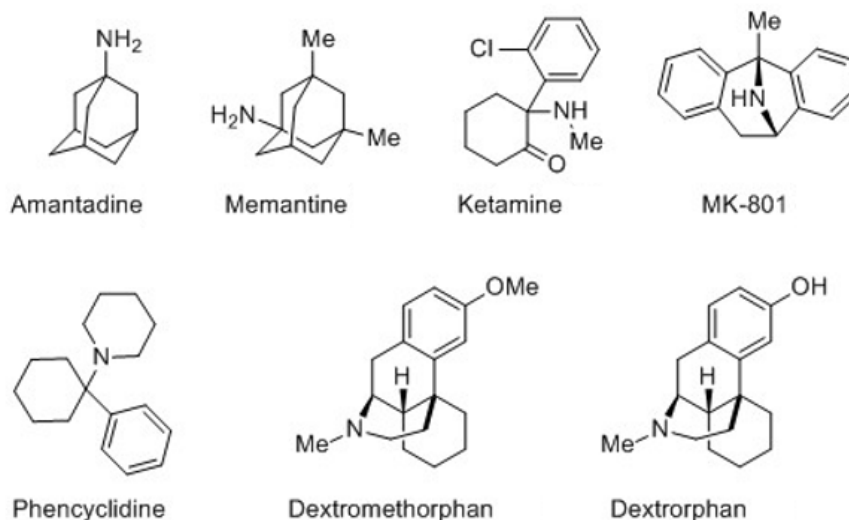


Figure 6. NMDA receptor channel blockers [34].

1.2.4 NMDA noncompetitive modulators

The first noncompetitive, subunit-selective NMDA antagonist was the phenylethanolamine ifenprodil. Ifenprodil is GluN2B-selective and is up to 400-fold more potent at GluN2B- than GluN2A-, GluN2C- and GluN2D-containing NMDA receptors [42, 43]. Both ifenprodil and closely related analogs, such as CP-101,606 and Ro 25-6981, bind at the GluN1-GluN2B ATD interface (*Figure 7, Figure 8*) [12, 43, 44]. Noncompetitive negative allosteric modulators 3-chloro-4-fluoro-N-[(4-[(2-(phenylcarbonyl)hydrazine) carbonyl]phenyl) methyl]-benzenesulfonamide (TCN-201) has been identified as a GluN2A-selective inhibitor and reside in the GluN1-GluN2A heterodimer LBD (*Figure 7, Figure 8*) [19, 45, 46]. A series of naphthalene and phenanthrene (UBP) derivatives that bind in the LBD region have been identified as potentiator and antagonists of the NMDA receptors. For example, UBP618 inhibits all GluN2 subunits with no selectivity, while UBP714 slightly potentiates with a modest selectivity for GluN2A and GluN2B subunits over GluN2D subunit [47]. UBP608 and UBP512 exclusively inhibits and potentiates for

the GluN2A-containing receptor, respectively (*Figure 7*) [48, 49]. Recently, a class of GluN2C- and GluN2D-selective potentiators (3-chlorophenyl)(6,7-dimethoxy-1-((4-methoxyphenoxy)methyl)3,4-dihydroisoquinolin-2(1H)-yl)methanone (CIQ) has been developed by our group with EC₅₀ values of 3-6 μM [50, 51]. CIQ has structural determinants of activity that reside within the pre-M1 M1 region (*Figure 7, Figure 8*) [52]. A class of pyrrolidinone (PYD) has been discovered as GluN2C potentiators. For example, PYD-106 exhibit potentiation at GluN2C subunit with an EC₅₀ value of 13 μM. Studies suggest that PYD derivatives bind at the interface between the LBD and ATD (*Figure 7, Figure 8*) [53, 54]. A series of GluN2C- or GluN2D-selective antagonists (E)-4-(6-methoxy-2-(3-nitrostyryl)-4-oxoquinazolin-3(4H)-yl)-benzoic acid (QNZ46) has been reported in a noncompetitive, voltage-independent and use-dependent manner. Studies revealed that QNZ46 shows inhibition within the presence of glutamate [45]. A class of dihydroquinoline-pyrazoline (DQP) was first developed by Dr. Tim Acker as GluN2C- and GluN2D-containing receptor antagonists (*Figure 7*) [2]. Based on site-directed mutagenesis, DQP has been advised to have structural determinants near the S2 region of the LBD of the NMDA receptor (*Figure 8*) [34]. This DQP class is described in this thesis.

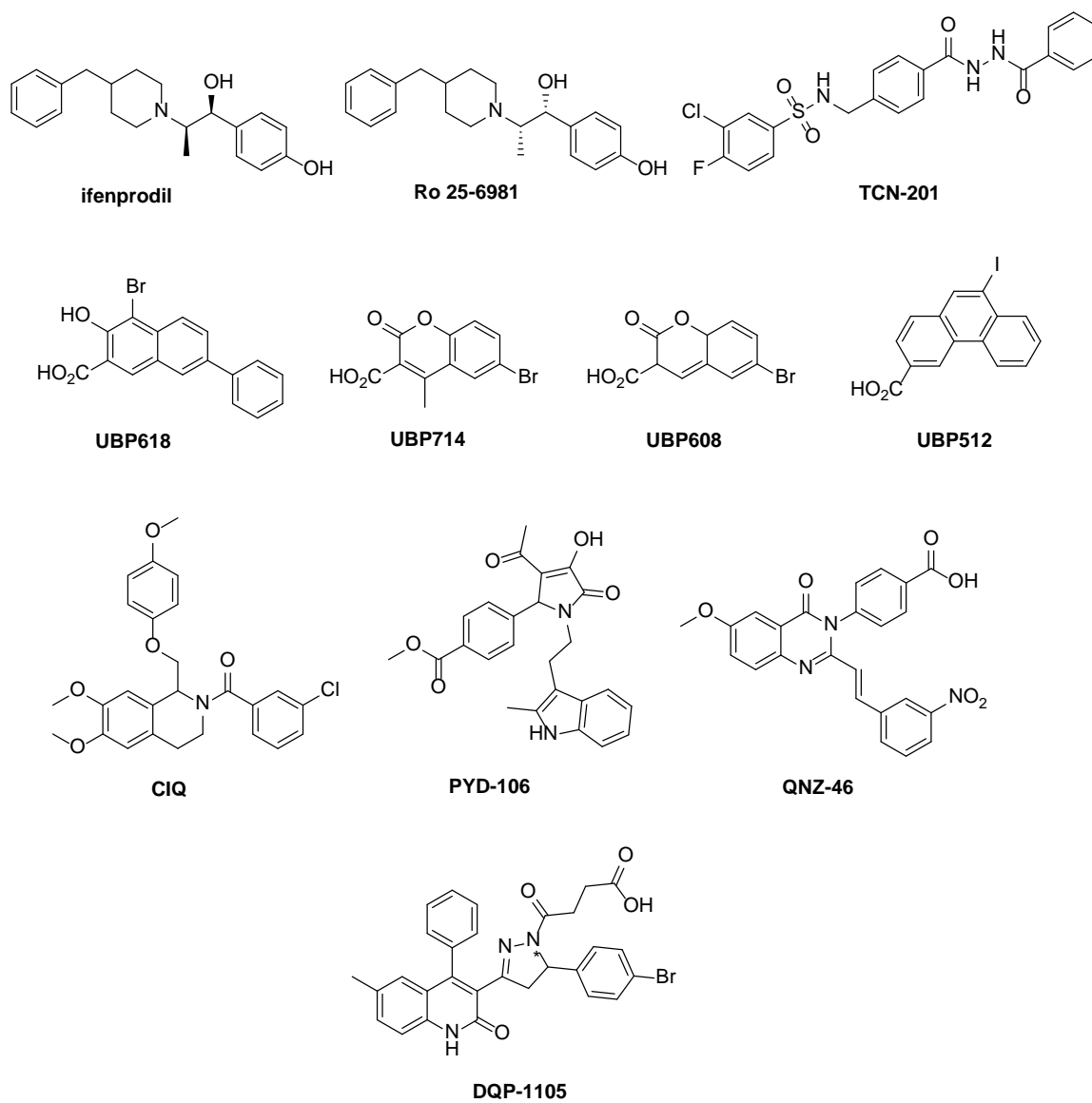


Figure 7. Subunit-selective antagonists [34].

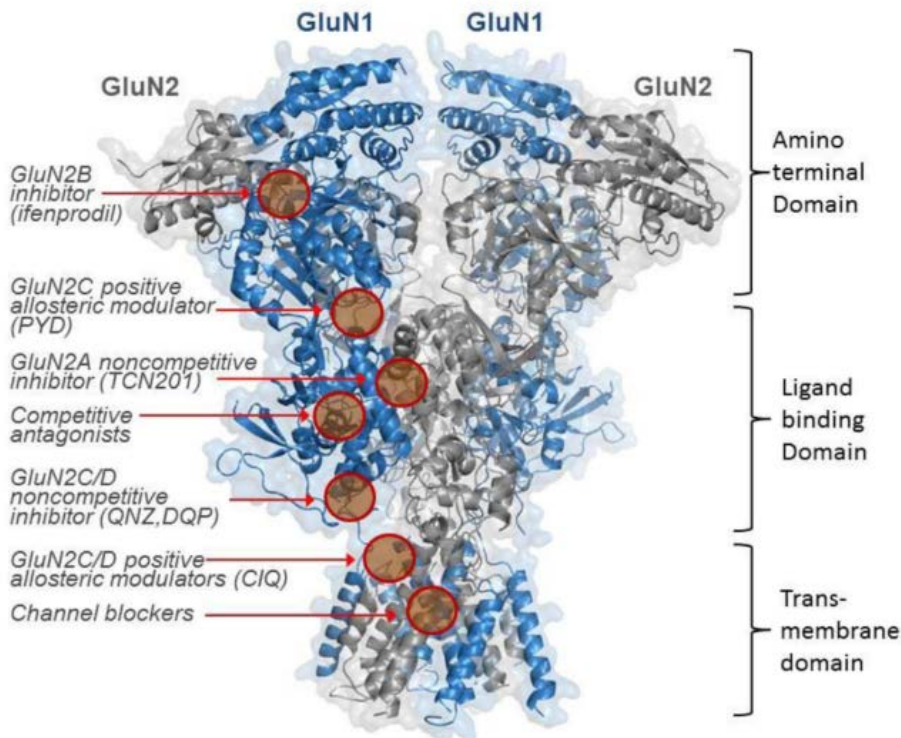


Figure 8. Homology Model of an NMDA receptor highlighting known binding sites. Ribbon diagram depicting the NMDA receptor where the GluN1 subunit is shown in blue and the GluN2 subunit is shown in grey. The figure was generated using the GluN2B crystal structure, PDB code 4PE5. Known or postulated binding sites are shown for several classes of ligands [34].

1.3 Therapeutic rationale for GluN2D-selective NMDA antagonists

Although various promising candidates have been studied in clinical trials, no treatments have been reported to be neuroprotective in Parkinson's disease (PD). For instance, L-dihydroxyphenylalanine (L-DOPA, levodopa), known as the biosynthetic precursor of dopamine, is an effective symptomatic treatment via replacement of dopaminergic stimulation [55]. However, after a period of treatment, most of the patients show motor complications such as dyskinesias and abnormal involuntary choreiform movements [56]. To reduce dyskinesia, the NMDA antagonist amantadine acts as an adjunct to L-DOPA therapy [57-59]. Although loss of dopaminergic neurons is one of the

most prominent features of Parkinson's disease, addressing only the dopaminergic deficit in PD cannot circumvent nonmotor symptoms such as dementia and impairment of autonomic nervous system function. These nonmotor symptoms are as important as motor complications [60, 61]. Therefore, the neuroprotective treatments need to be developed that will alter disease progression.

GluN2D subunits have been reported to regulate synaptic transmission in the striatum, thalamus, subthalamic nucleus (STN), globus pallidus (GPi), and substantia nigra [62-65]. The basal ganglia are a group of subcortical nuclei, which regulate movement and are imbalanced in movement disorders such as Parkinson's disease [66-68]. Since GluN2D is located at basal ganglia, GluN2D subunits have been considered as potential targets for treatment of neuropathological diseases [64]. Models of basal ganglia circuit connections between various nuclei are shown in *Figure 9*. Within the basal ganglia, the balance of activity in the parallel pathways plays a key role in regulating movement [69]. Because both excitatory glutamatergic input from the cortex and dopaminergic input from the substantia nigra pars compacta (SNc) are received by the striatum, the striatum is a critical component and interactions between dopamine receptors and NMDA receptors are essential for healthy brain and diseased brain [70-73]. In the healthy brain, the normal dopaminergic neuronal output from substantia nigra to the striatum leads to the inhibition of glutamatergic output from the STN to the GPi [74]. In Parkinson's brain, overstimulation of the GPi is due to an imbalance in the direct (D) and indirect (I) pathways. Excessive inhibitory input GPi to the motor thalamus (Thal) diminishes thalamic stimulation of the supplementary motor areas, which are indispensable for the normal spontaneous movements [75, 76]. Blockade of GluN2D could rectify circuit imbalance that develops

with loss of dopaminergic neurons. These studies raise the idea that GluN2D subunits have crucial roles in brain circuits and movements. Thus, more selective and drug-like GluN2D-selective NMDA receptor modulators could be helpful both in proof of concept and as potential therapies.

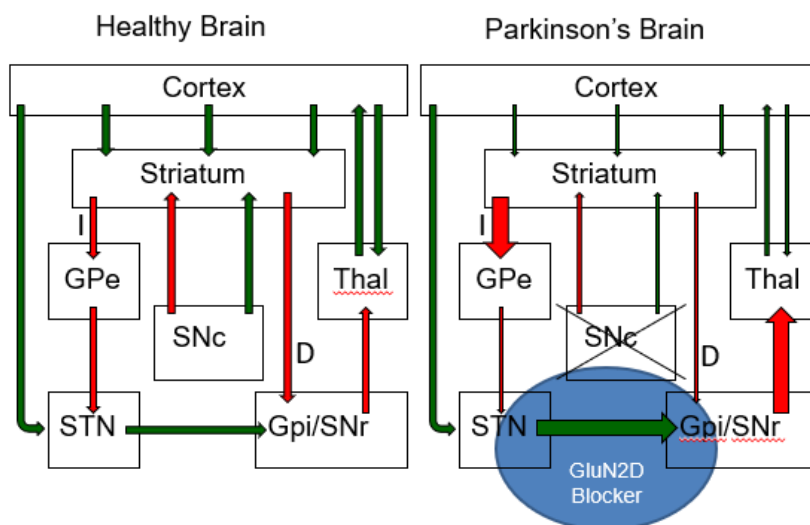


Figure 9. Models of basal ganglia circuits in the healthy brain and Parkinson's brain. GPe, external globus pallidus; STN, subthalamic nucleus; GPi, internal globus pallidus; SNr, substantia nigra pars reticulata; SNc, substantia nigra pars compacta. The thickness of arrows represents the functional state of a given circuit. Thicker arrows represent hyperactive pathways, whereas thinner arrows illustrate hypoactive circuits [66].

1.4 DQP-1105 properties

Compound 4-(5-(4-bromophenyl)-3-(6-methyl-2-oxo-4-phenyl-1,2-dihydroquinolin-3-yl)-4,5-dihydro-1H-pyrazol-1-yl)-4-oxobutanoic acid (DQP-1105) was selected from a Ca^{2+} -based screen of approximately one hundred thousand compounds from ChemDiv and Asinex diversity libraries as GluN2C/D-selective modulators [77, 78]. DQP-1105 exhibits inhibition at GluN2C- and GluN2D-containing receptors with an IC_{50} value of 7.0 μM and 2.7 μM , respectively [79]. The actions of DQP-1105 against current responses have been evaluated from recombinant NMDA receptors expressed in *X. laevis*

oocytes. With co-application of agonist plus increasing the concentrations of DQP-1105, the current response of GluN2C and GluN2D significantly decreased. When the concentration of DQP-1105 increased to 2.7 μM , the current response was reduced to 50% of maximum (Figure 10) [2]. Studies reported that the IC_{50} values evaluated at recombinant human NMDA receptors were similar to the values tested at recombinant rat NMDA receptors [2]. Although DQP-997, the initial screening hit, has the similar activity at GluN2C and GluN2D subunits, DQP-1105 has a more favorable combination of inhibition activity and selectivity for GluN2D subunit over GluN2A and GluN2B subunits [79]. The selectivity for GluN2D over GluN2C is about 3-fold and is unable to improve at this moment, more details will discuss in the conclusion chapter. Therefore, DQP-1105 is treated as the lead compound for this project to improve both the potency and selectivity at GluN2D over other GluN2 subunits.

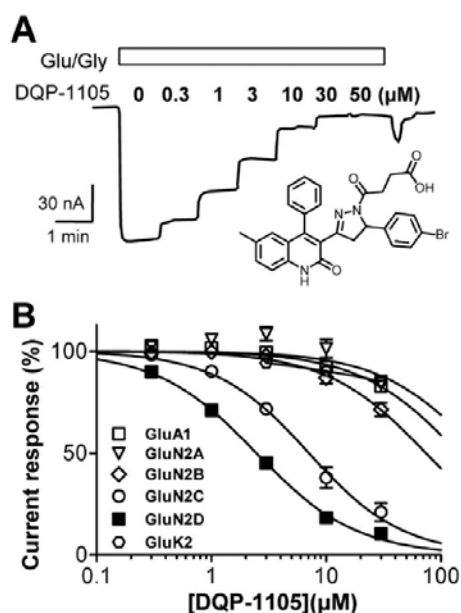
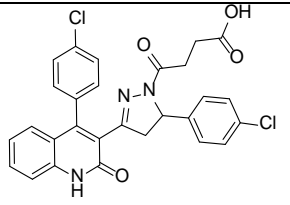
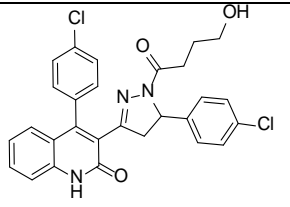
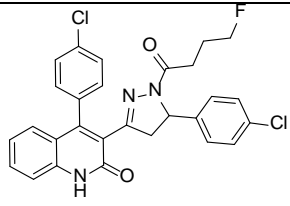


Figure 10. Subunit selectivity of DQP-1105. A, the representative current response of GluN1/GluN2D receptors during co-application of 100 μM glutamate, 30 μM glycine, and the designated concentration of DQP-1105. B, Composite concentration-effect curves determined via two-electrode voltage-clamp recording for DQP-1105 against recombinant AMPA, kainate, and four GluN2 subunits of the NMDA receptors [2].

For a better understanding of DQP-1105, two experiments have been established to determine the mechanism of its inhibition. One is to evaluate whether DQP-1105 acts as a noncompetitive antagonist. The study reported that by increasing the concentration of either glutamate or glycine, the level of inhibition of GluN1/GluN2D receptor response by DQP-1105 was not altered [2]. Another experiment was used to evaluate whether DQP-1105 inhibition is voltage-independent. The mean current-voltage relationship of GluN1/GluN2D receptors was established in the presence and absence of DQP-1105. The level of inhibition by DQP-1105 was the same at all voltages, ruling out actions within the pore [2]. Based on the results of these two experiments, DQP-1105 has been suggested as noncompetitive and voltage-independent antagonists of the NMDA receptors.

As was mentioned before, the substitutions on the DQP scaffold play a crucial role in the activity of inhibition and selectivity at GluN2D subunit over other glutamate receptor subunits. Dr. Timothy M. Acker started this project since 2010 and had synthesized over 60 compounds with DQP scaffold. Among these compounds, several candidates performed inhibition with IC_{50} values in the 100-500 nM range and show 50- to 200-fold selectivity at GluN2D-containing receptor over GluN2A and GluN2B subunits (*Table 1*) [79]. Carboxylic acid compound 997-23, a potent candidate with *para*-chloro substitution on the A ring and B ring, showed inhibition with an IC_{50} value of 430 nM at the GluN2D-containing receptor and performed 49- and 51-fold selectivity over GluN2A- and GluN2B-containing receptors, respectively. Primary alcohol 997-57, synthesized from the reduction of carboxylic acid 997-23, retained activity at the GluN2D-containing receptor, while improving the selectivity over GluN2A-containing receptor. However, compound 997-64 that substituted the alcohol with the mono fluorine isostere was inactive at all subunits.

Table 1. Acyl chain modifications^a [79].

997-	Structures	GluN2A IC ₅₀ GluN2D IC ₅₀	GluN2B IC ₅₀ GluN2D IC ₅₀	GluN2A IC ₅₀ (μ M)	GluN2B IC ₅₀ (μ M)	GluN2C IC ₅₀ (μ M)	GluN2D IC ₅₀ (μ M)
23		49	51	21	22	0.6	0.43
57		90	48	62	33	1.7	0.69
64		-	-	NE	NE	NE	NE
^a Compounds were synthesized by Dr. Tim Acker. IC ₅₀ values were obtained by fitting the Hill equation (see chapter 2.4.5) to the average composite concentration–effect curves. Data are from 5-24 oocytes between 2-4 frogs. NE indicates less than 30% inhibition at 100 μ M. The mean IC ₅₀ values plus confidence intervals are given in the appendix C.							

These three compounds were evaluated for potential blood-brain barrier (BBB) penetration using the MDR1-MDCK permeability assay [80]. Since the topological polar surface area (TPSA) of 997-23 and 997-57 were outside the optimal range for BBB penetration, and the efflux ratio of these compounds are high, 997-23 and 997-57 were suggested as being poorly brain penetrable. Compared with the carboxylic acid and alcohol, 997-64 with lower TPSA and efflux ratio has been identified to have a high potential for BBB penetration [79]. The same compounds were evaluated for plasma stability over a two-hour time course assay. All three compounds were stable in human, rat, and mouse

plasma. Metabolic stability of these three compounds was also reported via the human liver microsomes assay. The half-life of the carboxylic acid, alcohol, and mono fluorine were evaluated to be over 60 min, 13 min, and 35 min, respectively. According to this assay, carboxylic acid 997-23 exhibited the minimal degradation [79].

In conclusion, GluN2D subunits have been suggested to play a crucial role in brain circuits and movement. Thus, more active and drug-like GluN2D-selective NMDA receptor modulators could be helpful both in proof of concept and as potential therapies. A novel series of GluN2C/D-selective antagonists of the NMDA receptor have been synthesized with DQP-scaffold. Among all the compounds that have been purchased and synthesized, **997-23** is the most active compound at this stage but it is not brain penetrable. Our goal is to develop more potent and selective compounds with adequate brain penetration so that they could be use *in vivo*.

Chapter 2. SAR study of 997-series

2.1 Background of 997 project:

To develop the GluN2C/D-selective antagonists of NMDA receptor, DQP-1105 was chosen as the lead compound. DQP-1105 is a non-competitive, voltage-independent, and use-dependent negative allosteric modulator [2, 79]. The initial screening hit was compound 997, and thus all the compounds synthesized in Liotta laboratory that are derived from this scaffold are referred to as 997-#. Based on the research of Dr. Timothy M. Acker, a more potent dihydroquinolone-pyrazoline scaffold was identified with *para*-chlorine A ring substitution, *para*-chlorine or *meta*-fluorine B ring substitution and no C ring substitution (*Figure 11*) [79]. Modifications of the substitutions on these rings retained or lowered the activity and selectivity at GluN2C/D-containing receptors.

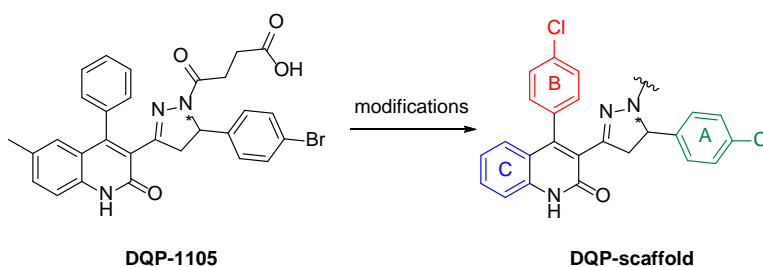


Figure 11. Structure of previously reported representative compound DQP-1105 and optimized scaffold [79].

After ring modifications, acyl chain was also optimized to obtain a more potent compound. From acyl chain modifications, more selective carboxylic acid (**997-23**) and alcohol (**997-57**) containing compounds were developed. Notably, the primary alcohol (**997-57**) improved selectivity at GluN2C/D 90-fold over GluN2A as compared to the carboxylic acid (**997-23**) which showed 48-fold selectivity (*Table 1*) [79].

As I mentioned in chapter 1, compounds **997-23**, **997-57** and **997-64** were selected

to assess the potential BBB penetration using an MDR1-MDCK permeability assay [80]. The results showed a low potential for BBB penetration of carboxylic acid (**997-23**) and alcohol (**997-57**) containing compounds. However, inactive compound **997-64** was predicted to be highly brain penetrable [79]. Following the progress of 997 project by Dr. Acker, we worked to develop more potent and selective compounds with adequate brain penetration so that they could be use *in vivo*.

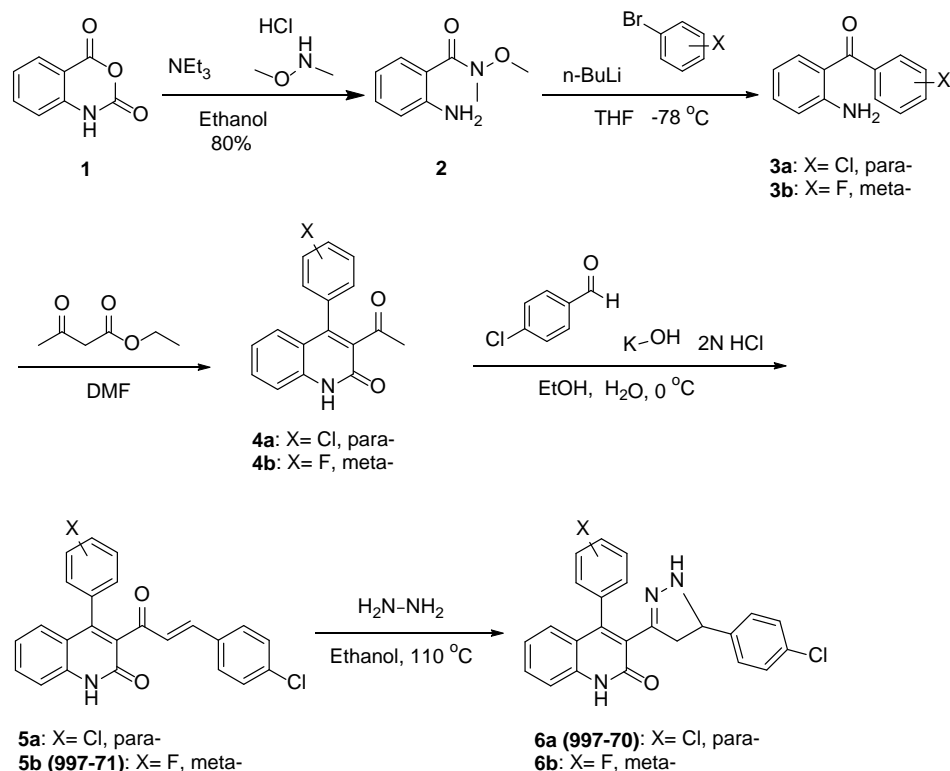
2.2 SAR results of 997-series with DQP-1105 scaffold

2.2.1 Acyl chain modification

Based on the SAR and BBB penetration results of **997-23** and **997-64**, carboxylic acid or alcohol placement on the terminal of the acyl chain resulted in low IC₅₀ values (i.e. they were potent analogues). However, these analogues were not brain penetrable, while fluorine on the terminal eliminated the activity but increased the predicted BBB penetration [79]. My project started with synthesizing candidates that retained the carboxylic acid or alcohol group as a terminal with additional fluorine group on the acyl chain.

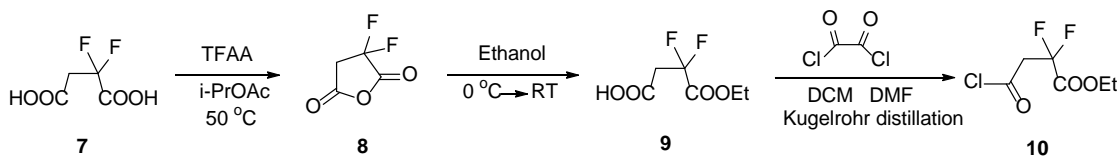
General synthetic procedures of these target compounds were shown in the following schemes. Commercially available isatoic anhydride **1** was reacted with dimethylhydroxylamine to give the Weinreb amide **2** in high yield. Then a 1:1 mixture of compound **2** and the appropriate bromobenzenes were treated with two equivalents of *n*-butyllithium via a lithium-halogen exchange reaction to yield benzophenones **3** [81]. Benzophenones **3** were condensed with ethyl acetoacetate to yield quinolone derivatives **4** [82]. The resultant methyl ketones **4** were treated with 4-chlorobenzaldehyde via a base-catalyzed condensation to yield the α,β -unsaturated ketones **5** [83]. Utilizing microwave irradiation, these ketones **5** were treated with hydrazine monohydrate to yield the

pyrazoline amines **6** (Scheme 1) [79].



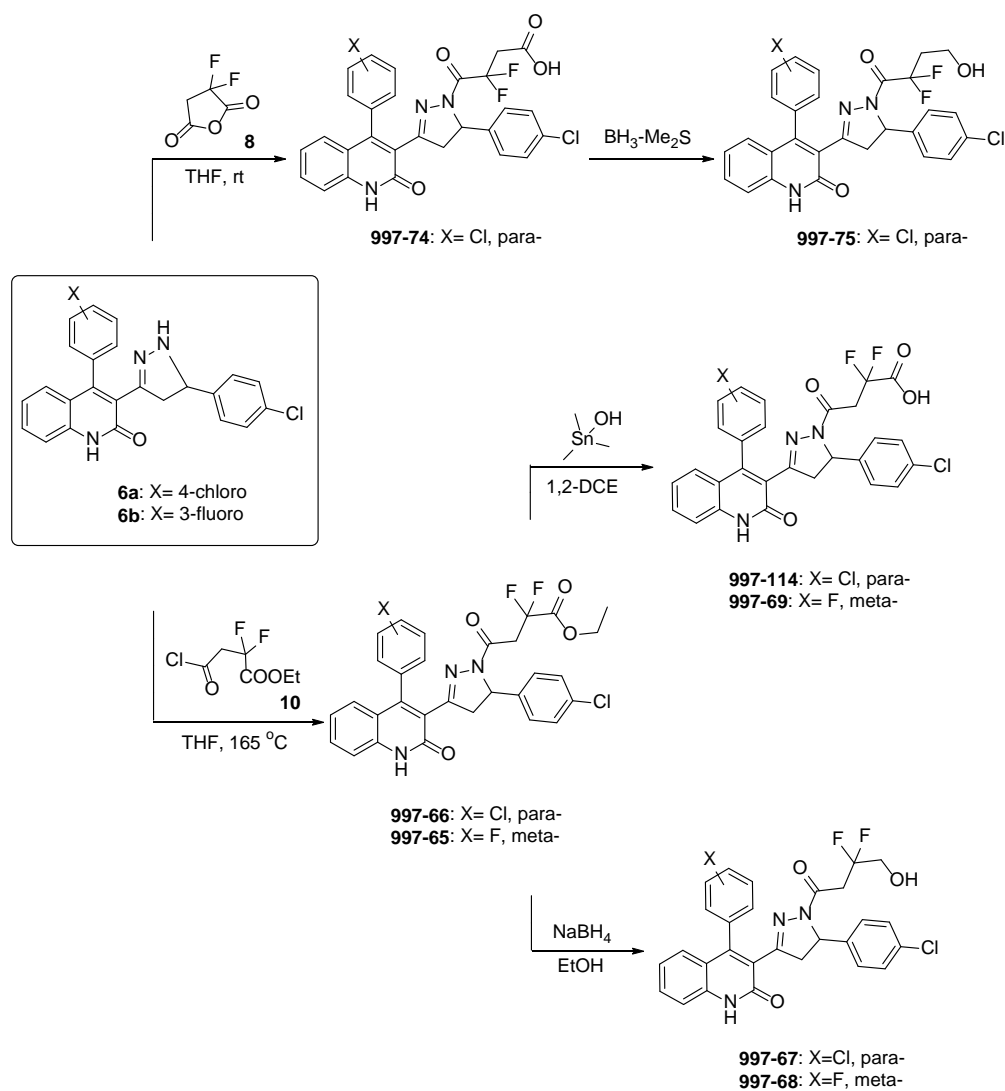
Scheme 1. Synthesis of dihydroquinolone pyrazoline amines.

The acyl chain component was synthesized separately. Commercially available 2,2-difluorosuccinic acid **7** and trifluoroacetic anhydride (TFAA) were refluxed in isopropyl acetate (i-PrOAc) yielding 2,2-difluorosuccinic anhydride compound **8** [84]. The anhydride **8** was reacted with absolute ethanol overnight and then treated with oxalyl chloride to yield acetyl chloride **10** after kugelrohr distillation [85, 86] (Scheme 2).



Scheme 2. Synthesis of acyl chains.

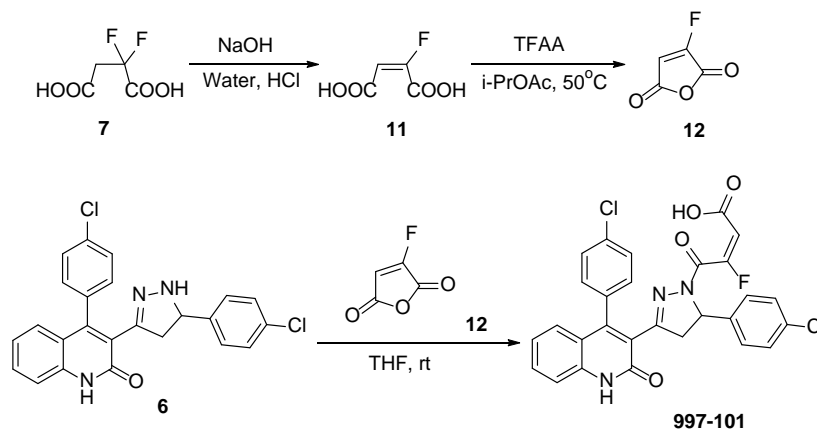
After synthesis of pyrazoline amine **6** and acyl chain precursors **8** and **10**, the pyrazoline amine **6** selectively attacked the more electrophilic carboxyl group of **10** to yield **997-65** and **997-66**, respectively [79]. Esters **997-65** and **997-66** were further reduced with sodium borohydride to yield 2,2-difluoro-substituted alcohols **997-67** and **997-68** [87]. Esters **997-65** and **997-66** were also hydrolyzed with trimethyltin hydroxide to give 2,2-difluoro-substituted carboxylic acids **997-69** and **997-114** [88]. Alternative pyrazoline amine **6** could directly react with 2,2-difluorosuccinic anhydride **8** at room temperature given 3,3-difluoro-substituted carboxylic acid **997-74**. Then, **997-74** was further reduced by borane dimethyl sulfide, to yield 3,3-difluoro-substituted alcohol **997-75** [79](Scheme 3).



Scheme 3. Synthesis of acylated quinolone pyrazoline products.

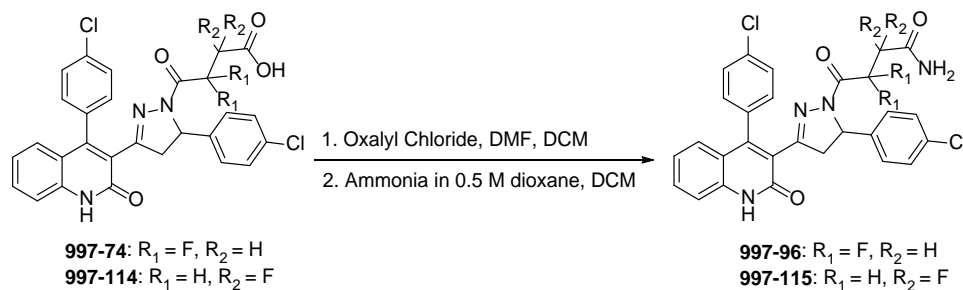
Instead of adding two fluorines on the acyl chain, mono-fluorine substituted compound **997-101** was synthesized to evaluate the activity and selectivity at the GluN2D-containing receptor. The acyl chain component was synthesized through two steps. Starting with commercially available 2,2-difluorosuccinic acid **7**, 2-fluoromaleic acid **11** was synthesized via elimination with sodium hydroxide. Then compound **11** was refluxed with trifluoroacetic anhydride in isopropyl acetate to yield fluoromaleic anhydride **12** [84]. Finally, the intermediate pyrazoline amine **6** was reacted with anhydride **12** to yield **997-**

101 [79] (Scheme 4).



Scheme 4. Synthesis of 997-101.

Amides **997-96** and **997-115**, which can be regarded as the bio-isosteres of carboxylic acids, were also synthesized via two steps. Carboxylic acids **997-74** and **997-114** were activated by oxalyl chloride to yield acetyl chlorides and then reacted with ammonia solution to yield **997-96** and **997-115** (Scheme 5).



Scheme 5. Synthesis of amides 997-96 and 997-115.

All target compounds were evaluated for activity in Dr. Stephen Traynelis laboratory using two-electrode voltage-clamp recordings performed in *Xenopus laevis* oocytes expressing recombinant GluN2A-D subunits [79] (**Table 2**). The intermediates pyrazoline amine **997-70** and α,β -unsaturated ketone **997-71** were inactive at all receptors. Two ester compounds **997-65** and **997-66** also showed no inhibition of NMDA receptors. With di-fluorine substitution, alcohol compounds **997-67**, **68** and **75** showed inhibitory

activity only at GluN2C and GluN2D receptors, with IC_{50} values ranging from 0.8 μ M to 2.0 μ M. Based on the IC_{50} value, compound **997-67** with *para*-chloro substitution on the top ring was determined to be more potent at GluN2C/D subunits in comparison to *meta*-fluoro substituted **997-68**. Compound **997-75** with the difluoro-substitution near the amide group showed much lower potency than **997-67** and **997-68**.

Notably, in previous reports, the potency at GluN2C/D-containing receptors ranged between 3-10 μ M [2, 79]. Consequently, an important goal of my project was to improve potency. With further development of the SAR, the potency of compounds that were synthesized was often under 1 μ M. Under our recording conditions, we can only conclude that compound **997-67** remained potent at GluN2C/D-containing receptors, but its selectivity over GluN2A- and GluN2B-containing receptors could not be determined because we could not test higher concentrations due to limited solubility. Compound 2,2-difluoro-substituted carboxylic acid **997-69** with *meta*-fluoro substitution on the top ring exhibited similar activity and selectivity at GluN2C/D subunits. Compound **997-114**, with *para*-chloro substitution on the top ring and 2,2-difluoro-substituted carboxylic acid, showed better inhibition with an IC_{50} value of 170 nM, but poorer selectivity at GluN2D over GluN2A/B-containing receptors in comparison to compound **997-23**, which lacked fluoro substitutions. Surprisingly, compound **997-74**, with difluoro-substitution adjacent to the amide group, improved potency at GluN2C- and GluN2D-containing receptors, possessing IC_{50} values of 390 nM and 50 nM respectively, and was 220-fold selective for GluN2D- over GluN2A-containing receptor. Although compound **997-101**, which is the *cis*-configuration of mono-fluoro maleic acid, retained the activity at the GluN2D receptor (IC_{50} = 60 nM) in comparison to **997-74**, the potency of GluN2A- and GluN2C-containing

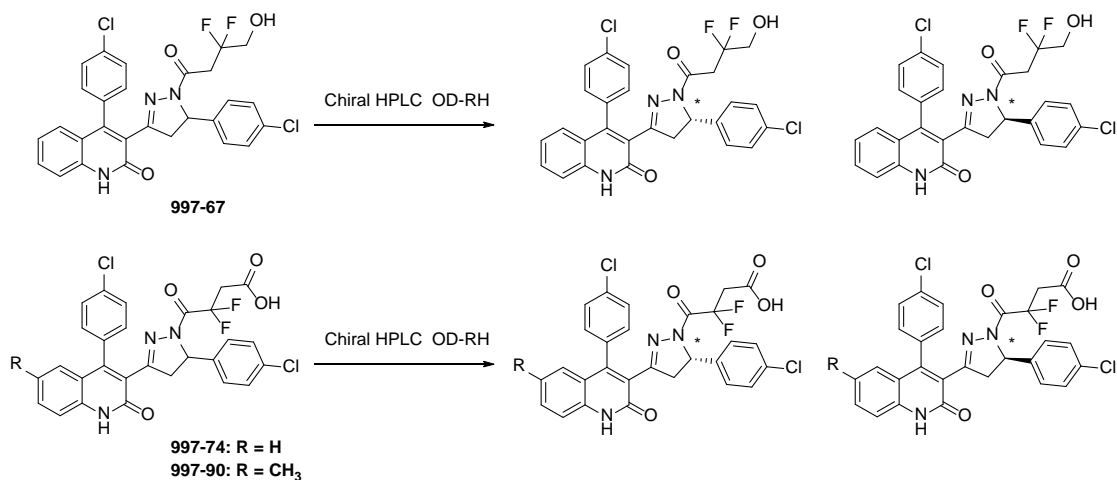
receptors were both increased, which consequently decreased the selectivity at GluN2D over GluN2A from 220-fold to 50-fold. Finally, replacing the carboxylic acid to the bioisostere amide yielded **997-96** and **997-115**, which dropped the potency 2- to 4-fold in comparison to their corresponding acids **997-74** and **997-114** (Table 2).

Table 2. Acyl chain modifications.

997-	<u>2A IC₅₀</u> 2D IC ₅₀	<u>2B IC₅₀</u> 2D IC ₅₀	GluN2A IC ₅₀ (μM)	GluN2B IC ₅₀ (μM)	GluN2C IC ₅₀ (μM)	GluN2D IC ₅₀ (μM)
65	-	-	NE	NE	NE	NE
66	-	-	NE	NE	NE	NE
67	-	-	NE	NE	1.6	0.8
68	-	-	NE	NE	4.3	1.4
69	56	96	28	48	0.6	0.5
70	-	-	NE	NE	NE	NE
71	-	-	NE	NE	NE	NE
74	220	138	11	6.9	0.39	0.05
75	-	-	NE	NE	17	2
96	150	14	30	2.8	0.5	0.2
101	50	183	3	11	0.07	0.06
114	33	48	5.67	8.15	0.338	0.17
115	-	-	NE	NE	1.44	0.343

IC₅₀ values were obtained by fitting the Hill equation (see chapter 2.4.5) to the average composite concentration-effect curves. Data were from 4-13 oocytes between 1-2 frogs. NE indicates less than 50% inhibition at 30 μM. The mean IC₅₀ values plus confidence intervals are given in the appendix C.

Based on the above SAR results, three potent racemic compounds **997-67**, **997-74**, and **997-90** were selected to separate their enantiomers via reverse phase chiral chromatography by using an OD-RH column [79] (Scheme 6).



Scheme 6. Enantiomer separation.

Evaluation of the purified enantiomers indicated that all three (-)-enantiomers modestly increased the selectivity and activity at GluN2C- and GluN2D -containing receptors over racemic compounds. (-)-**997-67** is 6-fold more potent than (+)-**997-67** at GluN2D subunit, while (-)-**997-74** is 85-fold more active than (+)-**997-74** at GluN2D receptors (Table 3).

Table 3. Stereoselectivity for the purified enantiomers.

997-	<u>2A IC₅₀</u> 2D IC ₅₀	<u>2B IC₅₀</u> 2D IC ₅₀	GluN2A IC ₅₀ (μM)	GluN2B IC ₅₀ (μM)	GluN2C IC ₅₀ (μM)	GluN2D IC ₅₀ (μM)
67	-	-	NE	NE	1.6	0.8
(-)-67	-	-	NE	NE	1.4	0.62
(+)-67	-	-	NE	NE	8.5	3.6
74	220	138	11	6.9	0.39	0.05
(-)-74	-	-	NE	NE	0.094	0.046
(+)-74	-	-	NE	NE	3.4	3.9
90	15	15	3	3	0.4	0.2
(-)-90	15	15	1.9	1.9	0.2	0.13
(+)-90	4	2	4.1	1.8	2.1	<1
IC ₅₀ values were obtained by fitting the Hill equation (see chapter 2.4.5) to the average composite concentration-effect curves. Data were from 4-13 oocytes between 1-2 frogs. NE indicates less than 50% inhibition at 30 μM. The mean IC ₅₀ values plus confidence intervals are given in the appendix C.						

The absolute stereochemistry of (+) 997-74 was assigned via X-ray crystallography as *R* configuration (See experimental, *Figure 12*, Appendix A *Figure 12*). According to this information, we can conclude that *S* enantiomers of 997-series were more potent than corresponding *R* enantiomers and racemic compounds. (*S*)-**997-74** was the most active compound thus far with an IC₅₀ value of 46 nM and was more selective at GluN2D over GluN2A- and GluN2B-containing receptors than the racemic **997-74**.

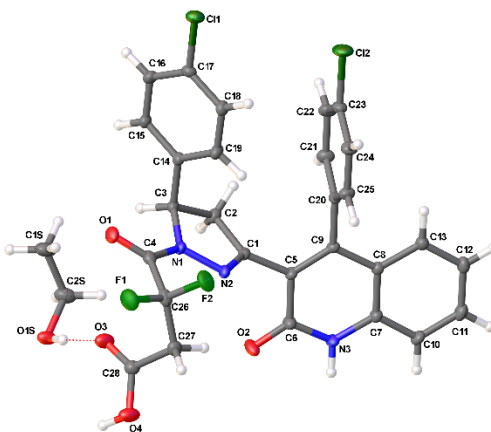
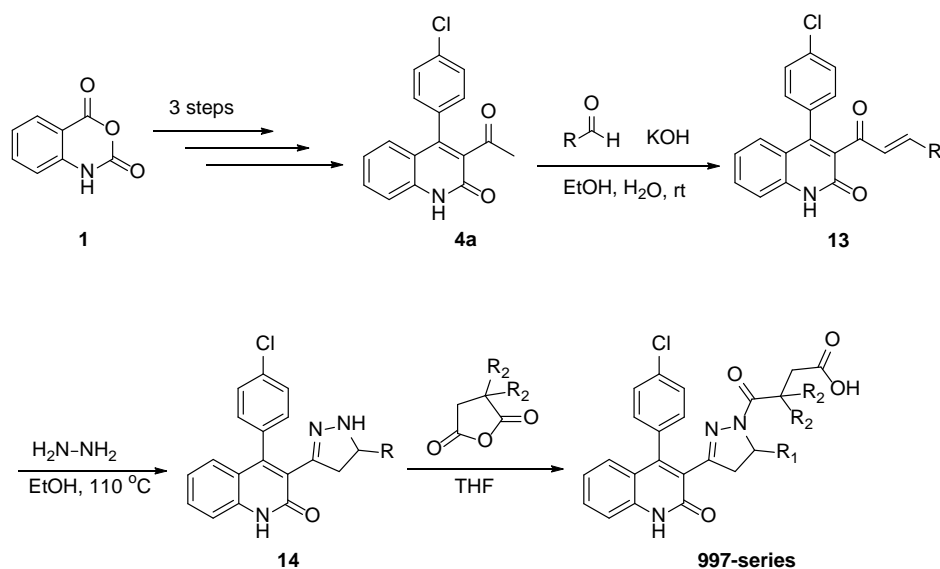


Figure 12. Crystallographic data for *R* configuration of 997-74.

2.2.2 A-phenyl ring modification

After exploring the effect of different acyl chains, the A-phenyl ring was modified next. Eleven compounds were synthesized by keeping the B-phenyl ring and C-quinolone ring constant. The acyl chains of these compounds were either a carboxylic acid or difluoro-substituted carboxylic acid. The synthesis route was similar as shown above. Starting with isatoic anhydride, quinolone derivative **4a** was formed via three steps [81, 82]. The resultant methyl ketones **4a** were treated with appropriate carbaldehyde via a base-catalyzed condensation to yield the α,β -unsaturated ketones [83]. Utilizing microwave irradiation, ketones were reacted with hydrazine monohydrate to yield the pyrazoline amines. The pyrazoline amines were then functionalized with succinic anhydride or 2,2-difluorosuccinic anhydride to yield compounds **997-79**, **997-80**, **997-83**, **997-88**, **997-92**, **997-104**, **997-110**, **997-111**, **997-112**, and **997-113** [79] (Scheme 7).

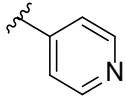
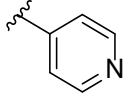
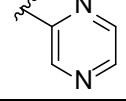
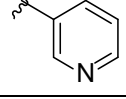
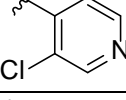
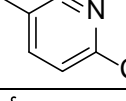
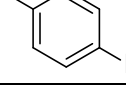
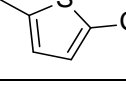
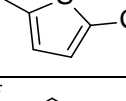
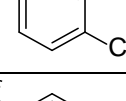
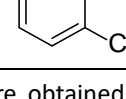


Scheme 7. Synthesis of 997-series with different A-ring modifications.

All target compounds were evaluated for activity by Dr. Stephen Traynelis' laboratory using two-electrode voltage-clamp recordings. Compared with pyrazoline amine **997-70**, which was inactive at receptors, pyrazoline amine **997-78** showed weak potency at GluN2B-, GluN2C-, and GluN2D-containing receptors (Table 4). However, compound **997-79** was inactive at all receptors after adding the acyl chain to **997-78**. Compounds **997-80**, **997-83**, and **997-88** were also inactive at all receptors, while compound **997-92** with *para*-chloro substitution showed weak activity at GluN2C- and GluN2D-containing receptors. Compound **997-104** with smaller halogen substitution, fluorine, decreased the potency 16-fold at GluN2D-containing receptor as well as lower the selectivity over GluN2B-containing receptor in comparison to **997-74**. 2-Chloro substituted thiophene **997-110** and **997-111** were synthesized and evaluated. Compound **997-110** with difluoro-substitution on the acyl chain performed IC₅₀ value of 160 nM, which is 3-fold less potent than **997-74**. However, 2-chlorothiophene improved the GluN2D-containing receptor selectivity over GluN2B-containing receptor to 625-fold.

Compound **997-112** and **997-113** with trifluoromethyl substitution, which showed better hydrophobicity and electron-withdrawing property than chlorine, were synthesized with and without difluoro substitution on the acyl chain. Compound **997-112** without difluoro substitution possessed better activity and selectivity at GluN2D-containing receptor in comparison to **997-23**, while compound **997-113** with difluoro-substitution resulted in lower inhibition and selectivity at GluN2D-containing receptor than **997-74** (*Table 4*). Therefore, the halogen substitution on the *para* position of the A ring may be important functionality to increase the potency at GluN2C/D-containing receptors, and the thiophene ring may improve the selectivity at GluN2D-containing receptors over GluN2B-containing receptors.

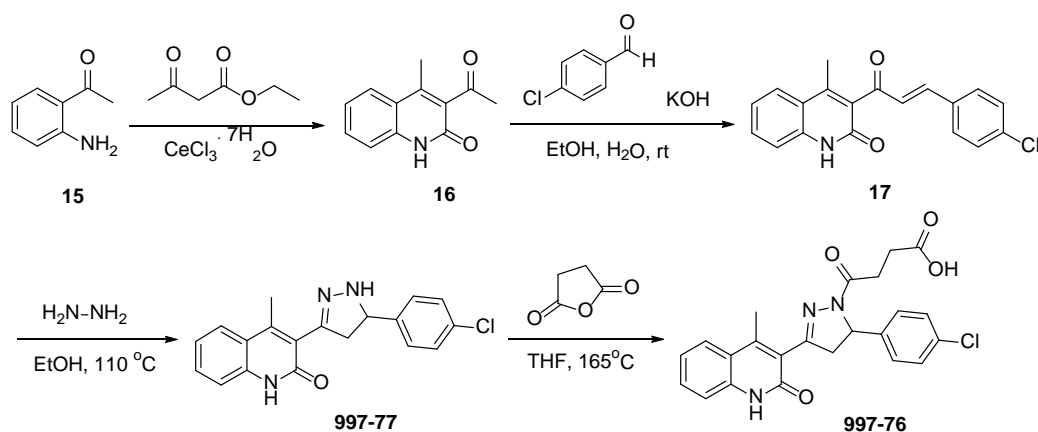
Table 4. A-ring modifications.

997-	R ₁	R ₂	2B IC ₅₀ 2D IC ₅₀	GluN2A IC ₅₀ (μ M)	GluN2B IC ₅₀ (μ M)	GluN2C IC ₅₀ (μ M)	GluN2D IC ₅₀ (μ M)
78		-	3	NE	54	20	19
79		H	-	NE	NE	NE	NE
80		H	-	NE	NE	NE	NE
83		H	-	NE	NE	NE	NE
88		H	-	NE	NE	NE	NE
92		H	-	NE	NE	8	8
104		F	37	20	30	1.6	0.81
110		F	625	30	100	0.43	0.16
111		H	43	21	34	1.3	0.8
112		H	100	13	20	0.35	0.2
113		F	36	2.3	2.9	0.17	0.08

IC₅₀ values were obtained by fitting the Hill equation (see chapter 2.4.5) to the average composite concentration-effect curves. Data were from 4-13 oocytes between 1-2 frogs. NE indicates less than 50% inhibition at 30 μ M. The mean IC₅₀ values plus confidence intervals are given in the appendix C.

2.2.3 B-phenyl ring modification

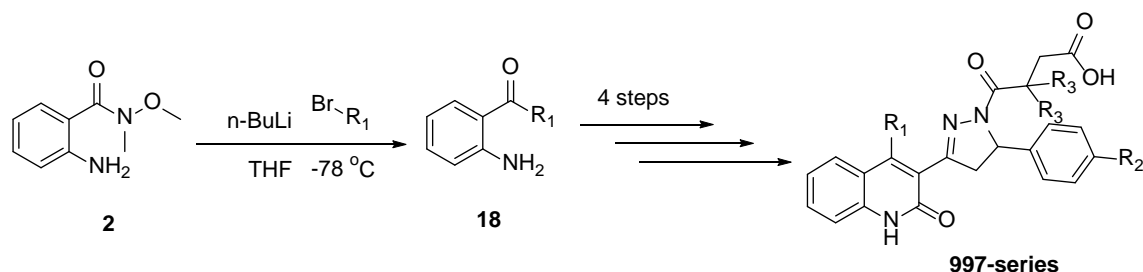
To explore the necessity of the top B-phenyl ring, compound **997-76** was synthesized first. Commercially available 2-aminoacetophenone was treated with ethyl acetoacetate, utilizing microwave irradiation, to yield quinolone derivative [82]. The resultant methyl ketone was treated with 4-chlorobenzaldehyde via a base-catalyzed condensation to yield the α,β -unsaturated ketones. Utilizing microwave irradiation, unsaturated ketone was reacted with hydrazine monohydrate to yield compound **997-77**. The pyrazoline amine **997-77** was treated with succinic anhydride to yield final compound **997-76** [79] (Scheme 8). This compound was inactive at all receptors (Table 5).



Scheme 8. Synthesis of 997-76 and 997-77.

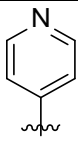
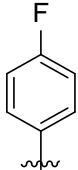
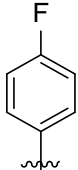
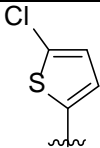
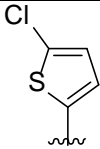
By following the same procedures as shown in chapter 2.3.1, the top ring was also modified with pyridine, 2-chlorothiophen, and *para*-fluorophenyl analogs. Commercially available 4-bromopyridine, 2-bromo-5-chlorothiophene, and 1-bromo-4-fluorobenzene were used in the second step (Scheme 9). All these compounds were evaluated for activity using two-electrode voltage-clamp recordings. In comparison to **997-23**, compound **997-82** showed poor activity at GluN2C- and GluN2D-containing receptors

with IC₅₀ values of 15 μM and 8.1 μM respectively, while compound **997-108** with thiophene retained or slightly increased the activity and selectivity at GluN2D- over GluN2A/B-containing receptors (Table 5). Difluoro substituted compound **997-109** improved the IC₅₀ value to 100 nM at GluN2D-containing receptor but decreased the selectivity over GluN2A- and GluN2B-containing receptors. Compounds **997-103** and **997-105** with fluoro substitution on both A-phenyl ring and B-phenyl ring dropped the inhibition potency to 3-5 μM no matter whether there was difluoro substitution on the acyl chain. These results updated the conclusion to that *para*-chloro and chlorothiophene are two favorable substitutions on the top ring for improving the potency at the GluN2D subunit.



Scheme 9. Synthesis of 997-series with B-phenyl ring modifications.

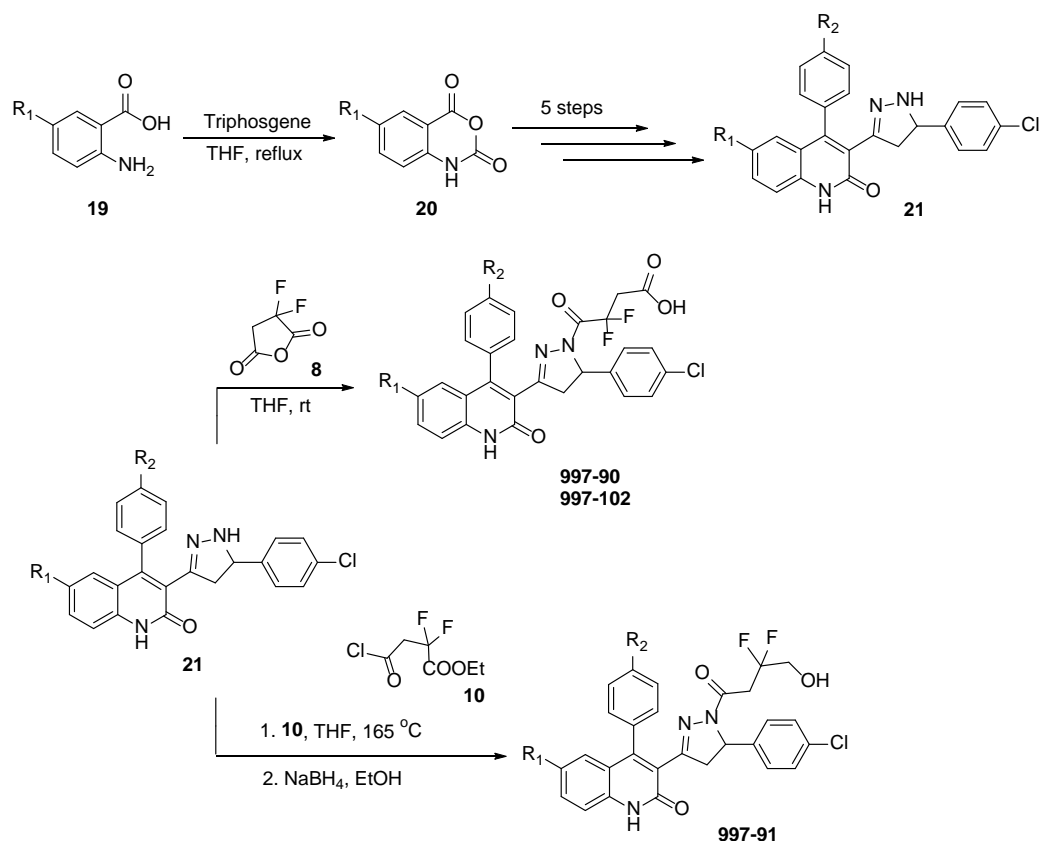
Table 5. B-ring modifications.

997-	R1	R2	R3	GluN2A IC ₅₀ (μ M)	GluN2B IC ₅₀ (μ M)	GluN2C IC ₅₀ (μ M)	GluN2D IC ₅₀ (μ M)
76	Me	Cl	H	NE	NE	NE	NE
77	Me	Cl	-	NE	NE	NE	NE
82		Cl	H	NE	NE	15	8.1
103		F	F	NE	NE	7	3.1
105		F	H	NE	NE	6.7	5.1
108		Cl	H	13	23	0.67	0.4
109		Cl	F	2.6	4	0.28	0.1

IC₅₀ values were obtained by fitting the Hill equation (see chapter 2.4.5) to the average composite concentration-effect curves. Data were from 4-13 oocytes between 1-2 frogs. NE indicates less than 50% inhibition at 30 μ M. The mean IC₅₀ values plus confidence intervals are given in the appendix C.

2.2.4 Quinolone ring modification

Former work suggested that the methyl group on the quinolone ring increased the selectivity of GluN2B over GluN2D [79]. Hence, two compounds with the methyl group were synthesized to improve the selectivity. Starting with 2-amino-5-methylbenzoic acid, triphosgene was added to form anhydride **1b** [79]. Then **1b** underwent 6 or 7 steps to give **997-90** and **997-91** (Scheme 10). Unexpectedly, for the difluoro-substituted compounds, the methyl group did not increase selectivity but instead decreased selectivity. Compound **997-102** with fluoro substitution on the quinolone ring showed moderate potency at GluN2D-containing receptor with an IC₅₀ value of 400 nM and poor selectivity over GluN2A- and GluN2B-containing receptors (*Table 6*). Based on these results, substitutions on the quinolone ring did not improve either the activity or selectivity at the GluN2D-containing receptor.



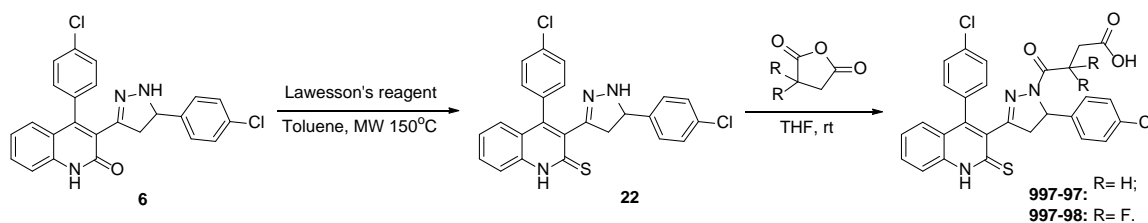
Scheme 10. Synthesis of 997-90, 997-91, and 997-102.

Table 6. Quinolone ring modifications (1).

997-	R1	R2	GluN2A IC ₅₀ (μM)	GluN2B IC ₅₀ (μM)	GluN2C IC ₅₀ (μM)	GluN2D IC ₅₀ (μM)
90	Me	Cl	3	3	0.4	0.2
91	Me	Cl	NE	NE	7.1	4.4
102	F	F	5.9	7.3	1	0.4

IC₅₀ values were obtained by fitting the Hill equation (see chapter 2.4.5) to the average composite concentration-effect curves. Data were from 4-13 oocytes between 1-2 frogs. NE indicates less than 50% inhibition at 30 μM. The mean IC₅₀ values plus confidence intervals are given in the appendix C.

According to the results from Strong, et al (2017), thioamide-containing compounds with CIQ scaffold were consistently more potent than amide-containing compounds because thioamide bonds have a larger rotational barrier [89-91]. Therefore, compounds **997-97** and **997-98** with thioamide were synthesized to explore the functionality of amide group in the quinolone ring. Pyrazoline amine **6** was converted to thioamide-containing compound **22** with Lawesson's reagent in toluene via microwave irradiation [92]. Then the compound **22** was forwarded to the final compound **997-97** and **997-98** (Scheme 11). Both the activity and selectivity were improved by adding the difluoro substitution. Compound **997-98** was less potent at GluN2D subunit with an IC₅₀ value of 140 nM in comparison to the most active compound **997-74** with an IC₅₀ value of 50 nM. However, compound **997-98** was inactive at GluN2A- and GluN2B-containing receptors, which resulted in better selectivity (Table 7).



Scheme 11. Synthesis of thioamide-containing compound 997-97 and 997-98.

Table 7. Quinolone ring modifications (2).

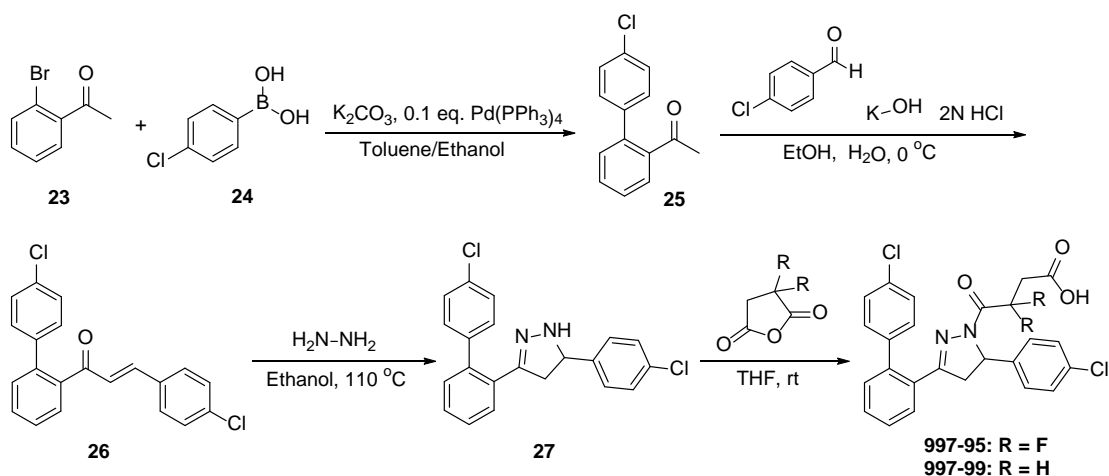
997-	R	$\frac{2A}{2D}$ IC ₅₀	$\frac{2B}{2D}$ IC ₅₀	GluN2A IC ₅₀ (μM)	GluN2B IC ₅₀ (μM)	GluN2C IC ₅₀ (μM)	GluN2D IC ₅₀ (μM)
97	H	46	86	16	30	0.48	0.35
98	F	-	-	NE	NE	0.44	0.14

IC₅₀ values were obtained by fitting the Hill equation (see chapter 2.4.5) to the average composite concentration-effect curves. Data were from 4-13 oocytes between 1-2 frogs. NE indicates less than 50% inhibition at 30 μM. The mean IC₅₀ values plus confidence intervals are given in the appendix C.

2.3 SAR results of 997-series with 997-95 scaffold

2.3.1 Development of 997-95 scaffold

Although **997-74** already provided an excellent IC_{50} value at the GluN2D receptor and increased the selectivity at GluN2D over GluN2A as 220-fold, the brain penetration study resulted that **997-74** was not brain penetrable. One possible reason why **997-74** cannot cross the blood-brain barrier (BBB) was its large molecular weight (over 500). Generally, as a CNS drug, the large molecular weight can lower the capacity of crossing BBB. Therefore, to improve BBB penetration, the size of 997-series was diminished. One direct way to minimizing the size is simply to remove one ring. **997-95** with phenyl group instead of quinolone moiety was synthesized first. 2'-Bromoacetophenone and 4-chlorophenylboronic acid were refluxed via Suzuki-Miyaura cross-coupling to yield methyl ketone. The resultant methyl ketones were treated with 4-chlorobenzaldehyde via a base-catalyzed condensation to yield the α,β -unsaturated ketones [83]. Utilizing microwave irradiation, these ketones were treated with hydrazine monohydrate to yield the pyrazoline amines. The pyrazoline amines were then functionalized with succinic anhydride or 2,2-difluorosuccinic anhydride to yield compounds **997-95** and **997-99** [79] (Scheme 12).



Scheme 12. Synthesis of 997-95 and its analogue.

All target compounds were evaluated for activity using two-electrode voltage-clamp recordings. Compound **997-95** with phenyl group instead of quinolone moiety showed IC_{50} value equal to 4.8 μM and 6.2 μM at GluN2C- and GluN2D-containing receptors, respectively (*Table 8*). Although **997-95** was less potent than **997-74**, it was still active and lower the molecular weight from 570 g/mol to 503 g/mol. Therefore, **997-95** was treated as a novel scaffold for further optimization. Compound **997-99** without difluoro-substitution increased IC_{50} to 16 μM and 12 μM at GluN2C- and GluN2D-containing receptors, and eliminated the activity at GluN2A- and GluN2B-containing receptors (*Table 8*).

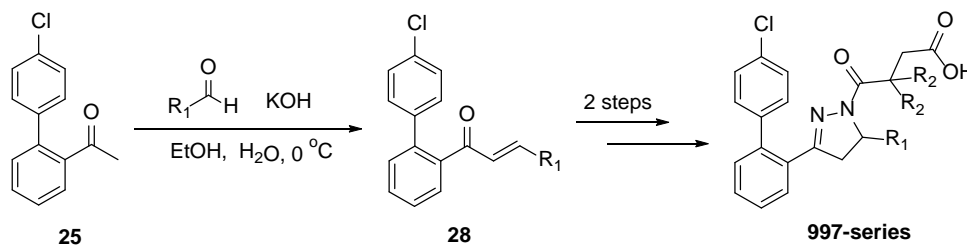
Table 8. SAR study of 997-95 and 997-99.

997-	R	$\frac{2A}{2D} IC_{50}$	$\frac{2B}{2D} IC_{50}$	GluN2A IC_{50} (μM)	GluN2B IC_{50} (μM)	GluN2C IC_{50} (μM)	GluN2D IC_{50} (μM)
95	F	5	1	30	6.4	4.8	6.2
99	H	-	-	NE	NE	16	12

Data were from 4-13 oocytes between 1-2 frogs. NE indicates less than 50% inhibition at 30 μM .

2.3.2 A-phenyl ring modification

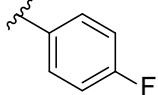
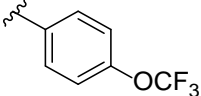
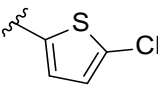
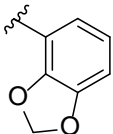
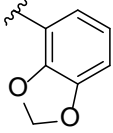
To explore the favorable substitution that contributes to the activity with **997-95** scaffold, the ring on the right side was first optimized. The synthetic pathways were the same to the procedures of forming **997-95** by choosing the appropriate aldehydes to yield α,β -unsaturated ketones (*Scheme 13*).



Scheme 13. Synthesis of 997-95 analogues with A-ring modifications.

Compound **997-116** with 4-fluorophenyl substitution on the right ring showed poor activity and selectivity at GluN2C- and GluN2D-containing receptors. Replacing 4-chlorophenyl to 4-trifluoromethoxyphenyl lead to compound **997-117**, which increased the potency at GluN2D-containing receptor with an IC_{50} value of 2.9 μ M. However, the selectivity at GluN2D subunit over GluN2A- and GluN2B-containing receptors were low. Similarly, compound **997-118** with 2-chlorothiophene performed IC_{50} value of 3.7 μ M at GluN2D subunit and poor selectivity over other subunits. Compounds **997-119** and **997-122** with benzo[1,3]dioxole were inactive at all receptors (*Table 9*).

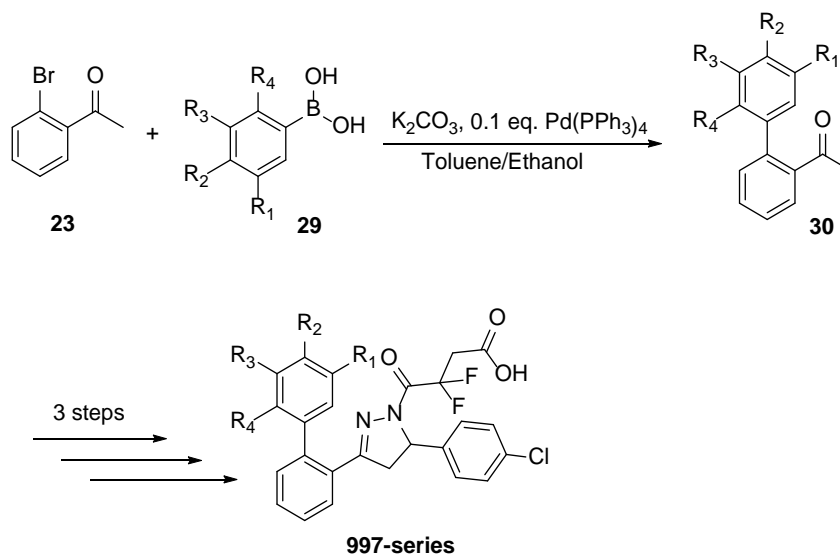
Table 9. SAR study of compounds with right ring modification.

997-	R ₁	R ₂	2B IC ₅₀ 2D IC ₅₀	GluN2A IC ₅₀ (μ M)	GluN2B IC ₅₀ (μ M)	GluN2C IC ₅₀ (μ M)	GluN2D IC ₅₀ (μ M)
116		F	3	NE	23	12	7.4
117		F	3	17	8.8	3.4	2.9
118		F	3	9	12	3.7	3.7
119		F	-	NE	NE	NE	NE
122		H	-	NE	NE	NE	NE

IC₅₀ values were obtained by fitting the Hill equation (see chapter 2.4.5) to the average composite concentration-effect curves. Data were from 4-13 oocytes between 1-2 frogs. NE indicates less than 50% inhibition at 30 μ M. The mean IC₅₀ values plus confidence intervals are given in the appendix C.

2.3.3 B-phenyl ring modification

The top ring was also modified to improve the activity and selectivity. Starting with commercially available 2'-Bromoacetophenone and appropriate phenylboronic acid, compounds **997-100**, and **997-120** to **997-124** were synthesized via the same procedures as shown in chapter 2.5.1.



Scheme 14. Synthesis of 997-95 analogues with B-ring modifications.

Compound **997-100** with meta-fluoro substitution on the phenyl ring lost activity at all receptors. Both **997-120** with 4-chloro-3-fluoro substitution and **997-123** with 3,5-dichloro substitution increased the potency at GluN2D-containing receptor with IC_{50} values of 3.4 μ M and 4.7 μ M, respectively. The GluN2D selectivity of **997-120** over other subunits remained poor, while **997-123** slightly improved the selectivity. Compound **997-121** with 2,4-difluoro substitution decreased the activity of 2-fold in comparison to **997-95**. Notably, compound **997-124** with 4-trifluoromethyl substitution on the top ring possessed an IC_{50} value of 3.6 μ M at the GluN2D-containing receptor and improved the selectivity over GluN2A-containing receptor (*Table 10*). Therefore, the **997-95** scaffold preferred

more hydrophobic and electron-withdrawing substitution on the top ring.

Table 10. SAR study of compounds with B-ring modification.

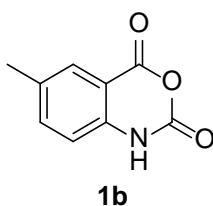
997-	R ₁	R ₂	R ₃	R ₄	GluN2A IC ₅₀ (μ M)	GluN2B IC ₅₀ (μ M)	GluN2C IC ₅₀ (μ M)	GluN2D IC ₅₀ (μ M)
100	H	H	F	H	NE	NE	NE	NE
120	H	F	Cl	H	11	8.8	5.2	3.4
121	H	F	H	F	NE	NE	14	12
123	Cl	H	Cl	H	NE	15	7.3	4.7
124	H	CF ₃	H	H	NE	14	3.6	3.6

IC₅₀ values were obtained by fitting the Hill equation (see chapter 2.4.5) to the average composite concentration-effect curves. Data were from 4-13 oocytes between 1-2 frogs. NE indicates less than 50% inhibition at 30 μ M. The mean IC₅₀ values plus confidence intervals are given in the appendix C.

2.4 Chemistry Experimental

All the commercially available chemicals were purchased from Sigma-Aldrich and Alfa Aesar and used without further purification. Reaction progress was monitored using thin layer chromatography (TLC) on pre-coated aluminum plates (silica gel 60 F254, 0.25 mm) and liquid chromatography-mass spectrometry (LCMS, Varian). Flash column chromatography using a Teledyne ISCO Combiflash Companion with Teledyne RediSep disposable normal phase silica columns is used to purify crude compounds. The purity of final compounds was evaluated in two solvents systems (MeOH/water and ACN/water) by HPLC (Varian). Proton, carbon and fluorine NMR spectra were recorded on Mercury 300 (300 MHz), VNMRS 400 (400 MHz), or INOVA 400 (400 MHz) instruments. Proton and carbon NMR spectra utilize the related solvent peak as references, while fluorine NMR spectra employ trifluoroacetic acid (TFA) residual peak as a reference. All chemical shifts and coupling constants were reported in parts per million and Hertz (Hz), respectively. The high-resolution mass spectrometry (HRMS) was evaluated from Emory University Mass Spectrometry Center on either a VG 70-S Nier Johnson or JEOL instrument.

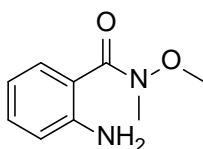
2.4.1 Synthetic procedures



6-methyl-2H-benzo[d][1,3]oxazine-2,4(1H)-dione (19). Triphosgene (6.7 g, 23 mmol, 0.34 equiv. WARNING, triphosgene is toxic and should be handled with care, refer to MSDS before handling) in THF (0.23 molar) was added in a solution of 2-amino-5-methylbenzoic acid (10 g, 66 mmol, 1.0 equiv.) in THF using syringe pump at a flow rate

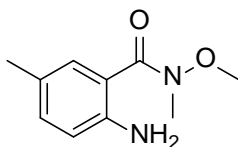
of 25 ml/h. The mixture was refluxed at 70 °C for around two hours. The mixture was poured onto an ice bath, and the resultant solid was filtered and washed with MeOH to yield the desired products. Yield 8.8 g, 75%. ^1H NMR (400 MHz, DMSO-*d*₆) δ 11.63 (s, 1H), 7.68 (s, 1H), 7.54 (d, *J* = 8.6 Hz, 1H), 7.03 (dd, *J* = 8.2, 2.3 Hz, 1H), 2.31 (d, *J* = 1.5 Hz, 3H). ^{13}C NMR (100 MHz, DMSO-*d*₆) δ 159.90, 147.12, 139.22, 137.92, 132.94, 128.30, 115.27, 109.97, 20.08.

General procedure A for the synthesis of 2-amino-*N*-methoxybenzamide. In a flame dried round-bottomed flask, triethylamine (1.5 equiv.) and *N,O*-dimethylhydroxylamine hydrochloride (1.5 equiv.) in ethanol (2.5 M, 90%) were stirred for 10 minutes. Compound **1** (1.0 equiv.) was then added slowly. The mixture was heated to reflux for approximately two hours. Upon completion, the mixture was poured onto ice/saturated sodium bicarbonate. The ethanol was removed *in vacuo*, and the mixture was extracted with ethyl acetate. The organic layer was washed 3X with brine, dried over magnesium sulfate, concentrated *in vacuo*.



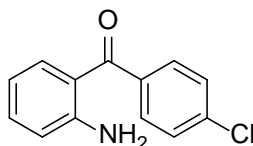
2-amino-*N*-methoxy-*N*-methylbenzamide (2). Compound **2** was prepared via general procedure **A** using **1** (10 g, 61 mmol), *N,O*-dimethylhydroxylamine hydrochloride (9.0 g, 92 mmol), and triethylamine (13 ml, 92 mmol). Purification with flash column chromatography using 20% EtOAc: Hexanes yielded the title compound (8.8 g, 80%) as a brown oil. ^1H NMR (400 MHz, DMSO-*d*₆) δ 7.18 (dt, *J* = 7.6, 1.2 Hz, 1H), 7.13 - 7.09 (m, 1H), 6.73 (d, *J* = 8.4 Hz, 1H), 6.54 (t, *J* = 7.4 Hz, 1H), 5.38 (s, 2H), 3.53 (d, *J* = 1.6 Hz, 3H), 3.21 (d, *J* = 1.2 Hz, 3H). ^{13}C NMR (100 MHz, DMSO-*d*₆) δ 169.88, 147.69, 131.39,

129.03, 117.69, 116.43, 115.65, 61.17, 34.20. HRMS (m/z): $[M+H]^+$ calculated for $C_9H_{13}N_2O_2$, 181.09715; found, 181.09739.

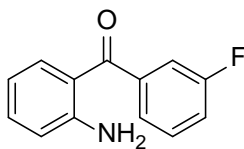


2-amino-N-methoxy-N,5-dimethylbenzamide (20). Compound **20** was prepared via general procedure **A** using **19** (8.9 g, 50 mmol), *N,O*-dimethylhydroxylamine hydrochloride (7.3 g, 75 mmol), and triethylamine (11 ml, 75 mmol). Purification with flash column chromatography using 20% EtOAc: Hexanes yielded the title compound (6.0 g, 62%) as a brown oil. 1H NMR (400 MHz, DMSO-*d*6) 6.97 (s, 1H), 6.94 (d, J = 9.0 Hz, 1H), 6.64 (d, J = 8.2 Hz, 1H), 5.13 (s, 2H), 3.54 (d, J = 1.6 Hz, 3H), 3.20 (d, J = 1.5 Hz, 3H), 2.14 (s, 3H). ^{13}C NMR (100 MHz, DMSO-*d*6) δ 169.26, 144.50, 131.46, 128.30, 123.54, 117.44, 115.98, 60.51, 33.69, 19.91.

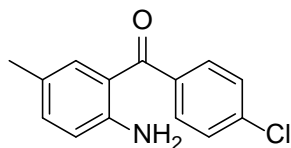
General procedure B for the synthesis of 2-aminobenzophenone intermediates. In a flame dried round-bottomed flask at -78 °C, compound **2** (1 equiv.) and an appropriately substituted bromo-benzene (1 equiv.) in THF (0.17 M) were stirred under nitrogen. *N*-butyllithium (2 equiv., 2.5 M in Hexanes) was added at a flow rate of 0.3 ml/min. Upon completion of the addition, 2 ml of 1N HCl per 1 ml of *n*-butyllithium was added while the temperature was still controlled at -78 °C. The mixture was then warm to room temperature with stirring, and the THF was removed *in vacuo*. The resultant mixture was extracted with ethyl acetate, washed with brine, dried over magnesium sulfate, and concentrated *in vacuo*. Purification with flash column chromatography (20% gradient) EtOAc: Hexanes gave the desired products.



(2-aminophenyl)(4-chlorophenyl)methanone (3a). Compound **3a** was prepared via general procedure **B** using 1-bromo-4-chlorobenzene (8.6 g, 45 mmol), **2** (8.1 g, 45 mmol) and N-butyllithium (36 ml, 89 mmol). Purification by flash chromatography using 20% isocratic EtOAc: Hexanes yielded the title compound as a yellow solid. Yield 6.6 g, 64%. ^1H NMR (400 MHz, DMSO-*d*₆) δ 7.56 (s, 4H), 7.31 - 7.19 (m, 2H), 7.15 (s, 2H), 6.86 (d, $J = 8.4$ Hz, 1H), 6.54 - 6.47 (m, 1H). ^{13}C NMR (100 MHz, DMSO-*d*₆) δ 202.21, 196.55, 151.96, 151.07, 138.62, 135.71, 134.43, 133.91, 133.70, 131.27, 130.48, 128.33, 116.94, 116.52, 115.99, 114.32, 114.19, 26.74, 21.94, 13.91.



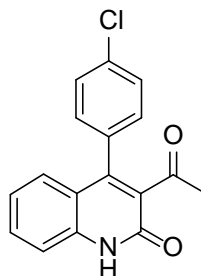
(2-aminophenyl)(3-fluorophenyl)methanone (3b). Compound **3b** was prepared via general procedure **B** using 1-bromo-3-fluorobenzene (4.3 g, 25 mmol), **2** (4.4 g, 25 mmol) and N-butyllithium (20 ml, 49 mmol). Purification by flash chromatography using 20% isocratic EtOAc: Hexanes yielded the title compound as a yellow solid. Yield 2.7 g, 51%. ^1H NMR (400 MHz, CDCl₃) δ 7.43-7.38 (m, 3H), 7.33 (d, $J = 8$ Hz, 1H), 7.27 (td, $J = 8$, 1 Hz, 1H), 7.22-7.17 (m, 1H), 6.71 (dd, $J = 8$, 1 Hz, 1H), 6.58 (td, $J = 8$, 4 Hz, 1H), 6.14 (s, 1H). ^{13}C NMR (100 MHz, CDCl₃) δ 197.22, 163.35, 160.89, 151.00, 141.99, 134.46, 134.18, 129.60, 124.62, 117.70, 116.95, 115.38. HRMS (m/z): $[\text{M}+\text{H}]^+$ calculated for C₁₃H₁₁NOF, 216.08192; found, 216.08169.



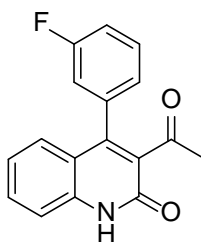
(2-amino-5-methylphenyl)(4-chlorophenyl)methanone. This compound was prepared via general procedure **B** using 1-bromo-4-chlorobenzene (1.8 g, 9.2 mmol), **20** (1.8 g, 9.2 mmol), and N-butyllithium (7.4 ml, 18 mmol). Purification by flash chromatography using 20% isocratic EtOAc: Hexanes yielded the title compound as a yellow solid. Yield 1.3 g, 58%. ^1H NMR (400 MHz, DMSO-*d*₆) δ 7.56 (s, 4H), 7.14 (dd, *J* = 8.4, 2.1 Hz, 1H), 7.03 (s, 1H), 6.95 (s, 2H), 6.79 (d, *J* = 8.2 Hz, 1H), 2.09 (s, 3H). ^{13}C NMR (100 MHz, DMSO-*d*₆) δ 196.46, 149.95, 138.73, 135.70, 135.62, 132.85, 130.43, 128.34, 122.51, 117.12, 115.92, 19.91.

General procedure C for the synthesis of quinolin-2(1H)-one intermediates. An appropriate 2-aminobenzophenone (1.0 equiv.) and the ethyl acetoacetate (1.5 equiv.) were dissolved in DMF (1.4 M) in a microwaveable vessel and microwaved at 180 °C for 8 minutes in the presence of 4 Angstrom molecular sieves. The reaction was then vented of gas and re-submitted to the microwave irradiation at 180 °C for another 8 minutes. The resultant mixture was transferred to a round-bottomed flask, and the solvent DMF was removed *in vacuo*. Ethyl acetate was added to the flask, and the solid was filtered. The filtrate was then concentrated *in vacuo*, and ethyl acetate was added again, followed by filtration of the solid that retained. The solids were collected and determined to be the desired product. In a large scale, an appropriate 2-aminobenzophenone (1.0 equiv.) and the ethyl acetoacetate (1.5 equiv.) were dissolved in DMF (0.4 M) in the presence of 4 Angstrom molecular sieves and refluxed overnight. The molecular sieves were filtered out, and the filtrate was concentrated *in vacuo*. Ethyl acetate was added, and then the mixture

was filtered, giving the product as solid. As the project moves, this procedure can be simplified. The resultant solids from filtration were directly used in the following step without further purification.

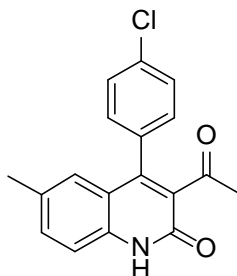


3-acetyl-4-(4-chlorophenyl)quinolin-2(1H)-one (4a). Compound **4a** was prepared via procedure **C** with **3a** (6.5 g, 28 mmol) and ethyl acetoacetate (5.3 ml, 42 mmol) in a large scale. Yield as white solid 10.2 g, 122%. ^1H NMR (400 MHz, DMSO-*d*₆) δ 12.30 (s, 1H), 7.58 (d, *J* = 7.8 Hz, 3H), 7.48 - 7.33 (m, 3H), 7.16 (t, *J* = 7.6 Hz, 1H), 7.05 (d, *J* = 8.3 Hz, 1H), 2.28 (s, 3H). HRMS (*m/z*): [*M*+*H*]⁺ calculated for C₁₇H₁₃ClNO₂, 298.06293; found, 298.06309.

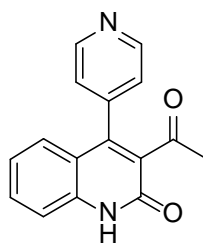


3-acetyl-4-(3-fluorophenyl)quinolin-2(1H)-one (4b). Compound **4b** was prepared via procedure **C** with **3b** (1.5 g, 7.0 mmol) and ethyl acetoacetate (1.3 ml, 11 mmol) under MW reaction. Yield as white solid 0.92 g, 47%. ^1H NMR (400 MHz, DMSO-*d*₆) δ 12.29 (s, 1H), 7.56 (p, *J* = 8.0 Hz, 2H), 7.41 (d, *J* = 8.0 Hz, 1H), 7.32 (t, *J* = 8.0 Hz, 1H), 7.24 (d, *J* = 8.0 Hz, 1H), 7.15 (t, *J* = 8.0 Hz, 2H), 7.04 (d, *J* = 12.0 Hz, 1H), 2.28 (s, 3H). ^{13}C NMR

(100 MHz, DMSO-*d*₆) δ 201.63, 159.27, 145.82, 138.48, 136.52, 133.34, 131.41, 130.74, 127.02, 125.08, 122.53, 118.64, 115.70, 31.48. HRMS (*m/z*): [M+H]⁺ calculated for C₁₇H₁₃NO₂F, 282.09248; found, 282.09235.

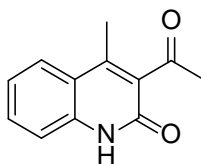


3-acetyl-4-(4-chlorophenyl)-6-methylquinolin-2(1H)-one (4c). Compound **4c** was prepared via procedure **C** with appropriate benzophenone (1.3 g, 5.4 mmol) and ethyl acetoacetate (1.0 ml, 8.1 mmol) under MW reaction. Yield as white solid 1.6 g, 97%. ¹H NMR (400 MHz, DMSO-*d*₆) δ 12.21 (s, 1H), 7.56 (d, *J*= 5.1 Hz, 2H), 7.40 (s, 1H), 7.33 (s, 3H), 6.82 (s, 1H), 2.25 (s, 3H), 2.22 (s, 3H). ¹³C NMR (100 MHz, DMSO-*d*₆) δ 201.84, 159.10, 136.54, 133.46, 133.20, 132.71, 131.50, 130.69, 128.59, 126.26, 118.62, 115.69, 31.53, 20.54. HRMS (*m/z*): [M+Na]⁺ calculated for C₁₈H₁₄ClNO₂Na, 334.06053; found, 334.06057.



3-acetyl-4-(pyridin-4-yl)quinolin-2(1H)-one. This compound was prepared via procedure **C** with appropriate benzophenone **18** (0.50 g, 2.5 mmol) and ethyl acetoacetate (0.48 ml, 3.8 mmol) under MW reaction. Yield as white solid 0.61g, 92%. ¹H NMR (400 MHz,

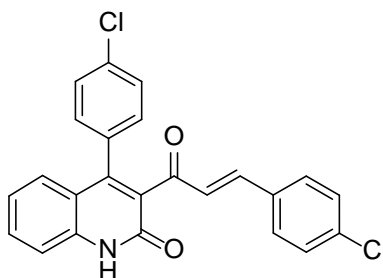
DMSO-*d*₆) δ 12.32 (s, 1H), 8.70 (s, 2H), 7.59 (s, 1H), 7.38 (s, 3H), 7.14 (s, 1H), 6.98 (s, 1H), 2.33 (s, 3H). ¹³C NMR (100 MHz, DMSO-*d*₆) δ 201.49, 159.23, 149.76, 144.97, 142.55, 138.65, 132.98, 132.85, 131.62, 126.90, 123.72, 122.64, 117.93, 115.78, 31.50.



3-acetyl-4-methylquinolin-2(1H)-one (16). The 2-acetylaniline (1.0 g, 7.4 mmol, 1 equiv.) and ethyl acetoacetate (0.92 ml, 7.4 mmol, 1 equiv.) were mixed with cerium (III) chloride heptahydrate (0.55 g, 1.5 mmol, 0.2 equiv.). The mixture was introduced into a microwaved vessel and was microwaved at 160 °C for 6 minutes. After cooled to room temperature, water (5-10 ml) was then added to the reaction mixture, and the mixture was stirred for another 5 min. The solid was collected by Buchner filtration, washed with water and ethyl acetate/hexanes (1:4), and then air-dried to give the product as white powder. Yield 417 mg, 28%. ¹H NMR (400 MHz, CDCl₃) δ 11.78 (s, 1H), 7.78 (d, J= 8.1 Hz, 1H), 7.55 (t, J= 7.5 Hz, 1H), 7.33 (d, J= 8.4 Hz, 2H), 2.67 (s, 3H), 2.49 (s, 3H). ¹³C NMR (100 MHz, DMSO-*d*₆) δ 203.54, 159.52, 143.64, 138.02, 132.88, 131.12, 125.65, 122.25, 119.12, 115.58, 31.33, 15.18.

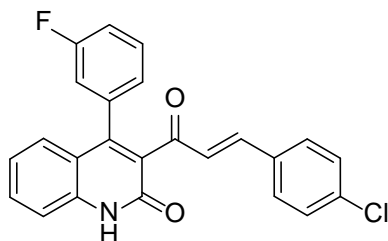
General procedure D for the synthesis of quinolin-2(1H)-one acrolyl intermediates. In a round-bottomed flask, the quinolin-2(1H)-one (1 equiv.) and potassium hydroxide (25 equiv.) were stirred in EtOH/H₂O (3:2, 0.05 M) at 0 °C for 45 minutes. 4-chlorobenzaldehyde or appropriate aldehyde (1 equiv.) was then added to the mixture. The reaction was stirred overnight. Upon completion, the reaction was quenched by slow addition of 2N hydrogen chloride (equal molar to KOH) and the resultant solid was filtered.

The solid was then extracted from DCM and washed with brine, dried with magnesium sulfate and concentrated *in vacuo*. As the project moves, this procedure can be simplified. The resultant solids from filtration were directly used in the following step without further purification.



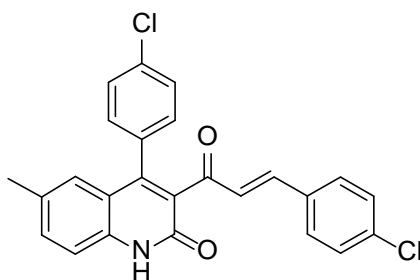
(E)-4-(4-chlorophenyl)-3-[3-(4-chlorophenyl)acryloyl]quinolin-2(1H)-one (5a).

Compound **5a** was prepared via the general procedure **D** using **4a** (2.5 g, 8.4 mmol), 4-chlorobenzaldehyde (1.2 g, 8.4 mmol), and potassium hydroxide (12 g, 210 mmol). Yield as white solid 2.0 g, 56%. ^1H NMR (400 MHz, DMSO-*d*₆) δ 12.24 (s, 1H), 7.72 (d, *J* = 8.6 Hz, 2H), 7.60 (t, *J* = 7.7 Hz, 1H), 7.50 (dd, *J* = 12.4, 3.8 Hz, 3H), 7.45 (d, *J* = 8.6 Hz, 3H), 7.34 (d, *J* = 8.6 Hz, 2H), 7.17 (t, *J* = 7.7 Hz, 1H), 7.07 (d, *J* = 8.1 Hz, 1H), 6.83 (d, *J* = 16.0 Hz, 1H). ^{13}C NMR (100 MHz, DMSO-*d*₆) δ 194.23, 166.48, 159.52, 146.99, 144.55, 138.82, 137.78, 135.32, 133.45, 133.28, 133.17, 131.57, 131.18, 130.90, 130.42, 129.71, 128.97, 128.77, 128.46, 128.17, 126.87, 122.37, 119.04, 115.78. HRMS (*m/z*): [*M*+*H*]⁺ calculated for C₂₄H₁₆Cl₂NO₂, 420.05526; found, 420.05560.

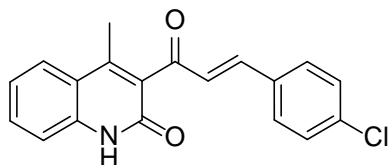


(E)-3-[3-(4-chlorophenyl)acryloyl]-4-(3-fluorophenyl)quinolin-2(1H)-one (5b/997-71).

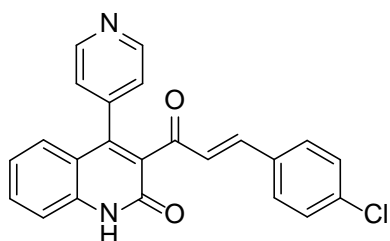
Compound **5b** was prepared via the general procedure **D** using **4b** (1.3 g, 4.6 mmol), 4-chlorobenzaldehyde (0.64 g, 4.6 mmol), and potassium hydroxide (6.4 g, 114 mmol). Yield as white solid 1.3 g, 71%. ¹H NMR (400 MHz, DMSO-*d*₆) δ 12.68 (s, 1H), 7.51-7.38 (m, 6H), 7.35-7.29 (m, 3H), 7.19-7.10 (m, 3H), 7.06 (dd, J= 9.4, 1.0 Hz, 1H), 6.82 (dd, J= 16.2, 1.0 Hz, 1H). ¹³C NMR (100 MHz, DMSO-*d*₆) δ 194.08, 162.86, 160.43, 159.49, 146.68, 144.58, 138.77, 136.60, 136.52, 135.31, 133.25, 131.44, 131.24, 130.32, 128.98, 128.06, 126.84, 125.24, 122.39, 118.90, 115.94, 115.67, 54.91, 17.44. HRMS (*m/z*): [M+H]⁺ calculated for C₂₄H₁₆ClFNO₂, 404.08481; found, 404.08629.

**(E)-4-(4-chlorophenyl)-3-[3-(4-chlorophenyl)acryloyl]-6-methylquinolin-2(1H)-one.**

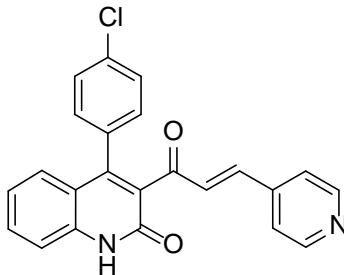
Compound **5c** was prepared via the general procedure **D** using **4c** (1.6 g, 5.2 mmol), 4-chlorobenzaldehyde (0.73 g, 5.2 mmol), and potassium hydroxide (7.3 g, 13 mmol). Yield as white solid 1.3 g, 58% and was used directly without purification. ¹H NMR (400 MHz, DMSO-*d*₆) δ 12.19 (s, 1H), 7.71 (d, J = 7.8 Hz, 2H), 7.50-7.32 (m, 9H), 6.83 (d, J = 17.1 Hz, 2H), 2.24 (s, 3H). ¹³C NMR (100 MHz, DMSO-*d*₆) δ 194.25, 159.34, 146.75, 144.28, 136.83, 135.27, 133.37, 133.25, 133.22, 132.51, 131.58, 131.36, 131.14, 130.85, 130.36, 129.37, 128.93, 128.43, 128.17, 126.11, 118.91, 115.72, 20.55.



(E)-3-(3-(4-chlorophenyl)acryloyl)-4-methylquinolin-2(1H)-one (17). Compound **17** was prepared via the general procedure **D** using **16** (0.30 g, 1.5 mmol), 4-chlorobenzaldehyde (0.21 g, 1.5 mmol), and potassium hydroxide (2.1 g, 37 mmol). Yield as white solid 0.40 g, 83% and was used to synthesize **997-77** directly without purification. ^1H NMR (400 MHz, DMSO-*d*₆) δ 11.97 (s, 1H), 7.83 (d, *J* = 7.3 Hz, 1H), 7.79 (d, *J* = 8.2 Hz, 2H), 7.58 (t, *J* = 7.3 Hz, 1H), 7.49 (t, *J* = 7.8 Hz, 3H), 7.38 (d, *J* = 7.7 Hz, 1H), 7.27 (t, *J* = 7.3 Hz, 1H), 7.11 (d, *J* = 15.6 Hz, 1H), 2.33 (s, 3H).

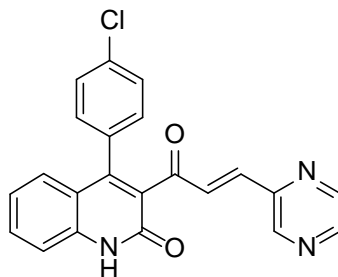


(E)-3-(3-(4-chlorophenyl)acryloyl)-4-(pyridin-4-yl)quinolin-2(1H)-one. Compound was prepared via the general procedure **D** using appropriate quinolin-2(1H)-one (0.59 g, 2.2 mmol), 4-chlorobenzaldehyde (0.31 g, 2.2 mmol), and potassium hydroxide (3.1 g, 56 mmol). Yield as white solid 0.91 g, 105% and was used to synthesize **997-81** directly without purification. ^1H NMR (400 MHz, DMSO-*d*₆) δ 12.33 (s, 1H), 8.64 (s, 2H), 7.71 (s, 2H), 7.61 (s, 1H), 7.55-7.46 (m, 4H), 7.36 (s, 2H), 7.17 (s, 1H), 7.03 (s, 1H), 6.86 (d, *J* = 16.4 Hz, 1H).



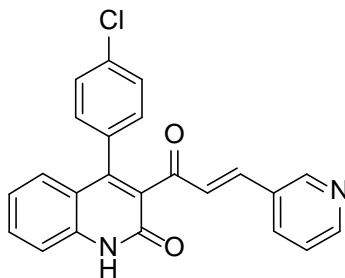
(E)-4-(4-chlorophenyl)-3-[3-(pyridin-4-yl)acryloyl]quinolin-2(1H)-one (13a).

Compound **13a** was prepared via the general procedure **D** using **4a** (1.2 g, 4.0 mmol), isonicotinaldehyde (0.38 ml, 4.0 mmol), and potassium hydroxide (5.7 g, 101 mmol). Yield as white solid 1.3 g, 85% and was used to synthesize **14a** directly without purification. ^1H NMR (400 MHz, DMSO-*d*₆) δ 12.31 (s, 1H), 8.60 (s, 2H), 7.63 (d, *J* = 5.2 Hz, 2H), 7.61-7.55 (m, 1H), 7.51 (d, *J* = 8.4 Hz, 2H), 7.47 (d, *J* = 5.9 Hz, 2H), 7.34 (d, *J* = 8.3 Hz, 2H), 7.18 (t, *J* = 7.6 Hz, 1H), 7.08 (d, *J* = 9.2 Hz, 1H), 7.04 (d, *J* = 16.5 Hz, 1H).



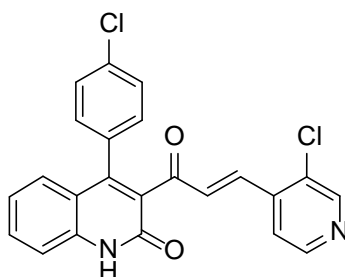
(E)-4-(4-chlorophenyl)-3-[3-(pyrazin-2-yl)acryloyl]quinolin-2(1H)-one (13b).

Compound **13b** was prepared via the general procedure **D** using **4a** (1.1 g, 3.7 mmol), pyrazine-2-carbaldehyde (0.40 g, 3.7 mmol), and potassium hydroxide (5.2 g, 92 mmol). Yield as white solid 0.51 g, 35% and was used to synthesize **14b** directly without purification. ^1H NMR (400 MHz, DMSO-*d*₆) δ 12.34 (s, 1H), 8.91 (s, 1H), 8.67 (d, *J* = 8.1 Hz, 2H), 7.63-7.41 (m, 5H), 7.36 (d, *J* = 6.6 Hz, 2H), 7.20-7.16 (m, 2H), 7.10 (s, 1H).



(E)-4-(4-chlorophenyl)-3-[3-(pyridin-3-yl)acryloyl]quinolin-2(1H)-one (13c).

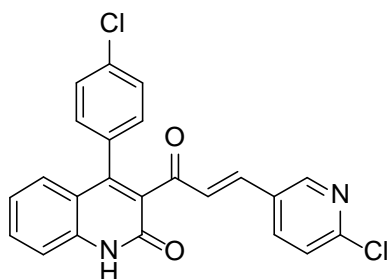
Compound **13c** was prepared via the general procedure **D** using **4a** (0.49 g, 1.7 mmol), nicotinaldehyde (0.18 g, 1.7 mmol), and potassium hydroxide (2.3 g, 41 mmol). Yield as white solid 0.50 g, 79% and was used to synthesize **14c** directly without purification. ^1H NMR (400 MHz, DMSO-*d*₆) δ 12.27 (s, 1H), 8.83 (s, 1H), 8.56 (d, *J* = 4.1 Hz, 1H), 8.13 (d, *J* = 6.8 Hz, 1H), 7.62-7.54 (m, 2H), 7.51 (d, *J* = 8.3 Hz, 2H), 7.46 (d, *J* = 8.4 Hz, 1H), 7.42 (dd, *J* = 7.2, 4.7 Hz, 1H), 7.36 (d, *J* = 7.9 Hz, 2H), 7.17 (t, *J* = 7.2 Hz, 1H), 7.08 (d, *J* = 7.7 Hz, 1H), 6.96 (d, *J* = 16.5 Hz, 1H). ^{13}C NMR (100 MHz, DMSO-*d*₆) δ 194.16, 167.88, 159.50, 151.24, 150.29, 147.14, 138.82, 134.78, 133.48, 133.12, 131.40, 130.88, 130.13, 129.17, 128.47, 126.90, 123.96, 122.42, 119.01.



(E)-4-(4-chlorophenyl)-3-[3-(3-chloropyridin-4-yl)acryloyl]quinolin-2(1H)-one (13d).

Compound **13d** was prepared via the general procedure **D** using **4a** (0.55 g, 1.9 mmol), 3-chloroisonicotinaldehyde (0.26 g, 1.9 mmol), and potassium hydroxide (2.6 g, 46 mmol). Yield as white solid 0.72 g, 92% and was used to synthesize **14d** directly without

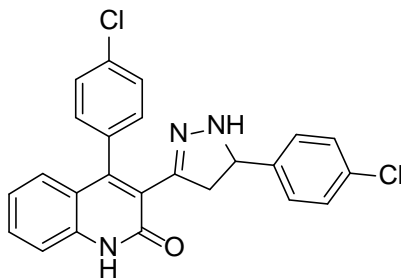
purification. ^1H NMR (400 MHz, DMSO-*d*6) δ 12.38 (s, 1H), 8.70 (s, 1H), 8.54 (s, 1H), 7.79 (d, $J = 3.5$ Hz, 1H), 7.62-7.54 (m, 2H), 7.51 (d, $J = 14.9$ Hz, 3H), 7.34 (d, $J = 7.0$ Hz, 2H), 7.23-7.10 (m, 3H). ^{13}C NMR (100 MHz, DMSO-*d*6) δ 193.35, 164.70, 159.46, 156.71, 149.94, 148.47, 148.05, 139.21, 138.93, 136.01, 133.68, 133.23, 132.82, 131.74, 131.11, 130.92, 130.63, 128.61, 127.08, 122.61, 121.68, 118.65.



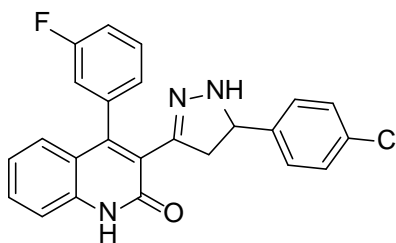
(E)-4-(4-chlorophenyl)-3-[3-(6-chloropyridin-3-yl)acryloyl]quinolin-2(1H)-one (13e).

Compound **13e** was prepared via the general procedure **D** using **4a** (0.55 g, 1.9 mmol), 6-chloronicotinaldehyde (0.26 g, 1.9 mmol), and potassium hydroxide (2.6 g, 46 mmol). Yield as white solid 0.68 g, 87% and was directly used to synthesize **14c** in the following step without further purification.

General procedure E for the synthesis of pyrazol-3-yl-quinolin-2(1H)-one intermediates. In an appropriate microwaveable vessel, the quinolin-2(1H)-one acryloyl intermediate (1 equiv.) was dissolved in EtOH (0.25 M, 190 proof or 200 proof) and hydrazine monohydrate (1.5 equiv.) was added. The mixture was microwaved for 20 minutes at 110 °C. Solid that present in the reaction vial was filtered to yield the desired product without further purification.

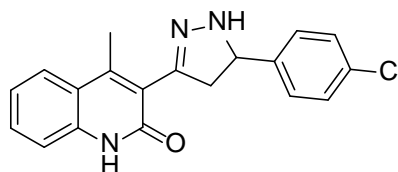


4-(4-chlorophenyl)-3-[5-(4-chlorophenyl)-4,5-dihydro-1H-pyrazol-3-yl]quinolin-2(1H)-one (5a/997-70). Compound **997-70** was prepared via general procedure **E** using **5a** (1.1 g, 2.7 mmol) and hydrazine monohydrate (0.20 ml, 4.0 mmol). Yield pale yellow solid 0.95 g, 81% and was used to synthesize **997-66**, **997-74** directly without purification. ^1H NMR (400 MHz, CDCl_3) δ 12.71 (s, 1H), 7.53-7.45 (m, 3H), 7.39 (d, J = 8.2 Hz, 1H), 7.31-7.27 (m, 3H), 7.24 (dd, J = 8.1, 1.5 Hz, 1H), 7.19-7.12 (m, 4H), 5.83 (s, 1H), 4.76 (dd, J = 10.8, 6.1 Hz, 1H), 3.32 (dd, J = 16.9, 10.9 Hz, 1H), 2.94 (dd, J = 16.7, 6.1 Hz, 1H). ^{13}C NMR (100 MHz, $\text{DMSO-}d_6$) δ 160.66, 148.38, 145.82, 142.63, 138.24, 134.76, 132.68, 131.40, 131.32, 130.70, 128.29, 128.14, 126.85, 125.63, 122.08, 119.37, 115.39, 61.96, 44.50. HRMS (m/z): $[\text{M}+\text{H}]^+$ calculated for $\text{C}_{24}\text{H}_{18}\text{Cl}_2\text{N}_3\text{O}$, 434.08214; found, 434.08235.



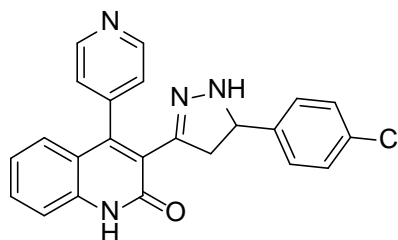
3-[5-(4-chlorophenyl)-4,5-dihydro-1H-pyrazol-3-yl]-4-(3-fluorophenyl)quinolin-2(1H)-one (6b). Compound **6b** was prepared via general procedure **E** using **5b** (1.2 g, 2.9 mmol) and hydrazine monohydrate (0.21 ml, 4.3 mmol). Yield pale yellow solid 0.80 g, 67% and was used to synthesize **997-65** and **997-69** directly without purification. ^1H NMR

(400 MHz, DMSO-*d*6) δ 12.11 (s, 1H), 7.57-7.47 (m, 2H), 7.39 (dd, J = 8.3, 0.6 Hz, 1H), 7.33-7.28 (m, 3H), 7.21-7.03 (m, 6H), 6.99 (d, J = 7.3 Hz, 1H), 4.61 (dd, J = 12.5, 7.6 Hz, 1H), 3.38-3.28 (m, 1H), 2.65-2.53 (m, 1H). ^{13}C NMR (100 MHz, CDCl_3) δ 186.85, 169.79, 163.86, 163.03, 161.93, 161.39, 141.94, 138.63, 138.05, 133.49, 131.44, 129.03, 128.70, 127.91, 127.58, 127.27, 126.92, 125.24, 123.18, 120.29, 119.70, 116.48, 53.70, 44.99. HRMS (m/z): $[\text{M}+\text{H}]^+$ calculated for $\text{C}_{24}\text{H}_{18}\text{ClFN}_3\text{O}$, 418.11169; found, 418.11158.



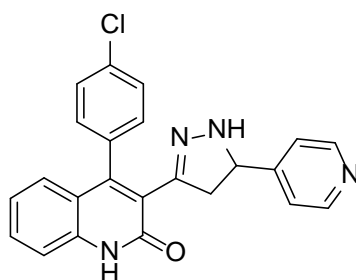
3-(5-(4-chlorophenyl)-4,5-dihydro-1H-pyrazol-3-yl)-4-methylquinolin-2(1H)-one

(997- 77). Compound **997-77** was prepared via general procedure **E** using **17** (0.39 g, 1.2 mmol) and hydrazine monohydrate (0.087 ml, 1.8 mmol). Yield pale yellow solid 55 mg, 14% and was used to synthesize **997-76** directly without purification. ^1H NMR (400 MHz, CDCl_3) δ 12.17 (s, 1H), 7.79 (d, J = 7.9 Hz, 1H), 7.55 (d, J = 8.4 Hz, 2H), 7.50 (t, J = 7.4 Hz, 1H), 7.39 (d, J = 8.1 Hz, 2H), 7.27-7.26 (m, 2H), 6.03 (s, 1H), 4.98 (dd, J = 10.4, 7.2 Hz, 1H), 3.50 (dd, J = 16.5, 10.6 Hz, 1H), 3.37 (dd, J = 16.8, 7.2 Hz, 1H), 2.64 (s, 3H). HRMS (m/z): $[\text{M}+\text{H}]^+$ calculated for $\text{C}_{19}\text{H}_{17}\text{ClN}_3\text{O}$, 338.10547; found, 338.10561.



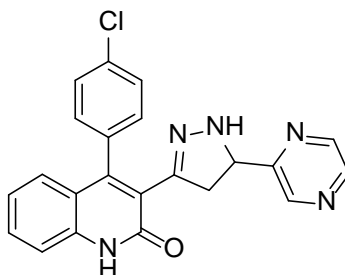
3-(5-(4-chlorophenyl)-4,5-dihydro-1H-pyrazol-3-yl)-4-(pyridin-4-yl)quinolin-2(1H)-one (997- 81). Compound **997-81** was prepared via general procedure **E** using appropriate

unsaturated ketone (0.88 g, 2.3 mmol) and hydrazine monohydrate (0.17 ml, 3.4 mmol). Yield pale yellow solid 0.17 g, 19% and was used to synthesize **997-82** directly without purification. ^1H NMR (400 MHz, DMSO-*d*₆) δ 12.18 (s, 1H), 8.68 (dd, *J*= 14.0, 4.4 Hz, 2H), 7.53 (t, *J*= 7.4 Hz, 1H), 7.42 (d, *J*= 8.1 Hz, 1H), 7.36 (d, *J*= 4.0 Hz, 1H), 7.32 (d, *J*= 7.7 Hz, 2H), 7.26 (d, *J*= 4.5 Hz, 1H), 7.23 (s, 1H), 7.15 (d, *J*= 7.9 Hz, 2H), 7.10 (d, *J*= 7.5 Hz, 1H), 6.95 (d, *J*= 7.9 Hz, 1H), 4.63 (t, *J*= 10.0 Hz, 1H), 3.40 (s, 1H), 2.68 (dd, *J*= 16.6, 9.4 Hz, 1H). ^{13}C NMR (100 MHz, DMSO-*d*₆) δ 167.29, 160.54, 151.11, 149.39, 146.77, 144.12, 142.42, 140.97, 138.29, 136.86, 135.16, 131.42, 130.71, 128.33, 128.24, 127.84, 126.55, 125.25, 124.42, 122.54, 118.55, 57.41, 43.03. HRMS (*m/z*): [*M*+*H*]⁺ calculated for C₂₃H₁₈ClN₄O, 401.11637; found, 401.11638.

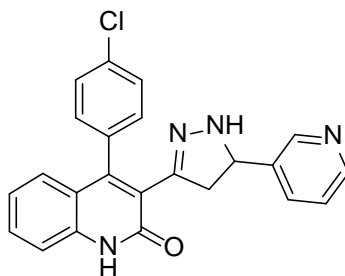


4-(4-chlorophenyl)-3-[5-(pyridin-4-yl)-4,5-dihydro-1H-pyrazol-3-yl]quinolin-2(1H)-one (14a/997-78). Compound **997-78** was prepared via general procedure **E** using **13a** (1.3 g, 3.4 mmol) and hydrazine monohydrate (0.25 ml, 5.1 mmol). Yield pale yellow solid 0.50 g, 38% and was used to synthesize **997-79** directly without purification. ^1H NMR (400 MHz, DMSO-*d*₆) δ 12.12 (s, 1H), 8.44 (d, *J*= 4.5 Hz, 2H), 7.56 (dt, *J*= 8.1, 2.0 Hz, 1H), 7.51 (d, *J*= 6.8 Hz, 1H), 7.47 (dd, *J*= 8.2, 2.0 Hz, 1H), 7.40 (d, *J*= 8.2 Hz, 1H), 7.35 (dd, *J*= 8.1, 1.9 Hz, 1H), 7.31 (s, 1H), 7.21 (dd, *J*= 8.4, 1.9 Hz, 1H), 7.10 (t, *J*= 7.7 Hz, 1H), 7.08 (d, *J*= 4.4 Hz, 2H), 6.98 (d, *J*= 8.1 Hz, 1H), 4.62 (t, *J*= 9.8 Hz, 1H), 3.38 (dd, *J*= 17.7, 12.4 Hz, 1H), 2.61 (dd, *J*= 16.8, 8.2 Hz, 1H). ^{13}C NMR (100 MHz, DMSO-*d*₆) δ 160.61, 152.18,

149.48, 148.47, 145.88, 138.23, 134.72, 132.68, 131.32, 128.20, 126.87, 125.44, 122.09, 121.63, 119.35, 115.36, 61.54, 44.06. HRMS (m/z): $[M+H]^+$ calculated for $C_{23}H_{18}ClN_4O$, 401.11637; found, 401.11646.

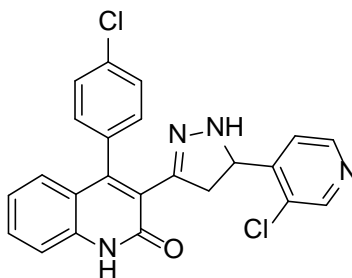


4-(4-chlorophenyl)-3-[5-(pyrazin-2-yl)-4,5-dihydro-1H-pyrazol-3-yl]quinolin-2(1H)-one (14b). Compound **14b** was prepared via general procedure **E** using **13b** (0.50 g, 1.3 mmol) and hydrazine monohydrate (0.094 ml, 1.9 mmol). Yield pale yellow solid 75 mg, 14% and was used to synthesize **997-80** directly without purification. 1H NMR (400 MHz, DMSO- d_6) δ 12.11 (s, 1H), 8.53 (d, J = 2.8 Hz, 2H), 8.49 (s, 1H), 7.51 (d, J = 7.5 Hz, 1H), 7.48 (dd, J = 8.2, 2.4 Hz, 1H), 7.41-7.38 (m, 3H), 7.30 (dd, J = 8.3, 1.6 Hz, 1H), 7.20 (dd, J = 8.0, 1.6 Hz, 1H), 7.10 (t, J = 7.6 Hz, 1H), 7.08 (d, J = 4.4 Hz, 2H), 6.98 (d, J = 8.1 Hz, 1H), 4.73 (td, J = 9.5, 2.1 Hz, 1H), 3.31 (dd, J = 16.7, 11.1 Hz, 1H), 2.97 (dd, J = 16.4, 8.3 Hz, 1H).



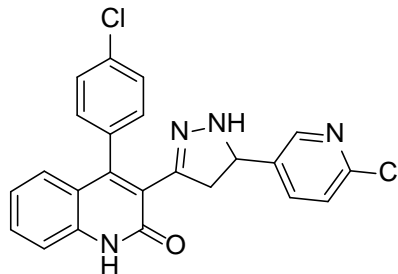
4-(4-chlorophenyl)-3-[5-(pyridin-3-yl)-4,5-dihydro-1H-pyrazol-3-yl]quinolin-2(1H)-one (14c). Compound **14c** was prepared via general procedure **E** using **13c** (0.49 g, 1.3

mmol) and hydrazine monohydrate (0.091 ml, 1.9 mmol). Yield pale yellow solid 0.43 g, 86% and was used to synthesize **997-83** directly without purification. ^1H NMR (400 MHz, DMSO-*d*₆) δ 12.12 (s, 1H), 8.44 (d, *J*= 4.7 Hz, 1H), 8.41 (s, 1H), 7.54 (t, *J*= 7.5 Hz, 2H), 7.49 (d, *J*= 8.6 Hz, 1H), 7.44 (d, *J*= 8.2 Hz, 1H), 7.40 (d, *J*= 8.2 Hz, 1H), 7.34 (d, *J*= 8.2 Hz, 1H), 7.28 (dd, *J*= 7.8, 4.7 Hz, 1H), 7.25 (d, *J*= 8.6 Hz, 2H), 7.10 (t, *J*= 7.6 Hz, 1H), 6.99 (d, *J*= 8.2 Hz, 1H), 4.66 (t, *J*= 10.0 Hz, 1H), 3.32 (dd, *J*= 16.8, 11.0 Hz, 1H), 2.68 (dd, *J*= 16.5, 9.0 Hz, 1H). ^{13}C NMR (100 MHz, DMSO-*d*₆) δ 160.67, 153.66, 152.71, 149.32, 148.45, 148.30, 148.17, 146.04, 138.76, 138.25, 134.77, 133.94, 132.68, 131.20, 130.75, 128.21, 128.16, 126.88, 125.54, 123.42, 122.11, 119.36, 115.41, 109.58, 60.34, 44.15.



4-(4-chlorophenyl)-3-[5-(3-chloropyridin-4-yl)-4,5-dihydro-1H-pyrazol-3-yl]quinolin-2(1H)-one (14d). Compound **14d** was prepared via general procedure **E** using **13d** (0.69 g, 1.7 mmol) and hydrazine monohydrate (0.12 ml, 2.5 mmol). Yield pale yellow solid 0.46 g, 64% and was used to synthesize **997-88** directly without purification. ^1H NMR (400 MHz, DMSO-*d*₆) δ 12.13 (s, 1H), 8.54 (s, 1H), 8.40 (d, *J*= 4.7 Hz, 1H), 7.54 (d, *J*= 6.3 Hz, 1H), 7.51 (d, *J*= 7.8 Hz, 1H), 7.41 (t, *J*= 9.6 Hz, 2H), 7.36-7.33 (m, 2H), 7.17 (d, *J*= 7.4 Hz, 1H), 7.08 (d, *J*= 4.3 Hz, 2H), 6.97 (d, *J*= 8.2 Hz, 1H), 4.85 (t, *J*= 8.4 Hz, 1H), 3.48 (dd, *J*= 16.4, 11.3 Hz, 1H), 2.54 (d, *J*= 7.8 Hz, 1H). ^{13}C NMR (100 MHz, DMSO-*d*₆) δ 160.53, 149.37, 148.62, 148.13, 145.84, 138.25, 134.68, 132.69, 131.33, 130.72, 130.53, 129.49, 128.18, 128.11, 126.87, 125.09, 122.99, 122.07, 119.30, 115.41, 58.71, 42.84. HRMS (*m/z*):

$[M+H]^+$ calculated for $C_{23}H_{17}Cl_2N_4O$, 435.07739; found, 435.07800.

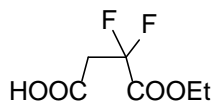


4-(4-chlorophenyl)-3-[5-(6-chloropyridin-3-yl)-4,5-dihydro-1H-pyrazol-3-yl]quinolin-2(1H)-one (14e). Compound **14e** was prepared via general procedure **E** using **13e** (0.68 g, 1.6 mmol) and hydrazine monohydrate (0.12 ml, 2.4 mmol). Yield pale yellow solid 60 mg, 8.6% and was used to synthesize **997-92** directly without purification. 1H NMR (400 MHz, DMSO-*d*₆) δ 12.14 (s, 1H), 8.24 (d, *J* = 2.3 Hz, 1H), 7.54 (dd, *J* = 8.4, 2.5 Hz, 3H), 7.48 (dd, *J* = 8.4, 2.1 Hz, 1H), 7.41 (dd, *J* = 8.2, 1.6 Hz, 2H), 7.32 (dd, *J* = 8.2, 2.4 Hz, 1H), 7.30 (d, *J* = 2.3 Hz, 1H), 7.25 (dd, *J* = 8.2, 1.9 Hz, 1H), 7.10 (t, *J* = 7.6 Hz, 1H), 6.99 (d, *J* = 8.2 Hz, 1H), 4.68 (td, *J* = 9.7, 2.5 Hz, 1H), 3.30 (dd, *J* = 16.8, 10.9 Hz, 1H), 2.68 (dd, *J* = 16.8, 8.2 Hz, 1H). ^{13}C NMR (100 MHz, DMSO-*d*₆) δ 160.64, 157.31, 153.31, 148.83, 148.50, 148.25, 146.13, 138.44, 138.27, 137.77, 134.71, 132.70, 131.11, 130.76, 128.21, 126.87, 125.38, 123.93, 122.12, 119.32, 115.43, 59.47, 43.99.

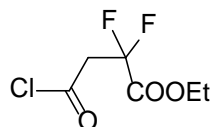


3,3-difluorodihydrofuran-2,5-dione (8). To a solution of 2,2-difluorosuccinic acid (1.5 g, 9.7 mmol, 1 equiv.) in *i*-PrOAc (20 ml, 0.5 M) was added trifluoroacetic anhydride (1.6 ml, 12 mmol, 1.2 equiv.) in one portion at ambient temperature. The reaction solution was stirred at 50 °C for approximately 1.5 hours. The mixture was distilled at 140 °C (the vapor

temperature was around 89-90 °C). The remaining liquid or solid was determined to be desired product. Yield colorless liquid was used to synthesize difluoro-substituted compounds via general procedure H directly. Yield 1.2 g, 87% ^1H NMR (400 MHz, CDCl_3) δ 3.535(t, J = 12.8 Hz, 2H). ^{19}F NMR (376 MHz, CDCl_3) δ -106.56 (t, J= 14 Hz, 2F).

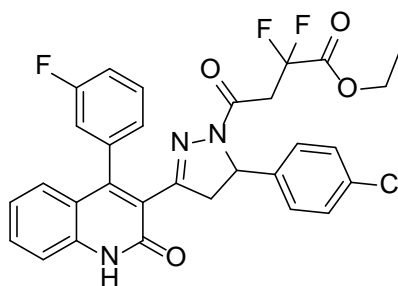


4-ethoxy-3,3-difluoro-4-oxobutanoic acid (9). Dry absolute ethanol (6.5 ml, 1.3 M) was added dropwise to **8** (1.1 g, 8.4 mmol) at 0 °C. The mixture was then warmed to room temperature and was stirred for 18 hours. Then the mixture was evaporated *in vacuo* and extracted with DCM/0.1 N HCl, dried with magnesium sulfate and concentrated *in vacuo*. Yield light pink liquid 800 mg, 52%. ^1H NMR (400 MHz, CDCl_3) δ 10.48 (s, 1H), 4.35 (q, J= 8 Hz, 2H), 3.29 (t, J= 16 Hz, 2H), 1.33 (t, J=8 Hz, 3H). ^{13}C NMR (100 MHz, CDCl_3) δ 172.65, 163.24, 113.35, 63.91, 40.24, 14.21. ^{19}F NMR (376 MHz, CDCl_3) δ -126.25 (t, J= 16 Hz, 2F).

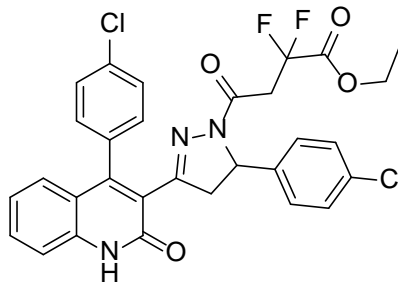


Ethyl 4-chloro-2,2-difluoro-4-oxobutanoate (10). In a round-bottomed flask, **9** (0.80 g, 4.4 mmol, 1 equiv.) was dissolved in DCM (8.4 ml, 0.3 M). Then oxalyl dichloride (0.94 ml, 11 mmol, 2.5 equiv.) was added dropwise, followed by one drop of DMF. The reaction was stirred for approximately 40 minutes. The solvent and excess oxalyl dichloride was removed under vacuum and the product was obtained by Kugelrohr distillation at 98 °C with full vacuum. Used to synthesize difluoro-substituted compounds via general procedure I immediately.

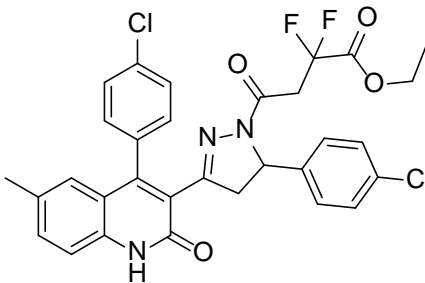
General procedure F for the synthesis of acylated quinolone pyrazoline products. In an appropriate microwaveable vessel, the pyrazol-3-yl-quinolin-2(1H)-one (1 equiv.) and **10** (1 equiv.) were dissolved in anhydrous THF (0.151 M) with 4 Angstrom molecular sieves. The reaction was microwaved at 165 °C for 20 minutes. The THF was removed under vacuum and the mixture was extracted with DCM, washed 3X with acidified (1N HCl) brine, dried over magnesium sulfate, filtered, concentrated *in vacuo*, and subjected to flash column chromatography using a 0-10% MeOH/DCM gradient.



Ethyl 4-{5-(4-chlorophenyl)-3-[4-(3-fluorophenyl)-2-oxo-1,2-dihydroquinolin-3-yl]-4,5-dihydro-1H-pyrazol-1-yl}-2,2-difluoro-4-oxobutanoate (997-65). Compound **997-65** was prepared via general procedure **F** using pyrazoline amine **6b** (0.72 g, 1.7 mmol) and acetyl chloride **10** (0.35 g, 1.7 mmol). Yield as yellow solid 89 mg, 9.0%; mp 98-103 °C. ¹H NMR (400 MHz, CDCl₃) δ 13.28 (s, 1H), 7.62-7.51 (m, 2H), 7.41 (d, J= 8.1 Hz, 1H), 7.30-7.04 (m, 9H), 5.46 (dd, J= 11.6, 3.4 Hz, 1H), 4.26 (qd, J= 7.2, 2.5 Hz, 2H), 3.86-3.79 (m, 1H), 3.45-3.24 (m, 3H), 1.24 (td, J= 7.2, 1.5 Hz, 3H). ¹³C NMR (100 MHz, CDCl₃) δ 163.77, 163.52, 163.14, 162.72, 161.37, 161.30, 153.93, 151.80, 139.49, 139.43, 138.40, 137.44, 133.55, 133.50, 132.14, 128.96, 128.05, 127.47, 127.36, 125.15, 123.51, 122.25, 120.01, 116.37, 114.01, 62.89, 59.08, 45.68, 39.64, 13.77. ¹⁹F NMR (376 MHz, CDCl₃) δ -104.34 (t, J= 14 Hz, 2F), -112.32 (d, J= 130.8 Hz, 1F). HRMS (*m/z*): [M+H]⁺ calculated for C₃₀H₂₄ClF₃N₃O₄, 582.14020; found, 582.14023.



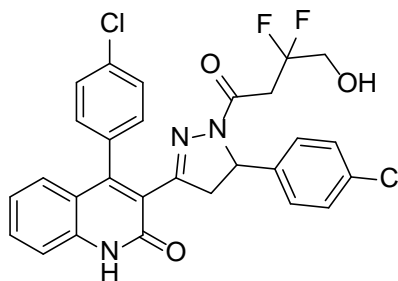
Ethyl 4-{5-(4-chlorophenyl)-3-[4-(4-chlorophenyl)-2-oxo-1,2-dihydroquinolin-3-yl]-4,5-dihydro-1H-pyrazol-1-yl}-2,2-difluoro-4-oxobutanoate (997-66). Compound **997-66** was prepared via general procedure **F** using pyrazoline amine **6a** (0.85 g, 2.0 mmol) and acetyl chloride **10** (0.39 g, 2.0 mmol). Yield as yellow solid 0.12 g, 10%; mp 116-121 °C. ¹H NMR (400 MHz, CDCl₃) δ 13.19 (s, 1H), 7.62-7.58 (m, 1H), 7.54 (dd, J= 8.3, 2.1 Hz, 1H), 7.50 (dd, J= 8.0, 2.2 Hz, 1H), 7.41 (d, J= 8.3 Hz, 1H), 7.32 (dd, J= 8.1, 2.1 Hz, 1H), 7.30-7.22 (m, 5H), 7.01 (dt, J= 8.3, 1.9 Hz, 2H), 5.44 (dd, J= 11.6, 4 Hz, 1H), 4.27 (q, J= 7.2 Hz, 2H), 3.74 (dd, J= 18.4, 11.8 Hz, 1H), 3.47-3.30 (m, 2H), 3.18 (dd, J= 18.3, 4 Hz, 1H), 1.25 (t, J= 7.2 Hz, 3H). ¹³C NMR (100 MHz, CDCl₃) δ 163.64, 163.57, 163.25, 162.79, 154.04, 152.23, 139.46, 138.45, 135.24, 133.71, 133.69, 132.23, 130.73, 130.53, 129.06, 128.95, 128.76, 128.08, 127.49, 123.61, 122.54, 120.24, 116.58, 116.50, 114.09, 63.03, 59.13, 45.77, 39.75, 13.90. ¹⁹F NMR (376 MHz, CDCl₃) δ -104.25 (t, J= 14.1 Hz, 2F). HRMS (*m/z*): [M+H]⁺ calculated for C₃₀H₂₄Cl₂F₂N₃O₄, 598.11064; found, 598.11078.



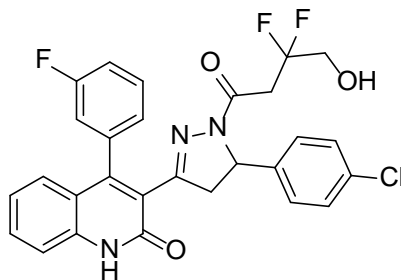
Ethyl 4-{5-(4-chlorophenyl)-3-[4-(4-chlorophenyl)-6-methyl-2-oxo-1,2-dihydroquinolin-3-yl]-4,5-dihydro-1H-pyrazol-1-yl}-2,2-difluoro-4-oxobutanoate. Compound was prepared via general procedure **F** using pyrazoline amine (0.65 g, 1.5 mmol) and acetyl chloride **10** (0.29 g, 1.5 mmol). The product was obtained after flash chromatography and using 1.3% MeOH/DCM. Yield as brown gel 0.27 g, 30%. ^1H NMR (400 MHz, DMSO-*d*₆) δ 12.24 (s, 1H), 7.59 (ddd, *J* = 14.4, 8.2, 2.4 Hz, 2H), 7.44-7.40 (m, 2H), 7.33 (t, *J* = 8.0 Hz, 2H), 7.31 (dd, *J* = 8.0, 2.5 Hz, 2H), 6.87 (d, *J* = 8.6 Hz, 2H), 6.82 (s, 1H), 5.37 (dd, *J* = 11.9, 4.1 Hz, 1H), 4.20-4.11 (m, 2H), 3.80 (dd, *J* = 18.6, 12.0 Hz, 1H), 3.43-3.15 (m, 2H), 2.94 (dd, *J* = 18.6, 4.5 Hz, 1H), 2.23 (s, 3H), 1.12 (t, *J* = 7.2 Hz, 3H). ^{13}C NMR (100 MHz, DMSO-*d*₆) δ 163.86, 162.54, 160.09, 159.94, 154.79, 149.98, 146.83, 140.26, 136.73, 134.29, 133.23, 131.92, 131.49, 131.28, 130.63, 129.24, 128.43, 128.33, 127.35, 126.65, 122.84, 119.01, 115.63, 62.54, 58.09, 28.97, 20.57, 13.50.

General procedure G for the synthesis of difluoro-substituted hydroxybutanoyl quinolone pyrazoline products. A solution of acylated quinolone pyrazoline product (1 equiv.) in absolute ethanol was added dropwise to stirred solution of sodium borohydride (0.5 equiv.) in absolute ethanol. (Overall 0.015 M EtOH). The mixture was cooled in an ice/salt bath and the temperature was kept at 16 °C by controlling the rate of addition. After the addition was completed, the mixture was stirred at room temperature for another 15

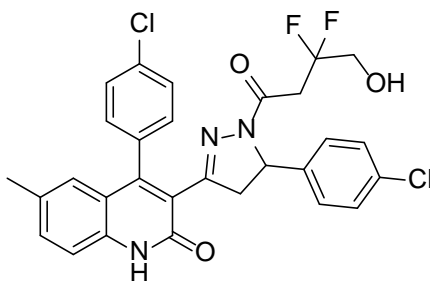
hours. The ethanol was evaporated and the residue was extracted with DCM and 4 N H₂SO₄. The aqueous phase was extracted twice with DCM. Then the organic phases were combined, washed twice with 2 N H₂SO₄, dried over magnesium sulfate, and evaporated *in vacuo*. Purification with flash column chromatography using 0-80% EtOAc: Hexanes.



4-(4-chlorophenyl)-3-[5-(4-chlorophenyl)-1-(3,3-difluoro-4-hydroxybutanoyl)-4,5-dihydro-1H-pyrazol-3-yl]quinolin-2(1H)-one (997-67). Compound **997-67** was prepared via general procedure **G** using **997-66** (0.11 g, 0.18 mmol) and sodium borohydride (3.4 mg, 0.09 mmol). Yield as yellow solid 20 mg, 20%; mp 181-185 °C. ¹H NMR (400 MHz, CDCl₃) δ 12.69 (s, 1H), 7.59 (quintet, J= 4.2 Hz, 1H), 7.52 (dd, J= 8.1, 2.1 Hz, 1H), 7.48 (dd, J= 8.1, 2.1 Hz, 1H), 7.39 (d, J= 8.3 Hz, 1H), 7.33 (dd, J= 8.1, 2.2 Hz, 1H), 7.28 (d, J= 8.3 Hz, 2H), 7.23 (d, J= 2.2 Hz, 1H), 7.22 (d, J= 4.5 Hz, 2H), 6.95 (d, J= 8.6 Hz, 2H), 5.44 (dd, J= 11.8, 4.1 Hz, 1H), 3.81 (sextet, J= 12 Hz, 2H), 3.71 (dd, J= 18.4, 11.8 Hz, 1H), 3.41-3.24 (m, 2H), 3.02 (dd, J= 18.4, 4.1 Hz, 1H), 2.72 (broad s, 1H). ¹³C NMR (100 MHz, CDCl₃) δ 163.03, 162.55, 154.30, 152.38, 142.44, 139.46, 138.38, 135.38, 133.89, 133.48, 132.34, 130.93, 130.37, 129.24, 128.96, 128.10, 127.34, 125.79, 123.73, 122.53, 121.68, 120.28, 117.76, 116.51, 64.19, 59.46, 45.92, 33.91. ¹⁹F NMR (376 MHz, CDCl₃) δ -100.90 (quintet, J= 11.2 Hz, 2F). HRMS (*m/z*): [M+H]⁺ calculated for C₂₈H₂₂Cl₂F₂N₃O₃, 556.10008; found, 556.10029.



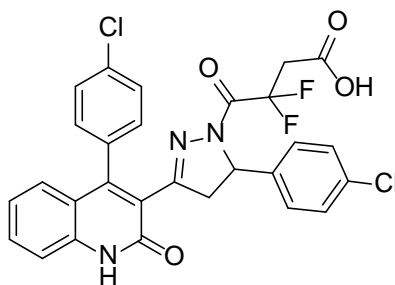
3-[5-(4-chlorophenyl)-1-(3,3-difluoro-4-hydroxybutanoyl)-4,5-dihydro-1H-pyrazol-3-yl]-4-(3-fluorophenyl)quinolin-2(1H)-one (997-68). Compound **997-68** was prepared via general procedure **G** using **997-65** (0.20 g, 0.34 mmol) and sodium borohydride (6.5 mg, 0.17 mmol). Yield as yellow solid 35 mg, 19%; mp 189-193 °C. ^1H NMR (400 MHz, CDCl_3) δ 12.73 (d, J = 16 Hz, 1H), 7.60-7.46 (m, 2H), 7.38 (dt, J = 8.3, 0.8 Hz, 1H), 7.28-7.17 (m, 6H), 7.10 (td, J = 8.4, 1.5 Hz, 1H), 7.03-6.97 (m, 2H), 5.45 (dd, J = 11.8, 4.1 Hz, 1H), 3.86-3.69 (m, 3H), 3.33-3.20 (m, 2H), 3.09 (dt, J = 18.4, 4.1 Hz, 1H), 2.72 (s, 1H). ^{13}C NMR (100 MHz, CDCl_3) δ 164.94, 162.58, 161.56, 161.48, 154.22, 152.09, 139.59, 139.51, 138.39, 137.28, 133.85, 133.80, 132.37, 129.25, 128.16, 127.41, 127.28, 125.42, 124.90, 123.73, 122.36, 121.64, 120.17, 116.24, 64.20, 59.51, 45.94, 38.56. ^{19}F NMR (376 MHz, CDCl_3) δ -101.11 (quintet, J = 12 Hz, 2F), -112.07 (d, J = 126.7 Hz, 1F). HRMS (m/z): $[\text{M}+\text{H}]^+$ calculated for $\text{C}_{28}\text{H}_{22}\text{ClF}_3\text{N}_3\text{O}_3$, 540.12963; found, 540.13022.



4-(4-chlorophenyl)-3-[5-(4-chlorophenyl)-1-(3,3-difluoro-4-hydroxybutanoyl)-4,5-dihydro-1H-pyrazol-3-yl]-6-methylquinolin-2(1H)-one (997-91). Compound **997-91** was prepared via general procedure **G** using ester (0.11 g, 0.18 mmol) and sodium

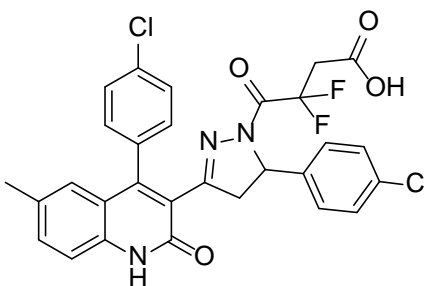
borohydride (3.4 mg, 0.09 mmol). The product was obtained after flash chromatography and came out at 60-65% EtOAc: Hexanes. Yield as yellow solid 8.2 mg, 8% overall; mp 215-218 °C. ¹H NMR (400 MHz, DMSO-*d*₆) δ 12.23 (s, 1H), 7.59 (dd, J= 8.2, 2.3 Hz, 1H), 7.53 (d, J= 8.2 Hz, 1H), 7.43-7.27 (m, 6H), 6.82 (d, J= 8.2 Hz, 3H), 5.48 (s, 1H), 5.38 (dd, J= 12.0, 4.1 Hz, 1H), 3.76 (dd, J= 18.4, 11.7 Hz, 1H), 3.62 (td, J= 14.5, 5.9 Hz, 2H), 3.16-2.97 (m, 2H), 2.78 (dd, J= 18.5, 4.1 Hz, 1H), 2.22 (s, 3H). ¹³C NMR (100 MHz, DMSO-*d*₆) δ 159.93, 153.82, 149.80, 140.75, 134.03, 133.22, 132.89, 131.73, 131.45, 131.40, 130.46, 128.36, 127.30, 126.55, 119.02, 115.60, 58.14, 45.41, 28.80, 25.85, 20.57; mp 215-218 °C. HRMS (*m/z*): [M+H]⁺ calculated for C₂₉H₂₄Cl₂F₂N₃O₃; found, 570.12080.

General procedure H for the synthesis of difluoro-substituted hydroxybutanoic acid quinolone pyrazoline products. Compound **8** (1 equiv.) was added in a solution of **6** (1 equiv.) in THF (0.045 molar) at room temperature. After around 24 hours, the crude was concentrated *in vacuo*, washed with ethyl acetate and 1 N HCl. The organic layer was dried over Mg₂SO₄, filtered and evaporated *in vacuo*. Finally, the crude compound was purified by flash chromatography using a 0-10% MeOH/DCM gradient to afford product.



4-(5-(4-chlorophenyl)-3-(4-(4-chlorophenyl)-2-oxo-1,2-dihydroquinolin-3-yl)-4,5-dihydro-1H-pyrazol-1-yl)-3,3-difluoro-4-oxobutanoic acid (997-74). Compound **997-74** was prepared via general procedure **H** using pyrazoline amine (0.10 g, 0.23 mmol) and **8** (31 mg, 0.23 mmol). The product was obtained after flash chromatography (0-10%

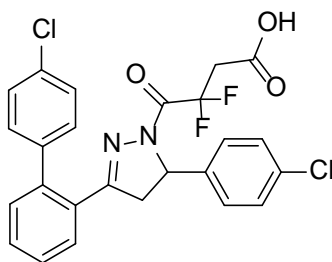
MeOH/DCM). Yield a yellow solid 86 mg, 66%; mp 194-198 °C. ¹H NMR (400 MHz, CDCl₃) δ 12.15 (s, 1H), 7.56 (p, J= 4.0 Hz, 1H), 7.50 (d, J= 7.9 Hz, 1H), 7.45 (d, J= 8.1 Hz, 1H), 7.33 (d, J= 8.3 Hz, 1H), 7.28-7.26 (m, 2H), 7.20 (d, J= 3.8 Hz, 2H), 7.17 (d, J= 7.3 Hz, 2H), 7.15 (d, J= 8.3 Hz, 1H), 6.88 (d, J= 7.5 Hz, 2H), 5.46 (dd, J= 11.5, 4.1 Hz, 1H), 3.68 (dd, J= 18.2, 12.1 Hz, 1H), 3.50-3.36 (m, 2H), 2.76 (dd, J= 18.3, 4.2 Hz, 1H). ¹³C NMR (100 MHz, CDCl₃) δ 171.22, 162.40, 160.22, 159.56, 154.70, 153.04, 139.11, 138.87, 138.41, 137.36, 135.33, 133.68, 132.75, 132.52, 131.05, 129.75, 128.99, 128.88, 127.76, 127.13, 124.11, 121.71, 120.21, 116.69, 110.01, 100.63, 60.42, 44.88, 41.25. HRMS (*m/z*): [M+H]⁺ calculated for C₂₈H₂₀Cl₂F₂N₃O₄, 570.07934; found, 570.08016.



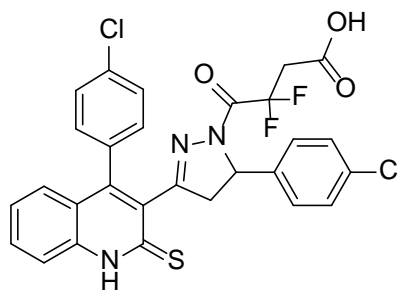
4-(5-(4-chlorophenyl)-3-(4-(4-chlorophenyl)-6-methyl-2-oxo-1,2-dihydroquinolin-3-yl)-4,5-dihydro-1H-pyrazol-1-yl)-3,3-difluoro-4-oxobutanoic acid (997-90).

Compound **997-90** was prepared via general procedure **H** using pyrazoline amine (0.43 g, 0.96 mmol) and **8** (0.13 g, 0.96 mmol). The product was obtained after flash chromatography (0-10% MeOH/DCM). Yield a yellow solid 0.12 g, 22%; mp 150-158 °C. ¹H NMR (400 MHz, DMSO-*d*₆) δ 12.92 (s, 1H), 12.27 (s, 1H), 7.54 (dd, J= 8.2, 1.9 Hz, 1H), 7.50 (dd, J= 8.2, 2.3 Hz, 1H), 7.42 (td, J= 7.8, 2.0 Hz, 2H), 7.34 (d, J= 8.6 Hz, 1H), 7.30 (d, J= 8.2 Hz, 2H), 7.25 (dd, J= 8.0, 2.1 Hz, 1H), 6.85 (d, J= 8.6 Hz, 2H), 6.79 (s, 1H), 5.50 (dd, J= 11.8, 4.3 Hz, 1H), 3.82 (dd, J= 18.8, 11.7 Hz, 1H), 3.32-3.20 (m, 2H), 2.71 (dd, J= 18.7, 4.7 Hz, 1H), 2.22 (s, 3H). ¹³C NMR (100 MHz, DMSO-*d*₆) δ 177.02, 162.17,

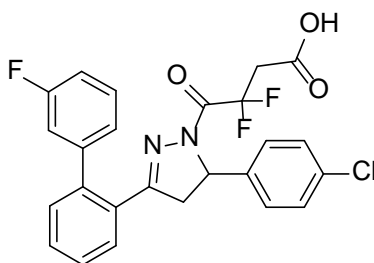
159.78, 156.29, 149.87, 139.78, 136.72, 133.74, 133.42, 133.01, 131.94, 131.52, 131.15, 130.11, 128.71, 128.52, 128.34, 127.44, 126.50, 122.95, 118.94, 115.66, 109.58, 59.45, 34.55, 34.24, 20.58. HRMS (m/z): $[M+H]^+$ calculated for $C_{29}H_{22}O_4N_3Cl_2F_2$, 584.09499; found, 584.09509.



4-(3-(4'-chloro-[1,1'-biphenyl]-2-yl)-5-(4-chlorophenyl)-4,5-dihydro-1H-pyrazol-1-yl)-3,3-difluoro-4-oxobutanoic acid (997-95). Compound **997-95** was prepared via general procedure **H** using pyrazoline amine (0.43 g, 1.2 mmol) and **8** (0.16 g, 1.2 mmol). The product was obtained after flash chromatography (0-10% MeOH/DCM). Yield a yellow solid 0.32 g, 75%; mp 172-176 °C. 1H NMR (400 MHz, DMSO- d_6) δ 12.95 (s, 1H), 7.69 (dd, $J = 7.5, 1.6$ Hz, 1H), 7.60 – 7.49 (m, 2H), 7.42 – 7.32 (m, 4H), 7.31 – 7.26 (m, 2H), 7.18 – 7.12 (m, 2H), 5.53 (dd, $J = 11.6, 4.4$ Hz, 1H), 3.63 (dd, $J = 18.4, 11.7$ Hz, 1H), 3.22 – 2.99 (m, 2H), 2.61 (dd, $J = 18.4, 4.5$ Hz, 1H). ^{13}C NMR (100 MHz, DMSO- d_6) δ 158.28, 139.87, 139.52, 139.32, 132.40, 132.04, 130.75, 130.39, 129.57, 129.42, 128.51, 128.40, 128.04, 127.35, 59.84, 43.76. HRMS (m/z): $[M+H]^+$ calculated for $C_{25}H_{19}O_3N_2Cl_2F_2$, 503.07353; found, 503.07228.

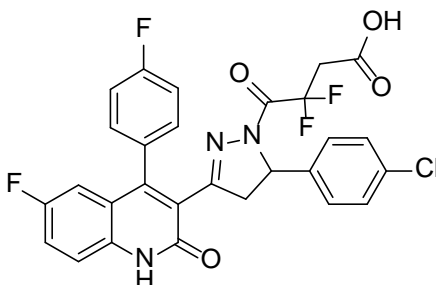


4-(5-(4-chlorophenyl)-3-(4-(4-chlorophenyl)-2-thioxo-1,2-dihydroquinolin-3-yl)-4,5-dihydro-1H-pyrazol-1-yl)-3,3-difluoro-4-oxobutanoic acid (997-98). Compound **997-98** was prepared via general procedure **H** using pyrazoline amine (0.21 g, 0.46 mmol) and **8** (63 mg, 0.46 mmol). The product was obtained after flash chromatography (0-10% MeOH/DCM). Yield a yellow solid 0.13 g, 47%; mp 105-108 °C. ^1H NMR (400 MHz, DMSO- d_6) δ 14.17 (s, 1H), 12.94 (s, 1H), 7.79 – 7.67 (m, 3H), 7.59 (dd, J = 8.2, 2.3 Hz, 1H), 7.44 (dt, J = 8.2, 1.9 Hz, 2H), 7.35 – 7.24 (m, 4H), 7.09 – 7.01 (m, 1H), 5.49 (dd, J = 12.0, 5.1 Hz, 1H), 3.46 (q, J = 16.8 Hz, 1H), 3.37 – 3.19 (m, 2H), 2.67 (s, 1H). ^{13}C NMR (100 MHz, DMSO- d_6) δ 178.71, 167.47, 156.91, 145.86, 139.80, 139.13, 133.70, 133.06, 132.30, 131.80, 130.78, 130.29, 128.66, 128.56, 128.13, 127.55, 127.00, 124.76, 122.15, 116.34, 114.64, 59.52, 44.65, 40.87. HRMS (m/z): $[\text{M}+\text{H}]^+$ calculated for $\text{C}_{28}\text{H}_{20}\text{O}_3\text{N}_3\text{Cl}_2\text{F}_2\text{S}$, 586.05760; found, 586.05716.



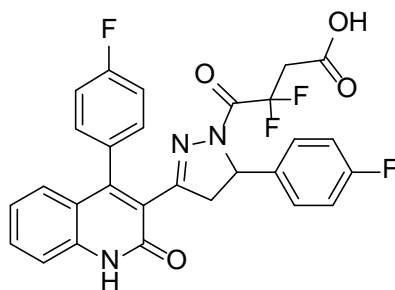
4-(5-(4-chlorophenyl)-3-(3'-fluoro-[1,1'-biphenyl]-2-yl)-4,5-dihydro-1H-pyrazol-1-yl)-3,3-difluoro-4-oxobutanoic acid (997-100). Compound **997-100** was prepared via general procedure **H** using pyrazoline amine (0.41 g, 1.2 mmol) and **8** (0.16 g, 1.2 mmol).

The product was obtained after flash chromatography (0-10% MeOH/DCM). Yield a yellow foam 57 mg, 10%. HRMS (m/z): $[M+H]^+$ calculated for $C_{25}H_{19}O_3N_2ClF_3$, 487.10308; found, 487.10335.

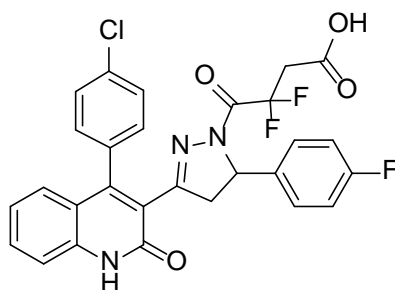


4-(5-(4-chlorophenyl)-3-(6-fluoro-4-(4-fluorophenyl)-2-oxo-1,2-dihydroquinolin-3-yl)-4,5-dihydro-1H-pyrazol-1-yl)-3,3-difluoro-4-oxobutanoic acid (997-102).

Compound **997-102** was prepared via general procedure **H** using pyrazoline amine (0.30 g, 0.69 mmol) and **8** (94 mg, 0.69 mmol). The product was obtained after flash chromatography (0-10% MeOH/DCM). Yield a yellow solid 59 mg, 15%; mp 233-238 °C. 1H NMR (400 MHz, DMSO- d_6) δ 12.94 (s, 1H), 12.42 (s, 1H), 7.56 – 7.42 (m, 3H), 7.31 (tt, $J = 5.6, 2.8$ Hz, 5H), 6.92 (dd, $J = 8.6, 2.8$ Hz, 2H), 6.70 (dt, $J = 9.7, 2.9$ Hz, 1H), 5.51 (dt, $J = 12.3, 3.8$ Hz, 1H), 3.86 (ddd, $J = 18.8, 11.9, 2.7$ Hz, 1H), 3.38 – 3.08 (m, 2H), 2.80 (dt, $J = 18.7, 3.8$ Hz, 1H). ^{13}C NMR (100 MHz, DMSO- d_6) δ 167.48, 163.44, 160.99, 159.75, 158.26, 158.13, 156.04, 155.88, 149.55, 149.52, 139.73, 135.38, 131.98, 131.38, 131.30, 130.72, 130.69, 130.42, 130.34, 128.35, 127.51, 124.32, 120.11, 119.98, 119.73, 117.76, 117.67, 115.86, 115.79, 115.65, 115.57, 114.60, 112.04, 111.80, 59.55, 44.63, 40.81. HRMS (m/z): $[M+H]^+$ calculated for $C_{28}H_{19}O_4N_3ClF_4$, 572.09947; found, 572.10004.

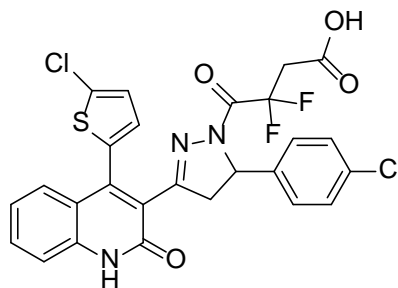


3,3-difluoro-4-(5-(4-fluorophenyl)-3-(4-(4-fluorophenyl)-2-oxo-1,2-dihydroquinolin-3-yl)-4,5-dihydro-1H-pyrazol-1-yl)-4-oxobutanoic acid (997-103). Compound **997-103** was prepared via general procedure **H** using pyrazoline amine (0.41 g, 1.0 mmol) and **8** (0.14 g, 1.0 mmol). The product was obtained after flash chromatography (0-10% MeOH/DCM). Yield a yellow foam 0.18 g, 32%. ^1H NMR (400 MHz, DMSO- d_6) δ 12.31 (s, 1H), 7.59 (tt, $J = 7.0, 1.5$ Hz, 1H), 7.48 – 7.39 (m, 2H), 7.34 – 7.25 (m, 3H), 7.19 – 7.11 (m, 1H), 7.10 – 7.00 (m, 3H), 6.95 (dt, $J = 7.7, 3.7$ Hz, 2H), 5.50 (dd, $J = 11.9, 4.6$ Hz, 1H), 3.90 – 3.71 (m, 1H), 3.44 – 3.30 (m, 2H), 2.79 (dt, $J = 18.6, 2.7$ Hz, 1H). ^{13}C NMR (100 MHz, DMSO- d_6) δ 167.24, 161.65, 161.37, 160.03, 156.24, 150.39, 138.64, 137.03, 131.61, 127.72, 127.64, 127.36, 123.15, 122.47, 119.29, 117.85, 115.65, 115.34, 115.22, 115.00, 112.82, 59.50, 48.62, 44.84. HRMS (m/z): $[\text{M}+\text{H}]^+$ calculated for $\text{C}_{28}\text{H}_{20}\text{O}_4\text{N}_3\text{F}_4$, 538.13954; found, 538.13879.



4-(3-(4-(4-chlorophenyl)-2-oxo-1,2-dihydroquinolin-3-yl)-5-(4-fluorophenyl)-4,5-dihydro-1H-pyrazol-1-yl)-3,3-difluoro-4-oxobutanoic acid (997-104). Compound **997-104** was prepared via general procedure **H** using pyrazoline amine (0.34 g, 0.81 mmol) and

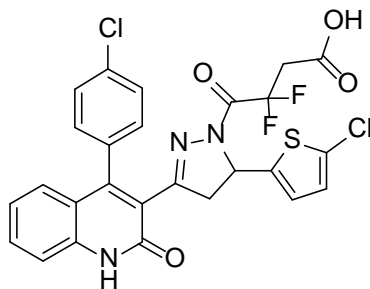
8 (0.11 g, 0.81 mmol). The product was obtained after flash chromatography (0-10% MeOH/DCM). Yield a yellow solid 0.30 g, 66%; mp 150-155 °C. ¹H NMR (400 MHz, DMSO-*d*₆) δ 7.62 – 7.48 (m, 3H), 7.46 – 7.40 (m, 2H), 7.27 (dt, *J* = 8.1, 1.9 Hz, 1H), 7.15 (dd, *J* = 8.4, 6.9 Hz, 1H), 7.10 – 6.99 (m, 3H), 6.89 (ddd, *J* = 8.9, 5.4, 1.8 Hz, 2H), 5.50 (dd, *J* = 11.9, 4.6 Hz, 1H), 3.98 – 3.72 (m, 2H), 3.41 – 3.28 (m, 1H), 2.81 – 2.66 (m, 1H). ¹³C NMR (100 MHz, Methanol-*d*₄) δ 169.65, 164.76, 164.27, 162.52, 162.32, 161.05, 157.98, 153.20, 139.79, 137.74, 136.08, 134.88, 133.23, 132.43, 131.35, 130.16, 128.99, 128.91, 128.80, 124.40, 123.96, 121.12, 117.20, 116.72, 116.45, 116.24, 61.78, 50.00, 46.42, 40.14. HRMS (*m/z*): [M+H]⁺ calculated for C₂₈H₂₀O₄N₃ClF₃, 554.10889; found, 554.10921.



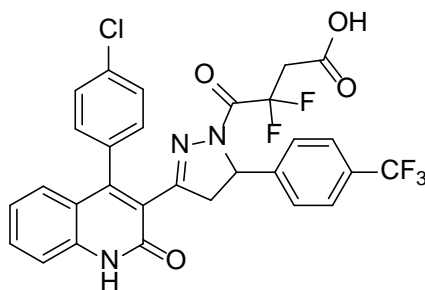
4-(5-(4-chlorophenyl)-3-(4-(5-chlorothiophen-2-yl)-2-oxo-1,2-dihydroquinolin-3-yl)-4,5-dihydro-1H-pyrazol-1-yl)-3,3-difluoro-4-oxobutanoic acid (997-109). Compound **997-109** was prepared via general procedure **H** using pyrazoline amine (0.2 g, 0.45 mmol) and **8** (62 mg, 0.45 mmol). The product was obtained after flash chromatography (0-10% MeOH/DCM). Yield a yellow foam 0.12 g, 44%. ¹H NMR (400 MHz, DMSO-*d*₆) δ 12.97 (s, 1H), 12.39 (s, 1H), 7.68 – 7.55 (m, 1H), 7.46 – 7.31 (m, 4H), 7.27 – 7.16 (m, 2H), 7.14 – 7.00 (m, 3H), 5.60 (dd, *J* = 11.9, 4.7 Hz, 1H), 3.93 – 3.80 (m, 1H), 3.55 – 3.17 (m, 2H), 2.84 (dd, *J* = 18.8, 4.9 Hz, 1H). ¹³C NMR (100 MHz, DMSO-*d*₆) δ 167.58, 159.57, 158.31, 155.89, 142.85, 139.81, 138.52, 133.01, 132.03, 131.92, 130.26, 129.39, 128.43, 127.54,

127.17, 126.96, 125.41, 122.73, 119.18, 115.72, 114.75, 112.28, 59.74, 44.70, 40.89.

HRMS (m/z): $[M+H]^+$ calculated for $C_{26}H_{18}O_4N_3Cl_2F_2S$, 576.03577; found, 576.03648.

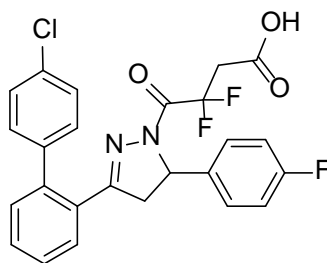


4-(3-(4-(4-chlorophenyl)-2-oxo-1,2-dihydroquinolin-3-yl)-5-(5-chlorothiophen-2-yl)-4,5-dihydro-1H-pyrazol-1-yl)-3,3-difluoro-4-oxobutanoic acid (997-110). Compound **997-110** was prepared via general procedure **H** using pyrazoline amine (0.20 g, 0.45 mmol) and **8** (62 mg, 0.45 mmol). The product was obtained after flash chromatography (0-10% MeOH/DCM). Yield a yellow foam 0.16 g, 60%. 1H NMR (400 MHz, $DMSO-d_6$) δ 12.93 (s, 1H), 12.34 (s, 1H), 7.58 (t, $J = 7.7$ Hz, 1H), 7.53 – 7.26 (m, 5H), 7.20 – 7.09 (m, 1H), 7.08 – 6.99 (m, 1H), 6.90 (t, $J = 3.6$ Hz, 1H), 6.71 (dt, $J = 7.3, 4.1$ Hz, 1H), 5.79 – 5.69 (m, 1H), 3.76 (td, $J = 11.6, 5.7$ Hz, 1H), 3.33 – 3.02 (m, 3H). ^{13}C NMR (100 MHz, $DMSO-d_6$) δ 167.49, 160.01, 158.31, 156.30, 150.23, 141.71, 138.72, 133.62, 133.51, 131.69, 130.90, 130.29, 128.54, 127.61, 127.36, 126.05, 124.65, 122.69, 122.51, 119.05, 117.05, 115.71, 114.56, 55.79, 43.82, 40.66. HRMS (m/z): $[M+H]^+$ calculated for $C_{26}H_{18}O_4N_3Cl_2F_2S$, 576.03577; found, 576.03628.

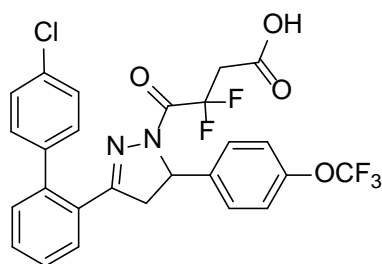


4-(3-(4-(4-chlorophenyl)-2-oxo-1,2-dihydroquinolin-3-yl)-5-(4-(trifluoromethyl)phenyl)-4,5-dihydro-1H-pyrazol-1-yl)-3,3-difluoro-4-oxobutanoic acid (997-113).

Compound **997-113** was prepared via general procedure **H** using pyrazoline amine (0.20 g, 0.43 mmol) and **8** (58 mg, 0.43 mmol). The product was obtained after flash chromatography (0-10% MeOH/DCM). Yield a yellow solid 0.14 g, 53%. ^1H NMR (400 MHz, DMSO- d_6) δ 12.97 (s, 1H), 12.34 (s, 1H), 7.65 – 7.53 (m, 4H), 7.49 – 7.40 (m, 3H), 7.26 (dd, $J = 8.2, 2.2$ Hz, 1H), 7.15 (ddd, $J = 8.2, 7.1, 1.2$ Hz, 1H), 7.08 – 7.00 (m, 3H), 5.62 (dd, $J = 12.0, 4.6$ Hz, 1H), 3.94 – 3.81 (m, 1H), 3.43 – 3.23 (m, 2H), 2.76 (dd, $J = 18.8, 4.6$ Hz, 1H). ^{13}C NMR (100 MHz, DMSO- d_6) δ 167.52, 159.89, 158.20, 156.18, 150.16, 145.24, 138.65, 133.68, 133.47, 131.65, 131.13, 130.10, 128.67, 128.51, 128.19, 127.87, 127.24, 126.28, 125.33, 125.29, 122.90, 122.49, 119.00, 117.11, 115.65, 114.64, 59.67, 44.64, 40.87. HRMS (m/z): $[\text{M}+\text{H}]^+$ calculated for $\text{C}_{29}\text{H}_{20}\text{O}_4\text{N}_3\text{ClF}_5$, 604.10570; found, 604.10660.

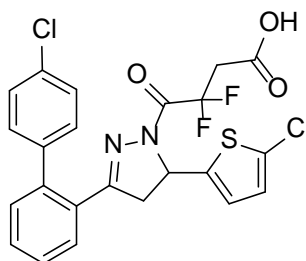


4-(3-(4'-chloro-[1,1'-biphenyl]-2-yl)-5-(4-fluorophenyl)-4,5-dihydro-1H-pyrazol-1-yl)-3,3-difluoro-4-oxobutanoic acid (997-116). Compound **997-116** was prepared via general procedure **H** using pyrazoline amine (0.40 g, 1.1 mmol) and **8** (0.16 g, 1.1 mmol). The product was obtained after flash chromatography (0-10% MeOH/DCM). Yield a yellow foam 0.28 g, 50%. ^1H NMR (400 MHz, DMSO- d_6) δ 12.93 (s, 1H), 7.69 (dd, $J = 7.5, 1.5$ Hz, 1H), 7.60 – 7.49 (m, 2H), 7.40 – 7.33 (m, 3H), 7.31 – 7.27 (m, 2H), 7.17 (dd, $J = 7.2, 2.5$ Hz, 4H), 5.53 (dd, $J = 11.6, 4.4$ Hz, 1H), 3.62 (dd, $J = 18.4, 11.6$ Hz, 1H), 3.20 – 3.03 (m, 2H), 2.61 (dd, $J = 18.4, 4.4$ Hz, 1H). ^{13}C NMR (100 MHz, DMSO- d_6) δ 167.69, 162.69, 160.27, 158.30, 139.92, 139.39, 136.84, 136.81, 132.45, 130.82, 130.45, 130.40, 129.67, 129.49, 128.47, 128.10, 127.58, 127.49, 117.15, 115.45, 115.24, 114.68, 59.85, 43.92, 40.87. HRMS (m/z): $[\text{M}+\text{H}]^+$ calculated for $\text{C}_{25}\text{H}_{19}\text{O}_3\text{N}_2\text{ClF}_3$, 487.10308; found, 487.10326.

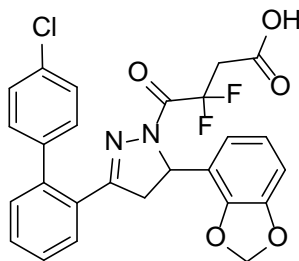


4-(3-(4'-chloro-[1,1'-biphenyl]-2-yl)-5-(4-(trifluoromethoxy)phenyl)-4,5-dihydro-1H-pyrazol-1-yl)-3,3-difluoro-4-oxobutanoic acid (997-117). Compound **997-117** was prepared via general procedure **H** using pyrazoline amine (0.30 g, 0.72 mmol) and **8** (98

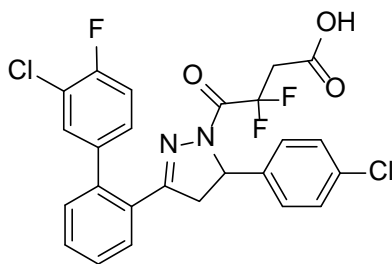
mg, 0.72 mmol). The product was obtained after flash chromatography (0-10% MeOH/DCM). Yield a yellow gel 0.12 g, 30%. ^1H NMR (400 MHz, DMSO- d_6) δ 7.70 (dd, $J = 7.6, 1.4$ Hz, 1H), 7.60 – 7.49 (m, 2H), 7.40 – 7.36 (m, 1H), 7.35 – 7.31 (m, 4H), 7.31 – 7.25 (m, 4H), 5.57 (dd, $J = 11.7, 4.4$ Hz, 1H), 3.62 (dd, $J = 18.4, 11.7$ Hz, 1H), 3.32 – 3.04 (m, 2H), 2.61 (dd, $J = 18.4, 4.4$ Hz, 1H). ^{13}C NMR (100 MHz, DMSO- d_6) δ 170.36, 167.71, 158.41, 147.60, 139.97, 139.92, 139.36, 132.48, 130.82, 130.48, 130.46, 129.60, 129.56, 128.47, 128.11, 127.43, 121.19, 114.69, 59.79, 43.77, 40.88. HRMS (m/z): $[\text{M}+\text{H}]^+$ calculated for $\text{C}_{26}\text{H}_{19}\text{O}_4\text{N}_2\text{ClF}_5$, 553.09480; found, 553.09433.



4-(3-(4'-chloro-[1,1'-biphenyl]-2-yl)-5-(5-chlorothiophen-2-yl)-4,5-dihydro-1H-pyrazol-1-yl)-3,3-difluoro-4-oxobutanoic acid (997-118). Compound **997-118** was prepared via general procedure **H** using pyrazoline amine (0.40 g, 1.1 mmol) and **8** (0.15 g, 1.1 mmol). The product was obtained after flash chromatography (0-10% MeOH/DCM). Yield a yellow foam 0.24 g, 45%. ^1H NMR (400 MHz, DMSO- d_6) δ 12.89 (s, 1H), 7.74 – 7.69 (m, 1H), 7.61 – 7.49 (m, 2H), 7.41 – 7.34 (m, 3H), 7.33 – 7.27 (m, 2H), 6.98 – 6.81 (m, 2H), 5.76 (dd, $J = 11.3, 3.8$ Hz, 1H), 3.60 (dd, $J = 18.4, 11.3$ Hz, 1H), 3.13 – 2.95 (m, 2H), 2.89 (dd, $J = 18.4, 3.9$ Hz, 1H). ^{13}C NMR (100 MHz, DMSO- d_6) δ 167.60, 158.32, 141.76, 139.93, 139.36, 132.48, 130.90, 130.50, 130.44, 129.53, 129.35, 128.44, 128.11, 127.52, 126.24, 124.61, 117.03, 114.56, 59.77, 56.26, 43.10. HRMS (m/z): $[\text{M}+\text{H}]^+$ calculated for $\text{C}_{23}\text{H}_{17}\text{O}_3\text{N}_2\text{Cl}_2\text{F}_2\text{S}$, 509.02995; found, 509.03005.

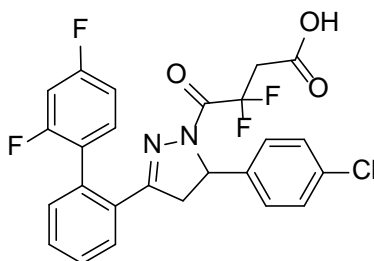


4-(5-(benzo[d][1,3]dioxol-4-yl)-3-(4'-chloro-[1,1'-biphenyl]-2-yl)-4,5-dihydro-1H-pyrazol-1-yl)-3,3-difluoro-4-oxobutanoic acid (997-119). Compound **997-119** was prepared via general procedure **H** using pyrazoline amine (0.30 g, 0.80 mmol) and **8** (0.11 g, 0.80 mmol). The product was obtained after flash chromatography (0-10% MeOH/DCM). Yield a yellow gel 0.11 g, 26%. ^1H NMR (400 MHz, $\text{DMSO-}d_6$) δ 7.72 – 7.68 (m, 1H), 7.59 – 7.46 (m, 2H), 7.40 – 7.26 (m, 5H), 6.88 – 6.77 (m, 2H), 6.70 – 6.60 (m, 1H), 5.99 (dd, $J = 47.4$, 1.0 Hz, 2H), 5.48 (dd, $J = 11.7$, 4.6 Hz, 1H), 3.71 – 3.57 (m, 1H), 3.42 – 3.31 (m, 1H), 3.11 – 2.99 (m, 1H), 2.73 (dd, $J = 18.2$, 4.6 Hz, 1H). ^{13}C NMR (100 MHz, $\text{DMSO-}d_6$) δ 167.88, 167.56, 164.06, 158.22, 147.34, 143.89, 139.90, 139.45, 132.39, 130.93, 130.45, 130.38, 129.52, 128.37, 128.09, 121.73, 121.45, 119.44, 114.01, 107.86, 101.09, 56.21, 53.08, 42.06. HRMS (m/z): $[\text{M}+\text{H}]^+$ calculated for $\text{C}_{26}\text{H}_{20}\text{O}_5\text{N}_2\text{ClF}_2$, 513.10343; found, 513.10384.

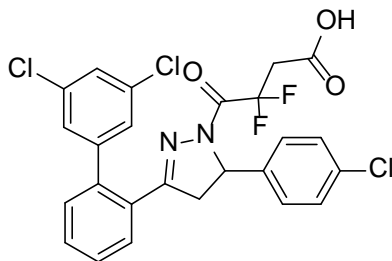


4-(3-(3'-chloro-4'-fluoro-[1,1'-biphenyl]-2-yl)-5-(4-chlorophenyl)-4,5-dihydro-1H-pyrazol-1-yl)-3,3-difluoro-4-oxobutanoic acid (997-120). Compound **997-120** was prepared via general procedure **H** using pyrazoline amine (0.50 g, 1.3 mmol) and **8** (0.18

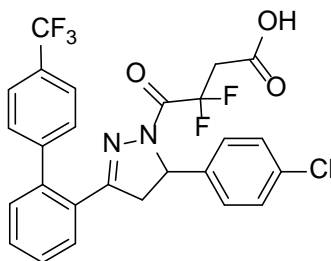
g, 1.3 mmol). The product was obtained after flash chromatography (0-10% MeOH/DCM). Yield a yellow foam 0.26 g, 38%. ^1H NMR (400 MHz, DMSO- d_6) δ 12.78 (s, 1H), 7.74 – 7.66 (m, 1H), 7.60 – 7.48 (m, 3H), 7.43 – 7.34 (m, 4H), 7.31 (ddd, J = 8.5, 4.8, 2.2 Hz, 1H), 7.23 – 7.16 (m, 2H), 5.54 (dd, J = 11.7, 4.7 Hz, 1H), 3.90 – 3.77 (m, 1H), 3.09 – 2.81 (m, 3H). ^{13}C NMR (100 MHz, DMSO- d_6) δ 167.39, 157.66, 155.48, 139.69, 138.85, 138.69, 138.65, 132.05, 131.15, 130.66, 130.33, 129.51, 129.46, 129.34, 129.26, 128.60, 128.31, 127.50, 119.81, 119.64, 116.96, 116.76, 114.52, 59.84, 43.63, 40.59. HRMS (m/z): $[\text{M}+\text{H}]^+$ calculated for $\text{C}_{25}\text{H}_{18}\text{O}_3\text{N}_2\text{Cl}_2\text{F}_3$, 521.06521; found, 521.06685.



4-(5-(4-chlorophenyl)-3-(2',4'-difluoro-[1,1'-biphenyl]-2-yl)-4,5-dihydro-1H-pyrazol-1-yl)-3,3-difluoro-4-oxobutanoic acid (997-121). Compound **997-121** was prepared via general procedure **H** using pyrazoline amine (0.50 g, 1.4 mmol) and **8** (0.18 g, 1.4 mmol). The product was obtained after flash chromatography (0-10% MeOH/DCM). Yield a yellow foam 0.27 g, 40%. ^1H NMR (400 MHz, DMSO- d_6) δ 12.74 (s, 1H), 7.75 – 7.68 (m, 1H), 7.68 – 7.55 (m, 1H), 7.56 (dt, J = 4.8, 2.0 Hz, 1H), 7.57 – 7.44 (m, 1H), 7.48 – 7.33 (m, 4H), 7.27 – 7.09 (m, 4H), 5.56 (dd, J = 11.7, 4.7 Hz, 1H), 3.82 (d, J = 13.4 Hz, 1H), 3.42 – 3.20 (m, 2H), 3.00 – 2.85 (m, 1H). ^{13}C NMR (100 MHz, DMSO- d_6) δ 164.39, 164.08, 158.26, 157.34, 139.74, 133.39, 132.10, 131.83, 131.17, 130.52, 130.17, 129.26, 128.87, 128.67, 128.62, 127.44, 126.57, 114.45, 114.03, 111.99, 104.17, 59.72, 53.10, 43.26, 40.56. HRMS (m/z): $[\text{M}+\text{H}]^+$ calculated for $\text{C}_{25}\text{H}_{18}\text{O}_3\text{N}_2\text{ClF}_4$, 505.09476; found, 505.09559.

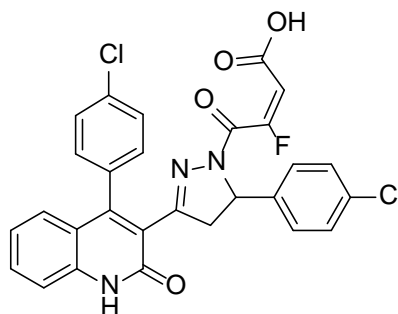


4-(5-(4-chlorophenyl)-3-(3',5'-dichloro-[1,1'-biphenyl]-2-yl)-4,5-dihydro-1H-pyrazol-1-yl)-3,3-difluoro-4-oxobutanoic acid (997-123). Compound **997-123** was prepared via general procedure **H** using pyrazoline amine (0.50 g, 1.2 mmol) and **8** (0.17 g, 1.2 mmol). The product was obtained after flash chromatography (0-10% MeOH/DCM). Yield a yellow foam 0.26 g, 39%. ^{13}C NMR (100 MHz, DMSO- d_6) δ 166.47, 157.23, 144.72, 139.75, 138.30, 137.81, 134.20, 134.13, 131.15, 130.37, 129.52, 129.31, 128.75, 128.62, 127.83, 127.56, 127.51, 127.41, 127.05, 126.88, 126.88, 59.87, 43.42, 24.82, 19.56. HRMS (m/z): $[\text{M}+\text{H}]^+$ calculated for $\text{C}_{25}\text{H}_{18}\text{O}_3\text{N}_2\text{Cl}_3\text{F}_2$, 537.03566; found, 537.03572.



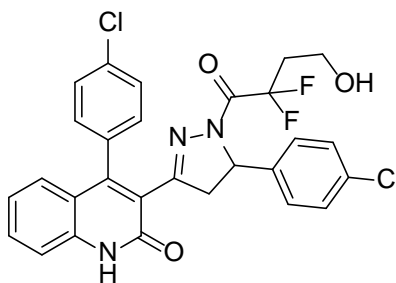
4-(5-(4-chlorophenyl)-3-(4'-(trifluoromethyl)-[1,1'-biphenyl]-2-yl)-4,5-dihydro-1H-pyrazol-1-yl)-3,3-difluoro-4-oxobutanoic acid (997-124). Compound **997-124** was prepared via general procedure **H** using pyrazoline amine (0.50 g, 1.3 mmol) and **8** (0.17 g, 1.3 mmol). The product was obtained after flash chromatography (0-10% MeOH/DCM). Yield a yellow foam 0.27 g, 40%. ^1H NMR (400 MHz, DMSO- d_6) δ 12.82 (s, 1H), 7.80 – 7.29 (m, 10H), 7.20 – 7.06 (m, 2H), 5.53 (dd, $J = 11.6, 4.4$ Hz, 1H), 3.86 – 3.27 (m, 2H), 3.09 – 2.87 (m, 1H), 2.66 (dd, $J = 18.4, 4.4$ Hz, 1H). ^{13}C NMR (100 MHz, DMSO- d_6) δ

167.52, 158.02, 144.87, 139.69, 139.55, 132.12, 131.15, 130.91, 130.50, 130.14, 129.68, 129.48, 128.75, 128.56, 128.49, 128.07, 127.76, 127.35, 125.56, 125.33, 125.29, 122.85, 114.51, 59.84, 43.62, 40.81. HRMS (m/z): $[M+H]^+$ calculated for $C_{26}H_{19}O_3N_2ClF_5$, 537.10098; found, 537.09927.



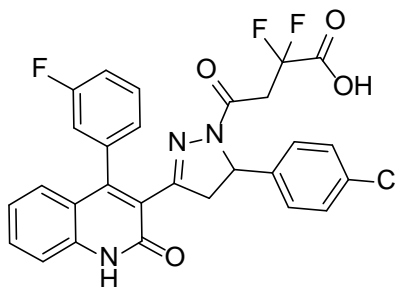
(E)-4-(5-(4-chlorophenyl)-3-(4-(4-chlorophenyl)-2-oxo-1,2-dihydroquinolin-3-yl)-4,5-dihydro-1H-pyrazol-1-yl)-3-fluoro-4-oxobut-2-enoic acid (997-101). 3-fluorofuran-2,5-dione (50 mg, 0.43 mmol, 1 equiv.) was added in a solution of pyrazoline amine **6a** (0.19 g, 0.43 mmol, 1 equiv.) in THF (0.045 molar) at room temperature. After around 24 hours, the crude was concentrated *in vacuo*, washed with ethyl acetate and 1 N HCl. The organic layer was dried over Mg_2SO_4 , filtered and evaporated *in vacuo*. Finally, the crude compound was purified by flash chromatography using a 0-10% MeOH/DCM gradient to afford product. Yield as yellow solid 71 mg, 30%; mp 132-138 °C. 1H NMR (400 MHz, $DMSO-d_6$) δ 12.33 (s, 1H), 7.64 – 7.55 (m, 2H), 7.51 (dd, $J = 8.2, 2.1$ Hz, 1H), 7.46 – 7.37 (m, 2H), 7.35 – 7.26 (m, 3H), 7.13 (tt, $J = 7.0, 1.2$ Hz, 1H), 7.06 – 6.99 (m, 1H), 6.84 (d, $J = 7.9$ Hz, 2H), 6.71 – 6.59 (m, 1H), 5.42 (dd, $J = 11.8, 4.5$ Hz, 1H), 3.71 (dd, $J = 18.6, 11.9$ Hz, 1H), 2.77 (dd, $J = 18.6, 4.5$ Hz, 1H). ^{13}C NMR (100 MHz, $DMSO-d_6$) δ 159.87, 153.40, 150.02, 149.89, 140.49, 138.60, 138.46, 133.69, 131.76, 131.62, 131.20, 131.07, 130.41, 130.28, 128.36, 128.24, 128.22, 127.35, 127.21, 127.08, 123.25, 123.12, 122.34, 122.22, 119.08, 118.94, 115.58, 115.45, 103.32, 58.14, 45.08. ^{19}F NMR (376 MHz, $DMSO-d_6$) δ -

106.75. HRMS (m/z): $[M+H]^+$ calculated for $C_{28}H_{19}O_4N_3Cl_2F$, 550.07312; found, 550.07346.



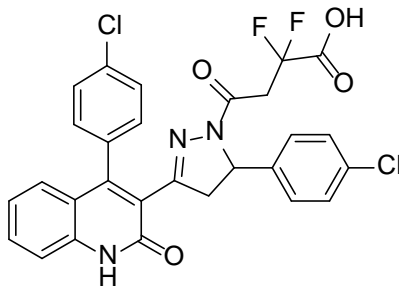
4-(4-chlorophenyl)-3-[5-(4-chlorophenyl)-1-(2,2-difluoro-4-hydroxybutanoyl)-4,5-dihydro-1H-pyrazol-3-yl]quinolin-2(1H)-one (997-75). Compound **997-74** (42 mg, 0.07 mmol, 1 equiv.) was dissolved in Tetrahydrofuran (0.03 molar) and cooled to 0 °C prior to the borane dimethyl sulfide (8.4 mg, 0.11 mmol, 1.5 equiv.) was added dropwise under nitrogen. The reaction mixture was stirred at 0 °C for 15 min and then at room temperature overnight. After the mixture was cooling again in an ice bath, methanol was added dropwise until effervescence ceased, and then the mixture was stirred at room temperature for another several minutes. The solvent was then evaporated *in vacuo*, and the crude was purified by column chromatography. Yield as yellow foam, 8.0 mg, 21%. 1H NMR (400 MHz, CD_3OD) δ 7.62-7.56 (m, 2H), 7.48 (dd, J = 8.2, 2.3 Hz, 1H), 7.43 (d, J = 7.3 Hz, 1H), 7.42 (dd, J = 8.3, 2.1 Hz, 1H), 7.26-7.22 (m, 3H), 7.19 (dd, J = 6.8, 1.0 Hz, 1H), 7.16 (dd, J = 8.2, 1.8 Hz, 1H), 6.84 (dd, J = 9.1, 4.4 Hz, 1H), 6.83 (d, J = 8.6 Hz, 1H), 5.44 (dd, J = 11.5, 4.4 Hz, 1H), 3.76 (dd, J = 18.6, 11.8 Hz, 1H), 3.64 (t, J = 6.3 Hz, 2H), 2.72 (dd, J = 18.6, 4.3 Hz, 1H), 2.48-2.24 (m, 3H). ^{13}C NMR (100 MHz, CD_3OD) δ 169.23, 157.70, 153.33, 142.79, 140.93, 140.05, 136.19, 134.98, 134.69, 129.92, 128.93, 128.66, 124.45, 121.32, 61.82, 46.15, 39.15, 30.91. HRMS (m/z): $[M+H]^+$ calculated for $C_{28}H_{22}O_3N_3Cl_2F_2$, 556.10008; found, 556.10084.

General procedure I for the synthesis of difluoro-substituted hydroxybutanoic acid quinolone pyrazoline products. To a solution of acylated quinolone pyrazoline product (1 equiv.) in 1,2-dichloroethane (4.89 mM), trimethyltin hydroxide (5 equiv.) was added in one portion. The mixture was heated at 80 °C and TLC was used to monitor the completion of reaction (1-2 hours). After the reaction was completed, the mixture was evaporated *in vacuo*, and the residue was taken up in ethyl acetate. The organic layer was washed with aqueous 2 N HCl and then washed with brine, dried over magnesium sulfate and concentrated *in vacuo*.



4-{5-(4-chlorophenyl)-3-[4-(3-fluorophenyl)-2-oxo-1,2-dihydroquinolin-3-yl]-4,5-dihydro-1H-pyrazol-1-yl}-2,2-difluoro-4-oxobutanoic acid (997-69). Compound **997-69** was prepared via general procedure **I** using **997-65** (0.35 g, 0.60 mmol) and trimethyltin hydroxide (0.54 g, 3.01 mmol). The product was obtained after flash chromatography (0-10% MeOH/DCM). Yield as yellow foam 0.16 g, 48%. ¹H NMR (400 MHz, CDCl₃) δ 12.22 (s, 1H), 7.84 (broad s, 1H), 7.58-7.46 (m, 2H), 7.32 (d, J= 8.1 Hz, 1H), 7.29-7.13 (m, 6H), 6.98 (dd, J= 31.2, 8.4 Hz, 1H), 6.84 (d, J= 7.9 Hz, 2H), 5.40 (dd, J= 12.0, 3.9 Hz, 1H), 3.90-3.74 (m, 1H), 3.43-3.32 (m, 2H), 2.95 (dd, J= 18.5, 3.3 Hz, 1H). ¹³C NMR (100 MHz, Chloroform-*d*) δ 163.95, 162.63, 161.48, 153.50, 152.89, 139.18, 139.11, 137.50, 137.23, 133.72, 133.67, 132.59, 129.23, 129.13, 127.23, 127.10, 124.28, 121.65, 120.35, 116.71, 59.45, 46.02, 29.89. HRMS (*m/z*): [M+H]⁺ calculated for C₂₈H₂₀ClF₃N₃O₄, 554.10889;

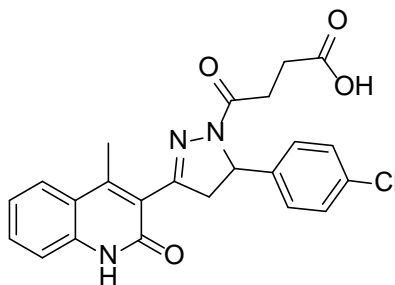
found, 554.11071.



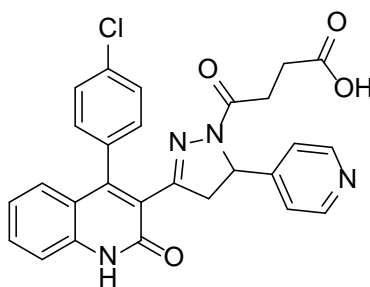
4-(5-(4-chlorophenyl)-3-(4-(4-chlorophenyl)-2-oxo-1,2-dihydroquinolin-3-yl)-4,5-dihydro-1H-pyrazol-1-yl)-2,2-difluoro-4-oxobutanoic acid (997-114). Compound **997-114** was prepared via general procedure **I** using **997-66** (0.60 g, 1.0 mmol) and trimethyltin hydroxide (0.91 g, 5.0 mmol). The product was obtained after flash chromatography (0-10% MeOH/DCM). Yield as yellow solid 0.26 g, 46%; mp 149-155 °C. ^1H NMR (400 MHz, Chloroform-*d*) δ 12.20 (s, 1H), 11.03 (s, 1H), 7.49 (ddd, $J = 11.5, 8.3, 3.3$ Hz, 2H), 7.43 (dd, $J = 8.2, 2.2$ Hz, 1H), 7.34 – 7.26 (m, 2H), 7.19 – 7.08 (m, 5H), 6.75 (d, $J = 8.1$ Hz, 2H), 5.39 (dd, $J = 11.7, 4.4$ Hz, 1H), 3.71 (dd, $J = 18.5, 11.7$ Hz, 1H), 3.43 (td, $J = 13.1, 4.9$ Hz, 2H), 2.80 (dd, $J = 18.4, 4.3$ Hz, 1H). ^{13}C NMR (100 MHz, Chloroform-*d*) δ 166.99, 164.09, 162.56, 153.61, 153.29, 139.08, 137.44, 135.53, 133.70, 133.32, 132.62, 131.16, 130.08, 129.13, 129.07, 128.93, 128.03, 127.12, 124.33, 121.76, 120.47, 116.81, 113.76, 59.40, 46.12, 40.36. HRMS (m/z): $[\text{M}+\text{H}]^+$ calculated for $\text{C}_{28}\text{H}_{20}\text{O}_4\text{N}_3\text{Cl}_2\text{F}_2$, 570.07934; found, 570.07966.

General procedure J for the synthesis of acylated quinolone pyrazoline products. In a microwaveable vial, pyrazoline amines (1 equiv.) and succinic anhydride (1 equiv.) were dissolved in Tetrahydrofuran (0.15 molar) with molecular sieves. The mixture was microwaved to 165 °C for 20 minutes, checked by LC-MS. The THF was evaporated *in vacuo* and the resultant residue was washed with DCM and brine. Product was obtained

after column chromatography using a flash chromatography system with a 2-10% gradient, using MeOH in DCM.

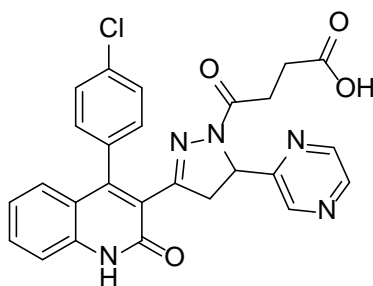


4-(5-(4-chlorophenyl)-3-(4-methyl-2-oxo-1,2-dihydroquinolin-3-yl)-4,5-dihydro-1H-pyrazol-1-yl)-4-oxobutanoic acid (997-76). Compound **997-76** was prepared via general procedure **J** using **997-77** (0.15 g, 0.44 mmol) and succinic anhydride (44 mg, 0.44 mmol). The product was obtained after flash chromatography (0-10% MeOH/DCM). Yield a yellow solid 29 mg, 15%; mp 228-232 °C. ^1H NMR (400 MHz, CD_3OD) δ 7.91 (d, J = 8.0 Hz, 1H), 7.57 (t, J = 7.7 Hz, 1H), 7.37-7.30 (m, 6H), 5.56 (dd, J = 11.8, 4.6 Hz, 1H), 3.82 (dd, J = 18.5, 11.8 Hz, 1H), 3.24 (dd, J = 18.6, 4.3 Hz, 1H), 3.09-2.95 (m, 2H), 2.63 (s, 3H), 2.60 (t, J = 6.8 Hz, 2H). HRMS (m/z): $[\text{M}+\text{H}]^+$ calculated for $\text{C}_{23}\text{H}_{21}\text{ClN}_3\text{O}_4$, 438.12151; found, 438.12189.



4-(3-(4-(4-chlorophenyl)-2-oxo-1,2-dihydroquinolin-3-yl)-5-(pyridin-4-yl)-4,5-dihydro-1H-pyrazol-1-yl)-4-oxobutanoic acid (997-79). Compound **997-79** was prepared via general procedure **J** using pyrazoline amine (0.15 g, 0.37 mmol) and succinic anhydride (37 mg, 0.37 mmol). The product was obtained after flash chromatography (0-

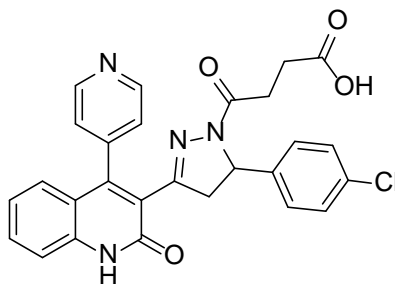
10% MeOH/DCM). Yield a yellow foam 37 mg, 20%. ^1H NMR (400 MHz, CD_3OD) δ 8.38 (d, J = 3.6 Hz, 2H), 7.56 (dd, J = 7.6, 1.2 Hz, 2H), 7.43-7.38 (m, 3H), 7.20-7.12 (m, 3H), 6.94 (d, J = 5.1 Hz, 2H), 5.41 (dd, J = 12.0, 4.3 Hz, 1H), 3.79 (dd, J = 18.6, 12.1 Hz, 1H), 2.92-2.84 (m, 1H), 2.81 (dd, J = 18.4, 4.3 Hz, 1H), 2.67-2.44 (m, 3H). ^{13}C NMR (100 MHz, CD_3OD) δ 176.18, 172.07, 167.34, 155.07, 153.33, 152.95, 150.46, 149.81, 140.00, 136.00, 135.43, 133.20, 132.84, 130.06, 124.35, 123.33, 122.55, 121.39, 60.13, 37.49, 30.14, 29.51. HRMS (m/z): $[\text{M}+\text{H}]^+$ calculated for $\text{C}_{27}\text{H}_{22}\text{ClN}_4\text{O}_4$, 501.13241; found, 501.13259.



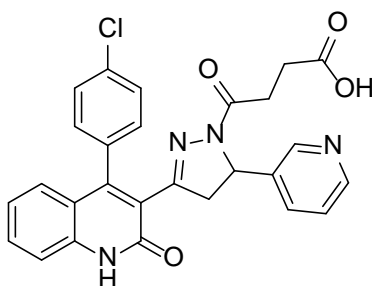
4-(3-(4-(4-chlorophenyl)-2-oxo-1,2-dihydroquinolin-3-yl)-5-(pyrazin-2-yl)-4,5-

dihydro-1H-pyrazol-1-yl)-4-oxobutanoic acid (997-80). Compound **997-80** was

prepared via general procedure **J** using pyrazoline amine (70 mg, 0.17 mmol) and succinic anhydride (17 mg, 0.17 mmol). The product was obtained after flash chromatography (0-10% MeOH/DCM). Yield a yellow foam 28 mg, 32%. ^1H NMR (400 MHz, CD_3OD) δ 8.51 (d, J = 1.1 Hz, 1H), 8.46 (d, J = 2.4 Hz, 1H), 8.39 (s, 1H), 7.57 (p, J = 4.3 Hz, 1H), 7.45 (td, J = 8.8, 2.3 Hz, 2H), 7.40 (d, J = 8.5 Hz, 1H), 7.31 (dd, J = 7.9, 2.1 Hz, 1H), 7.24 (dd, J = 8.1, 2.1 Hz, 1H), 7.17 (d, J = 3.9 Hz, 2H), 5.52 (dd, J = 11.8, 5.1 Hz, 1H), 3.79 (dd, J = 18.2, 12.0 Hz, 1H), 3.15 (dd, J = 18.4, 4.9 Hz, 1H), 2.69-2.56 (m, 2H), 2.47-2.43 (m, 2H). ^{13}C NMR (100 MHz, CD_3OD) δ 176.20, 172.33, 162.75, 156.60, 155.12, 153.40, 145.90, 144.66, 144.17, 139.98, 135.73, 135.54, 129.05, 124.31, 124.17, 121.36, 60.23, 60.18, 30.16, 29.59. HRMS (m/z): $[\text{M}+\text{H}]^+$ calculated for $\text{C}_{26}\text{H}_{21}\text{ClN}_5\text{O}_4$, 502.12766; found, 502.12813.

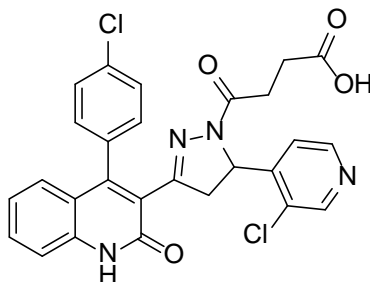


4-(5-(4-chlorophenyl)-3-(2-oxo-4-(pyridin-4-yl)-1,2-dihydroquinolin-3-yl)-4,5-dihydro-1H-pyrazol-1-yl)-4-oxobutanoic acid (997-82). Compound **997-82** was prepared via general procedure **J** using **997-81** (0.15 g, 0.37 mmol) and succinic anhydride (37 mg, 0.37 mmol). The product was obtained after flash chromatography (0-10% MeOH/DCM). Yield a yellow solid 23 mg, 12% ; mp 147-152 °C. ^1H NMR (400 MHz, DMSO-*d*₆) δ 12.34 (s, 1H), 12.07 (s, 1H), 8.72 (dd, *J*= 17.8, 5.0 Hz, 2H), 7.60 (t, *J*= 7.1 Hz, 1H), 7.45 (s, 1H), 7.44 (d, *J*= 12.8 Hz, 1H), 7.34 (d, *J*= 4.7 Hz, 1H), 7.30 (d, *J*= 8.5 Hz, 2H), 7.16 (t, *J*= 7.7 Hz, 1H), 6.98 (d, *J*= 7.9 Hz, 1H), 6.86 (d, *J*= 8.6 Hz, 2H), 5.35 (dd, *J*= 11.9, 4.3 Hz, 1H), 3.81 (dd, *J*= 18.4, 12.0 Hz, 1H), 2.92 (dd, *J*= 18.4, 4.6 Hz, 1H), 2.44-2.27 (m, 4H). ^{13}C NMR (100 MHz, CD₃OD) δ 176.81, 171.70, 159.79, 157.90, 154.85, 153.25, 152.24, 150.48, 146.98, 145.45, 143.21, 142.64, 141.73, 140.10, 134.30, 133.93, 132.07, 131.41, 129.88, 128.72, 128.44, 128.35, 124.50, 60.67, 38.43, 34.47, 29.47. HRMS (*m/z*): [*M*+*H*]⁺ calculated for C₂₇H₂₂O₄N₄Cl, 501.13241; found, 501.13254.



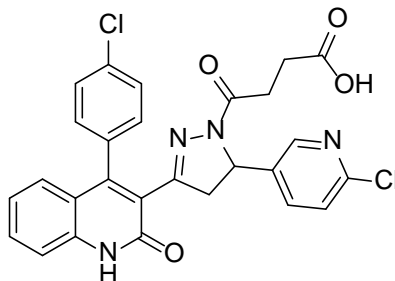
4-(3-(4-(4-chlorophenyl)-2-oxo-1,2-dihydroquinolin-3-yl)-5-(pyridin-3-yl)-4,5-dihydro-1H-pyrazol-1-yl)-4-oxobutanoic acid (997-83). Compound **997-83** was

prepared via general procedure **J** using pyrazoline amine (0.43 g, 1.1 mmol) and succinic anhydride (0.11 mg, 1.1 mmol). The product was obtained after flash chromatography (0-10% MeOH/DCM). Yield a yellow foam 87 mg, 16%. $^1\text{H NMR}$ (400 MHz, CD_3OD) δ 8.40 (d, $J= 3.1$ Hz, 1H), 8.35 (s, 1H), 7.61-7.54 (m, 2H), 7.48 (ddd, $J= 8.2, 3.5, 2.3$ Hz, 1H), 7.43-7.36 (m, 2H), 7.35-7.31 (m, 1H), 7.29-7.25 (m, 2H), 7.21-7.15 (m, 2H), 5.47 (dd, $J= 12.3, 4.1$ Hz, 1H), 3.78 (ddd, $J= 18.5, 11.9, 3.7$ Hz, 1H), 3.33 (dd, $J= 12.0, 3.9$ Hz, 1H), 2.96 (dt, $J= 18.4, 4.1$ Hz, 1H), 2.84-2.76 (m, 1H), 2.66-2.58 (m, 1H), 2.50-2.43 (m, 2H). $^{13}\text{C NMR}$ (100 MHz, CD_3OD) δ 175.93, 171.80, 162.59, 154.97, 149.01, 148.26, 141.29, 139.81, 135.79, 135.36, 135.31, 134.08, 132.95, 132.37, 131.70, 129.84, 129.67, 128.81, 125.38, 124.16, 124.13, 121.18, 116.84, 58.66, 46.23, 29.99, 29.37. HRMS (m/z): $[\text{M}+\text{H}]^+$ calculated for $\text{C}_{27}\text{H}_{22}\text{ClN}_4\text{O}_4$, 501.13241; found, 501.13235.

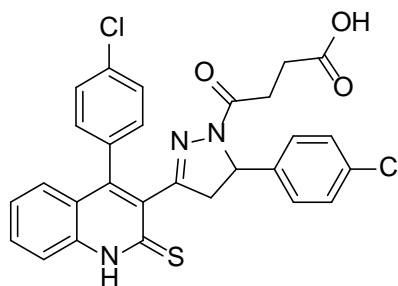


4-(3-(4-(4-chlorophenyl)-2-oxo-1,2-dihydroquinolin-3-yl)-5-(3-chloropyridin-4-yl)-4,5-dihydro-1H-pyrazol-1-yl)-4-oxobutanoic acid (997-88). Compound **997-88** was prepared via general procedure **J** using pyrazoline amine (0.45 g, 1.0 mmol) and succinic anhydride (0.10 g, 1.0 mmol). The product was obtained after flash chromatography (0-10% MeOH/DCM). Yield a yellow solid 0.13 g, 23%; mp 182-186 °C. $^1\text{H NMR}$ (400 MHz, CD_3OD) δ 8.50 (s, 1H), 8.34 (d, $J= 4.7$ Hz, 1H), 7.60 (dd, $J= 8.2, 1.9$ Hz, 1H), 7.58 (dd, $J= 8.2, 1.6$ Hz, 1H), 7.56 (dd, $J= 8.2, 2.3$ Hz, 1H), 7.43-7.37 (m, 4H), 7.20-7.14 (m, 3H), 6.67 (d, $J= 5.1$ Hz, 1H), 5.68 (dd, $J= 12.0, 4.5$ Hz, 1H), 3.92 (dd, $J= 18.4, 12.1$ Hz, 1H), 3.01-

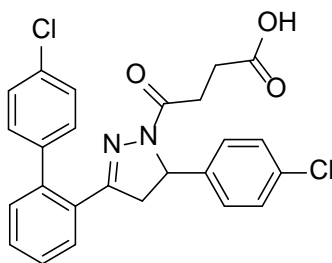
2.95 (m, 1H), 2.75 (dd, $J = 18.3, 4.7$ Hz, 1H), 2.66-2.48 (m, 3H). ^{13}C NMR (100 MHz, CD_3OD) δ 176.21, 172.16, 155.13, 150.20, 149.24, 149.09, 148.44, 144.98, 141.50, 140.01, 138.13, 135.45, 133.23, 132.92, 131.59, 129.99, 129.90, 129.02, 124.37, 122.43, 121.37, 117.06, 111.58, 57.98, 45.22, 30.00, 29.54. HRMS (m/z): $[\text{M}+\text{H}]^+$ calculated for $\text{C}_{27}\text{H}_{21}\text{O}_4\text{N}_4\text{Cl}_2$, 535.09344; found, 535.09384.



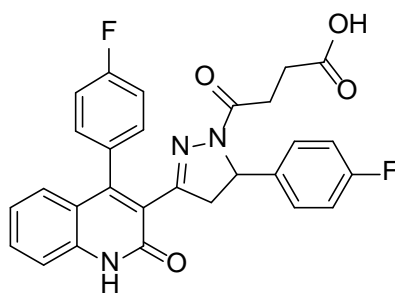
4-(3-(4-(4-chlorophenyl)-2-oxo-1,2-dihydroquinolin-3-yl)-5-(6-chloropyridin-3-yl)-4,5-dihydro-1H-pyrazol-1-yl)-4-oxobutanoic acid (997-92). Compound **997-92** was prepared via general procedure **J** using pyrazoline amine (50 mg, 0.11 mmol) and succinic anhydride (11 mg, 0.11 mmol). The product was obtained after flash chromatography (0-10% MeOH/DCM). Yield a yellow solid 17 mg, 28%. ^1H NMR (400 MHz, $\text{DMSO}-d_6$) δ 12.30 (s, 1H), 12.16 (s, 1H), 8.12 (d, $J = 2.7$ Hz, 1H), 7.57 (d, $J = 7.8$ Hz, 2H), 7.51 (dd, $J = 8.2, 2.3$ Hz, 1H), 7.41 (dd, $J = 17.8, 8.4$ Hz, 3H), 7.32 (dd, $J = 8.2, 1.9$ Hz, 1H), 7.21 (dd, $J = 8.4, 2.6$ Hz, 1H), 7.15 (t, $J = 7.6$ Hz, 1H), 7.04 (d, $J = 8.2$ Hz, 1H), 5.44 (dd, $J = 11.7, 4.3$ Hz, 1H), 3.72 (dd, $J = 18.5, 12.3$ Hz, 1H), 2.93 (dd, $J = 18.5, 4.1$ Hz, 1H), 2.41 (s, 2H). 2.33 (d, $J = 5.4$ Hz, 2H). ^{13}C NMR (100 MHz, CD_3OD) δ 173.50, 168.90, 160.18, 152.94, 148.97, 147.77, 140.79, 138.60, 136.78, 134.07, 131.17, 130.62, 128.27, 127.32, 124.10, 123.25, 119.10, 115.63, 108.82, 56.05, 28.95, 28.37, 28.17. HRMS (m/z): $[\text{M}+\text{H}]^+$ calculated for $\text{C}_{27}\text{H}_{21}\text{Cl}_2\text{N}_4\text{O}_4$, 535.09344; found, 535.09426.



4-(5-(4-chlorophenyl)-3-(4-(4-chlorophenyl)-2-thioxo-1,2-dihydroquinolin-3-yl)-4,5-dihydro-1H-pyrazol-1-yl)-4-oxobutanoic acid (997-97). Compound **997-97** was prepared via general procedure **J** using pyrazoline amine (0.21 g, 0.46 mmol) and succinic anhydride (46 mg, 0.46 mmol). The product was obtained after flash chromatography (0-10% MeOH/DCM). Yield a yellow solid 58 mg, 23%; mp 143-148 °C. ^1H NMR (400 MHz, DMSO- d_6) δ 14.13 (s, 1H), 7.78 – 7.67 (m, 2H), 7.65 (dd, $J = 8.2, 2.3$ Hz, 1H), 7.46 (ddd, $J = 12.2, 8.3, 2.2$ Hz, 2H), 7.34 – 7.28 (m, 2H), 7.28 – 7.22 (m, 2H), 7.07 (dd, $J = 8.1, 1.2$ Hz, 1H), 6.80 (d, $J = 8.1$ Hz, 2H), 5.33 (dd, $J = 12.1, 5.0$ Hz, 1H), 3.91 – 3.78 (m, 1H), 2.73 (dt, $J = 17.2, 6.8$ Hz, 2H), 2.59 (dt, $J = 17.1, 6.6$ Hz, 1H), 2.36 (t, $J = 7.1$ Hz, 2H). ^{13}C NMR (100 MHz, DMSO- d_6) δ 178.99, 173.52, 168.73, 153.82, 145.85, 141.20, 139.04, 133.53, 133.29, 132.16, 131.44, 131.42, 131.34, 130.68, 128.44, 128.08, 127.49, 127.04, 124.71, 122.20, 116.33, 58.30, 45.10, 28.64, 28.26. HRMS (m/z): $[\text{M}+\text{H}]^+$ calculated for $\text{C}_{28}\text{H}_{22}\text{O}_3\text{N}_3\text{Cl}_2\text{S}$, 550.07534; found, 550.07629.

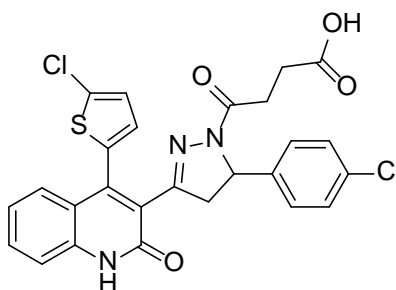


4-(3-(4'-chloro-[1,1'-biphenyl]-2-yl)-5-(4-chlorophenyl)-4,5-dihydro-1H-pyrazol-1-yl)-4-oxobutanoic acid (997-99). Compound **997-99** was prepared via general procedure **J** using pyrazoline amine (0.17 g, 0.46 mmol) and succinic anhydride (46 mg, 0.46 mmol). The product was obtained after flash chromatography (0-10% MeOH/DCM). Yield a yellow foam 0.13 g, 59%. ^1H NMR (400 MHz, Chloroform-*d*) δ 7.66 (dd, $J = 7.4, 1.7$ Hz, 1H), 7.50 – 7.40 (m, 2H), 7.31 (dd, $J = 7.2, 1.7$ Hz, 1H), 7.27 – 7.20 (m, 4H), 7.19 – 7.13 (m, 2H), 7.00 – 6.94 (m, 2H), 5.37 (dd, $J = 11.6, 4.2$ Hz, 1H), 3.20 (dd, $J = 17.9, 11.6$ Hz, 1H), 3.01 – 2.79 (m, 2H), 2.67 (t, $J = 6.3$ Hz, 2H), 2.45 (dd, $J = 17.9, 4.2$ Hz, 1H). ^{13}C NMR (100 MHz, Chloroform-*d*) δ 177.92, 170.12, 156.20, 140.71, 139.79, 139.65, 133.92, 133.66, 130.88, 130.61, 130.37, 130.18, 129.44, 129.18, 128.68, 128.16, 127.00, 59.59, 44.67, 28.91. HRMS (m/z): $[\text{M}+\text{H}]^+$ calculated for $\text{C}_{25}\text{H}_{21}\text{O}_3\text{N}_2\text{Cl}_2$, 467.09237; found, 467.09256.



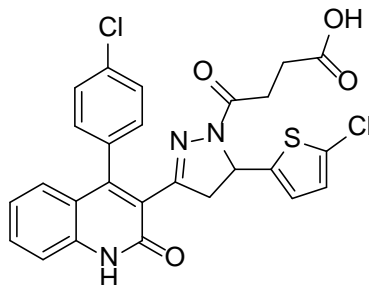
4-(5-(4-fluorophenyl)-3-(4-(4-fluorophenyl)-2-oxo-1,2-dihydroquinolin-3-yl)-4,5-dihydro-1H-pyrazol-1-yl)-4-oxobutanoic acid (997-105). Compound **997-105** was prepared via general procedure **J** using pyrazoline amine (0.20 g, 0.50 mmol) and succinic

anhydride (50 mg, 0.50 mmol). The product was obtained after flash chromatography (0-10% MeOH/DCM). Yield a yellow solid 0.16 g, 62%; mp 108-110 °C. ¹H NMR (400 MHz, Methanol-*d*₄) δ 7.64 – 7.51 (m, 1H), 7.41 (dd, *J* = 9.5, 5.0 Hz, 2H), 7.33 – 7.13 (m, 8H), 6.95 – 6.87 (m, 3H), 5.35 (dd, *J* = 11.8, 4.4 Hz, 1H), 3.80 – 3.59 (m, 2H), 2.89 – 2.61 (m, 2H), 2.55 – 2.39 (m, 2H). ¹³C NMR (100 MHz, Methanol-*d*₄) δ 171.82, 165.61, 163.15, 162.85, 162.29, 155.33, 153.42, 139.88, 139.07, 133.28, 133.20, 133.03, 132.28, 132.20, 129.03, 128.86, 128.77, 124.28, 121.66, 117.04, 116.80, 116.68, 116.45, 116.22, 60.54, 46.99, 30.33, 29.61. HRMS (*m/z*): [M+H]⁺ calculated for C₂₈H₂₂O₄N₃F₂, 502.15729; found, 502.15790.

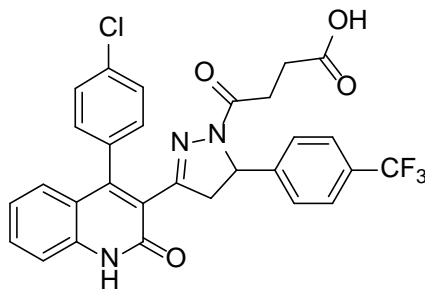


4-(5-(4-chlorophenyl)-3-(4-(5-chlorothiophen-2-yl)-2-oxo-1,2-dihydroquinolin-3-yl)-4,5-dihydro-1H-pyrazol-1-yl)-4-oxobutanoic acid (997-108). Compound **997-108** was prepared via general procedure **J** using pyrazoline amine (0.14 g, 0.32 mmol) and succinic anhydride (32 mg, 0.32 mmol). The product was obtained after flash chromatography (0-10% MeOH/DCM). Yield a yellow foam 62 mg, 36%. ¹H NMR (400 MHz, DMSO-*d*₆) δ 12.34 (s, 1H), 12.08 (s, 1H), 7.59 (ddt, *J* = 8.4, 7.1, 1.7 Hz, 1H), 7.39 (ddt, *J* = 14.6, 8.3, 1.7 Hz, 2H), 7.32 (dd, *J* = 8.9, 2.2 Hz, 2H), 7.25 (t, *J* = 3.4 Hz, 1H), 7.20 (ddt, *J* = 8.2, 7.1, 1.6 Hz, 1H), 7.07 (t, *J* = 3.2 Hz, 1H), 7.03 – 6.95 (m, 2H), 5.44 (dt, *J* = 12.0, 3.6 Hz, 1H), 3.77 (ddd, *J* = 18.3, 12.0, 2.4 Hz, 1H), 2.85 (dt, *J* = 18.4, 3.6 Hz, 1H), 2.77 – 2.54 (m, 2H), 2.39 (ddd, *J* = 14.3, 6.8, 1.9 Hz, 2H). ¹³C NMR (100 MHz, DMSO-*d*₆) δ 173.52, 168.83,

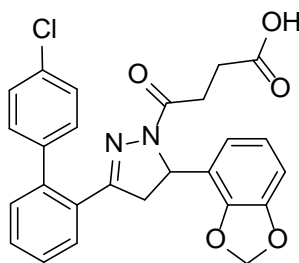
159.75, 152.45, 142.55, 141.07, 138.39, 133.42, 131.69, 131.65, 129.94, 129.42, 128.36, 127.36, 127.06, 126.93, 125.98, 122.63, 119.35, 115.62, 58.43, 45.10, 28.60, 28.27. HRMS (m/z): $[M+H]^+$ calculated for $C_{26}H_{20}O_4N_3Cl_2S$, 540.05461; found, 540.05475.



4-(3-(4-(4-chlorophenyl)-2-oxo-1,2-dihydroquinolin-3-yl)-5-(5-chlorothiophen-2-yl)-4,5-dihydro-1H-pyrazol-1-yl)-4-oxobutanoic acid (997-111). Compound **997-111** was prepared via general procedure **J** using pyrazoline amine (0.15 g, 0.34 mmol) and succinic anhydride (34 mg, 0.34 mmol). The product was obtained after flash chromatography (0-10% MeOH/DCM). Yield a yellow solid 81 mg, 44%. 1H NMR (400 MHz, $DMSO-d_6$) δ 12.40 (s, 1H), 12.22 (s, 1H), 7.73 – 7.61 (m, 2H), 7.51 (dddd, $J = 44.8, 15.2, 6.5, 2.4$ Hz, 4H), 7.26 (q, $J = 8.7, 7.6$ Hz, 1H), 7.15 (d, $J = 8.2$ Hz, 1H), 7.00 (dt, $J = 6.2, 3.0$ Hz, 1H), 6.79 (q, $J = 4.1, 3.4$ Hz, 1H), 5.67 (dt, $J = 11.3, 3.1$ Hz, 1H), 3.76 (ddd, $J = 18.2, 11.4, 2.0$ Hz, 1H), 3.26 (dt, $J = 18.2, 3.0$ Hz, 1H), 2.70 – 2.42 (m, 4H). ^{13}C NMR (100 MHz, $DMSO-d_6$) δ 173.45, 168.80, 160.20, 153.10, 150.01, 143.36, 138.61, 134.04, 133.20, 131.47, 131.01, 130.80, 128.28, 128.16, 127.35, 127.14, 126.00, 123.98, 123.14, 122.40, 119.14, 115.61, 54.37, 44.00, 28.46, 28.17. HRMS (m/z): $[M+H]^+$ calculated for $C_{26}H_{20}O_4N_3Cl_2S$, 540.05461; found, 540.05485.



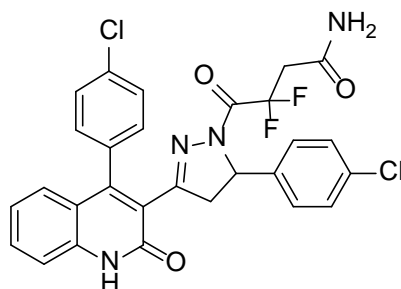
4-(3-(4-(4-chlorophenyl)-2-oxo-1,2-dihydroquinolin-3-yl)-5-(4-(trifluoromethyl)phenyl)-4,5-dihydro-1H-pyrazol-1-yl)-4-oxobutanoic acid (997-112). Compound **997-112** was prepared via general procedure **J** using pyrazoline amine (0.20 g, 0.43 mmol) and succinic anhydride (43 mg, 0.43 mmol). The product was obtained after flash chromatography (0-10% MeOH/DCM). Yield a yellow solid 0.14 g, 56%. ^1H NMR (400 MHz, DMSO- d_6) δ 7.63 – 7.54 (m, 4H), 7.47 (dd, $J = 8.2, 2.3$ Hz, 1H), 7.43 (dd, $J = 8.2, 2.0$ Hz, 2H), 7.27 (dd, $J = 8.2, 2.2$ Hz, 1H), 7.14 (ddd, $J = 8.3, 7.1, 1.2$ Hz, 1H), 7.05 – 6.98 (m, 3H), 5.45 (dd, $J = 12.1, 4.5$ Hz, 1H), 3.77 (dd, $J = 18.5, 12.1$ Hz, 1H), 2.76 (dd, $J = 18.5, 4.5$ Hz, 1H), 2.68 – 2.44 (m, 2H), 2.33 (t, $J = 7.1$ Hz, 2H). ^{13}C NMR (100 MHz, DMSO- d_6) δ 173.69, 168.93, 160.12, 152.64, 149.91, 146.63, 138.58, 134.01, 133.21, 131.44, 130.50, 128.33, 127.86, 127.54, 127.24, 126.11, 125.53, 125.30, 123.43, 122.38, 119.12, 115.60, 58.42, 45.13, 28.63, 28.53. HRMS (m/z): $[\text{M}+\text{H}]^+$ calculated for $\text{C}_{29}\text{H}_{22}\text{O}_4\text{N}_3\text{ClF}_3$, 568.12454; found, 568.12507.



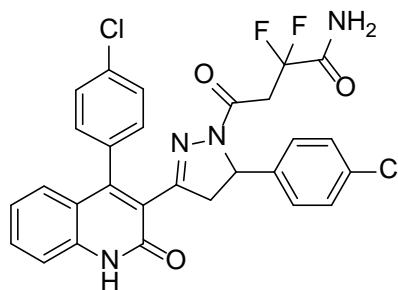
4-(5-(benzo[d][1,3]dioxol-4-yl)-3-(4'-chloro-[1,1'-biphenyl]-2-yl)-4,5-dihydro-1H-pyrazol-1-yl)-4-oxobutanoic acid (997-122). Compound **997-122** was prepared via general procedure **J** using pyrazoline amine (0.20 g, 0.53 mmol) and succinic anhydride (53 mg, 0.53 mmol). The product was obtained after flash chromatography (0-10% MeOH/DCM). Yield a yellow solid 94 mg, 37%; mp 85-90 °C. ¹H NMR (400 MHz, DMSO-*d*₆) δ 12.19 (s, 1H), 7.72 (dd, *J* = 7.6, 1.5 Hz, 1H), 7.54 (dtd, *J* = 18.2, 7.4, 1.5 Hz, 2H), 7.43 – 7.36 (m, 1H), 7.34 – 7.24 (m, 4H), 6.90 – 6.76 (m, 2H), 6.52 (dd, *J* = 7.9, 1.2 Hz, 1H), 5.98 (dd, *J* = 33.7, 1.0 Hz, 2H), 5.39 (dd, *J* = 11.7, 4.3 Hz, 1H), 3.42 (dd, *J* = 17.9, 11.8 Hz, 1H), 2.72 – 2.56 (m, 2H), 2.55 – 2.51 (m, 1H), 2.40 (t, *J* = 6.7 Hz, 2H). ¹³C NMR (100 MHz, DMSO-*d*₆) δ 173.60, 168.92, 155.25, 147.22, 143.57, 139.80, 139.65, 132.19, 130.52, 130.48, 130.30, 129.85, 129.38, 128.07, 127.97, 123.01, 121.43, 119.09, 107.46, 100.93, 54.75, 42.59, 28.44, 28.30. HRMS (*m/z*): [M+H]⁺ calculated for C₂₆H₂₂O₅N₂Cl, 477.12227; found, 477.12172.

General procedure K for the synthesis of difluoro-4-oxobutanamide. In a round-bottomed flask, difluoro-substituted carboxylic acid (1 equiv.) was dissolved in DCM (0.3 M). Then oxalyl dichloride (2.5 equiv.) was added dropwise, followed by one drop of DMF. The reaction was stirred for approximately 40 minutes. The solvent and excess oxalyl dichloride was removed under vacuum and the product was obtained by Kugelrohr distillation at 98 °C with full vacuum. Used immediately. Then a solution of resultant

compound in DCM was added slowly to excess ammonia solution (0.5 M in dioxane) under nitrogen. The mixture was stirred at room temperature overnight. The completion of the reaction was monitored by LC-MS. The solvent was evaporated *in vacuo*, and the crude was purified by amine column chromatography using 0-10% MeOH/DCM gradient.



4-(5-(4-chlorophenyl)-3-(4-(4-chlorophenyl)-2-oxo-1,2-dihydroquinolin-3-yl)-4,5-dihydro-1H-pyrazol-1-yl)-3,3-difluoro-4-oxobutanamide (997-96). Compound **997-96** was prepared via general procedure **K** using **997-74** (0.25 g, 0.44 mmol), oxalyl dichloride (0.14 mg, 1.1 mmol), and ammonia solution (18 ml, excess). The product was obtained after flash chromatography (amine column, 0-10% MeOH/DCM). Yield as yellow solid 0.11 g, overall 43%; mp 152-158 °C. ^1H NMR (400 MHz, DMSO- d_6) δ 12.31 (s, 1H), 7.62 – 7.46 (m, 3H), 7.42 (dtd, $J = 8.3, 4.2, 2.5$ Hz, 2H), 7.34 – 7.21 (m, 3H), 7.19 – 7.10 (m, 2H), 7.06 – 6.99 (m, 1H), 6.95 – 6.90 (m, 1H), 5.53 – 5.42 (m, 1H), 3.85 – 3.72 (m, 1H), 3.26 – 3.00 (m, 2H), 2.70 (ddd, $J = 18.5, 4.6, 1.5$ Hz, 1H). ^{13}C NMR (100 MHz, DMSO- d_6) δ 159.92, 155.33, 150.05, 139.88, 138.59, 133.61, 133.39, 131.79, 131.57, 131.08, 130.05, 128.54, 128.48, 128.22, 127.44, 127.21, 123.02, 122.44, 119.01, 115.60, 59.44, 44.65, 41.50. HRMS (m/z): $[\text{M}+\text{H}]^+$ calculated for $\text{C}_{28}\text{H}_{21}\text{O}_3\text{N}_4\text{Cl}_2\text{F}_2$, 569.09533; found, 569.09572.



4-(5-(4-chlorophenyl)-3-(4-(4-chlorophenyl)-2-oxo-1,2-dihydroquinolin-3-yl)-4,5-dihydro-1H-pyrazol-1-yl)-2,2-difluoro-4-oxobutanamide (997-115). Compound **997-115** was prepared via general procedure **K** using **997-114** (0.34 g, 0.60 mmol), oxalyl dichloride (0.19 g, 1.5 mmol), and ammonia solution (25 ml, excess). The product was obtained after flash chromatography (amine column, 0-10% MeOH/DCM). Yield as yellow solid 0.11 g, overall 31%; mp 133-137 °C. ^1H NMR (400 MHz, DMSO- d_6) δ 12.31 (s, 1H), 7.87 (d, $J = 79.1$ Hz, 2H), 7.64 – 7.51 (m, 3H), 7.43 (dt, $J = 8.3, 1.9$ Hz, 2H), 7.30 (dq, $J = 9.3, 2.4$ Hz, 3H), 7.15 (ddd, $J = 8.2, 7.0, 1.2$ Hz, 1H), 7.03 (dd, $J = 8.2, 1.4$ Hz, 1H), 6.88 – 6.82 (m, 2H), 5.37 (dd, $J = 11.9, 4.4$ Hz, 1H), 3.82 – 3.70 (m, 1H), 3.37 – 3.09 (m, 2H), 2.85 (dd, $J = 18.6, 4.4$ Hz, 1H). ^{13}C NMR (100 MHz, DMSO- d_6) δ 164.98, 164.70, 162.56, 160.09, 153.92, 150.08, 140.52, 138.61, 134.05, 133.30, 131.80, 131.56, 131.33, 130.58, 128.40, 128.30, 127.33, 123.06, 122.45, 119.12, 115.86, 115.61, 58.10, 45.39, 37.82. HRMS (m/z): $[\text{M}+\text{H}]^+$ calculated for $\text{C}_{28}\text{H}_{21}\text{O}_3\text{N}_4\text{Cl}_2\text{F}_2$, 569.09533; found, 569.09536.

2.4.2 Evaluation of Enantiomers

Reverse phase chiral chromatography was used to separate racemic compounds by using a ChiralPak OD-RH column (30 mm X 250 mm, 5 μM). The racemic compound was dissolved in methanol and diluted with a solvent of 60% ACN (0.1% Formic acid): 40% H_2O (0.1% Formic acid). The system was pre-flashed with 60% ACN (0.1% Formic acid): 40% H_2O (0.1% Formic acid) and then the sample was injected into the system (4-6 ml per

injection with 2-3 mg/ml compound) with flow rate of 10 ml/min. One enantiomer came out around 17-18 minutes, while the other enantiomer came out around 21 minutes. The enantiomeric excess (e.e.) of (*S*)-**997-74** and (*R*)-**997-74** was determined using an Agilent 1200 HPLC pump on a ChiralPak OD-RH column (4.6 mm X 150 mm, 5 μ M) using the following conditions: Flow rate 1 ml/min, injection volume 10 μ l, 60% ACN (0.1% Formic acid) : 40% H₂O (0.1% Formic acid); both enantiomers of **997-74** are 100% e.e.. Optical rotation data was collected using a Perkin-Elmer 314 instrument. (*S*)-**997-74**, $[\alpha]_{\text{D}}^{20}$ -56.0 (c = 1 mg/ml, MeOH), (*R*)-**997-74** $[\alpha]_{\text{D}}^{20}$ + 55.0 (c = 1 mg/ml, MeOH). The melting point of (*S*)-**997-74** was 185-187 °C.

2.4.3 X-ray

Single colorless plate-shaped crystals (+) **997-74** were recrystallized by methanol and ethyl acetate. A suitable crystal (0.50 * 0.40 * 0.18) was selected and mounted on a loop with paratone oil on a Bruker APEX-II CCD diffractometer. The crystal was cooled to $T = 100(2)$ K operated by an Oxford Cryosystems low-temperature apparatus during the data collection. The structure was solved using Olex2 (Dolomanov et al., 2009) as the graphical interface for the crystallographic calculation and with Superflip (L. palatinus & G. Chapuis, 2007) via the Charge Flipping solution method. The model was refined with ShelXL-97 (Sheldrick, 2008) by using Least Squares minimization. Crystal Data: C₃₀H₂₅Cl₂F₂N₃O₅, $M_r = 616.43$, monoclinic, P2₁ (No. 4), $a = 8.2731(9)$ Å, $b = 9.5335(10)$ Å, $c = 18.434(2)$ Å, $\beta = 94.719(2)^\circ$, $\alpha = \gamma = 90^\circ$, $V = 1449.0(3)$ Å³, $T = 100(2)$ K, $Z = 2$, $Z' = 1$, $\mu(\text{MoK}\alpha) = 0.282$, 18906 reflections measured, 8732 unique ($R_{\text{int}} = 0.0223$) which were used in all calculations. The final wR_2 was 0.0856 (all data) and R_I was 0.0335 ($I > 2(I)$). Crystal was selected and solved by Marika Wieliczko and John Bacsá, Ph.D. at the

Emory X-crystallography core facility.

2.4.4 Two-electrode voltage-clamp recording

Two-electrode voltage-clamp recording that performed in *Xenopus laevis* oocytes were injected with mRNA to express recombinant rat GluN1/GluN2A, GluN1/GluN2B, GluN1/GluN2C, and GluN1/GluN2D. The recordings using *Xenopus laevis* were permitted by Emory University Institutional Animal Care and Use Committee (IACUC). cDNAs for rat NMDA subunits GluN1-1a (GenBank U08261; hereafter GluN1), GluN2A (GenBank D13211), GluN2B (GenBank U11419), GluN2C (GenBank M91563), GluN2D (GenBank L31611), GluA1 (GenBank X17184), and GluK2 (GenBank Z11548) were provided by Drs. S. Heinemann from Salk Institute, S. Nakanishi from Kyoto University, and P. Seeburg from the University of Heidelberg. An automatic injector (Nanoject II, Drummond Scientific) was used for cRNA injection using the pipettes filled with mineral oil. The cRNA that transcribed in vitro via the mMessage Machine kit (Ambion) was diluted with nuclease-free water, and then injected at GluN1/GluN2 with a ratio of 1:2. The oocytes were stored in Barth's solution that contained 88 mM NaCl, 5.0 mM Tris-HCl, 2.4 mM NaHCO₃, 1.0 mM KCl, 0.84 mM MgSO₄, 0.41 mM CaCl₂, 0.33 mM Ca(NO₃)₂, 0.1 mg/ml gentamycin sulfate, 1.0 U/ml penicillin, and 1µg/ml streptomycin at a pH of 7.4 and temperatures of 15-17 °C for two to five days before the two-electrode voltage-clamp recordings. When recording, the oocytes were placed in a perfusion chamber and continually washed with the recording solution comprised of 90 mM NaCl, 1.0 mM KCl, 0.50 mM BaCl₂, 0.005 mM EDTA, and 10 mM HEPES at a pH of 7.4 and a temperature of 23 °C. Glass electrodes with a tip resistance of 0.5 to 2.5 MΩ were obtained from thin-walled glass capillary tubes. Voltage electrodes and current electrodes were filled with 0.3

M and 3.0 M KCl, respectively. The recordings were executed with the oocytes membrane potential holding at -40 mV by an OC-725 amplifier (Warner Instrument Co). All compounds were dissolved in dimethyl sulfoxide (DMSO) as 20 mM stock solutions and future diluted to reach the desired concentration (0.05-0.5% (vol/vol) DMSO) in recording solution comprised of 30 μ M glycine and 100 μ M glutamate. Each compound was recorded 3-7 times in the least 4 oocytes from at least 2 different *Xenopus laevis*.

2.4.5 Data Analysis

To evaluate the inhibition of compounds, the concentration-response curve was fitted with the average two-electrode voltage-clamp recording results with the equation

$$response = 100 / \{1 + [(inhibitor\ concentration) / IC_{50}]^N\}$$

where IC_{50} is the concentration of compounds that inhibit half maximal of the current response and N is the Hill slope. Compounds with less than 30% inhibition at 30 μ M will display NE (not effective) in the figures.

To assess the potentiation of compounds, the concentration-response curve was fitted with the average recording results with the equation

$$response = 100 / \{1 + [EC_{50} / (agonist\ concentration)]^N\}$$

where EC_{50} is the concentration of compounds that potentiate half maximal of the current response and N is the Hill slope. EC_{50} is used to evaluate several antagonists.

Chapter 3. QSAR study of 997-series

3.1 Introduction

Quantitative structure-activity relationship (QSAR) is a valuable tool to find statistically reliable correlations between chemical structures and biological activities by building mathematical or computational models and predict biological and pharmaceutical activities of prospective compounds [93-95]. Due to the large number of compounds that need to be synthesized from HTS, as well as the high cost and time-consuming conventional syntheses methods and biological assays, QSAR is a useful alternative to rapid predict the candidates [95]. QSAR follows several general steps: dataset preparation, descriptor calculation, descriptor selection, dataset division (training and test sets), model building (select appropriate statistical data analysis method), validation, and model evaluation [96] (*Figure 13*). The molecular descriptors are typically numerical values that represent a set of chemical and structural information to apply mathematical calculation. Molecular descriptors contain the essential physicochemical information, such as electronic, hydrophobic, lipophilicity, geometrical, solubility, steric, and topological properties [97]. Not all the descriptors are necessary to build an appropriate model. Because only a small set of descriptors carries useful information, descriptor selection acts as a crucial step to get rid of the redundant or irrelevant descriptors. By generating the appropriate statistical model, QSAR identifies the significant correlation between the molecular descriptors and their relative biological activities. Many statistical methods have been reported to build QSAR models, such as multiple linear regression (MLR), partial least-squares (PLS), principal component analysis/regression (PCA/PCR), artificial neural networks (ANN), k -nearest neighbors (k NN), Bayesian neural nets, and genetic algorithm

(GA) [93]. These approaches could be widely applied in drug discovery, lead optimization, toxicity prediction, regulatory decisions, and mechanistic interpretation [96]. However, there are several limitations of applying QSAR that need to be tackled. A sufficient number of compounds must be included in the dataset with their bioactivity data. The number of molecular descriptors could be restricted by the size of the dataset. Moreover, the outliers from the dataset may result in inaccuracy of the results [94]. For all the type of methods, QSAR assumes that all the compounds in the data set bind to the identical site of the target receptor [98]. QSAR methods can also be categorized by its dimensionality (1D- to 6D-QSAR) [93, 95]. In this thesis, I will focus on the 2D- and 3D-QSAR.

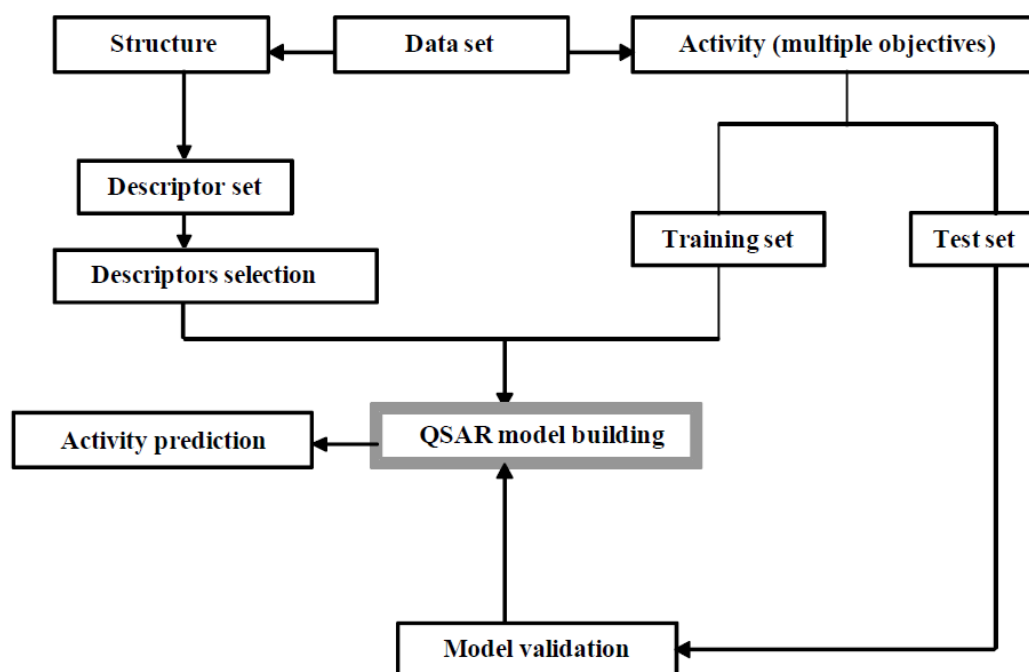


Figure 13. Flowchart of a general QSAR study.

3.2 2D-QSAR study of 997-series

3.2.1 Introduction of 2D-QSAR

2D-QSAR plays a significant role in revealing the relationships between molecular structures and biological activities. 2D model-based descriptors are the key elements,

which include octanol/water partition ($\log P$), topological polar surface area (TPSA), pK_a , and 2D molecular fingerprints [99-101]. The molecular fingerprints, such as atom pairs, topological torsions, and circular substructures, are arrays of binary or integer digits that correspond to the presence and absence of all chemical substructures [102, 103]. 2D-QSAR can be classified as linear methods and non-linear methods [95]. MLR belongs to a linear method which simply provides a linear relationship between 2D descriptors and biological activities. PLS is another linear approach that can deal with highly correlated descriptors by performing PCA before running the regression [99, 104-106]. Another method of predictions, called decision trees, applies a series of descriptor-based regulations to each compound. The non-linear k NN algorithm requires the function of the Euclidean distance of the normalized input descriptors and predicts the activities based on the known activities of the k nearest neighbors from training sets [99]. Some machine learning techniques, such as random forest, support vector machine (SVM), ANN, are commonly used in the pharmaceutical industry [99]. These techniques are all non-linear models and perform better prediction. QSAR models can be categorized as regression models and classification models [99]. Regression models are typically used to evaluate the correlation between the predicted activities and measured activities for the cross-validation set or test set. Correlation charts obtained from the models provide the information of the strength of the correlation, the presence of outliers, and the range of the data values [99]. Several statistical parameters are used to evaluate and assess regression models and include the root-mean-square deviation (RMSE), R-squared (r^2), and Q-squared (q^2) [107]. RMSE is analogous to the standard deviation (SD) for the distribution of prediction errors. r^2 is the square of Pearson's correlation coefficient which determines the performance of a regression model

[99]. The value of r^2 is ranged from 0 to 1. A value of 0 means no correlation, while a value of 1 indicates a perfect correlation. Another statistic q^2 is used to assess the accuracy of prediction. The max value of q^2 is 1.0 which indicates a perfect prediction, while a negative value shows a worse prediction than all compounds predict the mean value. One of the purposes of building 2D-QSAR models is to predict the activity of un-synthesized candidates, which can help chemists construct their hypothesis and save time and money on undesirable compounds. Another purpose is to evaluate and highlight regions of molecules that favorably or unfavorably contribute to the biological activity [108]. In this thesis, I will focus on building a 2D-QSAR model and analyze which functional groups are unfavorable for increasing the activity of 997 series.

3.2.2 AutoQSAR study of 997-series

3.2.2.a Introduction of autoQSAR

AutoQSAR is an automated application to create, validate, distribute, and deploy predictive QSAR models. A single workflow within autoQSAR includes descriptor generation, feature selection, creation of a large number of QSAR models using a variety of methods, such as kernel-based partial least squares (KPLS), naïve bayes, and ensemble-based recursive partitioning with multiple random training/test set splits, and QSAR models ranking by performance. Reliable predictions are enabled using a consensus or a single QSAR model. Using autoQSAR for QSAR modeling has several key benefits. For instance, QSAR models can be generated and employed with confidence. AutoQSAR can be used to identify approaches most/least likely to be successful before manual QSAR modeling, which could save time for researchers. Moreover, autoQSAR has no descriptor limitation, and easily integrates into informatics platform. An estimate of the applicability

domain of the QSAR model using structural similarity among the training set provides a yes/no indication of whether to trust the model predictions. AutoQSAR can easily connect to existing cheminformatics platforms and regenerate the models as more data become available to improve prediction accuracy. Therefore, autoQSAR can be used with drug discover projects to provide confidence when making predictions of new candidates.

3.2.2.b Data preparation and autoQSAR model creation

The 997-series were prepared for autoQSAR model generation and the IC₅₀ data were converted into pIC₅₀ values. 122 out of total of 149 compounds with defined GluN2D pIC₅₀ values use in this experiment. AutoQSAR models were generated using the GluN2D pIC₅₀ values as prediction property. The dataset was randomly split into a validation set (25%), and the rest of compounds were separated into a training set (75%) and test set (25%) (structures 122 total, 68 training, 23 test, 31 validation). The number of models to build for each model type (MLR, PLS, PCR, Kernel-based PLS, Naïve Bayes, and ensemble recursive partitioning (RP)) was set as default 50, while the maximum allowed correlation between any pair of independent variables was set as 0.8. Descriptors used in this experiment were set as the default binary fingerprints (radial, linear, dendritic, molprint2D) or molecular properties (canvasMolDescriptors).

3.2.2.c AutoQSAR model analysis

The ten top-ranked QSAR models were kept for future prediction (*Table 11*). All these models performed well with good R² and Q² values and a small null hypothesis Q² values, which show that the activity data does not correlate well with molecular weight. Model code `kpls_dendritic_1` indicated that the QSAR model was generated by KPLS fitting with dendritic fingerprints, using the first split of the learning set into a test and

training set.

Table 11. Ten top-ranked QSAR models.

Model Code	Score	S.D.	R ²	RMSE	Q ²	Q ² MW (Null)
kpls_dendritic_1	0.8701	0.2846	0.8742	0.2788	0.8725	0.2996
kpls_linear_19	0.8544	0.3055	0.8537	0.2933	0.8620	0.3085
kpls_dendritic_50	0.8437	0.2998	0.8607	0.3004	0.8514	0.3629
kpls_dendritic_19	0.8234	0.3086	0.8507	0.3158	0.8400	0.3085
kpls_linear_50	0.8193	0.2963	0.8638	0.3122	0.8395	0.3629
kpls_linear_42	0.8035	0.3603	0.7973	0.3169	0.8296	-0.1734
kpls_dendritic_28	0.7989	0.3458	0.8145	0.3434	0.7957	0.2219
kpls_dendritic_13	0.7973	0.3563	0.7959	0.3460	0.8089	0.2806
kpls_dendritic_42	0.7967	0.3648	0.7922	0.3339	0.8109	-0.1734
kpls_desc_50	0.7728	0.4032	0.7596	0.3072	0.8446	0.3629

The best QSAR model for predicting the GluN2D pIC₅₀ values was the first model shown in the table with model code of kpls_dendritic_1. The correlation coefficient of the training set was 0.8742, while the correlation coefficient of the test set was 0.8725, which demonstrated that there was a strong linear association between the dendritic fingerprints and GluN2D pIC₅₀ values. The report for the best model kpls_dendritic_1 and a scatter plot of the performance in predicting GluN2D pIC₅₀ of this model (*Figure 14*, Appendix B) are

shown as below for an example:

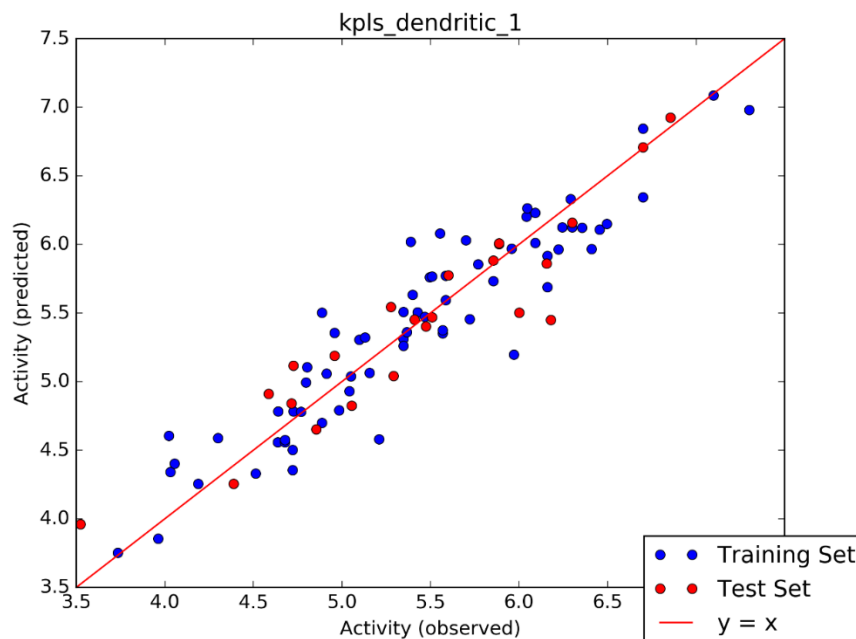


Figure 14. Observed and predicted GluN2D pIC₅₀ values of training (blue) and test (red) sets.

3.2.2.d Analyzing predictions and identifying outliers.

After generating the top-ranked QSAR models, the models can be used to make predictions of GluN2D pIC₅₀ for 997 compounds. The models were tested using a validation set which is a compound set that was not used prior in neither the training nor test set. The 10 models are therefore completely naïve to the compounds within the validation set. The results from the validation set provides a good idea of how well a model will perform when used to predict compounds congeneric to training set.

A consensus model prediction was performed using all 10 models. Predictions made with autoQSAR were analyzed to evaluate its accuracy and the ability to identify compounds that fall outside the applicability domain of the model (training set). The estimate of the domain of applicability provides a yes/no indication of whether to trust the

prediction of a model. The resulting scatter plot is shown in *Figure 15*. The X-Axis represents the GluN2D pIC₅₀ values, while the Y-Axis represents the predicted GluN2D pIC₅₀ values. *Figure 15* show a scatter plot colored by alerts on the predicted GluN2D pIC₅₀ domains. Compounds that are colored in green show a domain alert, which indicated that these compounds were outliers that fall outside the applicability domain and the predictions were not expected to be accurate. The best fit line was also plotted with an equation of

$$y = 0.76x + 1.30 (R^2 = 0.84)$$

where y represented predicted GluN2D pIC₅₀ values, while x represented observed GluN2D pIC₅₀ values. The plot showed the consensus QSAR model predictions in the predicted GluN2D pIC₅₀ values reproduce experimental pIC₅₀ well with an R² of 0.84.

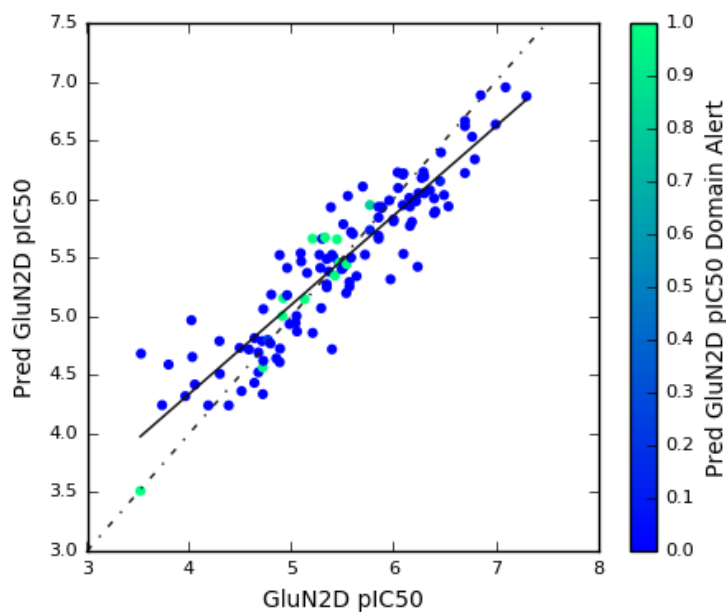


Figure 15. Observed and predicted GluN2D pIC₅₀ values with domain alert of outliers.

Eleven compounds were colored in green as outliers. Two of them, **1248** and **997-78**, lacked the acyl chain (*Figure 16*). Since the acyl chain was suggested as an essential

fragment of 997 structure, these two compounds were removed from the plot.

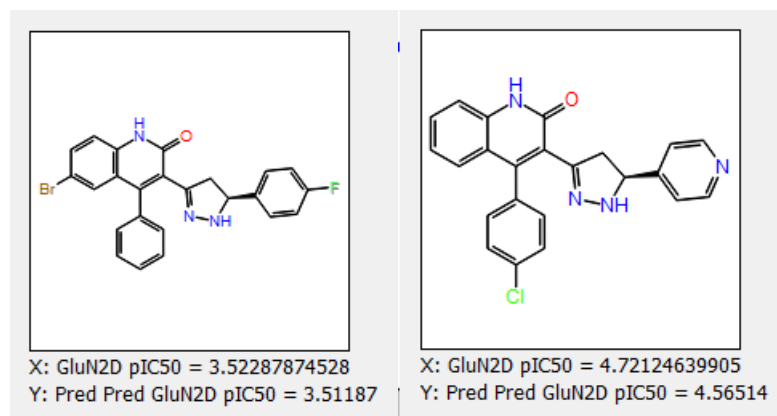


Figure 16. Outliers 1248 and 997-78.

However, the other 9 compounds were structurally related but assigned as outliers because they fell outside the 95% confidence interval used to set the applicability domain alerts (*Figure 17*). Since the activity values of these compounds were significant to improve this project, these compounds were kept in the dataset.

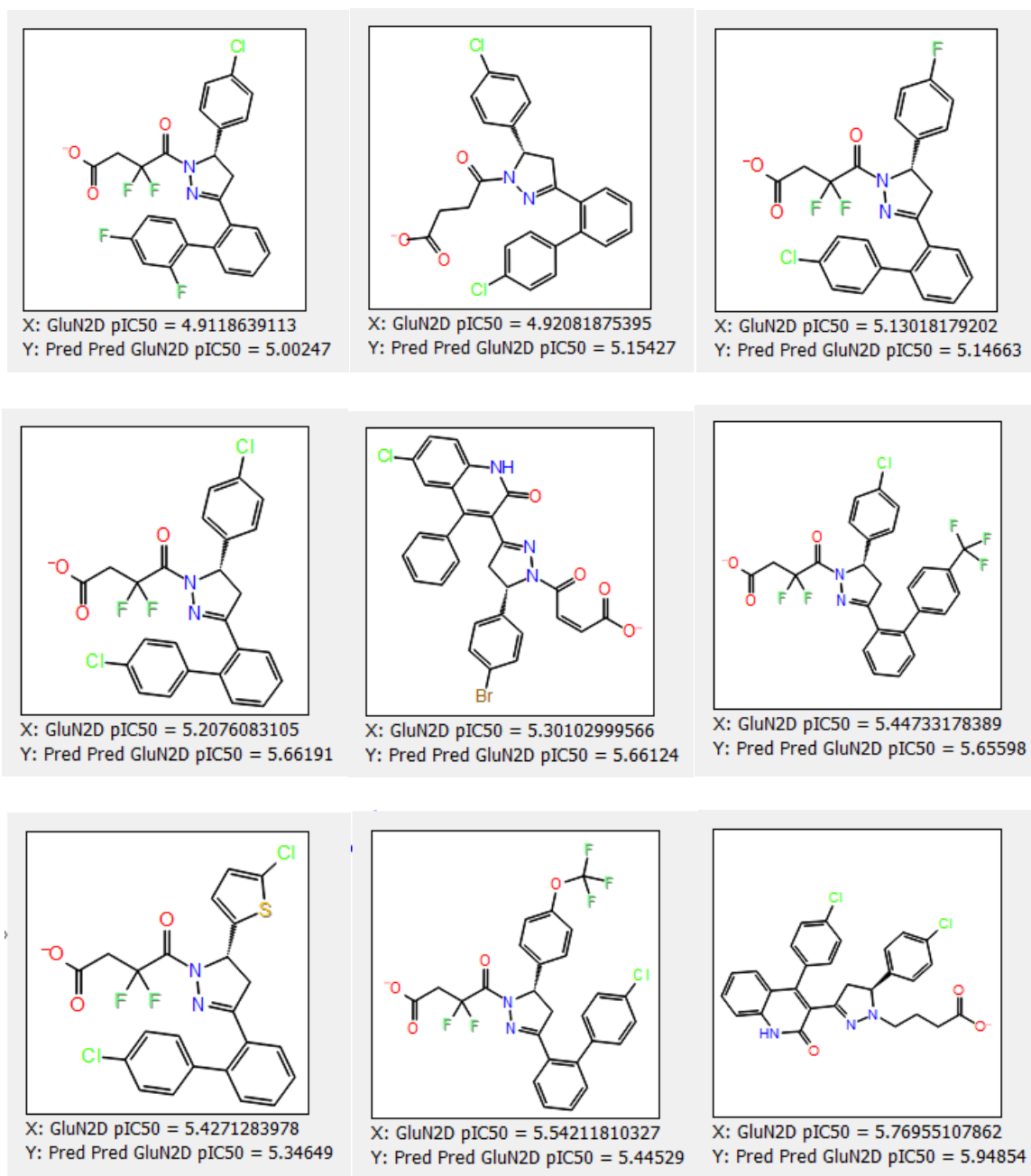


Figure 17. Outliers with structure related.

Based on the analysis of outliers, compounds **1248** and **997-78** were eliminated, and the plot was regenerated (Figure 18) with an equation of

$$y = 0.74x + 1.39 \quad (R^2 = 0.83)$$

Although the correlation coefficient R^2 was not improved, a better equation was obtained for future prediction. Using this QSAR model with regenerated equation and domain alert, we can predict the future candidates with more confident. As new compounds become available, the QSAR model can be automatically regenerated leading to improved predictive accuracy and applicability. With the QSAR model refining, the future compounds can be predicted with the 95% confidence interval.

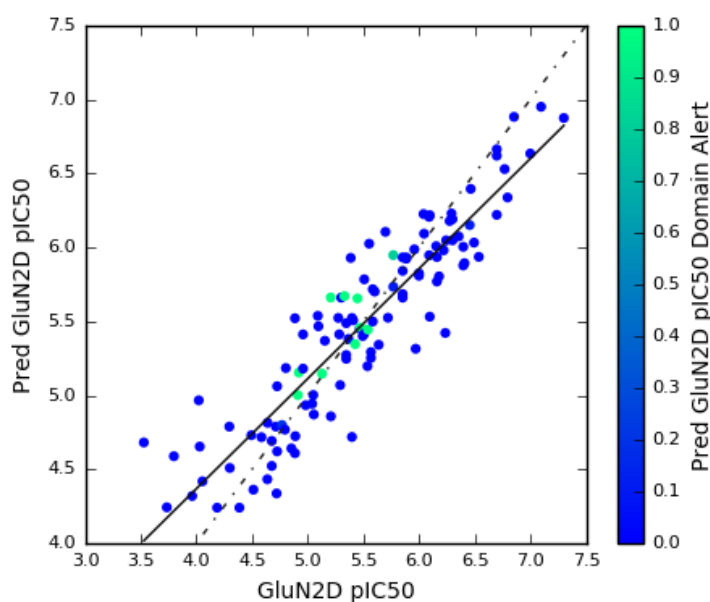


Figure 18. Observed and predicted GluN2D pIC50 values with domain alert of outliers without compound 1248 and 997-78.

According to the autoQSAR model selection, the best statistical method is the kernel-based PLS (KPLS) regression with dendritic fingerprints. Therefore, a 2D-QSAR model using KPLS method is built to future explore regions of molecules that favorably or unfavorably contribute to the biological activity.

3.2.3 KPLS model

3.2.3.a Introduction of KPLS

Numerous QSAR prediction tools exist, here we implemented a kernel-based PLS (KPLS) method, which is a fast and effective method for QSAR predictions in the Schrödinger modeling suite [108, 109]. We used the KPLS model to identify and highlight regions of our congeneric series that contributes positively and negatively to the biological activity. The KPLS regression method is an extension of PLS regression methods which incorporate nonlinearity into the scalar products of independent variables via a “kernel” nonlinear function. The kernel used by Schrödinger is a Gaussian function,

$$K(i, j) = \exp(-d_{ij}^2/\sigma_{ij}^2)$$

where d_{ij} is the Euclidean distance between independent variables i and j , and σ is the non-linearity parameter [110]. The KPLS method uses Canvas dendritic fingerprints and is used in KPLS regression model generation [110]. Each Canvas fingerprint bit represents a unique chemical fragment [111, 112]. The advantage of using the KPLS method is that the atomic contributions of a model can be mapped to molecules allowing the favorable and unfavorable fragments to be analyzed and visualized [108]. According to the autoQSAR model selection, the KPLS method was selected to build a 2D-QSAR model for 997 active compounds.

3.2.3.b KPLS model creation

The 997-series were prepared as described above. Dendritic fingerprints were generated due to the robustness of structural characterization of the fingerprints [108]. All compounds with the GluN2D-containing receptors (compounds with a valid pIC₅₀, a total of 122 compounds) were selected. GluN2D pIC₅₀ were selected as the Y variables, while

dendritic fingerprints represented as X variables. The dataset was randomly split into a 75% training set and 25% test set (generate seed: 3360439155). To estimate the uncertainty in the predictions for the test set, bootstrapping was used to sample the training set randomly with replacement to generate a new test set of the same size [110]. In this case, 10 bootstrapping cycles were used. KPLS model was built, and the results are shown below (Table 12):

Table 12. QSAR statistics of KPLS model.

#KPLS Factors	Training SD	R ²	Test RMSE	Q ²
1	0.5049	0.6316	0.4507	0.6686
2	0.3622	0.8125	0.4507	0.6685
3	0.2803	0.8890	0.3891	0.7530
4	0.2350	0.9228	0.3865	0.7563
5	0.1971	0.9464	0.4329	0.6943
6	0.1788	0.9564	0.4295	0.6990
7	0.1467	0.9710	0.4668	0.6444
8	0.1317	0.9769	0.4894	0.6092
9	0.1194	0.9812	0.5069	0.5807
10	0.1080	0.9849	0.5134	0.5700

3.2.3.c Results and discussion:

It was observed that both the Q² and R² values of the training and test sets increased as the KPLS factors (independent variables) increased. To select good models, the number

of KPLS factors should neither be excessively larger nor small to prevent over- or under-fitting (Rule of thumb is to not exceed KPLS factors more than the (number of compounds/5) or more than 10). Here we selected four KPLS factors, which showed a RMSE value of 0.3865, R^2 and Q^2 values of 0.9228 and 0.7563 respectively. A scatter plot show the GluN2D pIC_{50} values (X variable) versus the predicted GluN2D pIC_{50} values (Y variables) as predicted by this model (*Figure 19*).

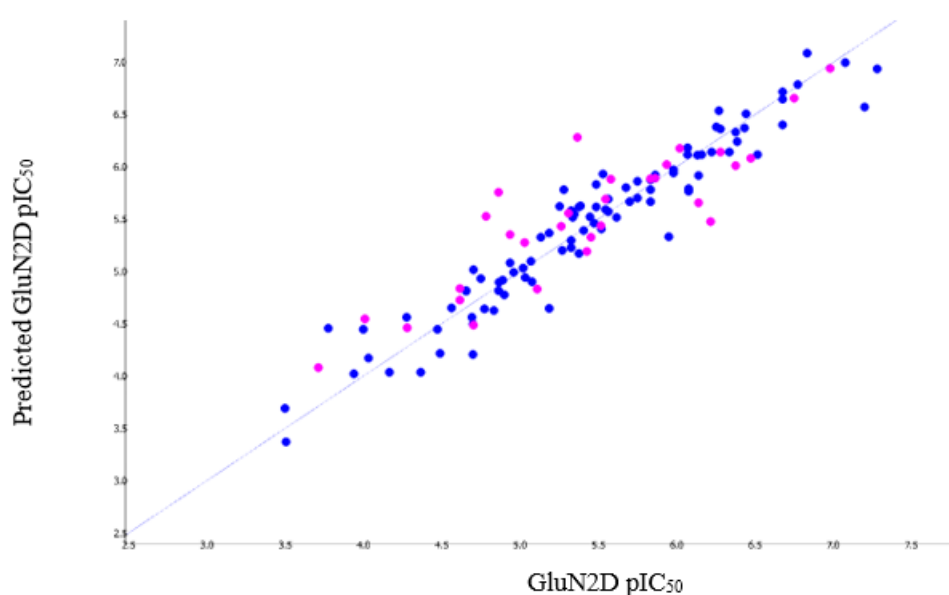


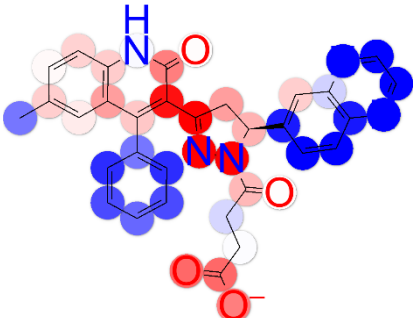
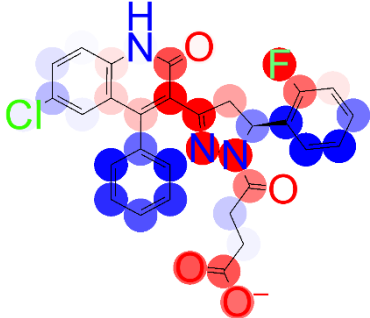
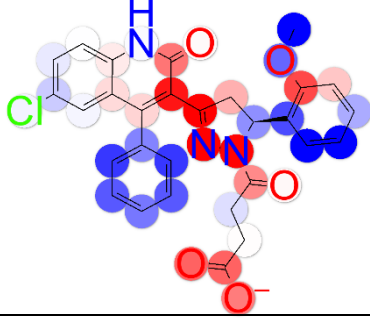
Figure 19. Predicted and observed GluN2D pIC_{50} for training set (blue) and test set (magenta) compounds using KPLS models constructed from dendritic fingerprints.

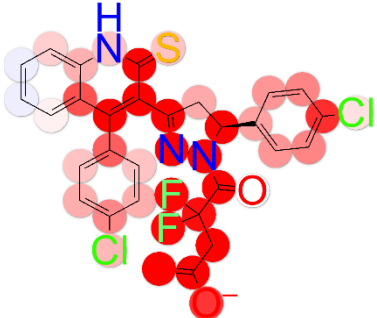
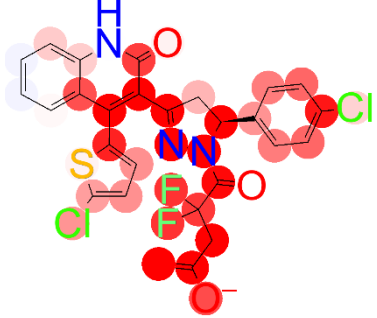
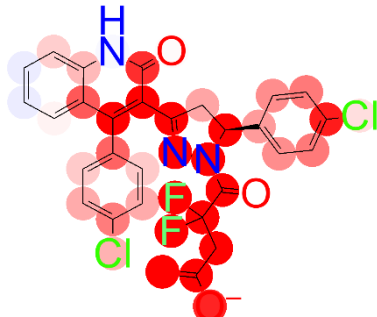
The training set compounds are colored in blue, and the test set is colored magenta. The dots are evenly distributed around the diagonal line, indicating the GluN2D pIC_{50} values are well predicted. Because of the fingerprints are used to build this model, the contributions of each atom to the model could be visualized as shown in Table. The visualized models of each compound are shown with the atomic contributions or the sensitivity of the predictions of each atom highlighted by color. The red colored spheres

represented the positive atomic contributions that increase the predicted activity, while the blue color indicated the negative atomic contributions that decrease the predicted activity.

The saturation color represents the magnitude of the atomic contribution (*Table 13*).

Table 13. Visualized structures of least active and most active compounds. Red circles contribute positive to the model whereas blue circles contribute negative to the model.

	Observed pIC ₅₀	Predicted pIC ₅₀	Visualized Structures
2071	3.529	3.393	
2065	4.301	4.483	
997-18	4.387	4.058	

997-98	6.854	7.109	
997-109	7.000	6.960	
997-74	7.301	6.956	

For the least active compounds **2071**, **2065**, and **997-18**, top B-phenyl ring without any substitutions are represented with solid blue colored spheres, which show a strong negative atomic contribution to the predicted activity at the GluN2D-containing receptor, in another word, is unfavorable to the predicted activity (*Table 13*). The methyl group on the quinolone ring of compound **2071** is also colored in blue, which negatively contributes to the predicted activity. Replacing methyl group to the chlorine substitution results in the increasing of the predicted activity. The A ring with naphthalene moiety of compound **2071** is strongly unfavored to its predicted activity. Compared with the naphthalene group, the electronegative *ortho*-fluorophenyl ring of compound **2065** positively contributes to the

predicted activity. The methoxy group instead of fluorine substitution on the phenyl ring slightly decreased the contribution effect, which results in a decreased predicted activity of compound **997-18**. However, the observed pIC₅₀ value of **997-18** is slightly higher than the observed value of **2065**. In addition, the α - and β -carbons of the acyl chain show moderate or slight negative contributions to the predicted activity. The visualized models of the most active compounds **997-98**, **997-109**, and **997-74** are also shown in Table. The *para*-chlorine substitutions on both A- and B-phenyl ring positively contribute to the predicted activity. The difluoro-substitution on the acyl chain for these compounds significantly improves the atomic contribution effect. The pyrazoline ring in the center of these compounds still positively contributes to the predicted activity. Notably, compound **997-98** with positive contributed thioamide group is predicted to be more active than compound **997-74**, however the observed activity value of compound **997-98** is lower than the value of compound **997-74**. Finally, the phenyl ring of the quinolone moiety retains slight negative or moderate contribution to the predicted activity, which could be eliminated or replaced with other substitutions.

In conclusion, the KPLS model highlighted features that influence the biological activity of the 997-series either positively or negatively. The KPLS model generated here can not only be used to better understand the SAR of the 997-series but also help rank and predict compounds for future synthesis and testing. Both autoQSAR and KPLS models can be used as predicting tools to provide future candidates, while the future compounds will be included in the dataset and regenerate more powerful QSAR models.

3.3 Field-based 3D-QSAR study of 997-series

3.3.1 Introduction of 3D-QSAR

Although 2D-QSAR has been used for decades and performs simple and fast prediction of the activities of a large number of compounds, this classical QSAR meets various limitations, such as no representation of stereochemistry since only 2D-structure considered, unavailability of suitable numerical descriptors, no unique solutions, high risk of chance correlations, and no directly suggested candidates [95]. Therefore, 3D-QSAR, based on three-dimensional information of the molecular structures, was developed as an extension to 2D-QSAR by Hansch and Free-Wilson [113, 114]. However, 3D-QSAR rely on various basic assumptions [95]. The first assumption is the existence of the relationship between molecular structure and biological activity. The second assumption is the receptor binding is directly proportional to the biological activity. The third assumption is molecular structures can be represented by a set of numerical descriptors like 2D-QSAR. Also, followed by the similarity principle and the neighborhood principle, compounds with common structures are assumed to have similar physicochemical properties, similar binding sites, and comparable biological activities [115]. Structural properties that related to its biological response are supposed to be determined by the steric and electrostatic forces. The observed biological response is assumed to be produced by the modeled ligand, rather than its metabolite or degradation product. Moreover, the protein binding site for all the modeled ligands is expected to be identical. Another assumption is the lowest energy conformation of the ligand, which is its bioactive conformation, exerts the binding effects. The geometry of the receptor binding site is assumed to be rigid with few exceptions [116-119]. As an assumption, the loss of translational and rotational degrees of freedom upon

binding follows a similar pattern for all compounds. Several major factors, such as temperature, diffusion, transport, salt concentration and pH, are suggested to be ignored because of the difficulty of handling, even though they contribute to the overall free energy of binding [116, 119, 120]. The last assumption is the property-activity correlation issue can be potentially solved by resulting QSAR model.

Generally, 3D-QSAR approaches were classified as structure-based and ligand-based QSAR. Structure-based QSAR is a valuable tool for fast lead discovery and optimization [121, 122]. However, the knowledge of high-resolution structural data of the target protein is required for structure-based QSAR. Ligand-based QSAR takes advantage of the information of known active and inactive compounds in order to search novel lead based on chemical similarity or predict potential drug candidates by building QSAR models [123, 124]. Ligand-based QSAR is a favorable tool when no or little structural information is obtainable [125]. For our project, the structural information is limited. Therefore, ligand-based QSAR was applied for 997-series.

3.3.2 Field-based QSAR

3.3.2.a Background

Field-Based QSAR is a technique for building 3D QSAR models for a set of aligned structures based on their electrostatic, hydrophobic, or steric fields [126]. The field-based QSAR models are an implementation of comparative molecular field analysis (CoMFA) [127] and comparative molecular similarity indices analysis (CoMSIA) [128, 129].

CoMFA is one of the most common 3D QSAR approaches to relate 3D structure properties to the biological activity. CoMFA is a ligand-based, alignment-dependent, and linear 3D-QSAR. PLS or PCA techniques are generally applied for CoMFA model

development [130]. CoMFA models are built by computing the value of fields on a rectangular grid that contains the whole molecule. The positions of grid, which represent the values of the fields, were treated as the independent variables to produce a correlation with the biological activity by using PLS technique. Visualized models are generated by PLS output and provide favorable and unfavorable regions in 3D [131]. Because the bioactive conformer of CoMFA model is generally assumed to possess the lowest energy conformation but the bioactive conformation is not always the minimum energy conformation when binds to the receptor, an erroneous model may be produced which limited the usage of CoMFA approach. Another limitation of applying CoMFA method is the lack of explanation for hydrophobicity or hydrogen bond interactions [130].

The other approach, CoMSIA, is also a useful tool for calculating the value of fields at points on a rectangular grid. The fields including hydrophobic, hydrogen bond donor and acceptor, and steric contribution are calculated and weighted the distance between the atom and the grid point using a Gaussian function [126]. CoMSIA computes the similarity indices by comparing each ligand compound with a probe, which has 1 Å radius and hydrophobicity, hydrogen bond properties, and charge of 1 [130].

The field-based QSAR models are based on CoMFA and CoMSIA approaches using a particular set of parameters. The Lennard-Jones steric potentials and the atomic charges for the electrostatic fields are taken from the OPLS_2005 force field by default. Hydrophobic fields depend on the types of each atom and hydrophobic parameters [132]. The Phase pharmacophore feature definitions determine hydrogen-bond donor and acceptor fields. Fields that are scaled by the standard deviation over the entire training set are then performed PLS regression [133].

Reliability of any 3D-QSAR techniques relies on the determination of the bioactive conformations or a conformer representative to the bioactive conformation [113, 134]. The bioactive conformation of the molecule represents the conformation when the molecule is bound to the receptor. Bioactive conformations of the molecules can be gained by X-ray crystallography, NMR spectroscopy, or theoretical protein/homology modeling [95]. X-ray crystallography provides reasonably accurate information for molecules, especially macromolecules, with several limitations, such as time-consuming data collection step, distorted structures due to crystal packing, crystal instability, and different conditions between crystallizing media and physiological condition [95]. Compared to X-ray crystallography, NMR spectroscopy identifies conformations in solution and it not restricted by one static conformation of the protein ligand complex. Because the data is obtained in solution, the results highly rely on the solvent. The advantage of dissolving molecules into solvents is that the solution conditions can match the physiological conditions by adjusting its conditions, such as pH, temperature, substrate, and ionic strength [95]. NMR spectroscopy is a favorable method for the case of receptors that have not been isolated or small molecules that cannot be crystallized.

Protein/homology modeling is a theoretical method that predicts the structure of the novel protein by comparing the sequence of proteins and finding known proteins in the database, such as PDB, which is homologous to the new protein. The sequence similarity between the known protein and the target protein determines the applicability and quality of this method [95]. The use of crystal structures or homology models in structure-based drug discovery (SBDD) relies on crystal structures co-resolved with ligands of interest. Structures co-resolved with ligands shape the binding pocket and produces better results

compares to structures in the apo-state when used in docking studies. No crystal structure or homologue of the NMDA receptor with compounds similar to the 997-series is available and thus SDBB cannot be used in this study. We therefore turned to small molecule NMR to identify the most prevalent conformers in solution structures, one of which has previously been shown to be representative of the bioactive conformation bound to a receptor [135, 136]. In this chapter, NMR analysis of molecular flexibility in solution (NAMFIS) was used in an attempt to see if we could identify in solution conformers of the 997-series and use these conformers to generate a 3D-QSAR. After determining the in solution conformers, the 997-series were flexibly aligned to them. To align all the molecules, several methods have been proposed, such as atom overlapping based superimposition, binding sites-based superimposition, fields/pseudofields based superimposition, and multiple conformers-based superimpositions. The most popular method is the atom overlapping based superimposition. This approach encompasses the corresponding atom to atom pairing between the molecules and best matches the preselected atom positions. This method has the advantage of identifying dissimilarity between similar molecules, while it is difficult to select matching atoms between the molecules with dissimilar structural types [95]. After superimposition, all molecules are placed in the center of a lattice or grid box to compute steric or electrostatic interaction energies between the ligands and different probes, such as a proton or sp^3 hybridized carbocation, positioned at each intersection of the lattice [134, 137].

3.3.2.b Field-based QSAR experimental section

A representative dataset of the 997-series containing 122 compounds was used to perform a 3D-QSAR study. The IC_{50} values used in this study were determined using a two-

electrode voltage-clamp recording that was done at least in triplicate to ensure statistical significant results. GluN2D IC₅₀ values were converted to pIC₅₀ for use in this study. Field-based QSAR models were built using the Field-Based QSAR module (Schrödinger, Inc., LLC, New York, USA, 2017).

First, we prepare the 3D structures of all the compounds. Since no binding pocket information was available, NMR analysis of molecular flexibility in solution (NAMFIS) was used in this study to determine the possible bioactive conformations of the 997-series [136]. The NMR experiments (proton NMR and 2D-NOESY) were performed by Dr. T. Kaiser for compound 997-23. Proton assignments were made, and the NOE distances for protons in close proximity were calculated. The data were subjected to NAMFIS analysis to deconvolute the computationally derived conformer pool into the most prevalent in solution structures. The conformational search parameters were as follow: 100,000-steps (10,000 steps per rotatable bond) of Monte Carlo Macro Model (MCMM) and Mixed torsional/Low-Mode (MTLM) sampling were performed on (S)-997-23 using three different individual force fields (AMBER*, MMFFs, and OPLS3) within the MacroModel module of Maestro. The GBSA/H₂O and GBSA/CHCl₃ solvation models were used along with a relaxed 30 kJ/mol energy cut-off. To ensure complete energy convergence, the resulting structures were subjected to 2500 steps of PRCG minimization with a gradient of 0.05, followed by 250 steps of FMNR minimization. Conformers resulting from the conformational searches were combined and redundant conformation removed using a 0.1 Å atom deviation of the heavy atoms. The global minimum was found between 408 and 5081 times for the different searches, assuring complete coverage of conformational space (*Figure 20*). Redundant conformers were removed with a heavy-atom RMSD less than

0.1Å resulting in a 133-conformer pool.

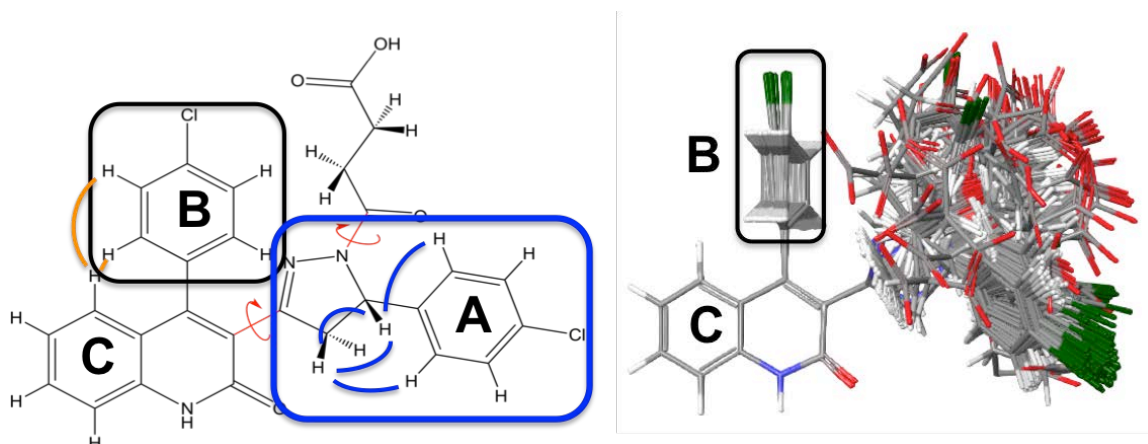
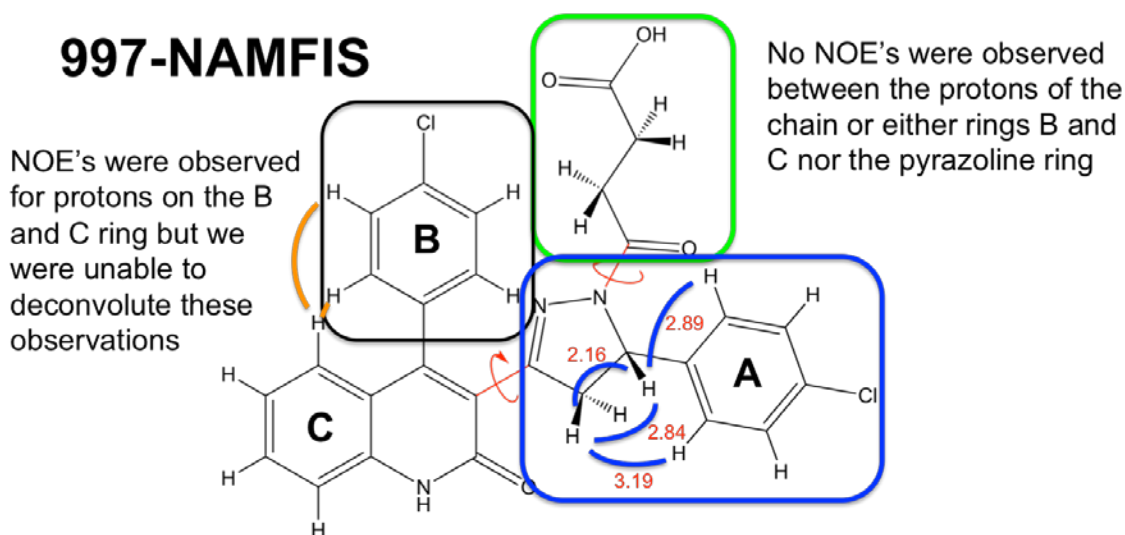


Figure 20. (Left) A 2D representation of compound 997-23. The observed NOE distances are shown in blue and orange. (Right) Complete conformation pool of (S)-997-23. The conformers were aligned on the quinolone showing a limited number of conformers between the B and the C rings.

Analyses of the NMR data of 997-23 showed 4 NOE distance between the pyrazoline and the A ring. Two NOE distances were also observed between the B and the C ring, but we were unable to deconvolute the data to assign the protons accurately. This was not detrimental since only one conformer were observed for the orientation between the B and the C ring. The 4 NOE distances were used to deconvolute the conformational pool, which resulted in two conformers with an SSD fit of 2.5 (*Figure 21*). The population of the NAMFIS conformers was 55 and 44% respectively (*Figure 21*). We expected to observe NOE's between the protons of the propanoic acid and either the A ring or the pyrazoline ring, however, none was detected. The orientation of the A ring and the pyrazoline was determined and was used further in this study.



Quality	
SSD	2.5
Population	
NAMFIS-1	55
NAMFIS-2	44

NAMFIS used the four NOESY derived H-H distance to deconvolute the conformational pool with a Sum of Squared Distances (SSD) value of 2.5. Two conformations were found with populations of 55 and 44% respectively. The RMSD between the regions of interest was 0.1Å.

Figure 21. Signal was observed between the protons of the B and C rings. The conformational search revealed as expected only one dominant conformer with respect to the orientations of the B and the C rings. No signal was observed between the acid chain (green box) and either the A or the B ring. The only NOE distances observed between the pyrazoline and the A ring were denoted in red (Å).

In an attempt to determine the possible bioactive conformations of the propanoic acid chain a conformational search was performed using the NAMFIS-1 and NAMFIS-2 structures as input. A conformational search was performed only sampling the propanoic acid chain while keeping the rest of the structure fixed. The minimum energy conformer for both the NAMFIS-1 and NAMFIS-2 structures was selected as input structures. As a control, a conformational search of (S)-997-23 was performed from which the minimum structures were selected. The conformers from the above results were named NAMFIS-1a, NAMFIS-2a, and (S)-997-23-min (*Figure 22*). Molecular alignment between the target

structures determined above and the 997-series dataset was performed using the Flexible Ligand Alignment module in the Schrödinger modeling suite. This module uses a conformational search algorithm that aligns each molecule in the dataset to the target structure. All alignments were visually inspected, and if the alignment were poor, a maximum common substructure alignment was performed by using a SMARTS pattern to obtain the best alignment.

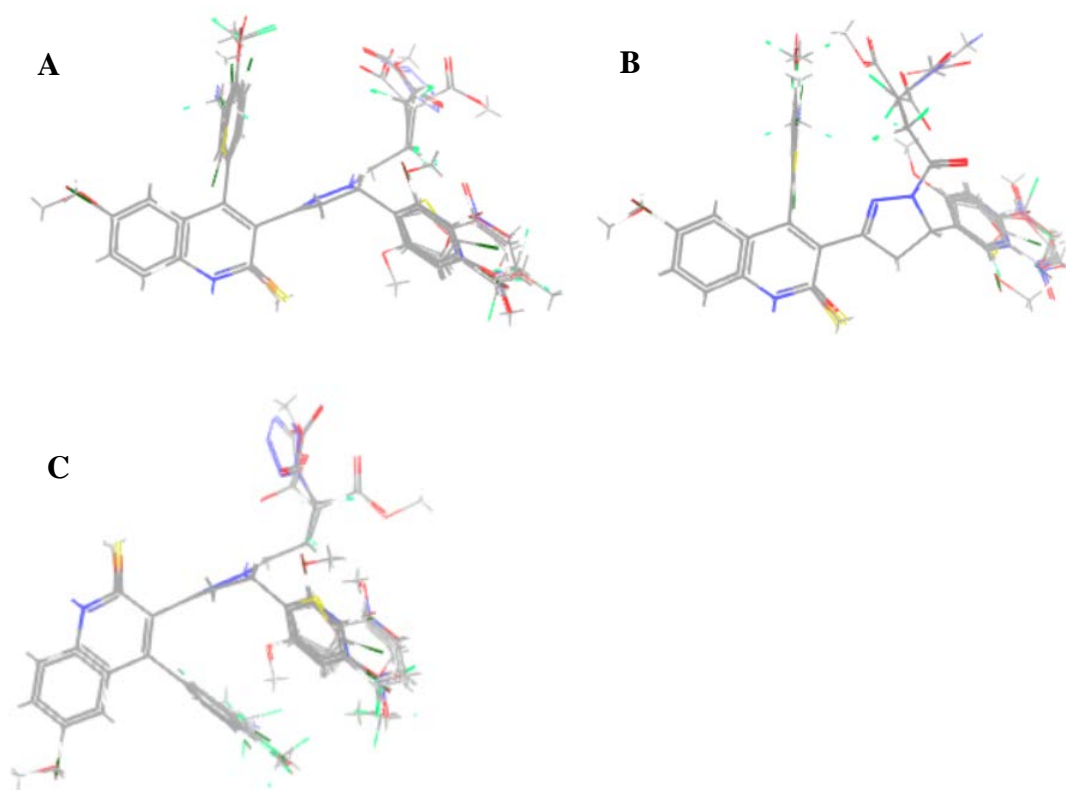


Figure 22. Alignments of A, NAMFIS-1a; B, NAMFIS-2a; and C, (S)-997-23-min.

The set of compounds with (S)-997-23-NAMFIS-1a conformation were first used to build the Field-Based QSAR model. A total of 122 compounds that is active at GluN2D-containing receptors were imported into Field-Based QSAR panel. The compounds were randomly assigned to the training set (75%) and test set (25%) (random seed: 123) followed by model building. Then the model was built. The Gaussian field (recommended) was used

in this experiment. The maximum PLS factors were set to 10. The rest of settings were kept as default. For example, the grid spacing was set to 1.0 Å, the grid beyond training set limits was extended by 3.0 Å, ignore force fields were set within 2.0 Å of any training set atom, truncate steric force fields and truncate electrostatic force fields were set at 30.0 kcal/mol, eliminate variables with StdDev was set less than 0.01, and the number of ligands to leave out for cross-validation was set as 1. After the model was built, QSAR statistics and field fractions were obtained as shown in *Table 14*. All other Field-Based QSAR models were generated using similar parameters as above unless specified otherwise.

Table 14. Field-based QSAR model of (S)-997-23 NAMFIS-1a with QSAR statistics.

# Factors	SD	R ²	Stability	RMSE	Q ²	Pearson-r
1	0.5353	0.5588	0.945	0.54	0.5049	0.7124
2	0.4680	0.6665	0.945	0.42	0.6983	0.8545
3	0.3968	0.7630	0.797	0.39	0.7391	0.8803
4	0.3555	0.8119	0.727	0.45	0.6655	0.8445
5	0.3343	0.8356	0.73	0.39	0.7492	0.8839

3.3.2.c Field-based QSAR results

To select what number of PLS factors should be used, the analysis of QSAR statistics was important to avoid under- or over-fitting. The standard deviation (SD) and stability decreased as the number of PLS factors increased, while the R-squared and R² scramble increased as the number of PLS factors increased. The stability indicated the sensitivity of the model to omissions from the training set. When the stability value is lower than the R² value, the dataset is suggestive of over-fitting. The test set statistics, RMSE, Q²,

and Pearson-r, were crucial for the quality of the predictions. The RMSE decreased when the number of PLS factors increased, while the Q^2 and Pearson-r increased when the number of PLS factors increased. If these test set statistics were not improved as the number of PLS factors increased, adding factors to the model possibly led to over-fitting. Based on these guidelines, the model was selected that had 3 PLS factors with a RMSE value of 0.39, Q^2 value of 0.7391, and the Pearson-r coefficient value of 0.8803 (Table 14). The resulting scatter plots of the training set and test set with 3 PLS factors are shown below (Figure 23).

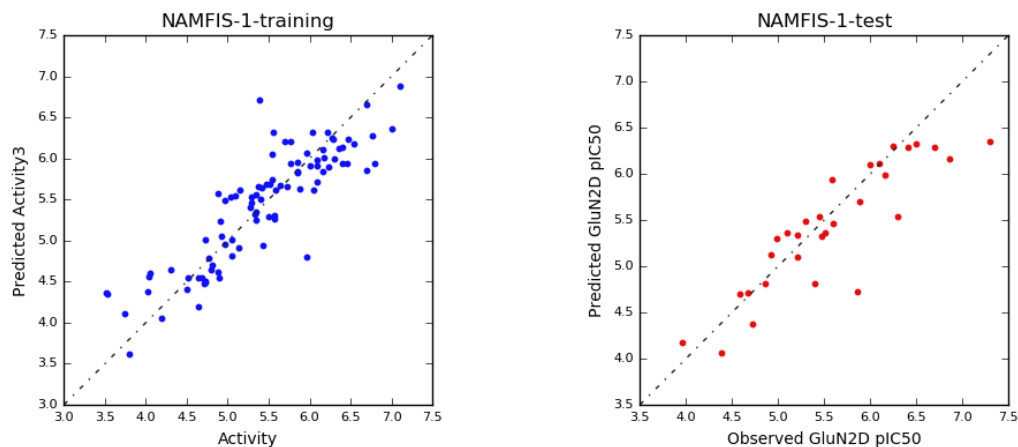


Figure 23. The plot of NAMFIS-1a training (in blue) and test (in red) sets results.

Finally, the QSAR model was visualized by using field-based QSAR visualization settings panel. The model can be viewed as solid contours from Gaussian steric, Gaussian electrostatic, Gaussian hydrophobic, Gaussian H-bond acceptor, and Gaussian H-bond donor fields. The default colors for field contours showed as below (Table 15):

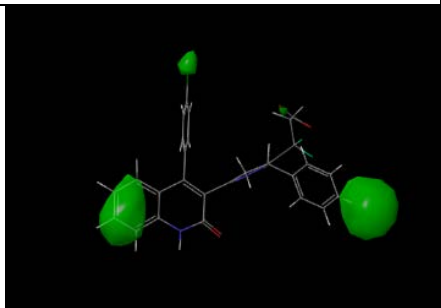
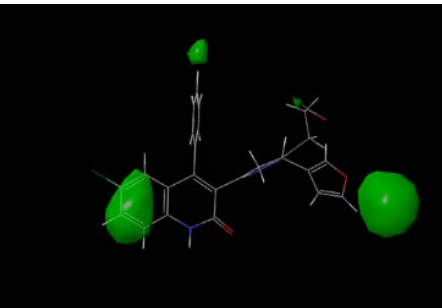
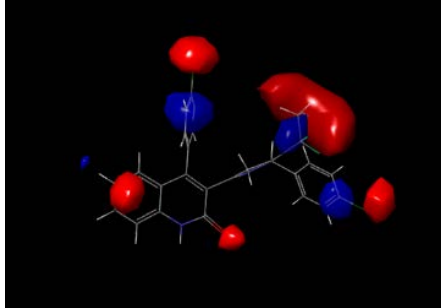
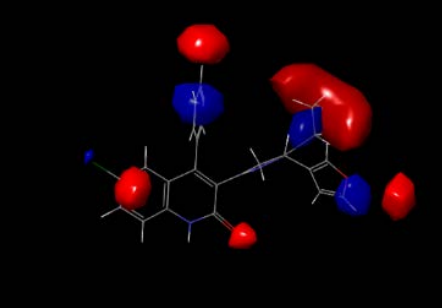
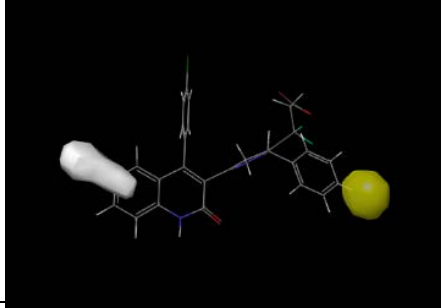
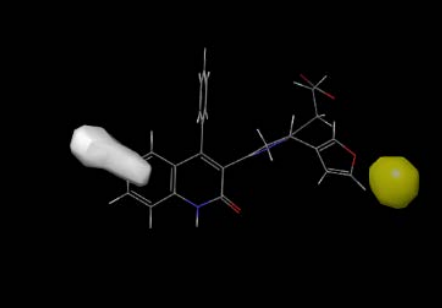
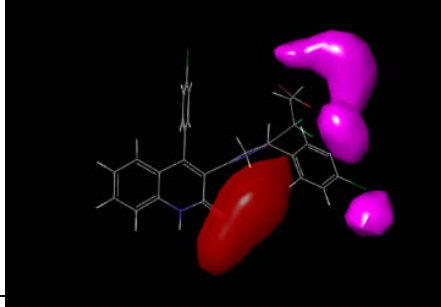
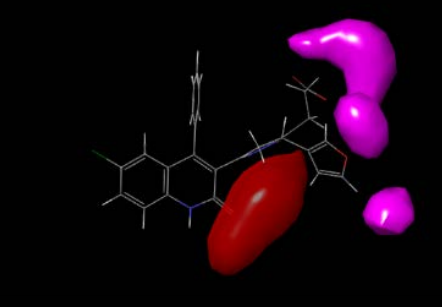
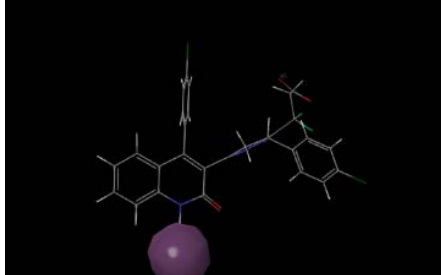
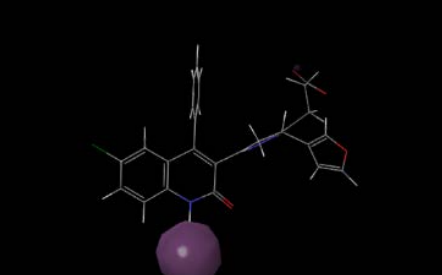
Table 15. The default colors for field contours.

Field Type	Positive	Negative
Gaussian Steric	Green	Yellow
Gaussian Electrostatic	Blue	Red
Gaussian Hydrophobic	Yellow	White
Gaussian H-bond Acceptor	Red	Magenta
Gaussian H-bond Donor	Purple	Cyan

The QSAR model was visualized using field-based QSAR visualization settings panel and are shown below (*Table 16*). The most active compound **997-74** and the least active compound **2063** are shown overlaid with contour maps for comparison. Contour maps obtained from field-based QSAR calculations identified favored and disfavored regions of the **997** series regarding steric, electrostatic, hydrophobic, H-bond acceptor, and H-bond donor properties for further optimization. The steric map showed the regions where steric bulk was favored (green contours). This map suggested that a steric feature was favored at the quinolone group and two halogen substitutions on two rings. For example, compound **997-74** with larger substitutions such as chlorine on the A- and B-rings were more potent at the GluN2D-containing receptor and showed positive steric effects at these regions. In compound **2063**, a furan substitution on the A-ring did not fill the positive steric region and partially explained the decreased potency at the GluN2D-containing receptor. The small green contour at the acyl chain showed that steric substitutions were preferred close to this region. The electrostatic map indicated the electropositive region in blue and the electronegative region in red. The blue electropositive contours, which were observed

close to the *para*-position of the phenyl ring and acyl chain, recommended positively charged substitutions to improve biologic activity. The red electronegative contours were observed close to the halogen substitutions and the acyl chain terminal, which indicated that increased electron density enhanced biological activity. Due to a lack of electronegative substitutions on the A and B rings, compound **2063** decreased the activity at the GluN2D-containing receptor. The hydrophobic contour map indicated that the substitution on the A ring preferred a hydrophobic group for enhancing the biologic activity, while the substitution on the quinolone ring preferred a hydrophilic group. Compared with compound **997-74** with chlorine substitution, compound **2063** without any hydrophobic group on the A ring has lower the bioactivity at the GluN2D-containing receptor. The H-bond acceptor contour indicated that the amide group at the quinolone ring and the nitrogen on the pyrazoline ring were preferred at these regions as hydrogen bond acceptors, while both the A ring and the acyl chain regions were disfavored H-bond acceptors. The H-bond donor contour only revealed that the amide group at the quinolone ring acted as a proton source and was favorable to increase the activity.

Table 16. Five field contours of the most active compound 997-74 and the least active compound 2063 with NAMFIS-1a structure.

NAMFIS-1a	997-74	2063
Steric	 The steric field contour of compound 997-74 is shown as a 3D model with green isosurfaces. The contours are distributed across the molecule, with larger volumes around the central ring system and the side chain, indicating steric bulk.	 The steric field contour of compound 2063 is shown as a 3D model with green isosurfaces. The distribution is similar to 997-74, with green volumes around the main structure and side chain.
Electrostatic	 The electrostatic field contour of compound 997-74 is shown as a 3D model with red and blue isosurfaces. Red volumes indicate electron-deficient regions, while blue volumes indicate electron-rich regions.	 The electrostatic field contour of compound 2063 is shown as a 3D model with red and blue isosurfaces. The distribution of red and blue volumes is similar to 997-74.
Hydrophobic	 The hydrophobic field contour of compound 997-74 is shown as a 3D model with white and yellow isosurfaces. The white volume is on the left side, and the yellow volume is on the right side.	 The hydrophobic field contour of compound 2063 is shown as a 3D model with white and yellow isosurfaces. The distribution is similar to 997-74.
H-bond Acceptor	 The H-bond Acceptor field contour of compound 997-74 is shown as a 3D model with red and magenta isosurfaces. The red volume is at the bottom, and the magenta volume is on the right side.	 The H-bond Acceptor field contour of compound 2063 is shown as a 3D model with red and magenta isosurfaces. The distribution is similar to 997-74.
H-bond Donor	 The H-bond Donor field contour of compound 997-74 is shown as a 3D model with a purple isosurface. The purple volume is located at the bottom of the molecule.	 The H-bond Donor field contour of compound 2063 is shown as a 3D model with a purple isosurface. The distribution is similar to 997-74.

Next, the (S)-997-23-NAMFIS-2a conformer was used to build another Field-Based QSAR model. The model was built as described for (S)-997-23-NAMFIS-1a. Follow model building, the QSAR statistics and field fractions were obtained and are shown below (*Table 17*).

Table 17. Field-based QSAR model of (S)-997-23 NAMFIS-2a with QSAR statistics.

# Factors	SD	R ²	Stability	RMSE	Q ²	Pearson-r
1	0.5460	0.5410	0.946	0.54	0.5049	0.7139
2	0.4706	0.6629	0.937	0.44	0.6810	0.8468
3	0.3885	0.7728	0.793	0.45	0.6666	0.8477
4	0.3585	0.8087	0.801	0.49	0.5886	0.8076
5	0.3177	0.8515	0.772	0.44	0.6787	0.8634

Based on these statistic results, when the number of PLS factors equal to 3, the best model was selected with the RMSE value of 0.45, the Q² value of 0.6666, and the Pearson-r coefficient value of 0.8477. Then the scatter plots of the training set and test set with 3 PLS factors were obtained and showed as below (*Figure 24*).

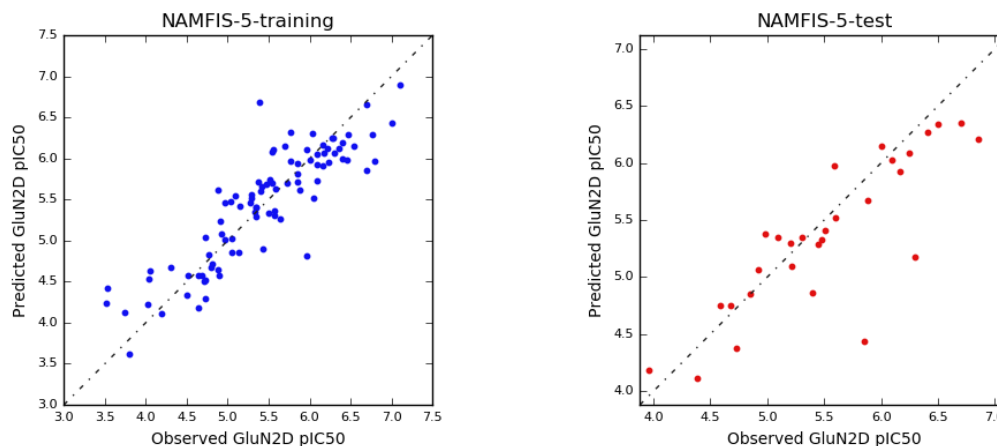
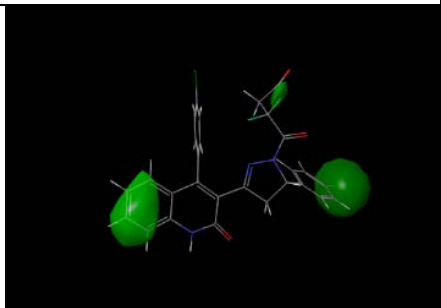
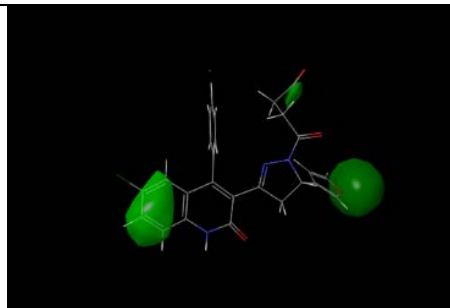
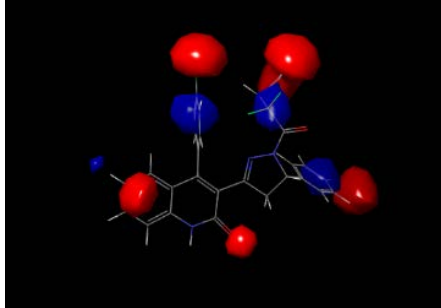
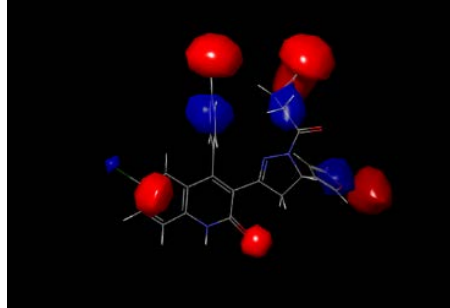
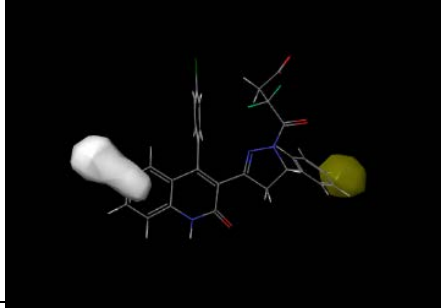
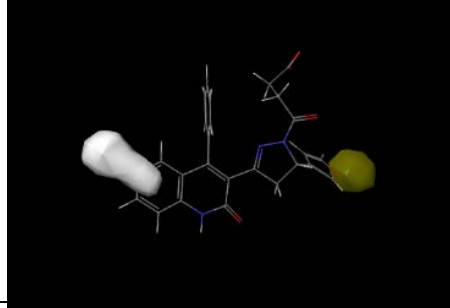
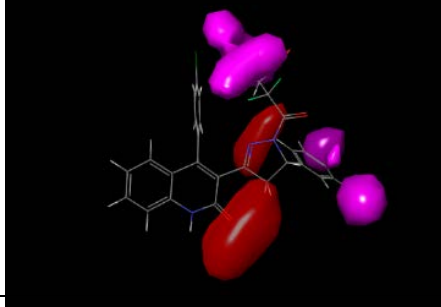
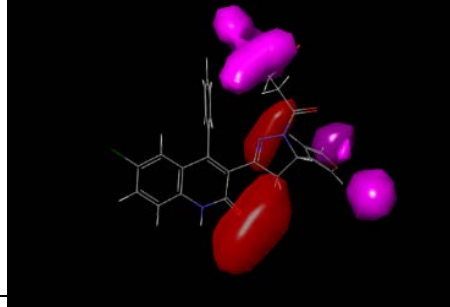
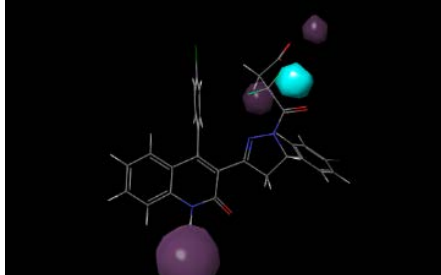
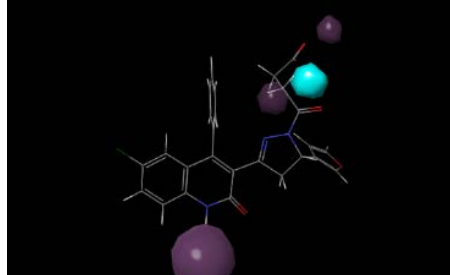


Figure 24. The plot of NAMFIS-2a training (in blue) and test (in red) sets results.

The QSAR model was visualized using Field-Based QSAR visualization settings panel and are shown below (Table 18). The most active compound **997-74** and the least active compound **2063** are shown overlaid with contour maps. The steric, electrostatic, hydrophobic, H-bond acceptor contours resulted similar outcomes to NAMFIS-1a model. However, the H-bond donor contour revealed that the amide group at the quinolone ring acted as a proton source and was favorable to increase the activity. Moreover, the H-bond donor contour also indicated that the α -carbon region of the acyl chain was disfavored H-bond donors, while the β -carbon region and the terminal of the acyl chain preferred an H-bond donor.

Table 18. Five field contours of the most active compound 997-74 and the least active compound 2063 with NAMFIS-2a structure.

NAMFIS-2a	997-74	2063
Steric		
Electrostatic		
Hydrophobic		
H-bond Acceptor		
H-bond Donor		

Field-Based QSAR model building of minimum energy conformer (S)-997-23-min as a control was performed using similar parameters as describe above. Following model building, the QSAR statistics and field fractions were obtained and are shown below (*Table 19*).

Table 19. Field-based QSAR model of (S)-997-23-min with QSAR statistics.

# Factors	SD	R ²	Stability	RMSE	Q ²	Pearson-r
1	0.5304	0.5669	0.944	0.54	0.5144	0.7191
2	0.4658	0.6697	0.944	0.43	0.6958	0.8521
3	0.3894	0.7717	0.769	0.42	0.7042	0.8687
4	0.3492	0.8186	0.723	0.46	0.6432	0.8404
5	0.3259	0.8438	0.716	0.40	0.7329	0.8791

Based on these statistic results, when the number of PLS factors equal to 3, the best model was selected with the RMSE value of 0.42, the Q² value of 0.7042, and the Pearson-r coefficient value of 0.8687. Then the scatter plots of the training set and test set with 3 PLS factors were obtained and showed as below (*Figure 25*).

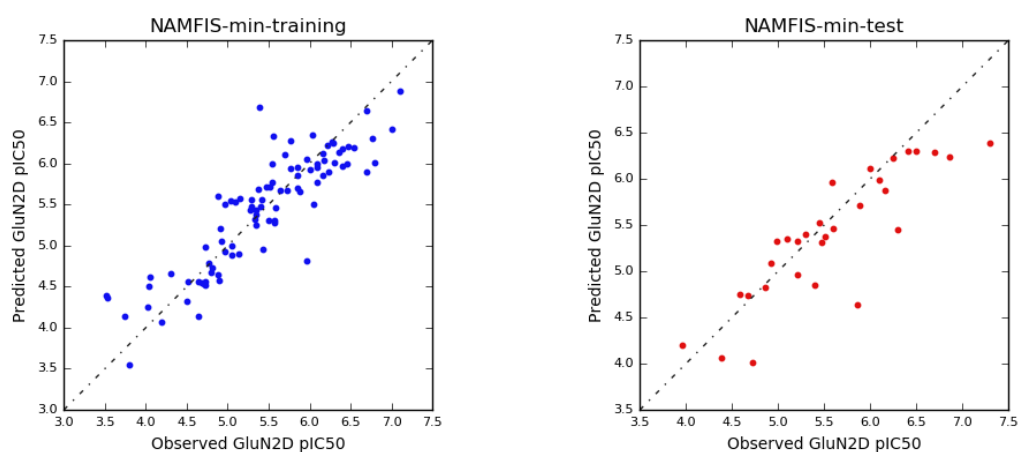
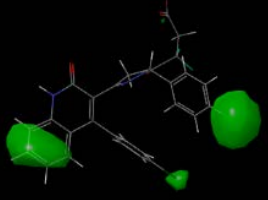
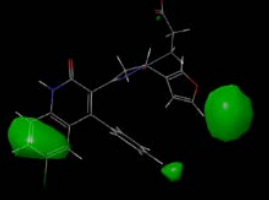
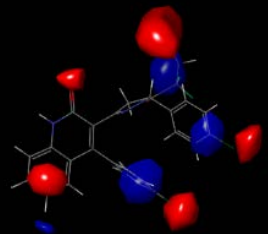
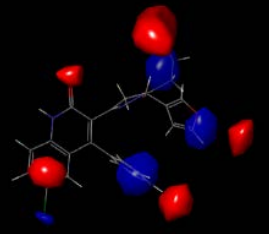
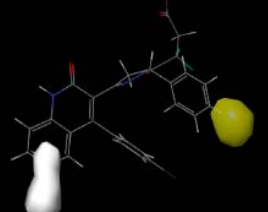
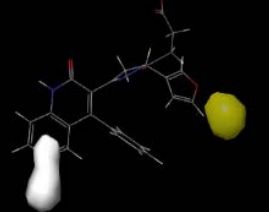
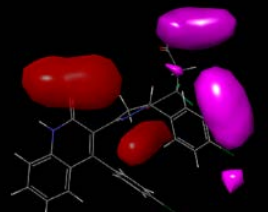
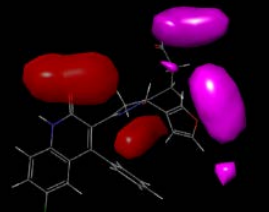
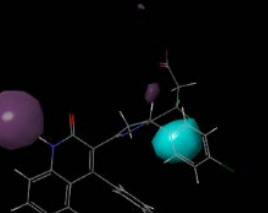
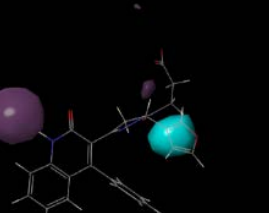


Figure 25. The plot of (S)-997-23-min training (in blue) and test (in red) results.

The QSAR model was visualized using Field-Based QSAR visualization settings panel and are shown below (*Table 20*Table 20). The most active compound **997-74** and the least active compound **2063** are shown overlaid with five contour maps. All the steric, electrostatic, hydrophobic, H-bond acceptor, and H-bond donor contours resulted similar outcomes to NAMFIS-2a model.

Table 20. Five field contours of the most active compound 997-74 and the least active compound 2063 with (S)-997-23 conformation.

min	997-74	2063
Steric		
Electrostatic		
Hydrophobic		
H-bond Acceptor		
H-bond Donor		

3.3.2.d Field-based QSAR discussion

The purpose of generating 3D Field-Based QSAR model was two fold, one to better understand the 3D properties of the 997-series that influence activity and two, to generate a predictive model to guide compound design in future efforts. Here we combined a biophysical and computational methods to better understand the activity profile of the 997-series in 3D. Three 3D-QSAR models were generated of which NAMFIS-1a showed the best predictability of the models (*Table 21*). The R^2 and Q^2 values were similar, 0.76 and 0.73 respectively when considering 3 PLS factors with the lowest RMSE value of 0.39. The NAMFIS-2a model had R^2 and Q^2 of 0.77 and 0.66 respectively with a RMSE of 0.45 (PLS = 3). Our control model (S)-997-23-min or the lowest energy model from a conformational search had a R^2 and Q^2 of 0.77 and 0.70 with RMSE of 0.42 (PLS = 3).

Table 21. Field-Based QSAR statistics.

# Factors = 3	SD	R^2	Stability	RMSE	Q^2	Pearson-r
NAMFIS-1a	0.3968	0.7630	0.797	0.39	0.7391	0.8803
NAMFIS-2a	0.3885	0.7728	0.793	0.45	0.6666	0.8477
min	0.3894	0.7717	0.769	0.42	0.7042	0.8687

The field contours provide some information to assess the molecular features for better activity at the GluN2D-containing receptor. For instance, the substitutions on both the A ring and B ring preferred steric bulk and electronegative groups. The substitution on the A ring was also favored a hydrophobic group. According to the Craig plot for various substituents with hydrophobic and electrostatic properties, trifluoromethyl and chlorine groups were hydrophobic and electronegative (*Figure 26*). Therefore, substitutions on the A ring and B ring preferred trifluoromethyl or chlorine groups, which confirmed that why

997-74 was the most active compound. From the H-bond acceptor and donor contours, the amide group at the quinolone ring played a crucial role for accepting and donating protons, while the acyl chain was favored an H-bond donor which verified that compound with difluoro-substitution was more active at the GluN2D-containing receptor.

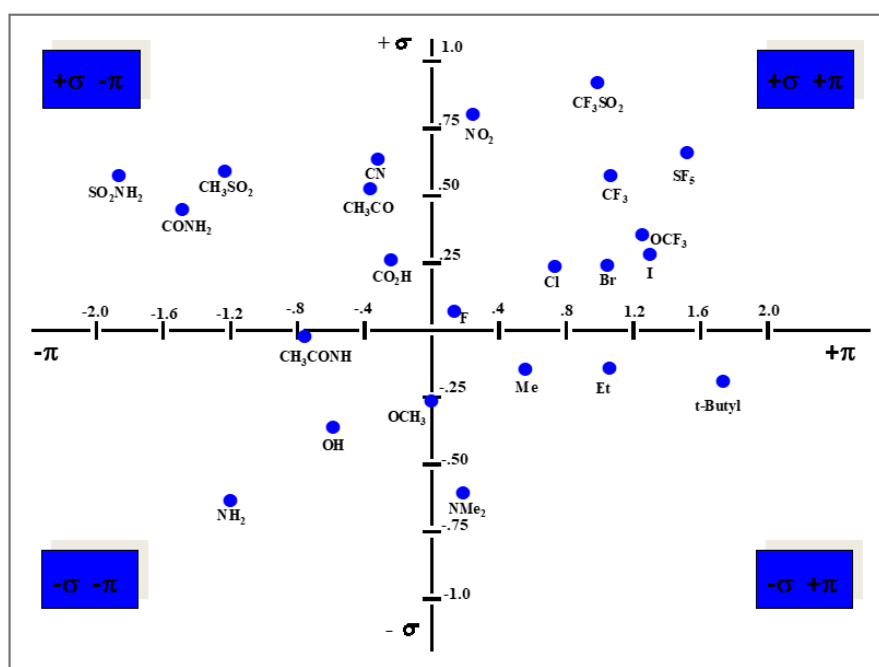


Figure 26. The Craig plot for various substituents with hydrophobic and electrostatic properties.

Although the Field-Based QSAR models was unable to clearly identify a bioactive conformation of 997 series, the QSAR statistics of these models could still treat as useful data for prediction of future compounds. According to the QSAR statistics of NAMFIS-1a, NAMFIS-2a, and the control of (S)-997-23 with 3 PLS factors, the predicted power of NAMFIS-1 conformations is relatively higher than the power of NAMFIS-2 conformations. The 3D QSAR model based on the NAMFIS-1a conformer could be used in combination with 2D QSAR models to guide prediction of future medicinal efforts of the 997-series.

Chapter 4. 1121 series

4.1 Introduction

Compound **1121** was obtained from high-throughput screening with a scaffold similar to the GluN2B selective antagonist, ifenprodil. Compound **1121** was evaluated its inhibition at GluN2 subunits via two-electrode voltage-clamp recording with IC₅₀ values of 14 and 13 μ M at GluN2C- and GluN2D-containing receptors, respectively (*Figure 27*). Also, **1121** showed slight selectivity for GluN2C- and GluN2D-containing receptors over GluN2A- and GluN2B-containing receptors. Even though the binding and conformational information remained unknown, **1121** was considered to be an interesting target of SAR studies.

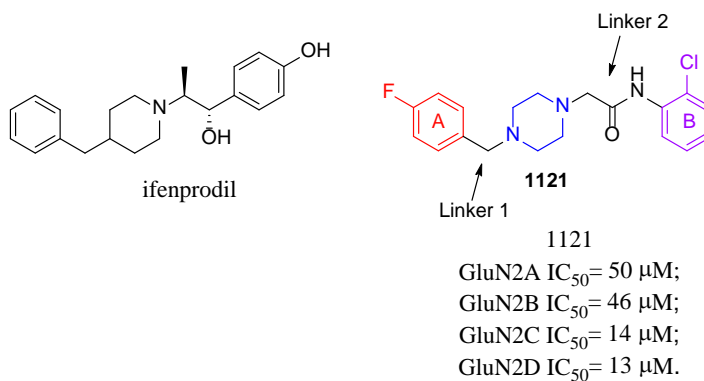


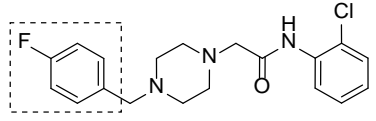
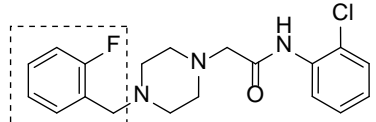
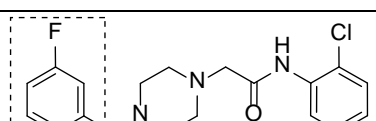
Figure 27. Structure of ifenprodil and 1121, and optimized scaffold of 1121.

4.2 A-ring modification

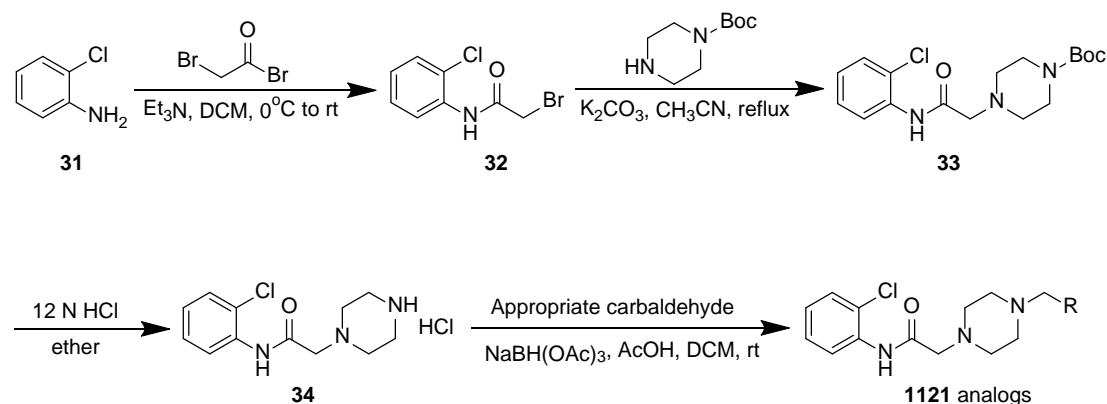
Compound **1121** was separated into five parts: A ring, B ring, piperazine ring and two linkers (*Figure 27*). To improve the activity at GluN2C/D-containing receptors and the selectivity at GluN2C/D over GluN2A and GluN2B receptors, substituents on aromatic rings could be modified. For example, replacing *para*-fluorine on the A ring of compound **1121** with other electrophilic or nucleophilic groups, including trifluoromethyl, cyanide, and amine groups, may increase or decrease the activity and selectivity. Therefore, the A

ring was first modified with other substitutions. Based on the SAR results of purchased compounds **1121**, **2030** and **2032**, the substitution on the *para* position of A ring was preferred (Table 22). Therefore, the modification of A ring was mainly focused on the *para* position.

Table 22. SAR of purchased compound 1121, 2030, and 2032.

	Structures	GluN2A IC ₅₀ (μM)	GluN2B IC ₅₀ (μM)	GluN2C IC ₅₀ (μM)	GluN2D IC ₅₀ (μM)
1121		50	46	14	13
2030		103	104	43	35
2032		NE	NE	94	73

Four steps are required to yield **1121** analogs. Commercially available bromoacetyl bromide and aniline (**31**) were reacted in the presence of triethylamine in DCM to yield the corresponding α -bromo acetamide (**32**). Then the α -bromo acetamide was refluxed with boc-piperazine in the presence of potassium carbonate in acetonitrile to yield the corresponding piperazine (**33**). Deprotection of the Boc group by the treatment of 12 N hydrogen chloride in ether, followed by the treatment of appropriate aldehyde in the presence of sodium triacetoxyborohydride gave the final **1121** analogs (Scheme 15) [138].

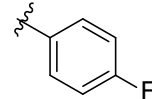
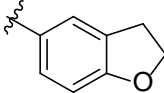
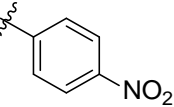
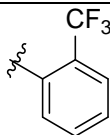
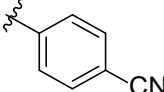
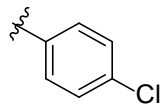
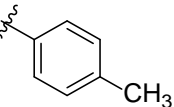
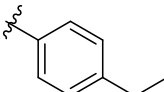
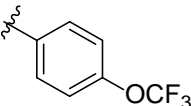
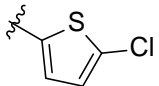


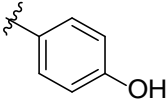
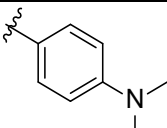
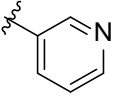
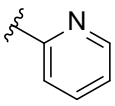
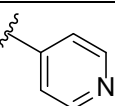
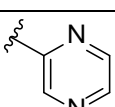
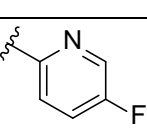
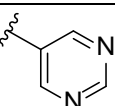
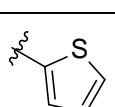
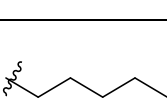
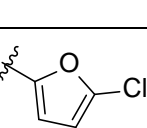
Scheme 15. Synthesis of 1121 analogs with A-ring modifications.

All target compounds were assayed for activity by Dr. Stephen Traynelis group using two-electrode voltage-clamp recordings performed in *Xenopus laevis* oocytes expressing recombinant GluN2A-D subunits [79]. Compound **1121-2** to **1121-6** were first synthesized and only compound **1121-3** and **1121-5** with nitro and cyanide substitutions were active and exhibited poor activity at GluN2C- and GluN2D-containing receptors. **1121-8** with methyl group showed poorer activity at all subunits than **1121**. Replacing the methyl group with an ethyl group was resulted in a loss of activity at all receptors. Compounds **1121-10** to **1121-13** also showed a decrease in potency at all subunits. Thus, the hypothesis is that the A ring requires hydrogen acceptor but may only tolerate a small group like methyl group or fluorine. If we optimize the A ring as pyridine ring with nitrogen as a hydrogen acceptor, the potency may remain or increase at GluN2C/D receptors. Compounds **1121-18**, **1121-19**, **1121-20**, **1121-21** and **1121-23** without halogen substitution lost their activities at all subunits. Compound **1121-22**, with fluorine on the *para*- position, remained potent at GluN2C and GluN2D subunits, while slightly increasing the selectivity over GluN2A and GluN2B subunits. Compound **1121-36** with bulky alkyl chain was inactive at all subunits. Notably, compared to **1121-11**, compound **1121-35** without fluorine substitution improved the activity with IC₅₀ values of 13 μ M and 11 μ M at GluN2C- and

GluN2D-containing receptors, respectively. Replacing 2-chlorothiophene to 2-chlorofuran eliminated the activity at all GluN2 subunits. Therefore, more aromatic thiophene group was preferred to retain the potency than furan [139] (*Table 23*).

Table 23. A-ring modification.

1121-	R	GluN2A IC ₅₀ (μM)	GluN2B IC ₅₀ (μM)	GluN2C IC ₅₀ (μM)	GluN2D IC ₅₀ (μM)
1*		50	46	14	13
2		NE	NE	NE	NE
3		NE	NE	45	32
4		NE	NE	NE	NE
5		NE	NE	54	37
6		NE	NE	NE	NE
8		64	101	44	26
9		NE	NE	NE	NE
10		NE	NE	NE	NE
11		NE	NE	35	42

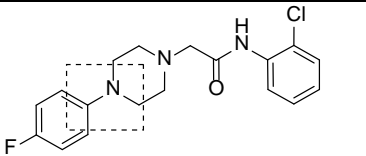
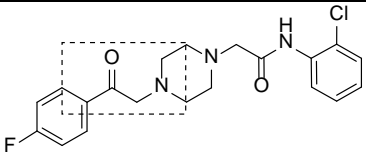
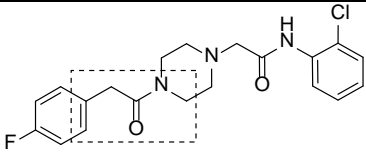
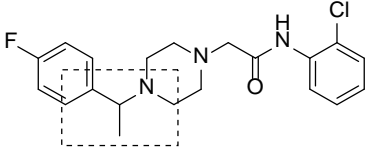
12		NE	61	68	71
13		NE	NE	NE	NE
18		NE	NE	NE	NE
19		NE	NE	NE	NE
20		NE	NE	NE	NE
21		NE	NE	NE	NE
22		100	100	22	18
23		NE	NE	NE	NE
35		NE	NE	13	11
36		NE	NE	NE	NE
37		NE	NE	NE	NE

IC₅₀ values were obtained by fitting the Hill equation (see chapter 2.4.5) to the average composite concentration-effect curves. Data were from 4-13 oocytes between 1-2 frogs. NE indicates less than 50% inhibition at 30 μM. The mean IC₅₀ values plus confidence intervals are given in the appendix E.

4.3 Linker modification

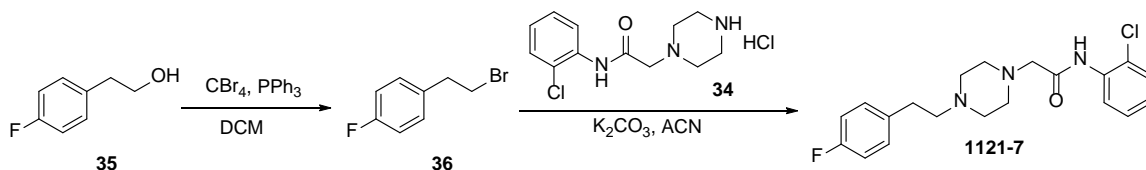
As well as optimizing the A ring, linker 1 between A ring and piperazine ring and linker 2 between piperazine and B ring were also modified. To modify linker 1, purchased compounds **2035**, **2101**, **2102**, and **2103** were evaluated. All these compounds showed poor activity at GluN2C- and GluN2D-containing receptors (*Table 24*).

Table 24. SAR of purchased compounds 2035, 2101, and 2103.

	Structures	GluN2A IC ₅₀ (μM)	GluN2B IC ₅₀ (μM)	GluN2C IC ₅₀ (μM)	GluN2D IC ₅₀ (μM)
2035		NE	NE	NE	NE
2101		NE	NE	NE	92
2102		NE	NE	NE	>100
2103		NE	NE	>100	60

To explore the linker function, a compound with ethyl group instead of the methyl linker was synthesized from 4-fluorophenyl ethanol (**35**). The ethanol was treated with tetrabromomethane and triphenylphosphine portionwise to give 2-bromoethyl-4-fluorobenzene (**36**) [140]. The resultant compound was then refluxed with piperazine (**34**)

and potassium carbonate in acetonitrile overnight to yield **1121-7** (Scheme 16) [141]. However, Compound **1121-7** was inactive at all receptors (Table 25, Scheme 16).



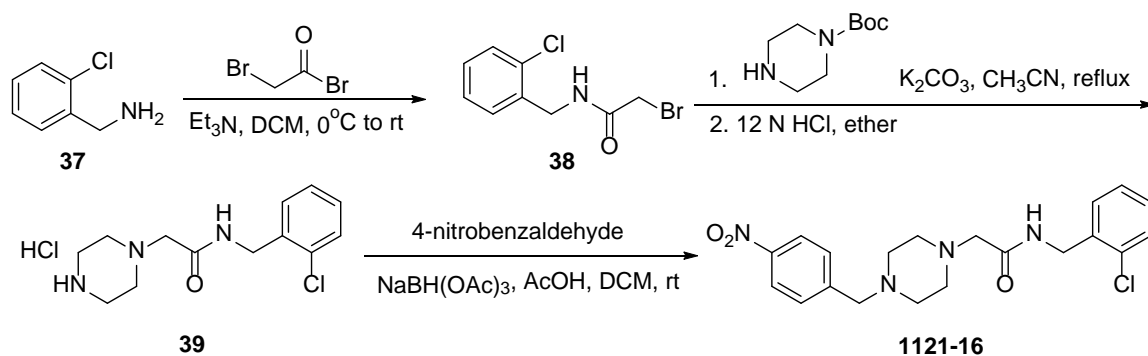
Scheme 16. Synthesis of 1121-7.

Table 25. Linker 1 modification.

1121-	GluN2A IC_{50} (μM)	GluN2B IC_{50} (μM)	GluN2C IC_{50} (μM)	GluN2D IC_{50} (μM)
7	50	46	14	13

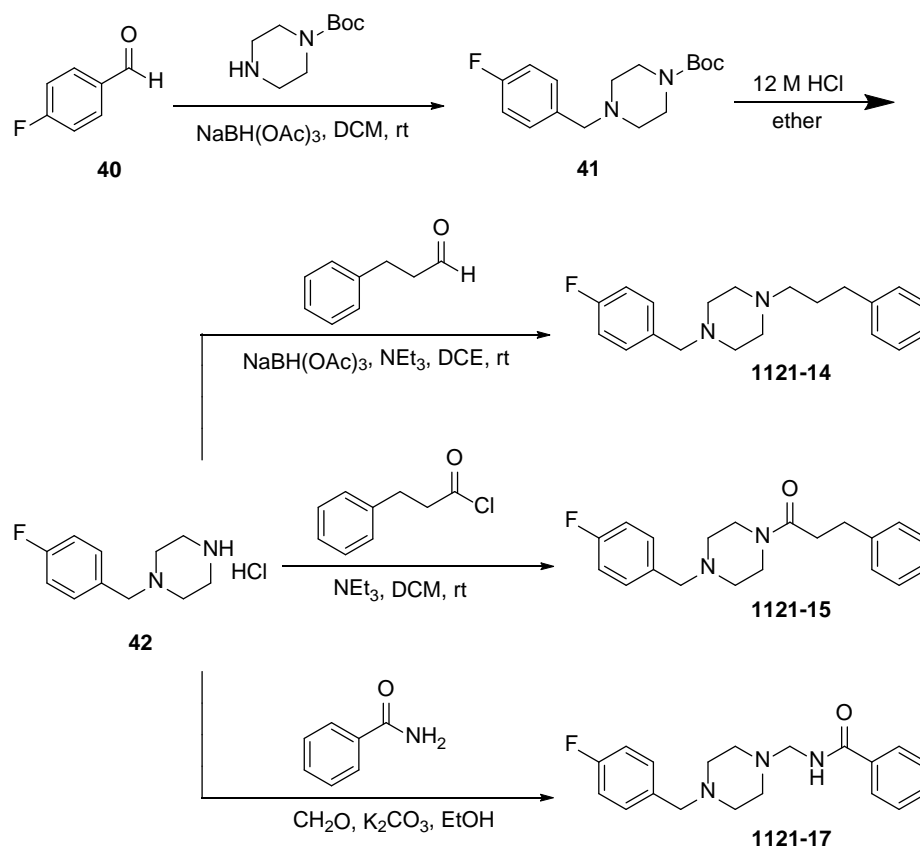
IC_{50} values were obtained by fitting the Hill equation (see chapter 2.4.5) to the average composite concentration-effect curves. The mean IC_{50} values plus confidence intervals are given in the appendix E.

Linker 2 also had the possibility of changing the activity. Started with 2-Chlorobenzylamine (**37**) and bromoacetyl bromide, α -bromo acetamide (**38**) was formed and treated with boc-piperazine in the presence of potassium carbonate to yield the corresponding piperazine. The Boc-protect group was removed by the treatment of 12 N hydrogen chloride, followed by the treatment of 4-nitrobenzaldehyde in the presence of sodium triacetoxyborohydride to give compound **1121-16**, which showed no activity at GluN2 receptors (Scheme 17, Table 26) [138].



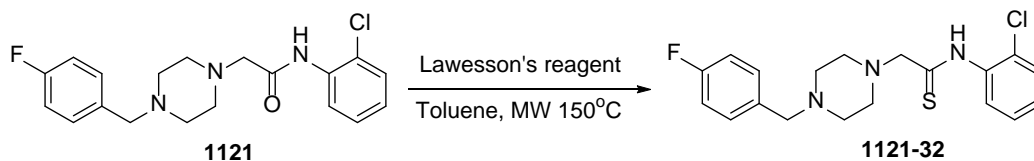
Scheme 17. Synthesis of 1121-16.

4-fluorobenzaldehyde (**40**) and Boc-piperazine were treated with sodium triacetoxyborohydride to form the corresponding piperazine (**41**). The Boc group was deprotected by the treatment of 12 N hydrogen chloride in ether. Then, 3-phenylpropanal in the presence of sodium triacetoxyborohydride was added to yield **1121-14** [142]. Compound **1121-15** was synthesized by adding 3-phenylpropanoyl chloride with triethylamine [86, 143]. The piperazine amine was refluxed with benzamide, paraformaldehyde and potassium carbonate in ethanol to give compound **1121-17** [144] (*Scheme 18*). Unfortunately, none of the compounds with these modified linkers were active (*Table 26*).



Scheme 18. Synthesis of 1121 analogues with linker modifications.

According to the from Strong, et al 2017, thioamide-containing compounds with CIQ scaffold were consistently more potent than amide-containing compounds because thioamide bonds have a larger rotational barrier [89-91]. Therefore, compound **1121-32** with thioamide linker was synthesized to explore the functionality of amide group in the linker 2. Compound **1121** was converted to thioamide-containing compound **1121-32** with Lawesson's reagent in toluene via microwave irradiation [92] (Scheme 19). The SAR result showed that compound **1121-32** had no inhibition at all GluN2 subunits (Table 26).



Scheme 19. Synthesis of thioamide compound 1121-32.

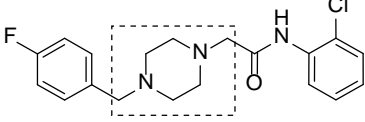
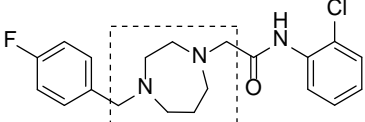
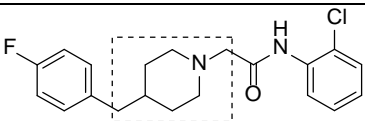
Table 26. Linker 2 modification.

1121-	GluN2A IC ₅₀ (μM)	GluN2B IC ₅₀ (μM)	GluN2C IC ₅₀ (μM)	GluN2D IC ₅₀ (μM)
14	NE	NE	NE	NE
15	NE	NE	NE	NE
16	NE	NE	NE	NE
17	NE	NE	NE	NE
32	NE	NE	NE	NE

IC₅₀ values were obtained by fitting the Hill equation (see chapter 2.4.5) to the average composite concentration-effect curves. Data were from 4-13 oocytes between 1-2 frogs. NE indicates less than 50% inhibition at 30 μM. The mean IC₅₀ values plus confidence intervals are given in the appendix E.

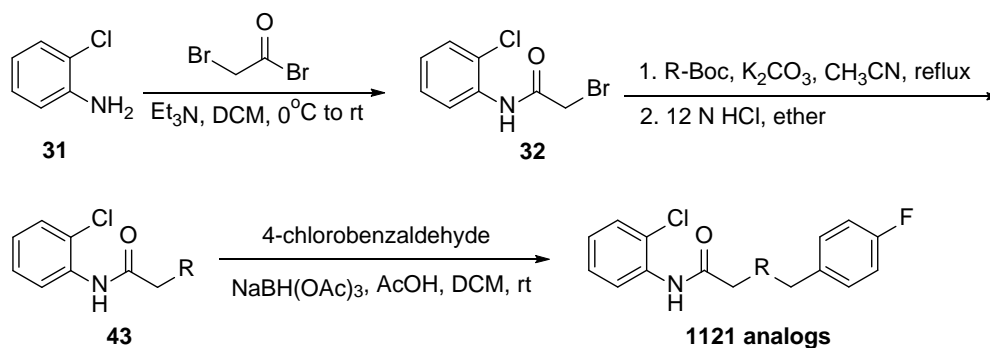
Besides the linkers, the piperazine ring is also significant for improving the GluN2D selectivity. Compared with **1121**, purchased compound **2106** and **2109** with 1,4-diazepane and piperidine groups respectively, lost all activity (*Table 27*). Hence, I hypothesize that, instead of replacing the piperazine ring, adding substitutions on piperazine ring or replacing the piperazine ring with another group may change the activity.

Table 27. SAR study of purchased compounds 1121, 2106, and 2109.

	Structures	GluN2A IC ₅₀ (μM)	GluN2B IC ₅₀ (μM)	GluN2C IC ₅₀ (μM)	GluN2D IC ₅₀ (μM)
1121		50	46	14	13
2106		NE	NE	NE	NE
2109		NE	NE	NE	NE

4.4 Piperazine ring modification

To explore the role of the piperazine ring, compounds **1121-24**, **1121-27** to **1121-31** were synthesized. Commercially available bromoacetyl bromide and aniline were reacted in the presence of triethylamine in DCM to yield the corresponding α -bromo acetamide in high yield. The intermediate α -bromo acetamide was treated with substituted boc-protected piperazine or other boc-protected compounds in the presence of potassium carbonate and then deprotected the boc group by the treatment of 12 N hydrogen chloride. 4-chlorobenzaldehyde was reacted with corresponding products in the presence of sodium triacetoxyborohydride to afford final compounds **1121-24**, **1121-27** to **1121-31** (Scheme 20) [138]. The IC₅₀ values were evaluated, but none of these compounds showed inhibition at any NMDA receptors (Table 28).



Scheme 20. Synthesis of 1121 analogues with piperazine ring modifications.

Table 28. Piperazine ring modification.

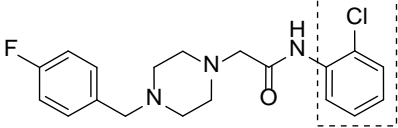
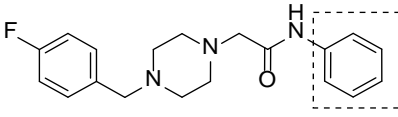
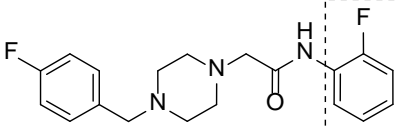
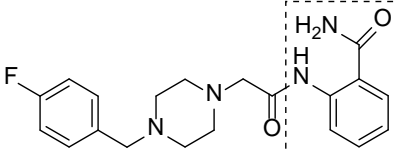
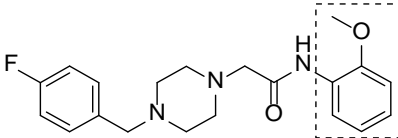
1121-	R	GluN2A IC ₅₀ (μM) pH 7.4	GluN2B IC ₅₀ (μM) pH 7.4	GluN2C IC ₅₀ (μM) pH 7.4	GluN2D IC ₅₀ (μM) pH 7.4
24		NE	NE	NE	NE
27		NE	NE	NE	NE
28		NE	NE	NE	NE
29		NE	NE	NE	NE
30		NE	NE	NE	NE
31		NE	NE	NE	NE

IC₅₀ values were obtained by fitting the Hill equation (see chapter 2.4.5) to the average composite concentration-effect curves. Data were from 4-13 oocytes between 1-2 frogs. NE indicates less than 50% inhibition at 30 μM. The mean IC₅₀ values plus CI are given in the appendix E.

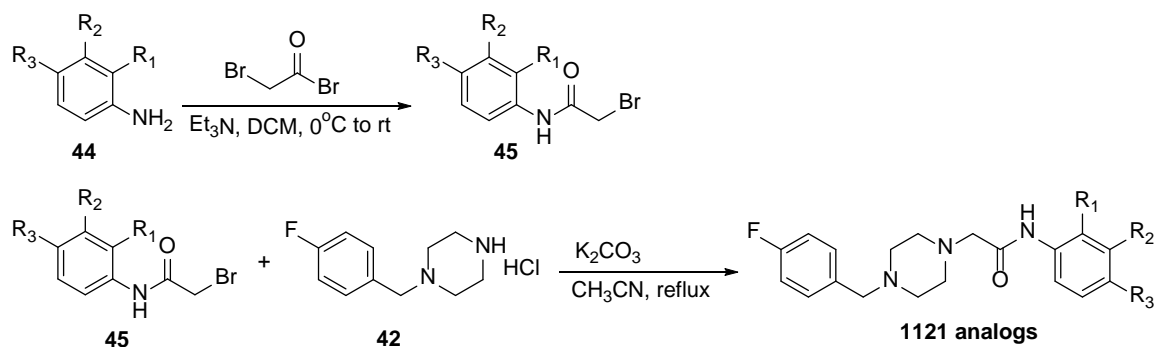
4.5 B-ring modification

Purchased compounds **2046**, **2031**, **2137**, and **2138** were evaluated their inhibition at GluN2 subunits. Compared to *ortho*-chloro substitution compound 1121, compounds with *ortho*-fluoro, *ortho*-amide, and *ortho*-methoxy substitutions decreased the potency at GluN2C- and GluN2D-containing receptors (*Table 29*). Therefore, a more hydrophobic and electron-withdrawing group may be preferred to the activity.

Table 29. SAR study of compounds with different B ring substitutions.

	Structures	GluN2A IC ₅₀ (μM) pH 7.4	GluN2B IC ₅₀ (μM) pH 7.4	GluN2C IC ₅₀ (μM) pH 7.4	GluN2D IC ₅₀ (μM) pH 7.4
1121		50	46	14	13
2046		NE	134	80	81
2031		139	106	51	28
2137		NE	NE	NE	NE
2138		NE	NE	NE	NE

Firstly, to explore which substituted position on the B ring was more favorable to the activity, compounds with *meta*- or *para*-chloro substitution were synthesized by replacing *ortho*-chloro substitution. The piperazine amine was first synthesized via two general steps as shown in the former chapters. In the meantime, α -bromo acetamide was formed using bromoacetyl bromide and appropriate anilines. The resultant α -bromo acetamide and the corresponding piperazine amine were refluxed in the presence of potassium carbonate in acetonitrile to yield the final compound **1121-25** and **1121-26** (*Scheme 21*). In comparison to compound **1121** which was active at GluN2C- and GluN2D-containing receptors, compounds **1121-25** and **1121-26** with *meta*- and *para*- substitution lost their activity at all GluN2 subunits (*Table 30*). According to these results, substitution at *ortho*-position on the B ring was more favorable of improving the potency at GluN2D subunit.



Scheme 21. Synthesis of 1121 analogues with different B ring substitutions.

According to above results, substitution at *ortho*-position on the B ring was more favorable of improving the potency at GluN2D subunit. Compound **1121-33** with more hydrophobic and electro-withdrawing trifluoromethyl group was synthesized through the same synthetic pathway as shown above (*Scheme 21*) and slightly decreased the potency at GluN2C- and GluN2D-containing receptor in comparison to compound **1121**.

Compound **1121-34** with lipophilic methyl group substituent was also synthesized but did not inhibit any of the GluN2 subunits (*Table 30*).

Table 30. B-ring modification.

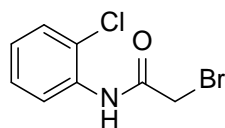
1121-	R ₁	R ₂	R ₃	GluN2A IC ₅₀ (μM)	GluN2B IC ₅₀ (μM)	GluN2C IC ₅₀ (μM)	GluN2D IC ₅₀ (μM)
25	H	Cl	H	NE	NE	NE	NE
26	H	H	Cl	NE	NE	NE	NE
33	CF ₃	H	H	NE	NE	~30	~20
34	CH ₃	H	H	NE	NE	NE	NE
IC ₅₀ values were obtained by fitting the Hill equation (see chapter 2.4.5) to the average composite concentration-effect curves. Data were from 4-13 oocytes between 1-2 frogs. NE indicates less than 50% inhibition at 30 μM. The mean IC ₅₀ values plus confidence intervals are given in the appendix E.							

4.6 Chemistry experimental of 1121-series

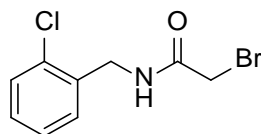
All the commercially available chemicals were purchased from Sigma-Aldrich and Alfa Aesar and used without further purification. Reaction progress was monitored using thin layer chromatography (TLC) on pre-coated aluminum plates (silica gel 60 F254, 0.25 mm) and liquid chromatography-mass spectrometry (LCMS, Varian). Flash column chromatography using a Teledyne ISCO Combiflash Companion with Teledyne RediSep disposable normal phase silica columns is used to purify crude compounds. The purity of final compounds was evaluated in two solvents systems (MeOH/water and ACN/water) by HPLC (Varian). Proton, carbon and fluorine NMR spectra were recorded on Mercury 300 (300 MHz), VNMRS 400 (400 MHz), or INOVA 400 (400 MHz) instruments. Proton and carbon NMR spectra utilize the related solvent peak as a reference. All chemical shifts and coupling constants were reported in parts per million and Hertz (Hz), respectively. The

high-resolution mass spectrometry (HRMS) was evaluated from Emory University Mass Spectrometry Center on either a VG 70-S Nier Johnson or JEOL instrument.

General procedure A for the synthesis of α -Bromoacetamide (32). Bromoacetyl bromide (1.1 equivalents) was added dropwise to a solution of benzylamine or aniline **31** (1 equiv.) and triethylamine (1.2 equiv.) dissolved in methylene chloride (0.55 molar) at 0 °C in an ice-bath. The cooling bath was then removed, and the reaction mixture was stirred at room temperature for 3 h. The reaction mixture was washed sequentially with 1 N HCl, saturated aqueous NaHCO₃ solution, and water and then dried over anhydrous MgSO₄. The solvent was removed by evaporation to afford the corresponding compound **32**.



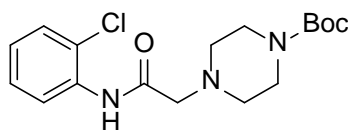
2-bromo-N-(2-chlorophenyl)acetamide (32). Compound **32** was prepared via general procedure **A** using 2-chloroaniline (8.2 ml, 78 mmol), 2-bromoacetyl bromide (7.5 ml, 86 mmol), and triethylamine (13 ml, 94 mmol). Yield as yellow solid 16 g, 82%. ¹H NMR (400 MHz, DMSO-*d*₆) δ 9.96 (s, 1H), 7.72 (d, *J* = 7.1 Hz, 1H), 7.52 (dd, *J* = 8.2, 1.1 Hz, 1H), 7.35 (t, *J* = 7.6 Hz, 1H), 7.23 (td, *J* = 7.6, 1.4 Hz, 1H), 4.17 (s, 2H). ¹³C NMR (100 MHz, DMSO-*d*₆) δ 165.35, 134.26, 129.61, 127.55, 126.82, 126.53, 125.99, 29.71.



2-bromo-N-(2-chlorobenzyl)acetamide (38). Compound **38** was prepared via general procedure **A** using (2-chlorophenyl)methanamine (0.85 ml, 7.1 mmol), 2-bromoacetyl bromide (0.68 ml, 7.8 mmol), and triethylamine (1.2 ml, 8.5 mmol). Yield as brown solid 1.4 g, 75%. ¹H NMR (300 MHz, DMSO-*d*₆) δ 8.82 (s, 1H), 7.47-7.44 (m, 1H), 7.36-7.28

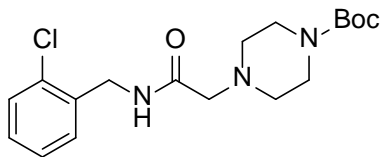
(m, 3H), 4.36 (d, $J = 5.9$ Hz, 2H), 3.95 (s, 2H). ^{13}C NMR (100 MHz, DMSO- d_6) δ 166.33, 135.70, 132.18, 129.21, 128.89, 127.24, 40.52, 29.30.

General Procedure B for the synthesis of 2-Benzamino-4-Boc Piperazine (33). To a solution of **32** (1 equiv.) in acetonitrile (0.48 molar) at room temperature was added potassium carbonate (2.5 equiv.) and *N*-Boc piperazine (1 equiv.). The mixture was refluxed for 6 h, and the reaction mixture was then cooled to room temperature. The solvent was removed by evaporation, and the residue was dissolved in dichloromethane, washed with water, and then dried over MgSO_4 . The solvent was removed in *vacuo* and yield the product.



tert-butyl 4-(2-((2-chlorophenyl)amino)-2-oxoethyl) piperazine-1-carboxylate (33).

Compound **33** was prepared via general procedure **B** using **32** (0.85 g, 3.4 mmol), *N*-boc piperazine (0.63 g, 3.4 mmol), and potassium carbonate (1.2 g, 8.5 mmol). Yield brown solid 1.1 g, 88%. ^1H NMR (400 MHz, DMSO- d_6) δ 9.77 (s, 1H), 8.14 (d, $J = 8.2$ Hz, 1H), 7.41 (d, $J = 8.2$ Hz, 1H), 7.24 (t, $J = 7.8$ Hz, 1H), 7.03 (td, $J = 7.4, 0.8$ Hz, 1H), 3.23 (s, 2H), 3.10 (s, 3H), 2.42 (t, $J = 4.6$ Hz, 4H), 1.30 (s, 9H). ^{13}C NMR (100 MHz, DMSO- d_6) δ 168.20, 153.77, 134.37, 129.25, 127.86, 125.03, 122.96, 121.39, 78.94, 61.16, 52.46, 28.07, 28.04.

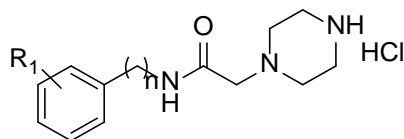


tert-butyl 4-(2-((2-chlorobenzyl)amino)-2-oxoethyl) piperazine-1-carboxylate (39).

Compound **39** was prepared via general procedure **B** using **38** (1.8 g, 7.0 mmol), *N*-boc

piperazine (1.3 g, 7.0 mmol), and potassium carbonate (2.4 g, 18 mmol). Yield brown solid 2.4 g, 91%. ^1H NMR (300 MHz, DMSO-*d*₆) δ 8.34 (t, J=5.9 Hz, 1H), 7.45-7.42 (m, 1H), 7.33-7.27 (m, 3H), 4.36 (d, J= 5.9 Hz, 2H), 3.35 (s, 4H), 3.04 (s, 2H), 2.42 (t, J= 4.7 Hz, 4H), 1.39 (s, 9H). ^{13}C NMR (100 MHz, DMSO-*d*₆) δ 169.49, 157.94, 153.82, 149.12, 136.40, 131.87, 129.09, 128.62, 127.18, 78.82, 60.94, 52.64, 39.88, 28.06.

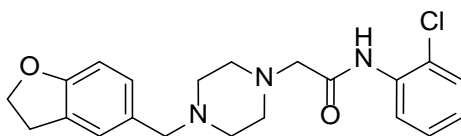
General Procedure C for the synthesis of 2-Benzamino Piperazine Hydrochloride 34.



Compound **33** (1 equiv.) was dissolved in a solution of ether and 12 N HCl and allowed to stir at room temperature for 40 minutes. The volatiles were removed in *vacuo* to afford the product without purification.

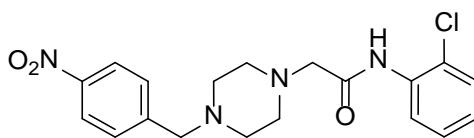
General Procedure D for the synthesis of 2-Benzamino-4-substituted Piperazine 1121 series.

To a solution of **34** (1 equiv.) in methylene chloride (0.17 molar) at room temperature under N₂ atmosphere was added sequentially aldehyde (2 equiv.), acetic acid (1 equiv.) and sodium triacetoxyborohydride (3 equiv.). The reaction mixture was stirred at the same temperature for 2 h. To the resulting reaction mixture was added 1 N aqueous NaOH solution while stirring. This mixture was stirred at room temperature for 0.5 h and then extracted with methylene chloride. The organic extract was dried over anhydrous MgSO₄. The solvent was removed by evaporation and the crude product was then purified by flash chromatography on silica gel using a 20-80% EA/Hexanes gradient.



***N*-(2-chlorophenyl)-2-(4-((2,3-dihydrobenzofuran-5-yl)methyl)piperazin-1-**

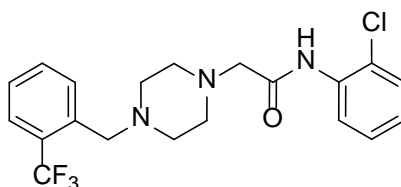
yl)acetamide (1121-2). Compound **1121-2** was prepared via general procedure D using piperazine hydrochloride **34** (0.12 g, 0.46 mmol), 2,3-dihydrobenzofuran-5-carboxaldehyde (0.12 ml, 0.91 mmol), acetic acid (0.026 ml, 0.46 mmol), and sodium triacetoxyborohydride (0.29 g, 1.4 mmol). The product was obtained after flash chromatography and came out at 50-60% EA/Hexanes. Yield a yellow oil 60 mg, 34%. ^1H NMR (300 MHz, DMSO-*d*₆) δ 9.92 (s, 1H), 8.29 (dd, *J*= 8.2, 1.1 Hz, 1H), 7.52 (dd, *J*= 8.2, 1.2 Hz, 1H), 7.35 (td, *J*= 8.2, 1.1 Hz, 1H), 7.15 (s, 1H), 7.13 (td, *J*= 7.6, 1.8 Hz, 1H), 6.98 (dd, *J*= 7.6, 1.8 Hz, 1H), 6.68 (d, *J*= 8.2 Hz, 1H), 4.49 (t, *J*= 8.8 Hz, 2H), 3.35 (s, 2H), 3.16 (s, 2H), 3.15 (t, *J*= 8.5 Hz, 2H), 2.57 (s, 4H), 2.44 (s, 4H). ^{13}C NMR (100 MHz, DMSO-*d*₆) δ 168.48, 134.42, 129.82, 129.29, 128.50, 127.99, 125.73, 124.88, 122.39, 120.91, 108.31, 70.85, 61.74, 61.26, 52.85, 52.75, 29.07. HRMS (*m/z*): [*M*+*H*]⁺ calculated for C₂₁H₂₄ClN₃O₂, 386.16298; found, 386.16336.



***N*-(2-chlorophenyl)-2-(4-(4-nitrobenzyl)piperazin-1-yl)acetamide (1121-3).**

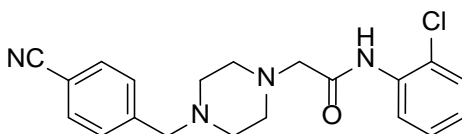
Compound **1121-3** was prepared via general procedure D using piperazine hydrochloride **34** (0.25 g, 0.99 mmol), 4-nitrobenzaldehyde (0.30 g, 2.0 mmol), acetic acid (0.056 ml, 0.99 mmol), and sodium triacetoxyborohydride (0.63 g, 3.0 mmol). The product was obtained after flash chromatography and came out at 60-70% EA/Hexanes. Yield a yellow solid 80 mg, 21%; m.p. 119-122 °C. ^1H NMR (300 MHz, DMSO-*d*₆) δ 9.91 (s, 1H), 8.28

(dd, $J = 8.2, 1.1$ Hz, 1H), 8.20 (dt, $J = 8.8, 1.8$ Hz, 2H), 7.60 (d, $J = 8.8$ Hz, 2H), 7.52 (dd, $J = 7.9, 1.5$ Hz, 1H), 7.35 (td, $J = 7.9, 1.8$ Hz, 1H), 7.13 (td, $J = 7.6, 1.7$ Hz, 1H), 3.64 (s, 2H), 3.18 (s, 2H), 2.61 (s, 4H), 2.50 (s, 4H). ^{13}C NMR (100 MHz, DMSO- d_6) δ 168.42, 146.66, 146.57, 134.39, 129.73, 129.27, 127.96, 124.89, 123.40, 120.97, 61.20, 60.88, 52.88, 52.78; mp 107-111 °C. HRMS (m/z): $[\text{M}+\text{H}]^+$ calculated for $\text{C}_{19}\text{H}_{21}\text{ClN}_4\text{O}_3$, 389.13749; found, 389.13721.



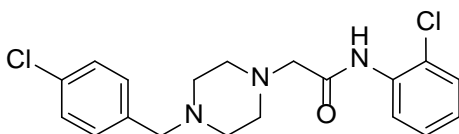
***N*-(2-chlorophenyl)-2-(4-(2-(trifluoromethyl)benzyl)piperazin-1-yl)acetamide (1121-**

4). Compound **1121-4** was prepared via general procedure D using piperazine hydrochloride **34** (0.26 g, 1.0 mmol), 2-(trifluoromethyl)benzaldehyde (0.27 ml, 2.0 mmol), acetic acid (0.058 ml, 1.0 mmol), and sodium triacetoxyborohydride (0.64 g, 3.0 mmol). The product was obtained after flash chromatography and came out at 30% EA/Hexanes. Yield a yellow oil 0.23 g, 56%. ^1H NMR (300 MHz, DMSO- d_6) δ 9.91 (s, 1H), 8.28 (d, $J = 8.2$ Hz, 1H), 7.77 (d, $J = 7.6$ Hz, 1H), 7.68 (t, $J = 7.6$ Hz, 2H), 7.52 (d, $J = 7.6$ Hz, 1H), 7.46 (t, $J = 7.6$ Hz, 1H), 7.35 (t, $J = 7.6$ Hz, 1H), 7.13 (td, $J = 8.2, 1.2$ Hz, 1H), 3.64 (s, 2H), 3.18 (s, 2H), 2.61 (s, 4H), 2.50 (s, 4H). ^{13}C NMR (100 MHz, DMSO- d_6) δ 168.40, 137.30, 134.42, 132.48, 130.54, 129.27, 127.95, 127.43, 125.79, 125.72, 124.89, 122.48, 121.00, 61.22, 57.66, 53.04, 52.84. HRMS (m/z): $[\text{M}+\text{H}]^+$ calculated for $\text{C}_{20}\text{H}_{21}\text{ClF}_3\text{N}_3\text{O}$, 412.13980; found, 412.13962.



***N*-(2-chlorophenyl)-2-(4-(4-cyanobenzyl)piperazin-1-yl)acetamide (1121-5).**

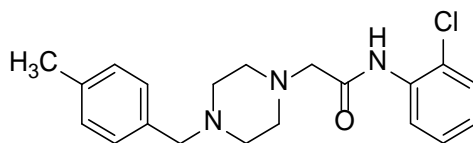
Compound **1121-5** was prepared via general procedure D using piperazine hydrochloride **34** (0.26 g, 1.0 mmol), 4-formylbenzonitrile (0.27 g, 2.0 mmol), acetic acid (0.058 ml, 1.0 mmol), and sodium triacetoxyborohydride (0.64 g, 3.0 mmol). The product was obtained after flash chromatography and came out at 50-60% EA/Hexanes. Yield a yellow gel 60 mg, 16%. ^1H NMR (300 MHz, CDCl_3) δ 9.94 (s, 1H), 8.46 (dd, J = 8.2, 1.2 Hz, 1H), 7.61 (d, J = 8.2 Hz, 1H), 7.60 (t, J = 6.2 Hz, 1H), 7.46 (d, J = 8.3 Hz, 2H), 7.37 (dd, J = 8.2, 1.8 Hz, 1H), 7.27 (td, J = 7.9, 1.4 Hz, 1H), 7.03 (td, J = 7.9, 1.8 Hz, 1H), 3.59 (s, 2H), 3.19 (s, 2H), 2.69 (s, 4H), 2.56 (s, 4H). ^{13}C NMR (100 MHz, CDCl_3) δ 168.41, 143.87, 134.37, 132.03, 129.39, 129.33, 128.92, 127.67, 124.37, 120.77, 118.81, 110.81, 62.10, 61.86, 53.23, 52.89. HRMS (m/z): $[\text{M}+\text{H}]^+$ calculated for $\text{C}_{20}\text{H}_{21}\text{ClN}_4\text{O}$, 369.14767; found, 369.14770.



2-(4-(4-chlorobenzyl)piperazin-1-yl)-*N*-(2-chlorophenyl)acetamide (1121-6).

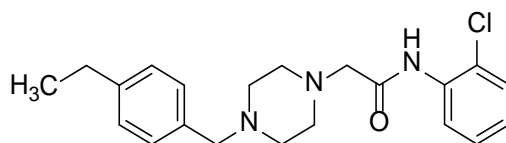
Compound **1121-6** was prepared via general procedure D using piperazine hydrochloride **34** (0.21 g, 0.84 mmol), 4-chlorobenzaldehyde (0.24 g, 1.7 mmol), acetic acid (0.048 ml, 0.84 mmol), and sodium triacetoxyborohydride (0.53 g, 2.5 mmol). The product was obtained after flash chromatography and came out at 50% EA/Hexanes. Yield a yellow gel 0.17 g, 54%. ^1H NMR (300 MHz, $\text{DMSO}-d_6$) δ 9.91 (s, 1H), 8.29 (dd, J = 8.2, 1.8 Hz, 1H), 7.52 (dd, J = 8.2, 1.2 Hz, 1H), 7.39-7.31 (m, 3H), 7.35 (d, J = 8.2 Hz, 2H), 7.12 (td, J = 7.6,

1.8 Hz, 1H), 3.36 (s, 2H), 3.17 (s, 2H), 2.58 (s, 4H), 2.46 (s, 4H). ^{13}C NMR (100 MHz, DMSO-*d*₆) δ 168.45, 137.24, 134.40, 131.47, 130.62, 129.29, 128.16, 127.99, 124.89, 124.05, 122.40, 120.92, 61.23, 60.99, 52.81, 52.78. HRMS (*m/z*): $[\text{M}+\text{H}]^+$ calculated for $\text{C}_{19}\text{H}_{22}\text{ON}_3\text{Cl}_2$, 378.11344; found, 378.11375.



***N*-(2-chlorophenyl)-2-(4-(4-methylbenzyl)piperazin-1-yl)acetamide (1121-8).**

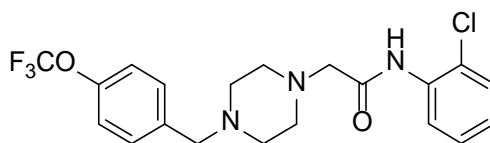
Compound **1121-8** was prepared via general procedure D using piperazine hydrochloride **34** (0.15 g, 0.61 mmol), 4-methylbenzaldehyde (0.15 g, 1.2 mmol), acetic acid (0.035 ml, 0.61 mmol), and sodium triacetoxyborohydride (0.39 g, 1.8 mmol). The product was obtained after flash chromatography and came out at 50-60% EA/Hexanes. Yield as a yellow solid 0.17 g, 78%, m.p. 102-105 °C. ^1H NMR (300 MHz, CDCl_3) δ 10.06 (s, 1H), 8.54 (dd, *J*= 8.2, 1.2 Hz, 1H), 7.44 (dd, *J*= 8.2, 1.2 Hz, 1H), 7.36-7.27 (m, 3H), 7.20 (d, *J*= 8.2 Hz, 2H), 7.12-7.07 (m, 1H), 3.57 (s, 2H), 3.24 (s, 2H), 2.74 (s, 4H), 2.62 (s, 4H), 2.41 (s, 3H). ^{13}C NMR (100 MHz, DMSO-*d*₆) δ 168.43, 135.95, 135.00, 134.39, 129.26, 128.82, 128.73, 127.95, 124.83, 122.36, 120.88, 61.71, 61.23, 54.93, 52.79, 20.70. HRMS (*m/z*): $[\text{M}+\text{H}]^+$ calculated for $\text{C}_{20}\text{H}_{25}\text{ClN}_3\text{O}$, 358.16807; found, 358.16731.



***N*-(2-chlorophenyl)-2-(4-(4-ethylbenzyl)piperazin-1-yl)acetamide (1121-9).**

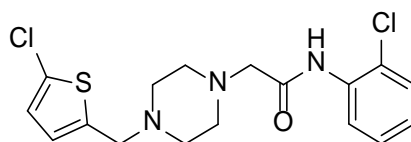
Compound **1121-9** was prepared via general procedure D using piperazine hydrochloride **34** (0.15 g, 0.61 mmol), 4-ethylbenzaldehyde (0.17 ml, 1.2 mmol), acetic acid (0.035 ml, 0.61 mmol), and sodium triacetoxyborohydride (0.39 g, 1.8 mmol). The product was

obtained after flash chromatography and came out at 50-60% EA/Hexanes. Yield as a yellow gel 0.17 g, 75%. ^1H NMR (300 MHz, DMSO-*d*₆) δ 9.92 (s, 1H), 8.30 (d, *J*= 8.2 Hz, 1H), 7.51 (dd, *J*= 8.2, 1.7 Hz, 1H), 7.34 (td, *J*= 7.6, 1.7 Hz, 1H), 7.20 (d, *J*= 8.2 Hz, 2H), 7.14 (d, *J*= 8.8 Hz, 3H), 3.44 (s, 2H), 3.16 (s, 2H), 2.57 (q, *J*= 7.6 Hz, 2H), 2.56 (s, 4H), 2.45 (s, 4H), 1.16 (t, *J*= 7.6 Hz, 3H). ^{13}C NMR (100 MHz, DMSO-*d*₆) δ 168.42, 142.33, 135.23, 134.39, 129.24, 128.86, 127.95, 127.52, 124.83, 122.34, 120.85, 61.72, 61.23, 52.79, 27.85, 15.65. HRMS (*m/z*): [*M*+*H*]⁺ (*Cl*³⁵) calculated for C₂₁H₂₇ClN₃O, 372.18372; found, 372.18270.



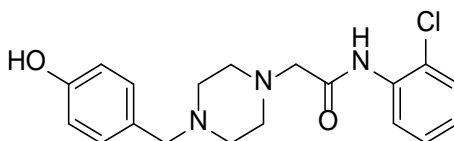
***N*-(2-chlorophenyl)-2-(4-(4-(trifluoromethoxy)benzyl)piperazin-1-yl)acetamide**

(1121-10). Compound **1121-10** was prepared via general procedure D using piperazine hydrochloride **34** (0.15 g, 0.58 mmol), 4-(trifluoromethoxy)benzaldehyde (0.16 ml, 1.2 mmol), acetic acid (0.033 ml, 0.58 mmol), and sodium triacetoxyborohydride (0.37 g, 1.7 mmol). The product was obtained after flash chromatography (EA/Hexanes). Yield as a yellow gel 0.17 g, 69%. ^1H NMR (300 MHz, DMSO-*d*₆) δ 9.92 (s, 1H), 8.30 (dd, *J*= 8.2, 1.1 Hz, 1H), 7.51 (dd, *J*= 8.2, 1.7 Hz, 1H), 7.44 (d, *J*= 8.8 Hz, 2H), 7.37-7.30 (m, 3H), 7.12 (td, *J*= 7.6, 1.8 Hz, 1H), 3.53 (s, 2H), 3.17 (s, 2H), 2.59 (s, 4H), 2.47 (s, 4H). ^{13}C NMR (100 MHz, DMSO-*d*₆) δ 168.42, 147.27, 137.66, 134.40, 130.51, 129.26, 127.95, 124.85, 122.37, 121.81, 120.89, 120.79, 61.20, 60.88, 52.78, 52.75. HRMS (*m/z*): [*M*+*H*]⁺ (*Cl*³⁵) calculated for C₂₀H₂₂ClF₃N₃O₂, 428.13472; found, 428.13461.



2-(4-((4-chlorocyclopenta-1,3-dien-1-yl)methyl)piperazin-1-yl)-N-(2-chlorophenyl)

acetamide (1121-11). Compound **1121-11** was prepared via general procedure D using piperazine hydrochloride **34** (0.16 g, 0.62 mmol), 5-chlorothiophene-2-carbaldehyde (0.13 ml, 1.2 mmol), acetic acid (0.035 ml, 0.62 mmol), and sodium triacetoxyborohydride (0.39 g, 1.9 mmol). The product was obtained after flash chromatography (EA/Hexanes). Yield as a yellow gel 0.15 g, 62%. ^1H NMR (300 MHz, DMSO-*d*₆) δ 9.91 (s, 1H), 8.29 (dd, *J* = 8.2, 1.8 Hz, 1H), 7.52 (dd, *J* = 8.2, 1.8 Hz, 1H), 7.34 (td, *J* = 7.6, 1.2 Hz, 1H), 7.12 (td, *J* = 7.6, 1.8 Hz, 1H), 6.94 (d, *J* = 3.5 Hz, 1H), 6.86 (d, *J* = 4.1 Hz, 1H), 3.65 (s, 2H), 3.18 (s, 2H), 2.59 (s, 4H), 2.51 (s, 4H). ^{13}C NMR (100 MHz, DMSO-*d*₆) δ 168.42, 141.85, 134.40, 129.27, 127.96, 126.19, 125.64, 124.88, 122.44, 120.94, 109.57, 61.13, 56.46, 52.72, 52.53. HRMS (*m/z*): [*M*+*H*]⁺ calculated for C₁₇H₂₀Cl₂N₃OS, 384.06986; found, 384.06983.

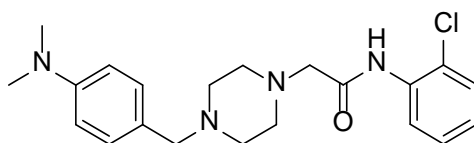


N-(2-chlorophenyl)-2-(4-(4-hydroxybenzyl)piperazin-1-yl)acetamide (1121-12).

Compound **1121-12** was prepared via general procedure D using piperazine hydrochloride **34** (0.25 g, 0.99 mmol), 4-hydroxybenzaldehyde (0.24 g, 2.0 mmol), acetic acid (0.056 ml, 0.99 mmol), and sodium triacetoxyborohydride (0.63 g, 3.0 mmol). The product was obtained after flash chromatography (EA/Hexanes), yield as yellow gel 99 mg, 28%. ^1H NMR (300 MHz, DMSO-*d*₆) δ 9.92 (s, 1H), 8.29 (dt, *J* = 8.2, 1.3 Hz, 1H), 7.52 (dt, *J* = 8.0, 1.1 Hz, 1H), 7.35 (tt, *J* = 7.7, 1.7 Hz, 1H), 7.18 – 7.04 (m, 2H), 6.73 – 6.66 (m, 1H), 3.16 (d, *J* = 2.3 Hz, 2H), 2.70 – 2.27 (m, 10H). ^{13}C NMR (75 MHz, DMSO-*d*₆) δ 168.47, 139.84,

134.40, 130.09, 129.29, 127.98, 124.89, 124.89, 120.96, 114.86, 61.26, 52.85, 52.65.

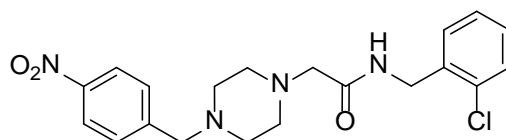
HRMS (m/z): $[M+H]^+$ (Cl^{35}) calculated for $C_{19}H_{23}ClN_3O_2$, 360.14733; found, 360.14797.



***N*-(2-chlorophenyl)-2-(4-(4-(dimethylamino)benzyl)piperazin-1-yl)acetamide (1121-**

13). Compound **1121-13** was prepared via general procedure D using piperazine hydrochloride **34** (0.19 g, 0.75 mmol), 4-(dimethylamino)benzaldehyde (0.11 g, 1.5 mmol), acetic acid (0.043 ml, 0.75 mmol), and sodium triacetoxyborohydride (0.48 g, 2.3 mmol).

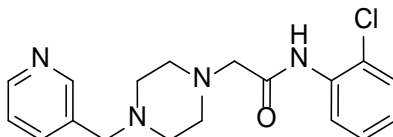
The product was obtained after flash chromatography (EA/Hexanes). Yield as a yellow solid 0.17 g, 58%, m.p. 114-117 °C. 1H NMR (300 MHz, DMSO- d_6) δ 9.92 (s, 1H), 8.30 (dd, J = 8.2, 1.1 Hz, 1H), 7.52 (dd, J = 8.2, 1.8 Hz, 1H), 7.34 (td, J = 7.6, 1.2 Hz, 1H), 7.14 (dd, J = 7.6, 1.8 Hz, 1H), 7.09 (dd, J = 8.8 2.3 Hz, 2H), 6.66 (d, J = 8.8 Hz, 2H), 3.35 (s, 2H), 3.15 (s, 2H), 2.86 (s, 6H), 2.56 (s, 4H), 2.43 (s, 4H). ^{13}C NMR (100 MHz, DMSO- d_6) δ 168.46, 149.61, 134.40, 129.73, 129.27, 127.96, 125.35, 124.85, 122.36, 120.88, 112.19, 61.65, 61.26, 52.85, 52.73, 40.27. HRMS (m/z): $[M+H]^+$ calculated for $C_{21}H_{26}ON_4Cl$, 385.17897; found, 385.17897.



***N*-(2-chlorobenzyl)-2-(4-(4-nitrobenzyl)piperazin-1-yl)acetamide (1121-16).**

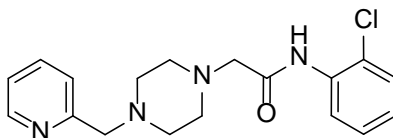
Compound **1121-16** was prepared via general procedure D using piperazine hydrochloride (0.25 g, 0.93 mmol), 4-nitrobenzaldehyde (0.28 g, 1.9 mmol), acetic acid (0.053 ml, 0.93 mmol), and sodium triacetoxyborohydride (0.59 g, 2.8 mmol). The product was obtained after flash chromatography (EA/Hexanes). Yield as yellow gel 0.27 g, 73%. 1H NMR (300

MHz, DMSO-*d*6) δ 8.26-8.21 (m, 1H), 8.20 (d, *J* = 8.8 Hz, 2H), 7.58 (d, *J* = 8.8 Hz, 2H), 7.44-7.41 (m, 1H), 7.31-7.26 (m, 3H), 4.36 (d, *J* = 6.5 Hz, 2H), 3.61 (s, 2H), 3.01 (s, 2H), 2.49 (s, 4H), 2.45 (s, 4H). ^{13}C NMR (100 MHz, DMSO-*d*6) δ 169.58, 146.70, 136.42, 131.90, 129.70, 129.08, 128.67, 128.54, 127.12, 123.37, 61.13, 60.99, 52.94, 52.47, 39.89. HRMS (*m/z*): $[\text{M}+\text{H}]^+$ calculated for $\text{C}_{20}\text{H}_{24}\text{O}_3\text{N}_4\text{Cl}$, 403.15314; found, 403.15308.



***N*-(2-chlorophenyl)-2-(4-(pyridin-3-ylmethyl)piperazin-1-yl)acetamide (1121-18).**

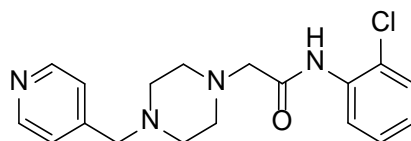
Compound **1121-18** was prepared via general procedure D using piperazine hydrochloride **34** (0.2 g, 0.79 mmol), nicotinaldehyde (0.15 ml, 1.6 mmol), acetic acid (0.045 ml, 0.79 mmol), and sodium triacetoxyborohydride (0.50 g, 2.4 mmol). The product was obtained after flash chromatography (EA/Hexanes). Yield as yellow solid 0.18 g, 68%; m.p. 90-94 °C. ^1H NMR (300 MHz, DMSO-*d*6) δ 9.91 (s, 1H), 8.50 (d, *J* = 1.8 Hz, 1H), 8.47 (dd, *J* = 4.7, 1.7 Hz, 1H), 8.28 (dd, *J* = 8.2, 1.8 Hz, 1H), 7.71 (dt, *J* = 8.2, 1.8 Hz, 1H), 7.52 (dd, *J* = 8.2, 1.8 Hz, 1H), 7.38-7.32 (m, 2H), 7.12 (td, *J* = 7.6, 1.1 Hz, 1H), 3.53 (s, 2H), 3.17 (s, 2H), 2.59 (s, 4H), 2.48 (s, 4H). ^{13}C NMR (100 MHz, DMSO-*d*6) δ 168.42, 150.08, 148.34, 139.11, 136.59, 134.39, 133.43, 129.28, 127.96, 124.88, 123.41, 122.41, 120.93, 109.55, 61.19, 59.01, 52.75, 52.70. HRMS (*m/z*): $[\text{M}+\text{H}]^+$ calculated for $\text{C}_{18}\text{H}_{22}\text{ClN}_4\text{O}$, 345.14767; found, 345.14721.



***N*-(2-chlorophenyl)-2-(4-(pyridin-2-ylmethyl)piperazin-1-yl)acetamide (1121-19).**

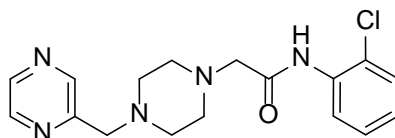
Compound **1121-19** was prepared via general procedure D using piperazine hydrochloride

34 (0.20 g, 0.79 mmol), nicotinaldehyde (0.15 ml, 1.6 mmol), acetic acid (0.045 ml, 0.79 mmol), and sodium triacetoxyborohydride (0.50 g, 2.4 mmol). The product was obtained after flash chromatography (EA/Hexanes). Yield as yellow gel 0.17 g, 62%. $^1\text{H NMR}$ (300 MHz, DMSO-*d*₆) δ 9.92 (s, 1H), 8.49 (dd, *J* = 4.7, 1.2 Hz, 1H), 8.29 (dd, *J* = 8.2, 1.8 Hz, 1H), 7.76 (td, *J* = 7.6, 1.8 Hz, 1H), 7.52 (dd, *J* = 8.2, 1.2 Hz, 1H), 7.43 (d, *J* = 8.2 Hz, 1H), 7.34 (td, *J* = 7.6, 1.2 Hz, 1H), 7.26 (qd, *J* = 4.7, 1.2 Hz, 1H), 7.12 (td, *J* = 7.6, 1.7 Hz, 1H), 3.62 (s, 2H), 3.18 (s, 2H), 2.61 (s, 4H), 2.53 (s, 4H). $^{13}\text{C NMR}$ (100 MHz, DMSO-*d*₆) δ 168.43, 158.24, 148.80, 136.50, 134.41, 129.28, 127.95, 124.88, 122.80, 122.44, 122.18, 120.94, 63.65, 61.22, 52.99, 52.82. HRMS (*m/z*): [$\text{M}+\text{H}$]⁺ calculated for C₁₈H₂₂ClN₄O, 345.14767; found, 345.14737.



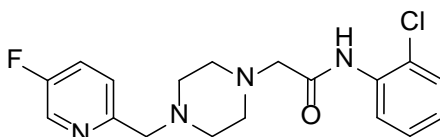
***N*-(2-chlorophenyl)-2-(4-(pyridin-4-ylmethyl)piperazin-1-yl)acetamide (1121-20).**

Compound **1121-20** was prepared via general procedure D using piperazine hydrochloride **34** (0.13 g, 0.53 mmol), isonicotinaldehyde (0.10 ml, 1.1 mmol), acetic acid (0.03 ml, 0.53 mmol), and sodium triacetoxyborohydride (0.34 g, 1.6 mmol). The product was obtained after flash chromatography (EA/Hexanes). Yield as yellow gel 0.10 g, 57%. $^1\text{H NMR}$ (300 MHz, DMSO-*d*₆) δ 9.91 (s, 1H), 8.51 (dd, *J* = 4.4, 1.5 Hz, 2H), 8.29 (dd, *J* = 8.2, 1.8 Hz, 1H), 7.52 (dd, *J* = 7.9, 1.5 Hz, 1H), 7.33 (d, *J* = 5.9 Hz, 3H), 7.13 (td, *J* = 7.6, 1.5 Hz, 1H), 3.54 (s, 2H), 3.18 (s, 2H), 2.61 (s, 4H), 2.49 (s, 4H). $^{13}\text{C NMR}$ (100 MHz, DMSO-*d*₆) δ 168.40, 149.55, 147.29, 134.39, 129.28, 127.96, 124.88, 123.77, 122.42, 120.94, 61.19, 60.50, 52.88, 52.76. HRMS (*m/z*): [$\text{M}+\text{H}$]⁺ calculated for C₁₈H₂₂ClN₄O, 345.14767; found, 345.14718.



***N*-(2-chlorophenyl)-2-(4-(pyrazin-2-ylmethyl)piperazin-1-yl)acetamide (1121-21).**

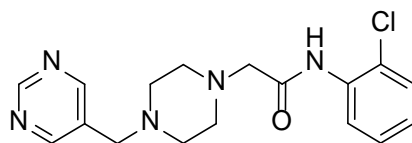
Compound **1121-21** was prepared via general procedure D using piperazine hydrochloride **34** (0.12 g, 0.46 mmol), pyrazine-2-carbaldehyde (0.10 g, 0.92 mmol), acetic acid (0.026 ml, 0.46 mmol), and sodium triacetoxyborohydride (0.29 g, 1.4 mmol). The product was obtained after flash chromatography (EA/Hexanes). Yield as yellow solid 83 mg, 52%; m.p. 75-78 °C. ¹H NMR (300 MHz, DMSO-*d*₆) δ 9.91 (s, 1H), 8.68 (d, *J*= 1.2 Hz, 1H), 8.59 (t, *J*= 1.8 Hz, 1H), 8.54 (d, *J*= 2.9 Hz, 1H), 8.28 (dd, *J*= 8.2, 1.7 Hz, 1H), 7.52 (dd, *J*= 8.2, 1.7 Hz, 1H), 7.35 (td, *J*= 7.6, 1.5 Hz, 1H), 7.13 (td, *J*= 7.6, 1.7 Hz, 1H), 3.70 (s, 2H), 3.18 (s, 2H), 2.60 (s, 4H), 2.56 (s, 4H). ¹³C NMR (100 MHz, DMSO-*d*₆) δ 168.42, 153.73, 144.89, 143.92, 143.29, 134.39, 129.28, 127.96, 124.90, 122.47, 120.99, 109.55, 61.17, 61.14, 52.90, 52.73. HRMS (*m/z*): [M+H]⁺ calculated for C₁₇H₂₁ClN₅O, 346.14291; found, 346.14274.



***N*-(2-chlorophenyl)-2-(4-((5-fluoropyridin-2-yl)methyl)piperazin-1-yl)acetamide**

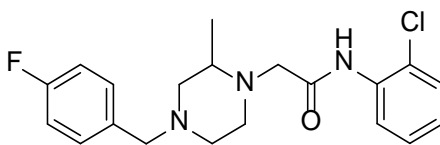
(1121- 22). Compound **1121-22** was prepared via general procedure D using piperazine hydrochloride **34** (0.10 g, 0.40 mmol), 5-fluoropicolinaldehyde (0.10 g, 0.80 mmol), acetic acid (0.023 ml, 0.40 mmol), and sodium triacetoxyborohydride (0.25 g, 1.2 mmol). The product was obtained after flash chromatography (EA/Hexanes). Yield as yellow solid 0.10 mg, 71%; m.p. 100-104 °C. ¹H NMR (300 MHz, DMSO-*d*₆) δ 9.97 (s, 1H), 8.46 (dd, *J*= 8.2, 1.2 Hz, 1H), 8.42 (d, *J*= 2.9 Hz, 1H), 7.45-7.36 (m, 3H), 7.27 (td, *J*= 8.2, 1.2 Hz, 1H),

7.04 (td, $J = 7.6, 1.8$ Hz, 1H), 3.68 (s, 2H), 3.19 (s, 2H), 2.71 (s, 4H), 2.63 (s, 4H). ^{13}C NMR (100 MHz, $\text{DMSO-}d_6$) δ 168.55, 156.86, 154.26, 137.46, 137.15, 134.45, 128.98, 127.68, 124.40, 124.02, 123.96, 123.32, 123.09, 122.69, 120.81, 63.57, 61.96, 53.40, 53.29. HRMS (m/z): $[\text{M}+\text{H}]^+$ calculated for $\text{C}_{18}\text{H}_{21}\text{ClFN}_4\text{O}$, 363.13824; found, 363.13764.



***N*-(2-chlorophenyl)-2-(4-(pyrimidin-5-ylmethyl)piperazin-1-yl)acetamide (1121-23).**

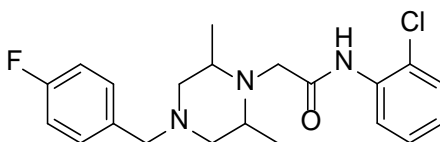
Compound **1121-23** was prepared via general procedure D using piperazine hydrochloride **34** (0.12 g, 0.46 mmol), pyrimidine-5-carbaldehyde (0.10 g, 0.92 mmol), acetic acid (0.026 ml, 0.46 mmol), and sodium triacetoxyborohydride (0.29 g, 1.4 mmol). The product was obtained after flash chromatography (EA/Hexanes). Yield as brown solid 92 mg, 58%; m.p. 95-99 °C. ^1H NMR (300 MHz, CDCl_3) δ 9.91 (s, 1H), 9.12 (s, 1H), 8.70 (s, 2H), 8.44 (dd, $J = 8.2, 1.8$ Hz, 1H), 7.36 (dd, $J = 8.2, 1.5$ Hz, 1H), 7.26 (td, $J = 8.2, 1.5$ Hz, 1H), 7.02 (td, $J = 7.6, 1.7$ Hz, 1H), 3.54 (s, 2H), 3.17 (s, 2H), 2.68 (s, 4H), 2.57 (s, 4H). ^{13}C NMR (100 MHz, CDCl_3) δ 168.31, 157.81, 157.27, 134.34, 131.27, 128.91, 127.68, 124.37, 122.52, 120.77, 61.81, 57.40, 53.17, 53.14. HRMS (m/z): $[\text{M}+\text{H}]^+$ calculated for $\text{C}_{17}\text{H}_{21}\text{ClN}_5\text{O}$, 346.14291; found, 346.14258.



***N*-(2-chlorophenyl)-2-(4-(4-fluorobenzyl)-2-methylpiperazin-1-yl)acetamide (1121-24).**

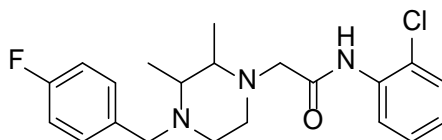
Compound **1121-24** was prepared via general procedure D using piperazine hydrochloride (0.20 g, 0.75 mmol), 4-fluorobenzaldehyde (0.14 ml, 1.5 mmol), acetic acid (0.038 ml, 0.75 mmol), and sodium triacetoxyborohydride (0.42 g, 2.2 mmol). The product

was obtained after flash chromatography (EA/Hexanes). Yield as a yellow oil 89 mg, 36%. ^1H NMR (400 MHz, $\text{DMSO-}d_6$) δ 10.09 (s, 1H), 8.32 (dd, $J = 8.2, 1.6$ Hz, 1H), 7.50 (dd, $J = 8.0, 1.4$ Hz, 1H), 7.37 – 7.29 (m, 3H), 7.17 – 7.07 (m, 3H), 3.38 (d, $J = 17.8$ Hz, 1H), 3.33 (s, 1H), 3.03 (d, $J = 17.2$ Hz, 1H), 2.81 (dt, $J = 11.3, 3.3$ Hz, 1H), 2.70 – 2.57 (m, 3H), 2.55 – 2.46 (m, 1H), 2.22 (t, $J = 10.2$ Hz, 1H), 1.92 (d, $J = 17.9$ Hz, 1H), 0.97 (d, $J = 6.2$ Hz, 3H). ^{13}C NMR (100 MHz, $\text{DMSO-}d_6$) δ 169.35, 162.41, 160.00, 134.35, 134.15, 134.12, 130.58, 130.50, 129.19, 127.90, 124.63, 122.06, 120.43, 114.92, 114.71, 60.83, 60.08, 57.80, 55.00, 52.93, 16.20. HRMS (m/z): $[\text{M}+\text{H}]^+$ calculated for $\text{C}_{20}\text{H}_{24}\text{ON}_3\text{ClF}$, 376.15864; found, 376.15796.



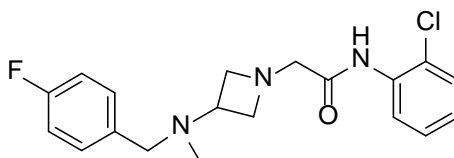
***N*-(2-chlorophenyl)-2-(4-(4-fluorobenzyl)-2,6-dimethylpiperazin-1-yl)acetamide**

(1121-27). Compound **1121-27** was prepared via general procedure **D** using piperazine hydrochloride (0.10 g, 0.36 mmol), 4-fluorobenzaldehyde (0.068 ml, 0.72 mmol), acetic acid (0.018 ml, 0.36 mmol), and sodium triacetoxyborohydride (0.20 g, 1.1 mmol). The product was obtained after flash chromatography (EA/Hexanes). Yield as a yellow gel 40 mg, 32%. ^1H NMR (400 MHz, Chloroform- d) δ 10.21 (s, 1H), 8.46 (dd, $J = 8.3, 1.5$ Hz, 1H), 7.40 – 7.21 (m, 4H), 7.01 (tdd, $J = 8.6, 3.5, 2.2$ Hz, 3H), 3.47 (s, 2H), 3.27 (s, 3H), 2.99 – 2.59 (m, 5H), 1.04 (d, $J = 6.1$ Hz, 6H). ^{13}C NMR (100 MHz, Chloroform- d) δ 134.81, 131.03, 129.23, 127.98, 124.53, 120.79, 115.55, 115.33, 61.94, 60.96, 57.19, 18.41. HRMS (m/z): $[\text{M}+\text{H}]^+$ calculated for $\text{C}_{21}\text{H}_{26}\text{ON}_3\text{ClF}$, 390.17429; found, 390.17367.



***N*-(2-chlorophenyl)-2-(4-(4-fluorobenzyl)-2,3-dimethylpiperazin-1-yl)acetamide**

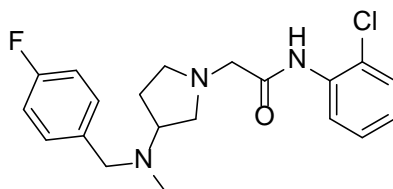
(1121-28). Compound **1121-28** was prepared via general procedure **D** using piperazine hydrochloride (0.14 g, 0.50 mmol), 4-fluorobenzaldehyde (0.093 ml, 0.99 mmol), acetic acid (0.025 ml, 0.50 mmol), and sodium triacetoxyborohydride (0.28 g, 1.5 mmol).. The product was obtained after flash chromatography (EA/Hexanes). Yield as a yellow gel 55 mg, 32%. ^1H NMR (400 MHz, Chloroform-*d*) δ 10.01 (s, 1H), 8.45 (dd, $J = 8.3, 1.6$ Hz, 1H), 7.41 – 7.20 (m, 4H), 7.01 (tdd, $J = 10.6, 5.3, 2.8$ Hz, 3H), 3.87 (d, $J = 37.4$ Hz, 1H), 3.54 – 3.33 (m, 1H), 3.31 – 3.07 (m, 2H), 2.87 – 2.33 (m, 6H), 1.29 (s, 3H), 1.19 (d, $J = 6.3$ Hz, 3H). ^{13}C NMR (100 MHz, Chloroform-*d*) δ 134.78, 130.57, 129.24, 127.99, 124.64, 122.76, 122.76, 121.11, 115.25, 115.20, 59.75, 57.70, 14.42, 13.07. HRMS (m/z): $[\text{M}+\text{H}]^+$ calculated for $\text{C}_{21}\text{H}_{26}\text{ON}_3\text{ClF}$, 390.17429; found, 390.17376.



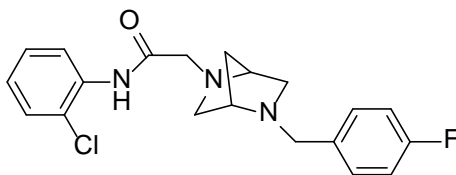
***N*-(2-chlorophenyl)-2-(3-((4-fluorobenzyl)(methyl)amino)azetidin-1-yl)acetamide**

(1121-29). Compound **1121-29** was prepared via general procedure **D** using piperazine hydrochloride (0.12 g, 0.47 mmol), 4-fluorobenzaldehyde (0.087 ml, 0.95 mmol), acetic acid (0.024 ml, 0.47 mmol), and sodium triacetoxyborohydride (0.26 g, 1.4 mmol).. The product was obtained after flash chromatography (EA/Hexanes). Yield as a yellow solid 39 mg, 26%; m.p. 68-71 °C. ^1H NMR (400 MHz, Chloroform-*d*) δ 9.55 (s, 1H), 8.33 (dd, $J = 8.2, 1.6$ Hz, 1H), 7.50 – 7.45 (m, 1H), 7.35 – 7.27 (m, 3H), 7.23 – 7.16 (m, 1H), 7.00 –

6.91 (m, 2H), 4.59 – 4.19 (m, 2H), 3.62 (q, $J = 4.5, 3.7$ Hz, 2H), 3.25 (d, $J = 25.6$ Hz, 6H), 2.06 (s, 3H). ^{13}C NMR (100 MHz, Chloroform-*d*) δ 134.63, 131.00, 130.39, 129.45, 129.22, 128.54, 127.94, 124.75, 121.43, 115.64, 115.45, 63.11, 58.62, 55.37, 55.37, 52.95, 38.36. HRMS (m/z): $[\text{M}+\text{H}]^+$ calculated for $\text{C}_{19}\text{H}_{22}\text{ON}_3\text{ClF}$, 362.14299; found, 362.14211.

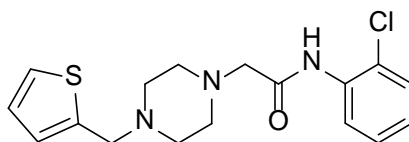


***N*-(2-chlorophenyl)-2-(3-((4-fluorobenzyl)(methyl)amino)pyrrolidin-1-yl)acetamide (1121-30)**. Compound **1121-30** was prepared via general procedure **D** using piperazine hydrochloride (0.32 g, 1.2 mmol), 4-fluorobenzaldehyde (0.23 ml, 2.4 mmol), acetic acid (0.061 ml, 1.2 mmol), and sodium triacetoxyborohydride (0.68 g, 3.6 mmol). The product was obtained after flash chromatography (EA/Hexanes). Yield as dark yellow gel 0.12 g, 30%. ^1H NMR (400 MHz, Chloroform-*d*) δ 9.74 (s, 1H), 8.41 (dd, $J = 8.3, 1.6$ Hz, 1H), 7.33 (dd, $J = 8.0, 1.5$ Hz, 1H), 7.30 – 7.20 (m, 3H), 7.03 – 6.92 (m, 3H), 3.57 – 3.41 (m, 2H), 3.36 – 3.21 (m, 3H), 2.92 – 2.70 (m, 4H), 2.13 (s, 3H), 2.11 – 1.88 (m, 2H). ^{13}C NMR (100 MHz, Chloroform-*d*) δ 169.00, 163.48, 134.71, 130.74, 130.66, 129.21, 127.94, 124.66, 122.96, 121.29, 115.44, 115.23, 63.88, 59.92, 59.11, 57.92, 54.13, 39.23, 28.79. HRMS (m/z): $[\text{M}+\text{H}]^+$ calculated for $\text{C}_{20}\text{H}_{24}\text{ON}_3\text{ClF}$, 376.15864; found, 376.15846.



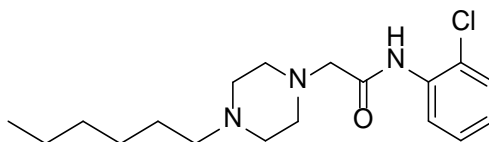
***N*-(2-chlorophenyl)-2-((1S,4S)-5-(4-fluorobenzyl)-2,5-diazabicyclo[2.2.1]heptan-2-yl)acetamide (1121-31)**. Compound **1121-31** was prepared via general procedure **D** using piperazine hydrochloride (0.36 g, 1.4 mmol), 4-fluorobenzaldehyde (0.25 ml, 2.7 mmol),

acetic acid (0.069 ml, 1.4 mmol), and sodium triacetoxyborohydride (0.76 g, 4.1 mmol).. The product was obtained after flash chromatography (EA/Hexanes). Yield as yellow gel 0.13 g, 28%. ^1H NMR (400 MHz, DMSO- d_6) δ 10.10 (s, 1H), 8.32 (dd, $J = 8.2, 1.5$ Hz, 1H), 7.51 (dd, $J = 8.1, 1.4$ Hz, 1H), 7.35 (ddd, $J = 8.4, 6.0, 2.3$ Hz, 3H), 7.18 – 7.05 (m, 3H), 3.73 – 3.61 (m, 3H), 3.01 (d, $J = 9.6$ Hz, 1H), 2.70 (ddd, $J = 14.6, 9.7, 2.5$ Hz, 3H), 2.57 (d, $J = 9.7$ Hz, 1H), 1.91 (s, 1H), 1.71 (q, $J = 9.1$ Hz, 3H). ^{13}C NMR (100 MHz, DMSO- d_6) δ 169.22, 162.25, 159.84, 135.96, 135.93, 134.43, 129.95, 129.87, 129.19, 127.90, 124.72, 122.39, 120.70, 114.92, 114.71, 63.03, 61.37, 59.28, 57.34, 57.05, 56.45, 34.00. HRMS (m/z): $[\text{M}+\text{H}]^+$ calculated for $\text{C}_{20}\text{H}_{22}\text{ON}_3\text{ClF}$, 374.14299; found, 374.14309.

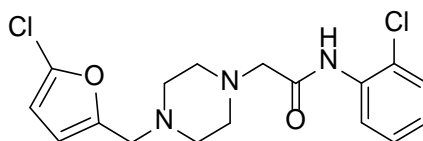


***N*-(2-chlorophenyl)-2-(4-(thiophen-2-ylmethyl)piperazin-1-yl)acetamide (1121-35).**

Compound **1121-35** was prepared via general procedure D using piperazine hydrochloride (0.16 g, 0.62 mmol), thiophene-2-carbaldehyde (0.12 ml, 1.2 mmol), acetic acid (0.035 ml, 0.62 mmol), and sodium triacetoxyborohydride (0.39 g, 1.9 mmol). The product was obtained after flash chromatography (EA/Hexanes). Yield as a yellow solid 0.13 g, 61%. ^1H NMR (400 MHz, DMSO- d_6) δ 9.92 (s, 1H), 8.30 (dt, $J = 8.3, 2.6$ Hz, 1H), 7.57 – 7.27 (m, 3H), 7.18 – 7.06 (m, 1H), 6.96 (h, $J = 3.5$ Hz, 2H), 3.72 (d, $J = 3.9$ Hz, 2H), 3.17 (s, 2H), 2.55 (d, $J = 31.6$ Hz, 8H). ^{13}C NMR (100 MHz, DMSO- d_6) δ 168.37, 134.38, 129.22, 127.91, 126.48, 126.17, 126.16, 125.49, 124.81, 122.36, 120.87, 61.13, 56.15, 52.70, 52.47. HRMS (m/z): $[\text{M}+\text{H}]^+$ calculated for $\text{C}_{17}\text{H}_{21}\text{ON}_3\text{ClS}$, 350.10884; found, 350.10876.



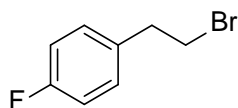
N-(2-chlorophenyl)-2-(4-hexylpiperazin-1-yl)acetamide (1121-36). Compound **1121-36** was prepared via general procedure D using piperazine hydrochloride (0.16 g, 0.62 mmol), pentanal (0.15 ml, 1.2 mmol), acetic acid (0.035 ml, 0.62 mmol), and sodium triacetoxyborohydride (0.39 g, 1.9 mmol). The product was obtained after flash chromatography (EA/Hexanes). Yield as a yellow gel 88 mg, 42%. ^1H NMR (400 MHz, Chloroform-*d*) δ 9.92 (s, 1H), 8.41 (dt, $J = 8.3, 1.4$ Hz, 1H), 7.31 (dt, $J = 8.1, 1.3$ Hz, 1H), 7.25 – 7.17 (m, 1H), 7.01 – 6.93 (m, 1H), 3.12 (d, $J = 1.1$ Hz, 2H), 2.64 (s, 5H), 2.35 – 2.26 (m, 2H), 1.52 – 1.38 (m, 2H), 1.32 – 1.18 (m, 7H), 0.90 – 0.78 (m, 3H). ^{13}C NMR (100 MHz, Chloroform-*d*) δ 168.73, 134.66, 129.10, 127.83, 124.49, 122.79, 120.98, 62.13, 58.77, 53.56, 53.49, 52.39, 31.88, 27.34, 27.20, 26.96, 22.71, 14.18. HRMS (m/z): $[\text{M}+\text{H}]^+$ calculated for $\text{C}_{18}\text{H}_{29}\text{ON}_3\text{Cl}$, 338.19937; found, 338.19929.



2-(4-((5-chlorofuran-2-yl)methyl)piperazin-1-yl)-N-(2-chlorophenyl)acetamide (1121-37). Compound **1121-37** was prepared via general procedure D using piperazine hydrochloride (0.17 g, 0.67 mmol), 5-chlorofuran-2-carbaldehyde (0.18 g, 1.3 mmol), acetic acid (0.038 ml, 0.67 mmol), and sodium triacetoxyborohydride (0.43 g, 2.0 mmol). The product was obtained after flash chromatography (EA/Hexanes). Yield as yellowish gel 0.13 g, 52%. ^1H NMR (400 MHz, Chloroform-*d*) δ 9.91 (s, 1H), 8.43 (dd, $J = 8.3, 1.6$ Hz, 1H), 7.35 (dd, $J = 8.1, 1.5$ Hz, 1H), 7.29 – 7.20 (m, 1H), 7.01 (td, $J = 7.7, 1.6$ Hz, 1H), 6.23 (d, $J = 3.2$ Hz, 1H), 6.09 (d, $J = 3.2$ Hz, 1H), 3.55 (s, 3H), 3.16 (s, 3H), 2.70 (s, 4H).

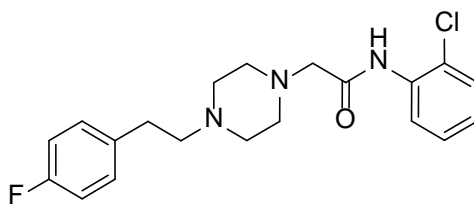
^{13}C NMR (100 MHz, Chloroform-*d*) δ 168.65, 134.67, 134.67, 129.21, 127.96, 124.64, 122.86, 121.04, 111.84, 106.94, 62.03, 54.66, 53.19, 52.93.

General Procedure E for the synthesis of 1-(2-bromoethyl)-4-fluorobenzene (36).



To a stirred solution of **35** (0.34 ml, 2.7 mmol 1 equiv.) in dichloromethane (0.45 M) at 0 °C was added tetrabromomethane (1.1 g, 3.4 mmol, 1.25 equiv.) and then triphenylphosphine (1.1 g, 4.1 mmol, 1.5 equiv.) in portions. The reaction mixture was stirred for 1 hour, concentrated under vacuum and added diethyl ether. The resultant solids were removed by filtration, and the filtrate was concentrated under vacuum. The residue was purified by flash column chromatography (EA/Hexanes) to give **36**. Yield 0.24 g, 43%. ^1H NMR (300 MHz, CDCl_3) δ 7.18 (dd, J = 8.2, 5.5 Hz, 2H), 7.02 (t, J = 8.6 Hz, 2H), 3.56 (t, J = 7.4 Hz, 2H), 3.15 (t, J = 7.4 Hz, 2H). ^{13}C NMR (100 MHz, CDCl_3) δ 130.16, 130.08, 115.51, 115.30, 38.44, 32.97.

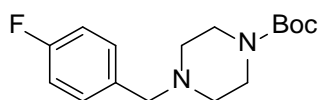
General Procedure F for the synthesis of *N*-(2-chlorophenyl)-2-(4-(4-fluorophenethyl)piperazin-1-yl)acetamide (1121-7).



A solution of **34** (0.25 g, 0.99 mmol, 1 equiv.), **36** (0.24 ml, 1.5 mmol, 1.5 equiv.) and potassium carbonate (1.1 g, 3.9 mmol, 8 equiv.) in acetonitrile was refluxed overnight. The mixture was partitioned between ethyl acetate and water. The combined organic layers were washed with water and brine, dried over MgSO_4 . The solvent was removed by evaporation and the crude product was then purified by flash chromatography on silica gel

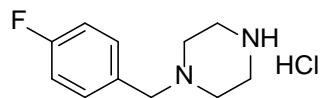
using a 20-80% EA/Hexanes gradient. Yield as yellow solid 0.15 g, 40%; m.p. 79-83 °C. ^1H NMR (300 MHz, CDCl_3) δ 9.92 (s, 1H), 8.30 (d, J = 8.2 Hz, 1H), 7.52 (d, J = 8.2 Hz, 1H), 7.35 (t, J = 7.6 Hz, 1H), 7.26 (dd, J = 8.5, 5.6 Hz, 2H), 7.12 (td, J = 7.6, 1.8 Hz, 2H), 7.08 (t, J = 8.8 Hz, 1H), 3.16 (s, 2H), 2.71 (dd, J = 15.2, 7.0 Hz, 4H), 2.57 (s, 8H). ^{13}C NMR (100 MHz, CDCl_3) δ 168.43, 162.25, 136.57, 136.53, 134.39, 130.42, 130.39, 130.31, 129.26, 127.95, 124.85, 122.39, 120.92, 114.97, 114.68, 61.23, 59.54, 52.91, 52.84, 52.72, 31.80. HRMS (m/z): $[\text{M}+\text{H}]^+$ calculated for $\text{C}_{20}\text{H}_{24}\text{ClFN}_3\text{O}$, 376.15864; found, 376.15910.

General Procedure G for the synthesis of *tert*-butyl 4-benzylpiperazine-1-carboxylate (41).



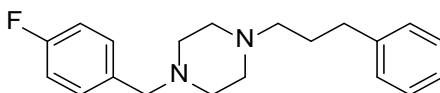
A mixture of **40** (5.0 g, 40 mmol, 1 equiv.) and *N*-Boc piperazine (8.3 g, 44 mmol, 1.1 equiv.) in dry DCM (0.7 molar) was stirred for 2 h at room temperature. Then sodium triacetoxymethylborohydride (13 g, 60 mmol, 1.5 equiv.) was added in portions with stirring. After the addition, the reaction mixture was stirred further overnight at room temperature. Water was added, and the resulting mixture was extracted twice with DCM. The organic layer was dried over anhydrous MgSO_4 , filtered and concentrated in *vacuo* to obtain **41**. Yield brown solid 5.8 g, 48%. ^1H NMR (300 MHz, $\text{DMSO}-d_6$) δ 7.33 (dd, J = 8.5, 5.6 Hz, 2H), 7.13 (t, J = 8.8 Hz, 2H), 3.45 (s, 2H), 3.29 (t, J = 4.7 Hz, 4H), 2.28 (t, J = 5.2 Hz, 4H), 1.38 (s, 9H). ^{13}C NMR (100 MHz, $\text{DMSO}-d_6$) δ 162.91, 159.68, 153.78, 134.01, 130.77, 130.66, 115.06, 114.77, 78.73, 61.02, 52.24, 28.05, 21.08. HRMS (m/z): $[\text{M}+\text{H}]^+$ calculated for $\text{C}_{16}\text{H}_{24}\text{FN}_2\text{O}_2$, 295.18163; found, 295.18156.

General Procedure H for the synthesis of Benzylpiperazine Hydrochloride 42.



Compound **41** (5.8 g, 20 mmol, 1 equiv.) was dissolved in a solution of ether and 12 N HCl and allowed to stir at room temperature for 40 minutes. The volatiles was removed in *vacuo* to afford the product without purification.

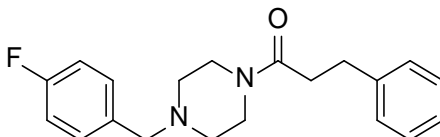
General Procedure I for the synthesis of 1-(4-fluorobenzyl)-4-(3-phenylpropyl)piperazine (1121-14).



In a dry flask, compound **42** (0.20 g, 1.0 mmol, 1 equiv.) was dissolved in 1,2-dichloroethane (0.1 molar) along with 3-phenylpropanal (0.20 ml, 1.5 mmol, 1.5 equiv.) and triethylamine (0.22 ml, 1.5 mmol, 1.5 equiv.). The solution was cooled to 0 °C, and sodium triacetoxyborohydride (0.33 g, 1.5 mmol, 1.5 equiv.) was then added. The reaction mixture was stirred for 1 h at 0 °C, allowed to warm to 25 °C. After stirring for 2 h, the resulting reaction mixture was added to a concentrated solution of sodium bicarbonate and shaken vigorously. The layers were separated, and the organic layer was washed once with water and once with brine. The organic extract was dried over anhydrous MgSO₄. The solvent was removed by evaporation, and the crude product was then purified by flash chromatography on silica gel using a 20-80% EA/Hexanes gradient. Yield yellow gel 0.13 g, 41%. ¹H NMR (300 MHz, DMSO-*d*₆) δ 7.32 (d, J= 5.2 Hz, 1H), 7.29 (d, J= 5.8 Hz, 1H), 7.25 (dd, J= 8.3, 1.2 Hz, 2H), 7.19-7.09 (m, 5H), 3.41 (s, 2H), 2.56 (t, J= 7.6 Hz, 2H), 2.34 (s, 8H), 2.24 (t, J= 7.6 Hz, 2H), 1.68 (p, J= 7.6 Hz, 2H). ¹³C NMR (100 MHz, DMSO-*d*₆)

δ 162.80, 142.05, 134.43, 130.62, 130.53, 128.28, 128.19, 125.61, 114.97, 114.68, 61.17, 57.13, 52.76, 52.59, 32.88, 28.24. HRMS (m/z): $[M+H]^+$ calculated for $C_{20}H_{26}FN_2$, 313.20745; found, 313.20738.

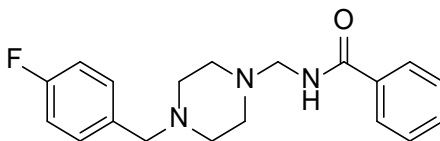
General Procedure J for the synthesis of 1-(4-(4-fluorobenzyl)piperazin-1-yl)-3-phenylpropan-1-one (1121-15).



To prepare 3-phenylpropanoyl chloride, 3-phenylpropanoic acid (0.25 g, 1.7 mmol, 1 equiv.) was dissolved in DCM (0.3 M), oxalyl dichloride (0.36 ml, 4.2 mmol, 2.5 equiv.) was added slowly, followed by one drop of DMF. The reaction was stirred for 40 minutes. The solvent and excess oxalyl dichloride were removed under vacuum (added methanol in the trap and mild evaporated) gave 3-phenylpropanoyl without further purification. To a solution of 3-phenylpropanoyl chloride (0.28 g, 1.7 mmol, 1.2 equiv.) and triethylamine (0.29 ml, 2.1 mmol, 1.5 equiv.) in DCM (0.14 molar) was added compound **42** (0.27 g, 1.4 mmol, 1 equiv.). After being stirred overnight at room temperature, the reaction mixture was diluted with 1N aqueous NaOH, extracted with DCM, dried over anhydrous $MgSO_4$. The solvent was removed by evaporation, and the crude product was then purified by flash chromatography on silica gel using a 20-80% EA/Hexanes gradient. Yield as colorless oil 0.18 g, 34%. 1H NMR (300 MHz, $DMSO-d_6$) δ 7.34 (d, $J=5.9$ Hz, 1H), 7.31 (d, $J=5.9$ Hz, 1H), 7.24 (dd, $J=8.8, 6.5$ Hz, 4H), 7.14 (t, $J=8.8$ Hz, 3H), 3.44 (s, 2H), 3.39 (p, $J=4.7$ Hz, 4H), 2.80 (t, $J=7.6$ Hz, 2H), 2.59 (t, $J=7.6$ Hz, 2H), 2.26 (d, $J=4.7$ Hz, 4H). ^{13}C NMR (100 MHz, $DMSO-d_6$) δ 169.79, 162.91, 141.38, 134.04, 130.76, 130.67, 128.44, 128.24, 125.86, 115.08, 114.79, 60.91, 52.62, 52.21, 44.85, 41.05, 33.95, 30.82. HRMS (m/z):

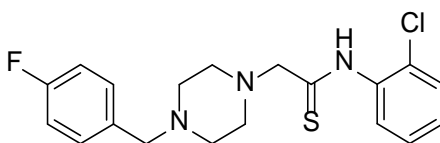
$[M+H]^+$ calculated for $C_{20}H_{24}FN_2O$, 327.18672; found, 327.18652.

General Procedure K for the synthesis of *N*-((4-(4-fluorobenzyl)piperazin-1-yl)methyl)benzamide (1121-17).



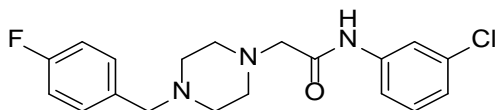
Benzamide (0.40 g, 3.3 mmol, 4 equiv.), potassium carbonate (0.16 g, 1.1 mmol, 3 equiv.), paraformaldehyde (0.21 g, 6.6 mmol, 8 equiv.), and compound **42** (0.20 g, 0.82 mmol, 1 equiv.) were combined in ethanol and refluxed for 18 hours. The reaction mixture was allowed to cool to room temperature and concentrated under reduced pressure. The resultant mixture was extracted with ethyl acetate, washed with brine, dried over magnesium sulfate, and concentrated. Purification with flash column chromatography EtOAc: Hexanes gave the desired products. Yield as yellow solid 0.17 g, 59%; mp 104-109 °C. 1H NMR (300 MHz, DMSO-*d*₆) δ 8.76 (t, *J* = 6.2 Hz, 1H), 7.87 (dd, *J* = 8.2, 1.8 Hz, 2H), 7.56-7.43 (m, 3H), 7.29 (td, *J* = 6.2, 2.6 Hz, 2H), 7.10 (t, *J* = 8.8 Hz, 2H), 4.11 (d, *J* = 6.4 Hz, 2H), 3.40 (s, 2H), 2.49 (s, 4H), 2.34 (s, 4H). ^{13}C NMR (100 MHz, DMSO-*d*₆) δ 166.91, 162.80, 134.47, 134.31, 131.28, 130.60, 130.50, 128.28, 127.34, 114.99, 114.71, 109.57, 61.13, 60.47, 52.44, 49.65. HRMS (*m/z*): $[M+H]^+$ calculated for $C_{19}H_{23}FN_3O$, 328.18197; found, 328.18245.

General Procedure L for the synthesis of *N*-(2-chlorophenyl)-2-(4-(4-fluorobenzyl)piperazin-1-yl)ethanethioamide (1121-32).



A mixture of **1121** (96 mg, 0.27 mmol) and Lawesson's reagent (0.11 g, 0.27 mmol) was refluxed in toluene for 3 h. The solvent was evaporated under vacuum and the resultant mixture was extracted with DCM, washed with NaHCO₃, dried over magnesium sulfate, and concentrated. Purification with flash column chromatography EtOAc: Hexanes gave the desired products. Yield as a yellow gel 46 mg, 46%. ¹H NMR (400 MHz, Chloroform-*d*) δ 7.20 – 7.13 (m, 2H), 7.01 (t, *J* = 7.6 Hz, 2H), 6.93 (t, *J* = 8.3 Hz, 2H), 6.55 (t, *J* = 7.6 Hz, 1H), 6.45 (d, *J* = 8.1 Hz, 1H), 4.12 – 3.88 (m, 4H), 3.86 – 3.56 (m, 4H), 2.62 (d, *J* = 46.0 Hz, 4H). ¹³C NMR (100 MHz, Chloroform-*d*) δ 198.96, 162.56, 142.87, 133.70, 133.67, 129.53, 128.19, 120.01, 118.46, 116.60, 116.39, 115.44, 115.22, 113.46, 113.29, 112.24, 55.60, 51.84, 50.74, 47.01. HRMS (*m/z*): [M+H]⁺ calculated for C₁₉H₂₂N₃ClF, 378.12015; found, 378.12039.

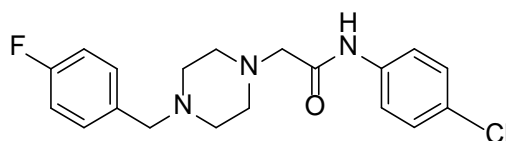
General Procedure M for the synthesis of 2-Benzamino-4-substituted Piperazine 1121 series. To a solution of **45** (1 equiv.) in acetonitrile (0.48 molar) at room temperature was added potassium carbonate (2.5 equiv.) and benzylpiperazine hydrochloride **42** (1 equiv.). The mixture was refluxed for 6 h and the reaction mixture was then cooled to room temperature. The solvent was removed by evaporation and the residue was dissolved in dichloromethane, washed with water, and then dried over MgSO₄. The solvent was removed by evaporation and the crude product was then purified by flash chromatography on silica gel using a 20-80% EA/Hexanes gradient.



***N*-(3-chlorophenyl)-2-(4-(4-fluorobenzyl)piperazin-1-yl)acetamide** (1121-25).

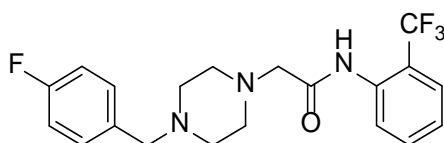
Compound **1121-25** was prepared via general procedure **M** using appropriate acetamide **45**

(0.20 g, 0.80 mmol), piperazine **42** (0.19 g, 0.80 mmol), and potassium carbonate (0.28 g, 2.0 mmol). The product was obtained after flash chromatography (EA/Hexanes). Yield as yellow solid 0.20 g, 67%; mp 79-82 °C. ¹H NMR (400 MHz, DMSO-*d*₆) δ 9.87 (s, 1H), 7.84 (t, *J* = 2.0 Hz, 1H), 7.52 (dd, *J* = 8.3, 2.0 Hz, 1H), 7.37 – 7.25 (m, 3H), 7.18 – 7.07 (m, 3H), 3.45 (s, 2H), 3.11 (d, *J* = 1.6 Hz, 2H), 2.47 (d, *J* = 39.9 Hz, 8H). ¹³C NMR (100 MHz, DMSO-*d*₆) δ 168.66, 159.99, 140.03, 132.95, 130.60, 130.52, 130.29, 123.02, 118.88, 117.80, 114.93, 114.72, 61.74, 61.07, 52.73, 52.26. HRMS (*m/z*): [M+H]⁺ calculated for C₁₉H₂₂ON₃ClF, 362.14299; found, 362.14258.



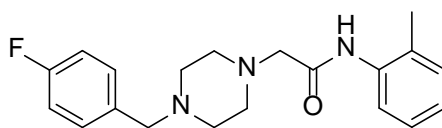
***N*-(4-chlorophenyl)-2-(4-(4-fluorobenzyl)piperazin-1-yl)acetamide (1121-26).**

Compound **1121-26** was prepared via general procedure **M** using appropriate acetamide **45** (0.20 g, 0.80 mmol), piperazine **42** (0.19 g, 0.80 mmol), and potassium carbonate (0.28 g, 2.0 mmol). The product was obtained after flash chromatography (EA/Hexanes). Yield as yellow solid 0.19 g, 64%; mp 143-145 °C. ¹H NMR (400 MHz, DMSO-*d*₆) δ 9.79 (s, 1H), 7.62 (d, *J* = 8.6 Hz, 2H), 7.31 (d, *J* = 8.7 Hz, 2H), 7.30 – 7.24 (m, 2H), 7.10 (t, *J* = 8.7 Hz, 2H), 3.31 (s, 2H), 3.07 (s, 2H), 2.47-2.38 (m, 8H). ¹³C NMR (100 MHz, DMSO-*d*₆) δ 168.39, 137.53, 130.60, 130.52, 128.48, 126.87, 120.96, 114.92, 114.71, 61.73, 61.06, 52.73, 52.27. HRMS (*m/z*): [M+H]⁺ calculated for C₁₉H₂₂ON₃ClF, 362.14354; found, 362.14237.



2-(4-(4-fluorobenzyl)piperazin-1-yl)-N-(2-(trifluoromethyl)phenyl)acetamide (1121-

33). Compound **1121-33** was prepared via general procedure **M** using appropriate acetamide **45** (0.61 g, 2.2 mmol), piperazine **42** (0.50 g, 2.2 mmol), and potassium carbonate (0.75 g, 5.4 mmol). The product was obtained after flash chromatography (EA/Hexanes). Yield as yellow gel 0.52 g, 61%. ^1H NMR (400 MHz, $\text{DMSO-}d_6$) δ 9.85 (s, 1H), 8.28 (d, $J = 8.2$ Hz, 1H), 7.78 – 7.60 (m, 2H), 7.32 (tdd, $J = 8.1, 5.0, 2.1$ Hz, 3H), 7.22 – 7.04 (m, 2H), 3.46 (s, 2H), 3.16 (s, 2H), 2.49 (d, $J = 57.2$ Hz, 8H). ^{13}C NMR (100 MHz, $\text{DMSO-}d_6$) δ 168.71, 162.44, 160.02, 135.23, 134.21, 134.18, 133.41, 130.60, 130.52, 126.12, 126.07, 125.35, 124.30, 123.05, 122.63, 114.92, 114.71, 61.11, 61.00, 52.86, 52.43. HRMS (m/z): $[\text{M}+\text{H}]^+$ calculated for $\text{C}_{20}\text{H}_{22}\text{ON}_3\text{F}_4$, 396.16935; found, 396.16937.



2-(4-(4-fluorobenzyl)piperazin-1-yl)-N-(o-tolyl)acetamide (1121-34). Compound **1121-34** was prepared via general procedure **M** using appropriate acetamide **45** (0.30 g, 1.3 mmol), piperazine **42** (0.30 g, 1.3 mmol), and potassium carbonate (0.45 g, 3.3 mmol). The product was obtained after flash chromatography (EA/Hexanes). Yield as yellow foam 0.26 g, 59%. ^1H NMR (400 MHz, $\text{DMSO-}d_6$) δ 9.36 (s, 1H), 7.84 (dd, $J = 8.1, 1.3$ Hz, 1H), 7.33 (ddd, $J = 8.4, 5.4, 2.3$ Hz, 2H), 7.25 – 7.08 (m, 4H), 7.03 (td, $J = 7.5, 1.4$ Hz, 1H), 3.47 (s, 2H), 3.11 (d, $J = 2.3$ Hz, 2H), 2.51 (d, $J = 52.4$ Hz, 8H), 2.22 (s, 3H). ^{13}C NMR (100 MHz, $\text{DMSO-}d_6$) δ 167.82, 162.42, 160.01, 136.03, 134.31, 134.28, 130.61, 130.53, 130.21, 128.32, 126.24, 124.14, 121.56, 114.93, 114.72, 61.45, 61.01, 52.85, 52.67, 40.15, 17.41. HRMS (m/z): $[\text{M}+\text{H}]^+$ calculated for $\text{C}_{20}\text{H}_{25}\text{ON}_3\text{F}$, 342.19762; found, 342.19755.

Chapter 5. Conclusion and Outlook

The GluN2 subunits of the NMDA receptors are critical in determining biophysical and pharmacological properties of the NMDA receptor. GluN2D subunits have been reported to regulate synaptic transmission in the basal ganglia. The basal ganglia are a group of subcortical nuclei that regulate movement, and can become imbalanced in terms of activity in movement disorders such as Parkinson's disease. Since GluN2D is located in multiple nuclei and cell types in the basal ganglia, GluN2D subunits have been treated as potential targets for neuropathological diseases.

To determine the potency and selectivity of DQP-1105 at GluN2 subunits, the composite concentration-effect curves for DQP-1105 against recombinant GluN1/GluN2A, GluN1/GluN2B, GluN1/GluN2C, and GluN1/GluN2D subunits have been evaluated using two-electrode voltage-clamp recordings expressed in *X. laevis* oocytes with co-application of 100 μM glutamate and 30 μM glycine [2]. The GluN1/GluN2C and GluN1/GluN2D subunits are more sensitive to the dose of DQP-1105 than the GluN1/GluN2A and GluN1/GluN2B subunits. The dose-response curve can help us figure out the inhibition effect at GluN2C for a EC_{90} (IC_{90}) value at GluN2D.

When the concentration of DQP-1105 increases to $\sim 30 \mu\text{M}$ and $\sim 100 \mu\text{M}$, the current responses decrease to 10% of the maximal at the GluN1/GluN2D and GluN1/GluN2C subunits, respectively (*Figure 28*). Since the maximum concentration of DQP-1105 used for oocytes recording is limited to the 100 μM , the IC_{90} values of GluN2A and GluN2B subunits cannot be compared to the GluN2D IC_{90} value. However, since the current responses even higher than 50% of the maximal at GluN2A and GluN2D when the concentration of DQP-1105 increases to 100 μM , we can conclude that the GluN2D subunit

is much more selective over GluN2A and GluN2B subunits using IC_{90} values. However, using IC_{50} values at GluN2A-D subunits already shows distinct selectivity for GluN2D over GluN2A and GluN2B subunits, and using IC_{90} values shows negligible improvement of selectivity for GluN2D over GluN2C subunits. Therefore, the inhibition activity of DQP-1105 and its analogs is suggested to evaluate using IC_{50} values unless noted otherwise.

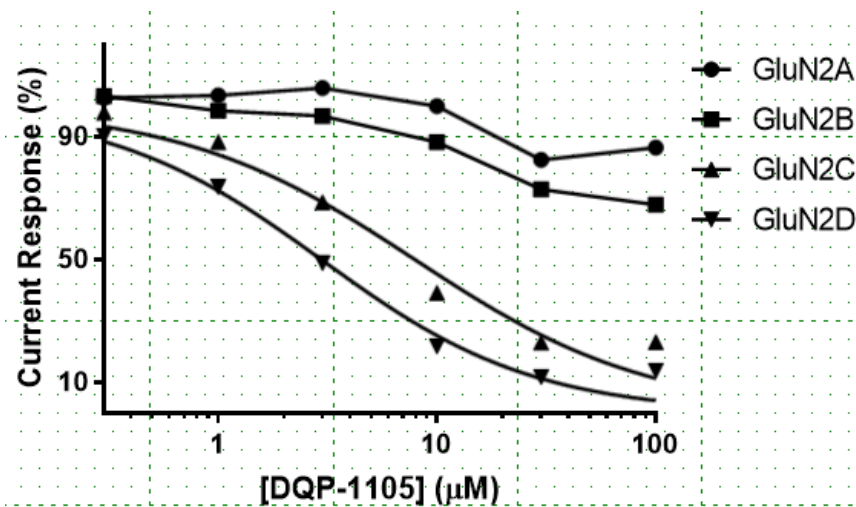


Figure 28. Composite concentration-effect curves for DQP-1105 against recombinant NMDA receptors. Data were analyzed using prism.

This dissertation has optimized a series of GluN2C/D-selective antagonists of the NMDA receptors that incorporate the DQP scaffold. The goal of this research is to develop more potent GluN2D-selective antagonists with adequate brain penetration so that they could be used *in vivo*. Among a total of 149 compounds in 997-series (both purchased and synthesized), compound (S)-**997-74** is the most potent antagonist of the GluN2D-containing receptors with an IC_{50} value of 46 nM, and is 220- and 138-fold selective over the GluN2A- and GluN2B-containing receptors respectively. Another compound **997-110**, which is 3-fold less potent than **997-74** at the GluN2D-containing receptors, is over 600-fold selective for GluN2D- over GluN2B-containing receptors. From the SAR study of 997-series, the proposed pharmacophore features that contribute to the GluN2D inhibition

are shown below (Figure 29).

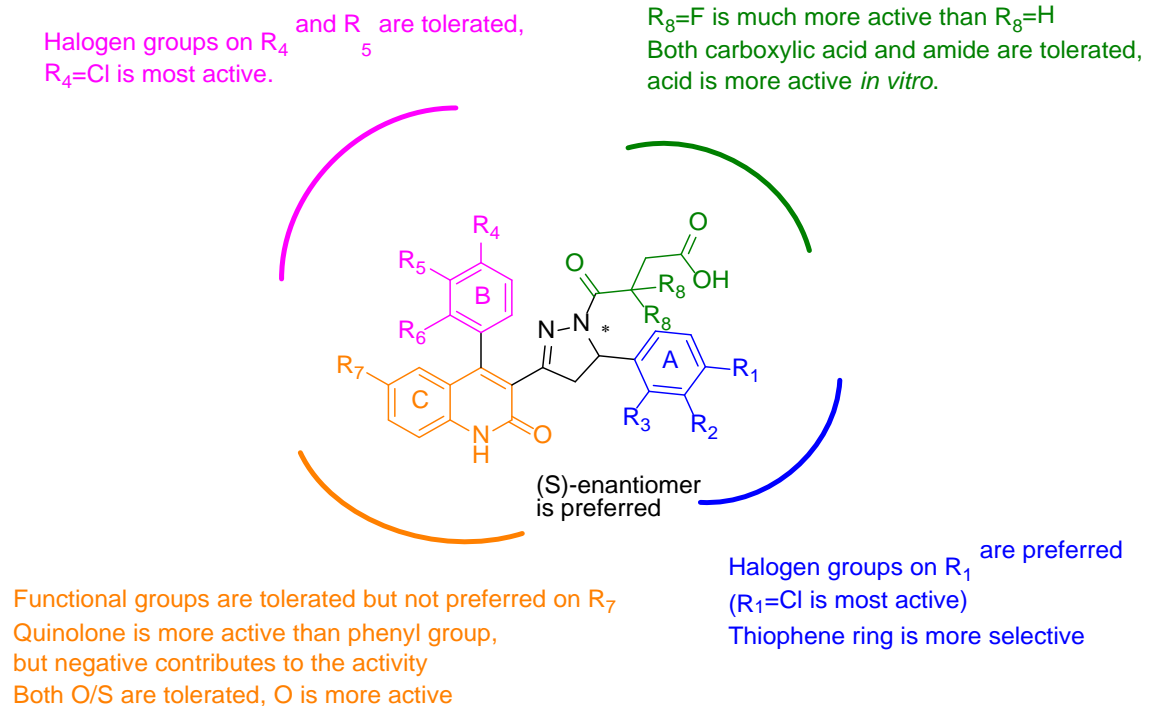
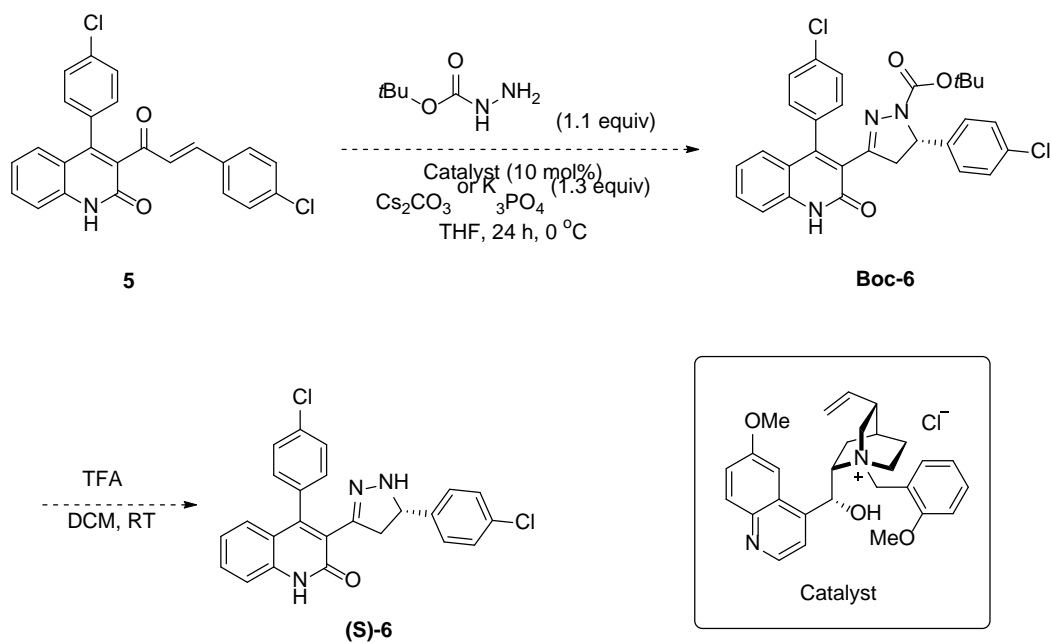


Figure 29. The proposed pharmacophore features that contribute to the GluN2D inhibition.

The halogen groups are preferred on the A- and B-rings. Compounds with electronegative chlorine substitutions at *para*-position on both rings are always more active than those with other substitutions. Replacing the phenyl A-ring by thiophene improves the selectivity at GluN2D subunits over GluN2B subunits. More potent compounds prefer a quinolone ring on the bottom with no substitution rather than a phenyl group. Furthermore, compounds with difluoro-substitution are invariably more potent than the related compounds without difluoro-substitution at the GluN2D-containing receptors. Although the carboxylic acid and amide groups are tolerated on the terminal of acyl chain, compounds with carboxylic acid show more potent inhibition at the GluN2D subunits *in vitro*. According to the enantiomer separation and the absolute stereochemistry determination, the (S)-enantiomers are always more potent than their racemic compounds,

while the (R)-enantiomers significantly decrease the activity at the GluN2D-containing receptors. Notably, in comparison to the racemic compounds, the corresponding (S)-enantiomers not only improve the activity, but also increase the selectivity for GluN2D-over GluN2A- and GluN2B-containing receptors.

Six compounds in 997-series have been separated into their enantiomers, and the (S)-enantiomer of each compound consistently exhibited better activity than the corresponding racemic compound and (R)-enantiomer. Thus, enantioselective synthesis of pyrazolines could be useful for directly form (S)-997- compounds in order to better understand the SAR and save effort on enantiomeric separations. One approach involves utilizing phase-transfer organometallic methodology. Specifically, unsaturated ketone **5** can be reacted with *N-tert*-butyloxycarbonyl hydrazine in the presence of cesium carbonate or tripotassium phosphate using 10 mol% quininium catalyst in THF at 0 °C for 24 hours to yield Boc-protected pyrazoline **Boc-6** in S-configuration [145]. Then the protecting group can be removed by TFA to yield pyrazoline amine (**S**)-**6** (*Scheme 22*) [146]. This pyrazoline amine can be directly used to synthesize final compounds in 997-series with appropriate acyl chain component.



Scheme 22. Purposed enantioselective synthesis of (*S*)-pyrazoline amines [145, 146].

Based on the SAR study of 997-series, 2D-QSAR models are built using KPLS regression and autoQSAR panel to reveal the relationships between 997-structures and the GluN2D subunit inhibitions. The autoQSAR panel creates 2D-QSAR models for predicting the GluN2D pIC₅₀ values and identifying compounds that locate outside the applicability domain of the model. From the 2D-QSAR model with the best performance, the GluN2D pIC₅₀ values and the predicted GluN2D pIC₅₀ values correlate with a simple linear regression. Using this QSAR model with regenerated equation and domain alert, we can predict the future candidates with more confidence. As new compounds become available, the QSAR model can be automatically regenerated leading to improved predictive accuracy and applicability. With the QSAR model refining, we expect that the future compounds can be predicted with the 95% confidence interval.

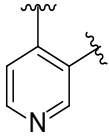
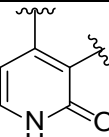
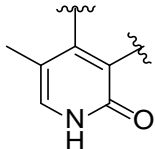
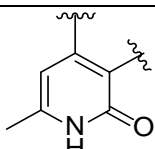
According to the autoQSAR model selection, the best statistical method is the kernel-based PLS (KPLS) regression with dendritic fingerprints. Therefore, a 2D-QSAR

model using KPLS method is built to future explore regions of molecules that favorably or unfavorably contribute to the biological activity. The KPLS regression model results in the visualized structure for each compound to exhibit the sensitivity of the predictions to the presence of each atom. The pyrazoline ring plays a crucial role in 997-series. Addition of chlorine to the *para* position of the phenyl rings improves the predicted activity at the GluN2D-containing receptor. Difluoro-substitution on the acyl chain contributes significantly to the predicted value of GluN2D pIC₅₀. Notably, the phenyl ring of the quinolone moiety is less favorable to the predicted activity, which can be eliminated or replaced with other substitutions.

The KPLS model can not only be used to better understand the SAR of the 997-series but also help rank and predict compounds for future synthesis and testing. Compounds with pyridine or pyridone ring as C-ring have been predicted their pIC₅₀ values using the KPLS model generated in this dissertation. Predicted compound (PC)-1 with pyridine ring is predicted as a less potent antagonist with predicted IC₅₀ value of 13 μM at the GluN2D-containing receptor, while PC-2 with pyridone ring is predicted as ten-fold more potent than PC-1. Adding a methyl group on the pyridone ring can alter the predicted activity at GluN2D-containing receptors. PC-3 with 5-methylpyridone ring is predicted to improve the GluN2D inhibitory activity with IC₅₀ value of 0.48 μM. PC-4 with 6-methylpyridone ring is predicted to slightly decrease the potency at GluN2D-containing receptors in comparison to the non-substituted PC-1 (*Table 31*). If the experimental IC₅₀ results of these compounds are close to the predicted IC₅₀ values at the GluN2D-containing receptors, this KPLS model can work as a powerful tool to predict future candidates in 997-series. Also, compounds with 5-methylpyridone can be treated as a new scaffold for future

optimization. However, if these predictions are not as expected, these compounds can be added to the existing dataset. As more data become available, KPLS models can be regenerated and the most powerful model can be used in the future predictions.

Table 31. Future compounds with predicted GluN2D IC₅₀ values from the KPLS model.

Predicted Compounds (PC)	C-ring	Predicted GluN2D pIC ₅₀	Predicted GluN2D IC ₅₀ (μM)
1		4.893	13
2		5.882	1.3
3		6.318	0.48
4		5.796	1.6

In this dissertation, we use the KPLS model with four KPLS factors, which is only 0.02 differ than the KPLS model with three KPLS factors. In general, it's not possible to differentiate between QSAR results that differ only by very small amounts.

One reason why the scores of top two ranked models of autoQSAR only differ by 0.02 is that 25% of the learning sets were used as a validation set to increase the reliability. Hence, the autoQSAR model only has 22 test compounds. The ratios of test errors between

two KPLS models using dendritic fingerprints and linear fingerprints are shown below (Figure 30). The ratio value less than 1 represents that the dendritic fingerprints result in lower test error than linear fingerprints, while the ratio more than 1 represents that the dendritic fingerprints lead to higher test error. Among 22 test compounds, only four of them show the ratio significantly more than 1. Therefore, the KPLS model with dendritic fingerprints has been selected to use because of its reliability.

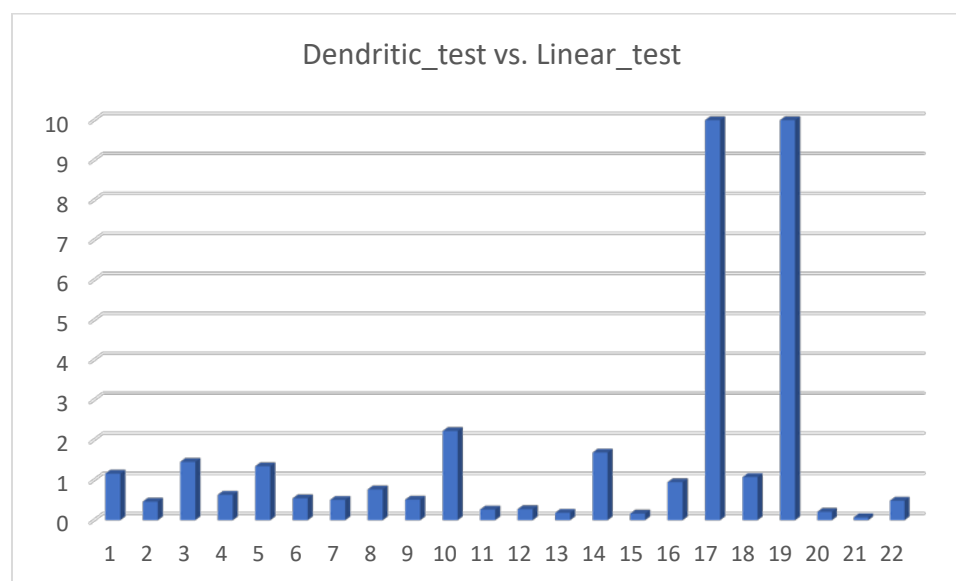


Figure 30. The ratios of test errors between two KPLS models using dendritic fingerprints and linear fingerprints.

The KPLS model built with dendritic fingerprints using Canvas is not validated but instead uses ten bootstrapping cycles to estimate the uncertainty. Therefore, 25% of the learning set (30 compounds) are used as the test set. The ratios of test errors between the KPLS model with four factors and the model with three factors are shown below (Figure 31). The ratio value less than 1 represents that the number of KPLS factors equal to 4 results in lower test error than linear fingerprints, while the ratio more than 1 represents that the number of KPLS factors equal to 3 leads to higher test error. Among 30 test compounds, eight of them show the ratio significantly more than 1. Therefore, the KPLS model 4 factors

have been selected to use because of its reliability.

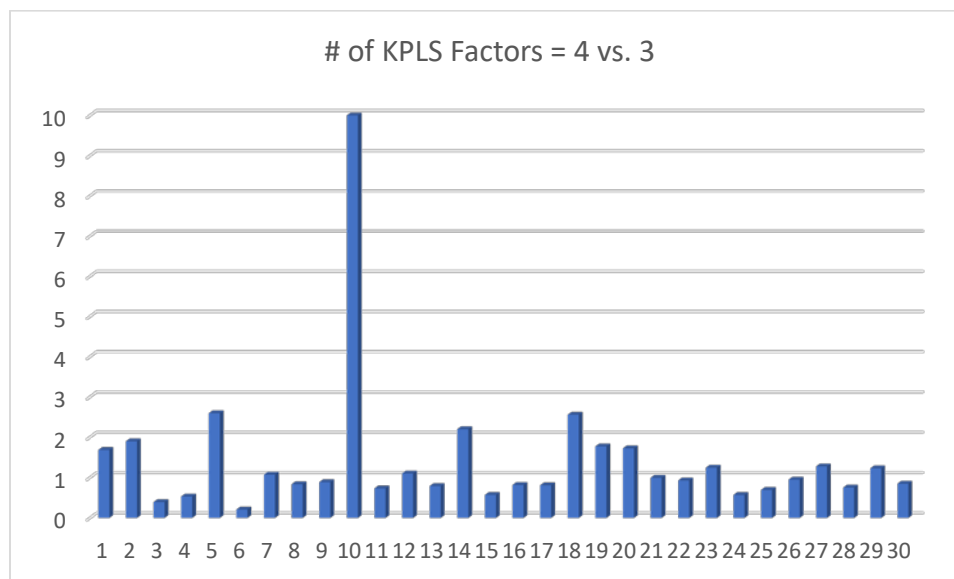


Figure 31. The ratios of test errors between the KPLS model with four factors and the model with three factors.

The accuracy of the QSAR results is measured by R^2 and Q^2 . R^2 is the correlation coefficient of the regression model fit for the training dataset, while Q^2 is the analogous statistic for prediction of the test dataset. They are expressed as follows,

$$r^2 = 1 - \frac{\sum_i^{training} (y_i - \hat{y}_i)^2}{\sum_i^{training} (y_i - \bar{y}_{training})^2}$$

$$q^2 = 1 - \frac{\sum_i^{testing} (y_i - \hat{y}_i)^2}{\sum_i^{testing} (y_i - \bar{y}_{testing})^2}$$

The value of R^2 ranges from 0 to 1. A value of 0 means no correlation, while a value of 1 indicates a perfect correlation. The max value of Q^2 is 1.0 which indicates a perfect prediction of the regression model, while a negative value shows a weak prediction.

Given a split of the learning dataset into training and testing groups, ideally, a model with highest R^2 and Q^2 is naturally selected the best candidate. In many cases, higher R^2 may come with a lower Q^2 . To include both information, the *score* is defined as,

$$score = Q^2 \times (1 - |R^2 - Q^2|)$$

The higher the *score*, the more accurate the model. Note that both R^2 and Q^2 are standardized values with the maximum value of 1, a small deviation between two models in their numerical values can still tell prediction performance of one model over the other. Another important point is that the split rearrangement of training and testing sets over the learning data may alter the score values among different models and change their ranking. It is thus useful to perform multiple trials of model tests with random assignment of training and testing sets and to obtain the statistical distribution of rankings of all models. The model with the highest ranking statistically can be selected as the optimal candidate. For example, five KPLS models have been generated using different training and test sets (randomly select, generate seed: 3360439155, 12345, 98765, 13579, 24680; sample size $n = 122$). Then the mean, SD, and confidence interval (CI) have been calculated for both KPLS models (Factor = 3 and 4). For 3 factors, R^2 and Q^2 fall within the interval of 0.882 ± 0.00312 and 0.700 ± 0.0197 , respectively with the probability of 95% (Table 32).

Table 32. Statistics for KPLS model with 3 factors.

# of KPLS Factors	SD	R^2	RMSE	Q^2
3	0.2803	0.8890	0.3891	0.7530
3	0.3001	0.8675	0.5664	0.5374
3	0.2664	0.8953	0.4780	0.6718
3	0.3093	0.8668	0.3060	0.8394
3	0.2756	0.8914	0.4354	0.7010
Mean =	0.28634	0.882	0.43498	0.70052
SD =	0.01779	0.013744	0.097292	0.111215
CI =	0.003157	0.002439	0.017264	0.019735

For 4 factors, R^2 and Q^2 fall within the interval of 0.913 ± 0.00184 and 0.706 ± 0.0180 , respectively with the probability of 95% (Table 33). Although the R^2 is higher for 4 factors, the Q^2 for 4 factors is only negligibly higher than that for 3 factors. Therefore, the KPLS models with 3 factors and 4 factors give the similar prediction accuracy.

Table 33. Statistics for KPLS model with 4 factors

# of KPLS Factors	SD	R^2	RMSE	Q^2
4	0.2350	0.9228	0.3865	0.7563
4	0.2643	0.8984	0.5508	0.5626
4	0.2342	0.9200	0.4711	0.6812
4	0.2612	0.9060	0.3077	0.8377
4	0.2410	0.9179	0.4415	0.6925
Mean =	0.24714	0.91302	0.43152	0.70606
SD =	0.014532	0.010383	0.091176	0.101533
CI =	0.002579	0.001842	0.016179	0.018017

The purpose of generating 3D Field-Based QSAR model is two fold, one to better understand the 3D properties of the 997-series that influence activity and two, to generate a predictive model to guide compound design in future efforts. We combine the biophysical and computational methods to better understand the activity profile of the 997-series in 3D. Three 3D-QSAR models are generated of which NAMFIS-1a showed the best predictability of the models.

The QSAR model can be viewed as solid contours from Gaussian steric, Gaussian electrostatic, Gaussian hydrophobic, Gaussian H-bond acceptor, and Gaussian H-bond

donor fields. The field contours provide some information to assess the molecular features for better activity at the GluN2D-containing receptor. For instance, the substitutions on both the A ring and B ring preferred steric bulk and electronegative groups. The substitution on the A ring was also favored a hydrophobic group. According to the Craig plot for various substituents with hydrophobic and electrostatic properties, trifluoromethyl and chlorine groups were hydrophobic and electronegative. Therefore, substitutions on the A ring and B ring preferred trifluoromethyl or chlorine groups, which confirmed that **997-74** was the most active compound. From the H-bond acceptor and donor contours, the amide group at the quinolone ring played a crucial role for accepting and donating protons, while the acyl chain was favored an H-bond donor which verified that compound with difluoro-substitution was more active at the GluN2D-containing receptor.

Although the Field-Based QSAR models is unable to clearly identify a bioactive conformation of 997 series, the QSAR statistics of these models could still treat as useful data for prediction of future compounds. According to the QSAR statistics of NAMFIS-1a, NAMFIS-2a, and the control of (S)-997-23 with 3 PLS factors, the predicted power of NAMFIS-1 conformations is relatively higher than the power of NAMFIS-2 conformations. The 3D QSAR model based on the NAMFIS-1a conformer could be used in combination with 2D QSAR models to guide prediction of future medicinal efforts of the 997-series.

Another series of GluN2C/D-selective antagonists with piperazine scaffold was explored. The information of **1121** series remains limited. Among the purchased and synthesized compounds in this series, compound **1121-35** with thiophene substitution on the A ring provided the best result at this stage with IC_{50} values of 13 μ M and 11 μ M at GluN2C- and GluN2D-containing receptors and inhibition at GluN2A- and GluN2B-

containing receptors that occurs at higher concentration ($IC_{50} > 50 \mu M$). The SAR of this series was relatively flat, with most substitution changes diminishing activity. Although this series has interesting drug-like scaffold, no clear indication of how to move forward was revealed by analysis of the analogues tested.

Within the optimization of GluN2C and GluN2D-selective antagonists, a number of neurological diseases could be prevented or treated. For example, the GluN2C receptor may participate in emotional learning, and modulation may be benefit. Additionally, the GluN2D-selective antagonists may decrease Ca^{2+} influx into dopaminergic neurons, which could be neuroprotective, and perhaps rectify circuit imbalance due to the dopamine depletion of Parkinson's disease. Therefore, an improvement of GluN2C/D-selective antagonists could have significant utility in treatment of neurological disease. We have leveraged the 997-project to the next stage with a concerted medicinal chemistry campaign and quantitative modelling. This project could move further if the selectivity for GluN2D over GluN2C subunits could improve and the most active compound could cross the blood-brain barrier (BBB).

The lead compound, DQP-1105, is highly selective for GluN2D subunit over GluN2A subunit. To evaluate the structural determinants of DQP-1105 action, a set of GluN2A and GluN2D chimeric receptors that transferred different portions of GluN2D into GluN2A has been constructed and used (*Figure 32A*) [2, 45]. Studies have reported that DQP-1105 did not increase the activity at the GluN2A subunits when transferring the ATD, the S1 region of the LBD, and the transmembrane helices M1, M2 with the reentrant loop M2 from GluN2D to GluN2A, respectively. However, transferring the S1-S2 region of the LBD or only the S2 portions of GluN2D into GluN2A led to a complete transfer of the

sensitivity of DQP-1105 from GluN2D to GluN2A (*Figure 32B*) [2]. Therefore, the structural determinants for subunit-selective DQP-1105 inhibition was suggested to reside in the S2 region of the LBD of the GluN2D subunit. To further identify the distinct regions of S2 that influence DQP-1105 activity and selectivity, a series of 12 chimeric receptors that revert each distinct region back to the wild-type GluN2A residues was constructed. Three of them (S2a, S2b, and S2c) markedly reduced the sensitivity to DQP-1105 (*Figure 32C*). Within these three regions, nine residues that differ between GluN2A and GluN2D have been mutated in GluN2D to the corresponding residues in GluN2A, respectively. GluN2D subunits with Gln701 and Leu705 mutated to the corresponding residues in GluN2A significantly reduced the potency of DQP-1105 more than 6-fold (*Figure 32D*). Therefore, the lower lobe of the LBD containing residues Gln701 and Leu705 (*Figure 32E*) is suggested as essential structural determinants for the antagonist activity of DQP-1105 and its analogs [2]. However, this GluN2A/GluN2D chimeras only suggested these regions were essential for selectivity, but other mutants of key residues in this region did not eliminate the effect. So, we did not have compelling data to show this is the binding site.

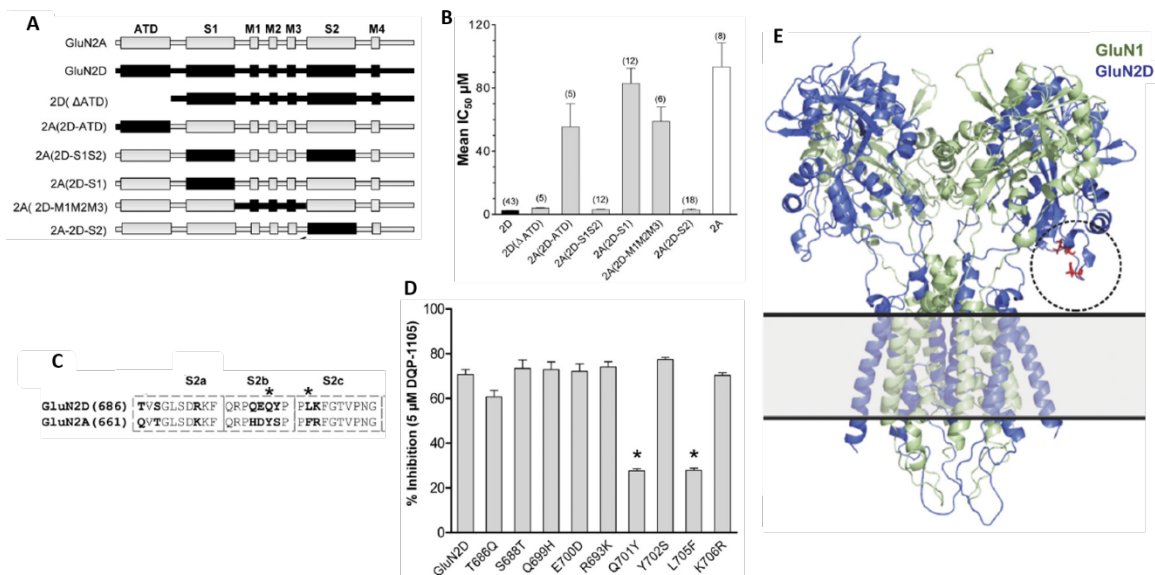


Figure 32. Identification of structural determinants of GluN2D-selective DQP-1105 using chimeric GluN2A-GluN2D receptors. **A**, linear representations of the polypeptide chains of GluN2A and GluN2D, as well as chimeric GluN2A-GluN2D subunits. **B**, Summary of the inhibition of the response by DQP-1105 for chimeric GluN2 subunits (Mean IC₅₀ values are shown). **C**, linear representation of the S2 regions of GluN2A(2D-S2) in which 2D-S2 regions have been reverted to the wild-type GluN2A residues. **D**, site-directed mutagenesis of residues with 2D-S2 chimeric regions. **E**, a GluN1/GluN2D receptor homology model (ATD omitted) with residues Gln701 and Leu705 (red) at the lower lobe of the LBD [2].

The S2 region of the GluN2D LBD containing residues Gln701 and Leu705 is suggested as essential structural determinants for the subunit selectivity of DQP-1105 and its analogs [2]. So, a set of GluN2A and GluN2C chimeric receptors that transferred different portions of GluN2C into GluN2A could be constructed to evaluate the structural determinants of DQP at GluN2C. Once the residues that are essential for the activity of DQP-1105 are determined, we can compare the S2 region of the GluN2C and GluN2D LBDs containing residues. However, GluN2C and GluN2D amino acid sequences have high similarity with four divergent residues (GluN2D Arg693, Glu700, Leu705, and Lys706) (Figure 33) [45]. One of the divergent residue Leu705 is important for GluN2D selectivity. Hence, to improve the selectivity for GluN2D over GluN2C, we can focus on the modulators which can bind with GluN2D Leu705. Molecules that bind with GluN2D

Arg693, Glu700, or Lys706 may also help with improving the selectivity over GluN2C subunit. The amino acids difference between GluN2C and GluN2D can help with determining the specific binding site and further improving the selectivity for GluN2D over GluN2A. However, to synthesize a compound based on these amino acid residues is still a challenge. A possible strategy is to make a set of mutant GluN2C or GluN2D with changes in the S2-region and screen a subset of 997-series including the compounds with relatively higher selectivity for GluN2D over GluN2C (plot GluN2C and GluN2D IC₅₀ values). The IC₅₀ values for wild-type GluN1/GluN2C or GluN1/GluN2D may or may not be different from that determined for the GluN2C or GluN2D mutations. The mutant receptors might help find changes that could increase the selectivity.

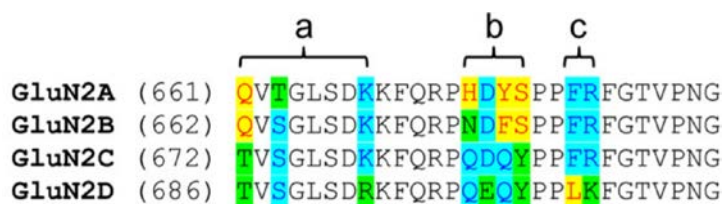


Figure 33. Amino acid sequence alignment of the S2a-c segment from GluN2A-D [45].

According to the visualized structures that generated from KPLS model with GluN2D pIC₅₀ in chapter 3, another KPLS model with GluN2C pIC₅₀ was generated to discover if fragments exist that are favored for activity at GluN2D, but negatively contribute to GluN2C potency. The visualized structures of 997-74 at GluN2C and GluN2D subunits are shown in Figure 8. The difluoro-substitution on the acyl chain moiety is crucial for selectivity for GluN2D over GluN2C due to the negative contribution of the difluoro group to the GluN2C activity. The A- and B-phenyl rings and the quinolone C-ring are less favored for the activity at GluN2D than GluN2C (*Figure 34*). Hence, to

improve the selectivity between GluN2C- and GluN2D-containing receptors, A-, B- and C-rings can be further optimized.

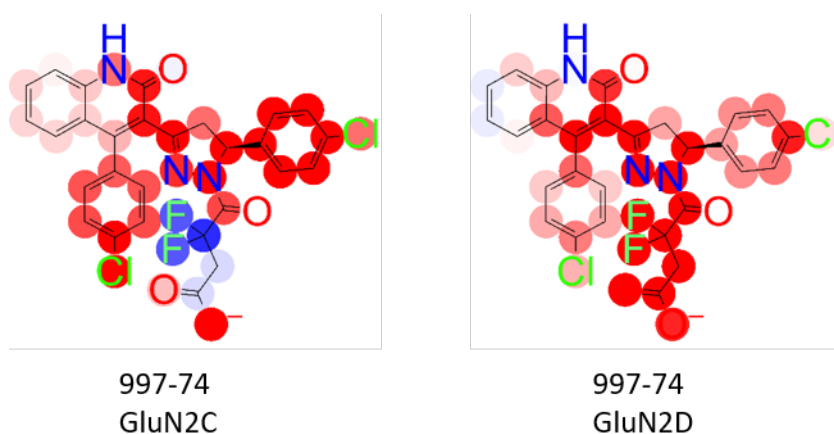
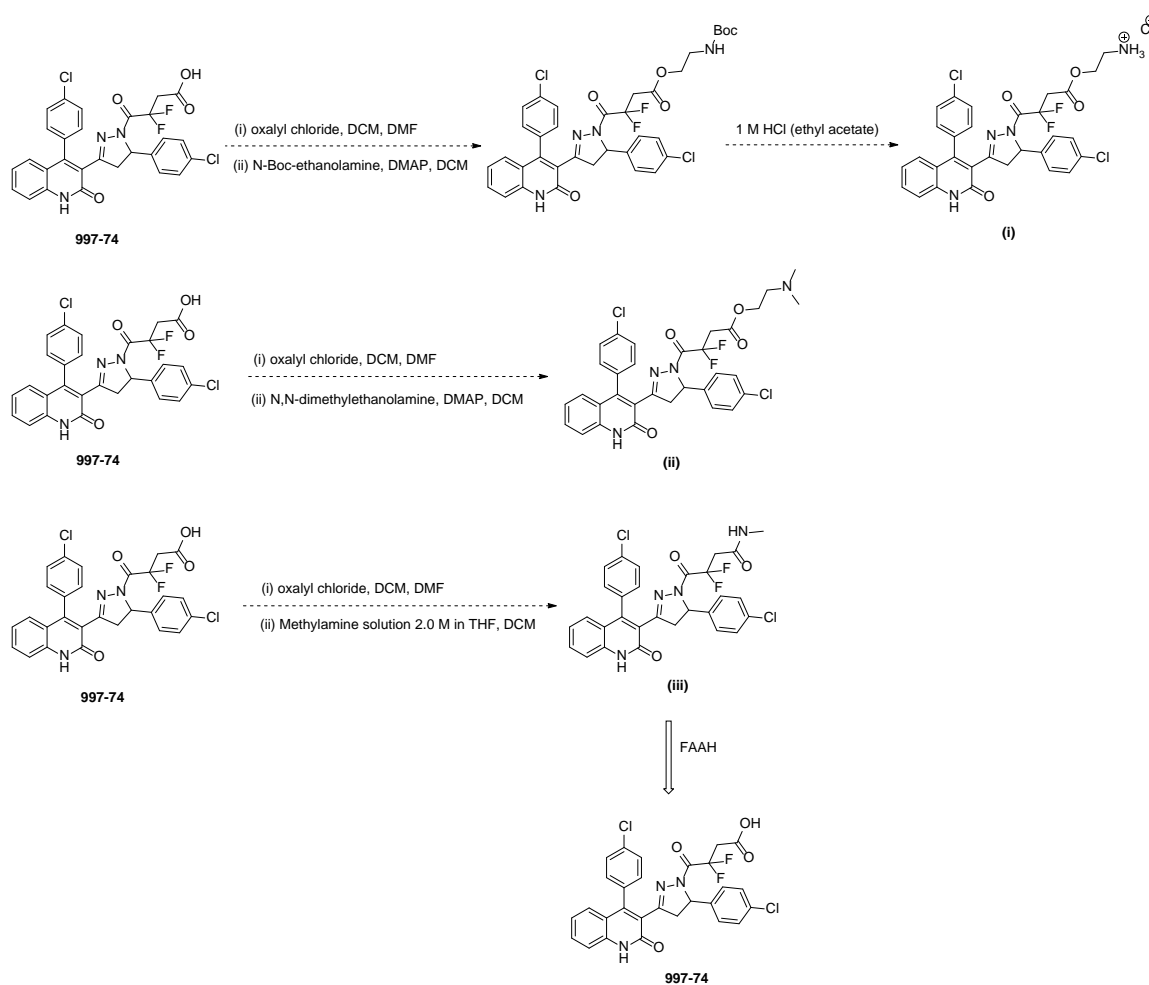


Figure 34. Visualized structures of 997-74 of the models built for GluN2C and GluN2D.

The developmental process for 997-series compounds as CNS drugs has had only limited success due to the inability of crossing the blood-brain barrier (BBB). Studies have reported that compounds with large molecular weight (> 500 Da) are unable to cross the BBB. Hence, the most active analog 997-74 with a molecular weight of 570 Da cannot simply solve the BBB penetration liability issue by further increasing its lipophilicity through substitutions with hydrophobic groups. However, the introduction of a prodrug to 997-74 can help increase its lipid solubility, thus producing higher uptake in the brain. The charged carboxylic acid moiety is responsible for the limited CNS drug distribution, which suggests carboxylate modification of 997-74 may improve BBB penetration. Studies have reported that ester and amide prodrugs of compounds with carboxylic acid moiety could enhance CNS drug distribution, followed by enzymatic hydrolysis [147]. The ester prodrugs can be synthesized by simple esterification. The carboxylic acid component of 997-74 can be activated by oxalyl chloride and *N*-Boc-ethanolamine or a substituted

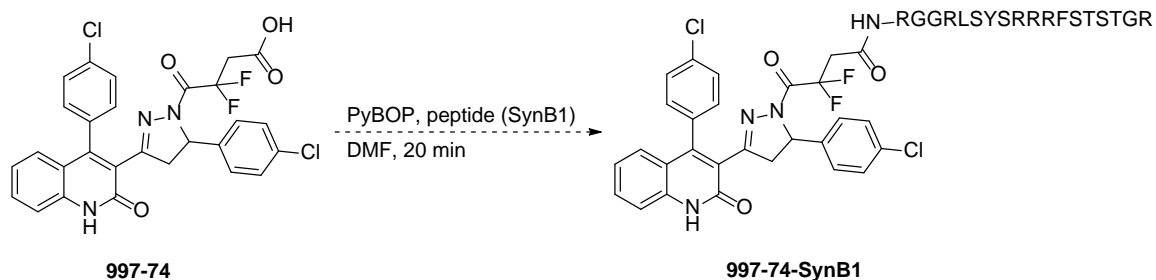
ethanolamine can be subsequently added to form the intermediate or prodrug (ii). The Boc-protecting group of ethanolamine intermediate can be removed using HCl to yield ester prodrug (i) (*Scheme 23*) [148]. Fatty-acid amide hydrolase (FAAH) is a membrane-bound serine hydrolase which is expressed in the brain [149]. The amide prodrugs can be used as FAAH-targeted prodrugs, which are suggested to increase drug exposure to the CNS [149]. Two amide prodrugs are selected to synthesize and are further evaluated. One is the amide compound 997-96 synthesized in chapter 2, and the other one is the methylamide (iii) which will be synthesized by other members in our group (*Scheme 23*).



Scheme 23. Strategies of synthesizing prodrugs of 997-74.

In addition, studies have reported that small synthetic peptides can cross the BBB efficiently and have been used to deliver drugs to the brain [150]. For the 997-series, small peptide vectors, pegelin (such as SynB1), can be used to improve the BBB penetration [151]. Compound 997-74 can be activated by benzotriazol-1-yl-oxopyrrolidine-phosphonium hexafluorophosphate (PyBOP), then the SynB1 peptide can be added to the mixture to form 997-74-SynB1 (*Scheme 24*) [150, 151].

There are many approaches that can be used to improve CNS drug delivery, not limited to the methods shown above [147]. Since minimizing the size of 997-series changes the structural scaffold (which may further influence the binding affinity of 997-compounds in its binding site), developing a prodrug approach to deliver the 997-compounds to the brain across the BBB can help move the project from *in vitro* to *in vivo*.



Scheme 24. The strategy of making 997-74-SynB1.

Appendix A: Crystal data and structure refinement for (R)-(+)-997-74

Compound	(+) 997-74
Formula	C ₃₀ H ₂₅ Cl ₂ F ₂ N ₃ O ₅
<i>D</i> _{calc.} / g cm ⁻³	1.413
μ /mm ⁻¹	0.282
Formula Weight	616.43
Color	colorless
Shape	plate
Max Size/mm	0.50
Mid Size/mm	0.40
Min Size/mm	0.18
<i>T</i> /K	100(2)
Crystal System	monoclinic
Flack Parameter	0.078(14)
Hooft Parameter	0.105(14)
Space Group	P2 ₁
<i>a</i> /Å	8.2731(9)
<i>b</i> /Å	9.5335(10)
<i>c</i> /Å	18.434(2)
α /°	90
β /°	94.719(2)
γ /°	90
<i>V</i> /Å ³	1449.0(3)
<i>Z</i>	2
<i>Z'</i>	1
θ _{min} /°	2.217
θ _{max} /°	30.599
Measured Refl.	18906
Independent Refl.	8732
Reflections Used	8341
<i>R</i> _{int}	0.0223
Parameters	417
Restraints	16
Largest Peak	0.356
Deepest Hole	-0.236
Goof	1.048
<i>wR</i> ₂ (all data)	0.0856
<i>wR</i> ₂	0.0829
<i>R</i> ₁ (all data)	0.0354
<i>R</i> ₁	0.0335

Appendix B: The report for the best AutoQSAR model kpls_dendritic_1

Report for Numeric Model kpls_dendritic_1

Ranking score = 0.870104

Training Set Test Set

S.D. R² RMSE Q²

0.2846 0.8742 0.2788 0.8725

Optimum number of factors = 3

ID Set Y(Obs) Y(Pred) Error

1 test 3.5229 3.9602 0.4374

2 train 3.7352 3.7529 0.0177

3 train 3.9626 3.8569 -0.1056

4 train 4.0223 4.6043 0.5820

5 train 4.0311 4.3414 0.3103

6 train 4.0555 4.4021 0.3466

7 train 4.1871 4.2548 0.0678

8 train 4.3010 4.5902 0.2892

9 test 4.3872 4.2548 -0.1324

10 train 4.5129 4.3316 -0.1813

11 test 4.5850 4.9100 0.3250

12 train 4.6383 4.5594 -0.0789

13 train 4.6402 4.7825 0.1423

14 train 4.6778 4.5592 -0.1185

15 train 4.6778 4.5744 -0.1034

16 test 4.7144 4.8429 0.1284
17 train 4.7212 4.5030 -0.2183
18 train 4.7212 4.3549 -0.3663
19 train 4.7258 4.7846 0.0587
20 test 4.7258 5.1171 0.3912
21 train 4.7696 4.7803 0.0108
22 train 4.7959 4.9938 0.1979
23 train 4.8041 5.1062 0.3021
24 test 4.8539 4.6537 -0.2002
25 train 4.8861 4.6994 -0.1866
26 train 4.8861 5.5029 0.6169
27 train 4.9119 5.0578 0.1460
28 train 4.9586 5.3563 0.3977
29 test 4.9586 5.1884 0.2298
30 train 4.9830 4.7903 -0.1927
31 train 5.0410 4.9293 -0.1117
32 train 5.0506 5.0377 -0.0129
33 test 5.0555 4.8256 -0.2299
34 train 5.0969 5.3056 0.2087
35 train 5.1302 5.3218 0.1916
36 train 5.1549 5.0633 -0.0916
37 train 5.2090 4.5793 -0.6297
38 test 5.2757 5.5437 0.2679

39 test 5.2924 5.0428 -0.2496
40 train 5.3468 5.3116 -0.0351
41 train 5.3468 5.2606 -0.0862
42 train 5.3468 5.5094 0.1626
43 train 5.3665 5.3624 -0.0041
44 train 5.3872 6.0200 0.6328
45 train 5.3979 5.6320 0.2340
46 test 5.4089 5.4516 0.0427
47 train 5.4271 5.5067 0.0796
48 train 5.4685 5.4735 0.0049
49 test 5.4738 5.4039 -0.0699
50 train 5.4949 5.7616 0.2668
51 train 5.5086 5.7674 0.2587
52 test 5.5086 5.4704 -0.0382
53 train 5.5528 6.0816 0.5288
54 train 5.5686 5.3525 -0.2161
55 train 5.5686 5.3748 -0.1939
56 train 5.5850 5.7712 0.1862
57 train 5.5850 5.5941 0.0090
58 test 5.6021 5.7749 0.1728
59 train 5.6990 6.0295 0.3306
60 train 5.7212 5.4566 -0.2647
61 train 5.7696 5.8542 0.0847

62 train 5.8539 5.7326 -0.1213
63 test 5.8539 5.8822 0.0284
64 train 5.8861 6.0038 0.1177
65 test 5.8861 6.0082 0.1221
66 train 5.9586 5.9694 0.0108
67 train 5.9706 5.1976 -0.7731
68 test 6.0000 5.5029 -0.4971
69 train 6.0410 6.2029 0.1619
70 train 6.0458 6.2639 0.2182
71 train 6.0915 6.0104 -0.0811
72 train 6.0915 6.2296 0.1381
73 test 6.1549 5.8603 -0.2946
74 train 6.1612 5.6892 -0.4720
75 train 6.1612 5.9166 -0.2445
76 test 6.1805 5.4498 -0.7307
77 train 6.2218 5.9637 -0.2581
78 train 6.2441 6.1255 -0.1186
79 train 6.2924 6.3292 0.0368
80 train 6.3010 6.1255 -0.1755
81 test 6.3010 6.1595 -0.1416
82 train 6.3565 6.1230 -0.2335
83 train 6.4089 5.9677 -0.4412
84 train 6.4559 6.1088 -0.3472

85 train 6.4949 6.1491 -0.3458

86 train 6.6990 6.8452 0.1462

87 test 6.6990 6.7070 0.0080

88 train 6.6990 6.3432 -0.3558

89 test 6.8539 6.9249 0.0710

90 train 7.0969 7.0873 -0.0096

91 train 7.3010 6.9813 -0.3197

Appendix C: Concentration-response data for 997-series at ionotropic glutamate receptors.

997-	$I_{3\mu\text{M}}/I_{\text{control}}$ (mean \pm SEM, %)				Avg. GluN2C IC ₅₀ (μM) (95% CI)	Avg. GluN2D IC ₅₀ (μM) (95% CI)
	GluN2A	GluN2B	GluN2C	GluN2D		
65	112 \pm 0.15	93 \pm 5.1	95 \pm 2.6	117 \pm 4.6	ND	ND
66	103 \pm 1.0	97 \pm 1.5	96 \pm 4.3	97 \pm 3.3	ND	ND
67	98 \pm 0.97	91 \pm 2.4	34 \pm 6.0	22 \pm 4.5	1.75 (0.97-3.14)	0.86 (0.56-1.32)
68	117 \pm 2.9	99 \pm 3.9	58 \pm 4.5	33 \pm 5.4	5.33 (3.14-9.02)	1.54 (0.91-2.62)
69	110 \pm 1.6	92 \pm 1.2	18 \pm 2.9	15 \pm 1.6	0.68 (0.55-0.85)	0.50 (0.48-0.52)
70	101 \pm 0.81*	99 \pm 0.74*	89 \pm 3.1*	86 \pm 3.7*	ND	ND
71	103 \pm 0.31*	99 \pm 1.3*	97 \pm 0.61*	95 \pm 0.78*	ND	ND
74	62 \pm 2.5	69 \pm 0.78	17 \pm 4.2	3.8 \pm 1.4	0.42 (0.26-0.67)	0.06 (0.03-0.09)
75	112 \pm 1.4	91 \pm 2.3	68 \pm 4.4	43 \pm 3.9	ND	2.36 (1.23-4.51)
76	103 \pm 0.8	101 \pm 2.0	96 \pm 1.5	103 \pm 5.0	ND	ND
77	102 \pm 2.0	97 \pm 3.1	89 \pm 0.90	90 \pm 1.6	ND	ND
78	100 \pm 2.3	93 \pm 5.3	87 \pm 2.9	89 \pm 5.0	ND	ND
79	101 \pm 5.6	100 \pm 3.5	108 \pm 2.1	101 \pm 6.3	ND	ND
80	93 \pm 2.8	96 \pm 2.3	93 \pm 4.4	91 \pm 1.1	ND	ND
81	105 \pm 1.5	95 \pm 2.0	107 \pm 3.9	115 \pm 8.4	ND	ND
82	109 \pm 2.5	96 \pm 1.3	86 \pm 2.6	73 \pm 0.43	ND	7.73 (7.53-7.94)
83	88 \pm 0.16*	90 \pm 0.24*	58 \pm 0.58*	44 \pm 0.37*	ND	ND
88	92 \pm 2.0*	92 \pm 0.46*	95 \pm 2.3	106 \pm 6.3	ND	ND
90	53 \pm 2.6	51 \pm 1.9	7.0 \pm 1.6	6.0 \pm 2.1	0.43 (0.37-0.50)	0.23 (0.20-0.28)
91	91 \pm 1.3	88 \pm 1.5*	65 \pm 2.2	57 \pm 3.4	ND	6.28 (4.74-8.32)
92	99 \pm 1.6*	89 \pm 2.3*	69 \pm 2.5	73 \pm 6.3	7.70 (5.25-11.3)	4.99 (4.15-6.01)
95	96 \pm 6.4	75 \pm 2.2	82 \pm 3.0	76 \pm 1.1	5.99 (5.33-6.74)	6.35 (5.39-7.49)
96	55 \pm 6.1	49 \pm 4.9	-2.8 \pm 6.7	9.7 \pm 3.7*	0.42 (0.28-0.62)	0.15 (0.08-0.29)
97	89 \pm 1.4	87 \pm 1.3	13 \pm 0.88	9.1 \pm 0.30	0.44 (0.37-0.54)	0.36 (0.33-0.40)
98	74 \pm 3.2	84 \pm 2.0	19 \pm 1.7	11 \pm 1.6	0.60 (0.45-0.80)	0.18 (0.14-0.23)

99	121 ± 4.8	101 ± 4.6	92 ± 4.2	81 ± 2.0	ND	ND
100	90 ± 2.8*	87 ± 2.4*	52 ± 2.3*	45 ± 2.6*	ND	ND
101	42 ± 2.0	85 ± 1.8	2.1 ± 0.88	4.2 ± 0.13	0.07 (0.06-0.08)	0.07 (0.06-0.08)
102	73 ± 3.2	80 ± 2.9	25 ± 2.7	9.6 ± 2.1	1.09 (0.89-1.33)	0.45 (0.39-0.51)
103	77 ± 1.1*	78 ± 3.3*	70 ± 1.7	52 ± 2.8	6.88 (6.05-7.81)	3.11 (2.36-4.11)
104	34 ± 2.5*	49 ± 0.05*	38 ± 2.7	20 ± 2.1	1.59 (1.21-2.09)	0.80 (0.69-0.94)
105	90 ± 2.0*	93 ± 1.5*	72 ± 2.7	62 ± 1.6	6.67 (5.91-7.51)	5.04 (4.42-5.75)
108	90 ± 2.2	86 ± 0.57	19 ± 1.4	13 ± 1.5	0.67 (0.59-0.76)	0.36 (0.32-0.40)
109	44 ± 3.3	62 ± 2.1	1.3 ± 1.3	0.16 ± 0.12	0.28 (0.23-0.34)	0.12 (0.11-0.13)
110	77 ± 4.1	78 ± 4.8*	13 ± 1.9	6.3 ± 1.1	0.43 (0.36-0.53)	0.17 (0.14-0.20)
111	105 ± 1.2	101 ± 2.3	30 ± 3.8	20 ± 3.1	1.34 (1.01-1.79)	0.78 (0.63-0.98)
112	84 ± 2.2	88 ± 1.1	9.4 ± 2.2	9.5 ± 2.7	0.36 (0.29-0.44)	0.25 (0.19-0.33)
113	39 ± 4.2	50 ± 3.1	5.2 ± 1.6	4.6 ± 1.5	0.19 (0.16-0.23)	0.08 (0.06-0.10)
114	77 ± 7.3	79 ± 7.6	10 ± 2.7	11 ± 2.4	0.34 (0.27-0.42)	0.15 (0.11-0.20)
115	68 ± 3.6*	59 ± 3.8*	36 ± 4.9	12 ± 3.2	1.75 (1.09-2.81)	0.33 (0.24-0.45)
116	117 ± 1.3	99 ± 3.4	91 ± 3.4	67 ± 8.4	10.2 (9.31-11.2)	5.14 (2.69-9.82)
117	87 ± 1.9	76 ± 1.9	52 ± 4.1	49 ± 4.8	3.27 (2.58-4.14)	2.63 (1.99-3.49)
118	80 ± 1.4	93 ± 4.6	59 ± 2.2	60 ± 1.2	3.70 (3.15-4.34)	3.70 (3.45-3.97)
119	103 ± 4.0*	94 ± 1.1*	75 ± 4.1*	64 ± 7.9*	ND	ND
120	87 ± 1.4	77 ± 3.2	62 ± 4.8	55 ± 1.0	4.35 (3.27-5.80)	3.31 (3.09-3.53)
121	102 ± 4.4*	84 ± 1.4*	84 ± 2.1	83 ± 1.5	ND	ND
122	110 ± 4.2	99 ± 0.68*	87 ± 3.1*	74 ± 1.0*	ND	ND
123	62 ± 7.2*	84 ± 2.3	72 ± 4.9	65 ± 2.0	5.61 (2.96-10.6)	4.69 (3.86-5.70)
124	62 ± 13*	85 ± 2.5	58 ± 0.85	58 ± 1.9	3.65 (3.36-3.97)	3.64 (3.15-4.22)

Data show the current response of coapplication of 3 μM of each compound with 100 μM glutamate and 30 μM glycine. The current response of control is set as 1. Data with * show the current response of coapplication of 30 μM of each compound with 100 μM glutamate and 30 μM glycine. Data are from between 2 and 15 oocytes from 1 to 4 frogs for each compound and receptor tested. The last column shows the mean IC₅₀ values of each compound with bottom and top 95% confidence interval. ND (not determined) indicates that we could not obtain adequate data to allow the concentration-effect curve to be fitted or indicates that the initial values generated a curve that didn't come close to the points.

Appendix D: Concentration-response data for 997-enantiomers at ionotropic glutamate receptors.

997-	$I_{3\ \mu\text{M}}/I_{\text{control}}$ (mean \pm SEM, %)				Avg. GluN2C IC ₅₀ (μM) (95% CI)	Avg. GluN2D IC ₅₀ (μM) (95% CI)
	GluN2A	GluN2B	GluN2C	GluN2D		
(-)-67	100 \pm 0.89	95 \pm 2.2	42 \pm 2.8	26 \pm 3.2	2.71 (1.93-3.82)	0.97 (0.68-1.40)
(+)-67	98 \pm 2.1	87 \pm 2.8	74 \pm 2.1	57 \pm 3.5	ND	7.02 (4.44-11.10)
(-)-74	67 \pm 3.9	73 \pm 4.8	9.3 \pm 1.8	3.5 \pm 1.0	0.11 (0.10-0.14)	0.055 (0.048-0.06)
(+)-74	95 \pm 0.47	87 \pm 1.4	56 \pm 3.8	55 \pm 2.7	3.10 (1.14-8.44)	2.24 (1.20-4.18)
(-)-90	33 \pm 4.5	34 \pm 5.0	7.0 \pm 2.2	3.4 \pm 1.2	0.21 (0.18-0.25)	0.13 (0.11-0.15)
(+)-90	72 \pm 2.9	53 \pm 3.6	36 \pm 3.0	31 \pm 9.8**	2.10 (1.73-2.55)	0.66 (0.37-1.19)

Data show the current response of coapplication of 3 μM of each compound with 100 μM glutamate and 30 μM glycine. The current response of control is set as 1. Data with ** show the current response of coapplication of 1 μM of each compound with 100 μM glutamate and 30 μM glycine. Data are from between 2 and 15 oocytes from 1 to 4 frogs for each compound and receptor tested. The last column shows the mean IC₅₀ values of each compound with bottom and top 95% confidence interval. ND (not determined) indicates that the initial values generated a curve that didn't come close to the points.

Appendix E: Concentration-response data for 1121-series at ionotropic glutamate receptors.

1121-	$I_{100\ \mu\text{M}}/I_{\text{control}}$ (mean \pm SEM, %)				Avg. GluN2C IC ₅₀ (μM) (95% CI)	Avg. GluN2D IC ₅₀ (μM) (95% CI)
	GluN2A	GluN2B	GluN2C	GluN2D		
1	60 \pm 8.0*	81 \pm 2.7*	34 \pm 4.2*	28 \pm 4.1*	11 (8.4-15)	9.7 (7.5-13)
2	85 \pm 2.9	69 \pm 3.1	79 \pm 2.2	77 \pm 2.2	ND	ND
3	70 \pm 2.8	77 \pm 0.57	31 \pm 4.2	29 \pm 3.6	44 (28-70)	ND
4	94 \pm 0.56	93 \pm 2.5	94 \pm 0.68	85 \pm 1.9	ND	ND
5	66 \pm 3.7	71 \pm 1.3	32 \pm 2.5	29 \pm 3.7	49 (45-53)	ND
6	76 \pm 1.6	83 \pm 1.3	43 \pm 4.0	43 \pm 2.6	ND	ND
7	84 \pm 2.5	60 \pm 1.8	91 \pm 2.1	81 \pm 0.72	ND	ND
8	50 \pm 8.2	48 \pm 9.7	33 \pm 7.0	20 \pm 2.1	ND	ND
9	92 \pm 1.7	86 \pm 1.2	65 \pm 0.69	59 \pm 1.5	ND	ND
10	84 \pm 1.8	85 \pm 0.68	60 \pm 0.33	54 \pm 1.9	ND	ND
11	54 \pm 1.9	67 \pm 3.4	24 \pm 1.5	27 \pm 2.1	41 (32-52)	48 (40-56)
12	81 \pm 2.2	37 \pm 2.0	41 \pm 2.5	40 \pm 2.7	66 (47-91)	ND
13	93 \pm 1.9	79 \pm 2.9	80 \pm 1.4	79 \pm 2.6	ND	ND
14	93 \pm 1.3	72 \pm 3.5	91 \pm 1.0	92 \pm 2.0	ND	ND
15	85 \pm 3.8	69 \pm 3.1	79 \pm 3.3	89 \pm 1.9	ND	ND
16	91 \pm 0.79	83 \pm 2.1	83 \pm 2.8	84 \pm 2.4	ND	ND
17	100 \pm 2.1	90 \pm 1.1	88 \pm 2.6	95 \pm 1.1	ND	ND
18	100 \pm 3.2	85 \pm 1.3	76 \pm 1.6	77 \pm 3.5	ND	ND
19	95 \pm 5.0	80 \pm 0.89	56 \pm 3.3	54 \pm 5.7	ND	ND
20	92 \pm 2.5	79 \pm 1.3	75 \pm 2.0	72 \pm 4.0	ND	ND
21	101 \pm 1.9	92 \pm 0.77	86 \pm 0.60	87 \pm 2.3	ND	ND
22	49 \pm 5.0	50 \pm 1.7	17 \pm 2.4	14 \pm 2.3	18 (4.3-75)	ND
23	97 \pm 0.70	93 \pm 2.4	89 \pm 2.3	89 \pm 1.1	ND	ND
24	87 \pm 1.5	95 \pm 3.2	62 \pm 2.4	49 \pm 2.7	ND	ND
25	88 \pm 2.3	77 \pm 4.0	59 \pm 5.2	53 \pm 5.0	89 (67-118)	51 (39-66)

26	95 ± 1.6	83 ± 1.8	86 ± 2.1	82 ± 0.80	ND	ND
27	99 ± 6.9	98 ± 1.1	99 ± 1.1	88 ± 1.2	ND	ND
28	97 ± 2.7	99 ± 4.3	93 ± 0.97	92 ± 4.3	ND	ND
29	97 ± 3.7	90 ± 1.4	90 ± 0.66	81 ± 0.62	ND	ND
30	99 ± 6.2	89 ± 1.8	67 ± 2.1	67 ± 2.7	ND	ND
31	86 ± 4.1	81 ± 1.5	87 ± 0.58	90 ± 5.1	ND	ND
32	101 ± 0.82*	101 ± 0.68*	99 ± 0.96*	101 ± 3.2*	ND	ND
33	85 ± 1.1*	98 ± 4.0*	48 ± 3.4*	42 ± 0.93*	ND	ND
34	103 ± 2.2*	101 ± 1.3*	93 ± 1.6*	89 ± 0.56*	ND	ND
35	72 ± 4.0*	77 ± 2.5*	29 ± 3.8*	26 ± 3.1*	7.8 (7.5-8.1)	9.0 (8.3-9.9)
36	98 ± 0.74*	98 ± 1.1*	96 ± 1.0*	88 ± 1.5*	ND	ND
37	87 ± 4.8*	92 ± 2.4*	71 ± 4.7*	60 ± 1.3*	ND	ND

Data show the current response of coapplication of 100 µM of each compound with 100 µM glutamate and 30 µM glycine. The current response of control is set as 1. Data with * show the current response of coapplication of 30 µM of each compound with 100 µM glutamate and 30 µM glycine. Data are from between 2 and 15 oocytes from 1 to 4 frogs for each compound and receptor tested. The last column shows the mean IC₅₀ values of each compound with bottom and top 95% confidence interval. ND (not determined) indicates that we could not obtain adequate data to allow the concentration-effect curve to be fitted or indicates that the initial values generated a curve that didn't come close to the points.

References

- [1] Traynelis, S.F., L.P. Wollmuth, C.J. McBain, F.S. Menniti, K.M. Vance, K.K. Ogden, K.B. Hansen, H. Yuan, S.J. Myers, and R. Dingledine, *Glutamate receptor ion channels: structure, regulation, and function*. *Pharmacol. Rev.*, 2010. 62(3): p. 405-496.
- [2] Acker, T.M., H. Yuan, K.B. Hansen, K.M. Vance, K.K. Ogden, H.S. Jensen, P.B. Burger, P. Mullasseril, J.P. Snyder, and D.C. Liotta, *Mechanism for noncompetitive inhibition by novel GluN2C/D N-methyl-D-aspartate receptor subunit-selective modulators*. *Mol. Pharmacol.*, 2011. 80(5): p. 782-795.
- [3] Paoletti, P., C. Bellone, and Q. Zhou, *NMDA receptor subunit diversity: impact on receptor properties, synaptic plasticity and disease*. *Nat. Rev. Neurosci.*, 2013. 14(6): p. 383.
- [4] Lüscher, C. and R.C. Malenka, *NMDA receptor-dependent long-term potentiation and long-term depression (LTP/LTD)*. *Cold Spring Harbor Perspect. Biol.*, 2012. 4(6): p. a005710.
- [5] Hunt, D.L. and P.E. Castillo, *Synaptic plasticity of NMDA receptors: mechanisms and functional implications*. *Curr. Opin. Neurobiol.*, 2012. 22(3): p. 496-508.
- [6] Vyklicky, V., M. Korinek, T. Smejkalova, A. Balik, B. Krausova, M. Kaniakova, K. Lichnerova, J. Cerny, J. Krusek, and I. Dittert, *Structure, function, and pharmacology of NMDA receptor channels*. *Physiol. Res.*, 2014. 63: p. S191.
- [7] Monyer, H., R. Sprengel, R. Schoepfer, A. Herb, M. Higuchi, H. Lomeli, N. Burnashev, B. Sakmann, and P.H. Seeburg, *Heteromeric NMDA receptors: molecular and functional distinction of subtypes*. *Science*, 1992. 256(5060): p. 1217-1221.
- [8] Hansen, K.B., K.K. Ogden, H. Yuan, and S.F. Traynelis, *Distinct functional and pharmacological properties of Triheteromeric GluN1/GluN2A/GluN2B NMDA receptors*. *Neuron*, 2014. 81(5): p. 1084-1096.
- [9] Karakas, E., N. Simorowski, and H. Furukawa, *Structure of the zinc-bound amino-terminal domain of the NMDA receptor NR2B subunit*. *EMBO J.*, 2009. 28(24): p. 3910-3920.
- [10] Yuan, H., C.-M. Low, O.A. Moody, A. Jenkins, and S.F. Traynelis, *Ionotropic GABA and glutamate receptor mutations and human neurologic diseases*. *Mol. Pharmacol.*, 2015. 88(1): p. 203-217.
- [11] Karakas, E. and H. Furukawa, *Crystal structure of a heterotetrameric NMDA receptor ion channel*. *Science*, 2014. 344(6187): p. 992-997.
- [12] Karakas, E., N. Simorowski, and H. Furukawa, *Subunit arrangement and phenylethanolamine binding in GluN1/GluN2B NMDA receptors*. *Nature*, 2011. 475(7355): p. 249.
- [13] Furukawa, H. and E. Gouaux, *Mechanisms of activation, inhibition and specificity: crystal structures of the NMDA receptor NR1 ligand-binding core*. *EMBO J.*, 2003. 22(12): p. 2873-2885.
- [14] Gielen, M., B.S. Retchless, L. Mony, J.W. Johnson, and P. Paoletti, *Mechanism of differential control of NMDA receptor activity by NR2 subunits*. *Nature*, 2009. 459(7247): p. 703.
- [15] Vance, K.M., N. Simorowski, S.F. Traynelis, and H. Furukawa, *Ligand-specific deactivation time course of GluN1/GluN2D NMDA receptors*. *Nat. Commun.*, 2011.

- 2: p. 294.
- [16] Yuan, H., K.B. Hansen, K.M. Vance, K.K. Ogden, and S.F. Traynelis, *Control of NMDA receptor function by the NR2 subunit amino-terminal domain*. J. Neurosci., 2009. 29(39): p. 12045-12058.
- [17] Rachline, J., F. Perin-Dureau, A. Le Goff, J. Neyton, and P. Paoletti, *The micromolar zinc-binding domain on the NMDA receptor subunit NR2B*. J. Neurosci., 2005. 25(2): p. 308-317.
- [18] Hansen, K.B., H. Furukawa, and S.F. Traynelis, *Control of assembly and function of glutamate receptors by the amino-terminal domain*. Mol. Pharmacol., 2010. 78(4): p. 535-549.
- [19] Hansen, K.B., K.K. Ogden, and S.F. Traynelis, *Subunit-selective allosteric inhibition of glycine binding to NMDA receptors*. J. Neurosci., 2012. 32(18): p. 6197-6208.
- [20] Furukawa, H., S.K. Singh, R. Mancusso, and E. Gouaux, *Subunit arrangement and function in NMDA receptors*. Nature, 2005. 438(7065): p. 185.
- [21] Santangelo, R.M., T.M. Acker, S.S. Zimmerman, B.M. Katzman, K.L. Strong, S.F. Traynelis, and D.C. Liotta, *Novel NMDA receptor modulators: an update*. Expert Opin. Ther. Pat., 2012. 22(11): p. 1337-1352.
- [22] Akazawa, C., R. Shigemoto, Y. Bessho, S. Nakanishi, and N. Mizuno, *Differential expression of five N-methyl-D-aspartate receptor subunit mRNAs in the cerebellum of developing and adult rats*. J. Comp. Neurol., 1994. 347(1): p. 150-160.
- [23] Paoletti, P., *Molecular basis of NMDA receptor functional diversity*. Eur. J. Neurosci., 2011. 33(8): p. 1351-1365.
- [24] Nicholls, D.G., *Release of glutamate, aspartate, and γ -aminobutyric acid from isolated nerve terminals*. J. Neurochem., 1989. 52(2): p. 331-341.
- [25] Errico, F., S. Rossi, F. Napolitano, V. Catuogno, E. Topo, G. Fisone, A. D'Aniello, D. Centonze, and A. Usiello, *D-aspartate prevents corticostriatal long-term depression and attenuates schizophrenia-like symptoms induced by amphetamine and MK-801*. J. Neurosci., 2008. 28(41): p. 10404-10414.
- [26] Fleck, M., D. Henze, G. Barrionuevo, and A. Palmer, *Aspartate and glutamate mediate excitatory synaptic transmission in area CA1 of the hippocampus*. J. Neurosci., 1993. 13(9): p. 3944-3955.
- [27] Yao, Y. and M.L. Mayer, *Characterization of a soluble ligand binding domain of the NMDA receptor regulatory subunit NR3A*. J. Neurosci., 2006. 26(17): p. 4559-4566.
- [28] Kemp, J., A. Foster, P. Leeson, T. Priestley, R. Tridgett, L. Iversen, and G. Woodruff, *7-Chlorokynurenic acid is a selective antagonist at the glycine modulatory site of the N-methyl-D-aspartate receptor complex*. Proc. Natl. Acad. Sci, 1988. 85(17): p. 6547-6550.
- [29] McNamara, D., E.C. Smith, D.O. Calligaro, P.J. O'Malley, L.A. McQuaid, and R. Dingledine, *5, 7-Dichlorokynurenic acid, a potent and selective competitive antagonist of the glycine site on NMDA receptors*. Neurosci. Lett., 1990. 120(1): p. 17-20.
- [30] Kinarsky, L., B. Feng, D.A. Skifter, R.M. Morley, S. Sherman, D.E. Jane, and D.T. Monaghan, *Identification of subunit-and antagonist-specific amino acid residues in the N-Methyl-D-aspartate receptor glutamate-binding pocket*. J. Pharmacol. Exp. Ther., 2005. 313(3): p. 1066-1074.

- [31] Parsons, C., W. Danysz, and G. Quack, *Memantine is a clinically well tolerated N-methyl-D-aspartate (NMDA) receptor antagonist—a review of preclinical data*. Neuropharmacology, 1999. 38(6): p. 735-767.
- [32] Blanpied, T.A., F.A. Boeckman, E. Aizenman, and J.W. Johnson, *Trapping channel block of NMDA-activated responses by amantadine and memantine*. J. Neurophysiol., 1997. 77(1): p. 309-323.
- [33] Huettner, J.E. and B.P. Bean, *Block of N-methyl-D-aspartate-activated current by the anticonvulsant MK-801: selective binding to open channels*. Proc. Natl. Acad. Sci, 1988. 85(4): p. 1307-1311.
- [34] Strong, K.L., Y. Jing, A.R. Prosser, S.F. Traynelis, and D.C. Liotta, *NMDA receptor modulators: an updated patent review (2013–2014)*. Expert Opin. Ther. Pat., 2014. 24(12): p. 1349-1366.
- [35] Chen, H.S.V. and S.A. Lipton, *The chemical biology of clinically tolerated NMDA receptor antagonists*. J. Neurochem., 2006. 97(6): p. 1611-1626.
- [36] Church, J., D. Lodge, and S.C. Berry, *Differential effects of dextrorphan and levorphanol on the excitation of rat spinal neurons by amino acids*. Eur. J. Pharmacol., 1985. 111(2): p. 185-190.
- [37] Franklin, P.H. and T.F. Murray, *High affinity [³H] dextrorphan binding in rat brain is localized to a noncompetitive antagonist site of the activated N-methyl-D-aspartate receptor-cation channel*. Mol. Pharmacol., 1992. 41(1): p. 134-146.
- [38] Wong, E., J.A. Kemp, T. Priestley, A.R. Knight, G.N. Woodruff, and L.L. Iversen, *The anticonvulsant MK-801 is a potent N-methyl-D-aspartate antagonist*. Proc. Natl. Acad. Sci, 1986. 83(18): p. 7104-7108.
- [39] WW Hasselmann, H., *Ketamine as antidepressant? Current state and future perspectives*. Curr. Neuropharmacol., 2014. 12(1): p. 57-70.
- [40] Jentsch, J.D. and R.H. Roth, *The neuropsychopharmacology of phencyclidine: from NMDA receptor hypofunction to the dopamine hypothesis of schizophrenia*. Neuropsychopharmacology, 1999. 20(3): p. 201-225.
- [41] Parsons, C., G. Quack, I. Bresink, L. Baran, E. Przegalinski, W. Kostowski, P. Krzascik, S. Hartmann, and W. Danysz, *Comparison of the potency, kinetics and voltage-dependency of a series of uncompetitive NMDA receptor antagonists in vitro with anticonvulsive and motor impairment activity in vivo*. Neuropharmacology, 1995. 34(10): p. 1239-1258.
- [42] Williams, K., *Ifenprodil discriminates subtypes of the N-methyl-D-aspartate receptor: selectivity and mechanisms at recombinant heteromeric receptors*. Mol. Pharmacol., 1993. 44(4): p. 851-859.
- [43] Chenard, B., J. Bordner, T. Butler, L. Chambers, M. Collins, D. De Costa, M. Ducat, M. Dumont, and C. Fox, *(1S, 2S)-1-(4-hydroxyphenyl)-2-(4-hydroxy-4-phenylpiperidino)-1-propanol: a potent new neuroprotectant which blocks N-methyl-d-aspartate responses*. J. Med. Chem., 1995. 38(16): p. 3138-3145.
- [44] Fischer, G., V. Mutel, G. Trube, P. Malherbe, J. Kew, E. Mohacsi, M. Heitz, and J. Kemp, *Ro 25-6981, a highly potent and selective blocker of N-methyl-D-aspartate receptors containing the NR2B subunit. Characterization in vitro*. J. Pharmacol. Exp. Ther., 1997. 283(3): p. 1285-1292.
- [45] Hansen, K.B. and S.F. Traynelis, *Structural and mechanistic determinants of a novel site for noncompetitive inhibition of GluN2D-containing NMDA receptors*. J.

- Neurosci., 2011. 31(10): p. 3650-3661.
- [46] Edman, S., S. McKay, L. Macdonald, M. Samadi, M. Livesey, G. Hardingham, and D. Wyllie, *TCN 201 selectively blocks GluN2A-containing NMDARs in a GluN1 co-agonist dependent but non-competitive manner*. Neuropharmacology, 2012. 63(3): p. 441-449.
- [47] Irvine, M.W., B.M. Costa, A. Volianskis, G. Fang, L. Ceolin, G.L. Collingridge, D.T. Monaghan, and D.E. Jane, *Coumarin-3-carboxylic acid derivatives as potentiators and inhibitors of recombinant and native N-methyl-D-aspartate receptors*. Neurochem. Int., 2012. 61(4): p. 593-600.
- [48] Monaghan, D.T., M.W. Irvine, B.M. Costa, G. Fang, and D.E. Jane, *Pharmacological modulation of NMDA receptor activity and the advent of negative and positive allosteric modulators*. Neurochem. Int., 2012. 61(4): p. 581-592.
- [49] Costa, B.M., M.W. Irvine, G. Fang, R.J. Eaves, M.B. Mayo-Martin, D.A. Skifter, D.E. Jane, and D.T. Monaghan, *A novel family of negative and positive allosteric modulators of NMDA receptors*. J. Pharmacol. Exp. Ther., 2010. 335(3): p. 614-621.
- [50] Santangelo Freel, R.M., K.K. Ogden, K.L. Strong, A. Khatri, K.M. Chepiga, H.S. Jensen, S.F. Traynelis, and D.C. Liotta, *Correction to synthesis and structure activity relationship of tetrahydroisoquinoline-based potentiators of GluN2C and GluN2D containing N-Methyl-d-aspartate receptors*. J. Med. Chem., 2014. 57(11): p. 4975-4975.
- [51] Santangelo Freel, R.M., K.K. Ogden, K.L. Strong, A. Khatri, K.M. Chepiga, H.S. Jensen, S.F. Traynelis, and D.C. Liotta, *Synthesis and structure activity relationship of tetrahydroisoquinoline-based potentiators of GluN2C and GluN2D containing N-methyl-D-aspartate receptors*. J. Med. Chem., 2013. 56(13): p. 5351-5381.
- [52] Ogden, K.K. and S.F. Traynelis, *Contribution of the M1 transmembrane helix and pre-M1 region to positive allosteric modulation and gating of N-methyl-D-aspartate receptors*. Mol. Pharmacol., 2013. 83(5): p. 1045-1056.
- [53] Zimmerman, S.S., A. Khatri, E.C. Garnier-Amblard, P. Mullasseril, N.L. Kurtkaya, S. Gyoneva, K.B. Hansen, S.F. Traynelis, and D.C. Liotta, *Design, synthesis, and structure-activity relationship of a novel series of GluN2C-selective potentiators*. J. Med. Chem., 2014. 57(6): p. 2334-2356.
- [54] Khatri, A., P.B. Burger, S.A. Swanger, K.B. Hansen, S. Zimmerman, E. Karakas, D.C. Liotta, H. Furukawa, J.P. Snyder, and S.F. Traynelis, *Structural determinants and mechanism of action of a GluN2C-selective NMDA receptor positive allosteric modulator*. Mol. Pharmacol., 2014. 86(5): p. 548-560.
- [55] Barbeau, A., *L-dopa therapy in Parkinson's disease: a critical review of nine years' experience*. Can. Med. Assoc. J., 1969. 101(13): p. 59.
- [56] Cenci, M.A., *Presynaptic mechanisms of l-DOPA-induced dyskinesia: the findings, the debate, and the therapeutic implications*. Front. Neurol., 2014. 5: p. 242.
- [57] Crosby, N.J., K. Deane, and C.E. Clarke, *Amantadine in Parkinson's disease*. Cochrane Libr., 2003.
- [58] Crosby, N.J., K. Deane, and C.E. Clarke, *Amantadine for dyskinesia in Parkinson's disease*. Cochrane Libr., 2003.
- [59] Bravo, S.A., C. Rangel-Barajas, and B.F. Garduño, *Pathophysiology of L-Dopa Induced Dyskinesia—Changes in D1/D3 Receptors and Their Signaling Pathway*,

- in *A Synopsis of Parkinson's Disease*. 2014, InTech.
- [60] Pantcheva, P., S. Reyes, J. Hoover, S. Kaelber, and C.V. Borlongan, *Treating non-motor symptoms of Parkinson's disease with transplantation of stem cells*. *Expert Rev. Neurother.*, 2015. 15(10): p. 1231-1240.
- [61] Savitt, J.M., V.L. Dawson, and T.M. Dawson, *Diagnosis and treatment of Parkinson disease: molecules to medicine*. *J. Clin. Invest.*, 2006. 116(7): p. 1744-1754.
- [62] Standaert, D.G., C.M. Testa, A.B. Young, and J.B. Penney, *Organization of N-methyl-D-aspartate glutamate receptor gene expression in the basal ganglia of the rat*. *J. Comp. Neurol.*, 1994. 343(1): p. 1-16.
- [63] Wenzel, A., M. Villa, H. Mohler, and D. Benke, *Developmental and regional expression of NMDA receptor subtypes containing the NR2D subunit in rat brain*. *J. Neurochem.*, 1996. 66(3): p. 1240-1248.
- [64] Swanger, S.A., K.M. Vance, J.-F. Pare, F. Sotty, K. Fog, Y. Smith, and S.F. Traynelis, *NMDA receptors containing the GluN2D subunit control neuronal function in the subthalamic nucleus*. *J. Neurosci.*, 2015. 35(48): p. 15971-15983.
- [65] Monyer, H., N. Burnashev, D.J. Laurie, B. Sakmann, and P.H. Seeburg, *Developmental and regional expression in the rat brain and functional properties of four NMDA receptors*. *Neuron*, 1994. 12(3): p. 529-540.
- [66] Lanciego, J.L., N. Luquin, and J.A. Obeso, *Functional neuroanatomy of the basal ganglia*. *Cold Spring Harbor Perspect. Med.*, 2012. 2(12): p. a009621.
- [67] Nelson, A.B. and A.C. Kreitzer, *Reassessing models of basal ganglia function and dysfunction*. *Annu. Rev. Neurosci.*, 2014. 37: p. 117-135.
- [68] Ikemoto, S., C. Yang, and A. Tan, *Basal ganglia circuit loops, dopamine and motivation: a review and enquiry*. *Behav. Brain Res.*, 2015. 290: p. 17-31.
- [69] DeLong, M. and T. Wichmann, *Changing views of basal ganglia circuits and circuit disorders*. *Clin. EEG Neurosci.*, 2010. 41(2): p. 61-67.
- [70] Alexander, G.E., *Biology of Parkinson's disease: pathogenesis and pathophysiology of a multisystem neurodegenerative disorder*. *Dialogues Clin. Neurosci.*, 2004. 6(3): p. 259.
- [71] Gardoni, F. and C. Bellone, *Modulation of the glutamatergic transmission by Dopamine: a focus on Parkinson, Huntington and Addiction diseases*. *Front. Cell. Neurosci.*, 2015. 9: p. 25.
- [72] Olivares, D., V. K Deshpande, Y. Shi, D. K Lahiri, N. H Greig, J. T Rogers, and X. Huang, *N-methyl D-aspartate (NMDA) receptor antagonists and memantine treatment for Alzheimer's disease, vascular dementia and Parkinson's disease*. *Curr. Alzheimer Res.*, 2012. 9(6): p. 746-758.
- [73] More, S.V. and D.-K. Choi, *Promising cannabinoid-based therapies for Parkinson's disease: motor symptoms to neuroprotection*. *Mol. Neurodegener.*, 2015. 10(1): p. 17.
- [74] Hallett, P.J. and D.G. Standaert, *Rationale for and use of NMDA receptor antagonists in Parkinson's disease*. *Pharmacol. Ther.*, 2004. 102(2): p. 155-174.
- [75] Johnson, K.A., P.J. Conn, and C.M. Niswender, *Glutamate receptors as therapeutic targets for Parkinson's disease*. *CNS Neurol. Disord.: Drug Targets*, 2009. 8(6): p. 475-491.
- [76] Caligiore, D., R.C. Helmich, M. Hallett, A.A. Moustafa, L. Timmermann, I. Toni, and G. Baldassarre, *Parkinson's disease as a system-level disorder*. *NPJ Parkinson's*

- Dis., 2016. 2: p. 16025.
- [77] Mosley, C.A., T.M. Acker, K.B. Hansen, P. Mullasseril, K.T. Andersen, P. Le, K.M. Vellano, H. Bräuner-Osborne, D.C. Liotta, and S.F. Traynelis, *Quinazolin-4-one derivatives: A novel class of noncompetitive NR2C/D subunit-selective N-methyl-D-aspartate receptor antagonists*. J. Med. Chem., 2010. 53(15): p. 5476-5490.
- [78] Hansen, K.B., P. Mullasseril, S. Dawit, N.L. Kurtkaya, H. Yuan, K.M. Vance, A.G. Orr, T. Kvist, K.K. Ogden, and P. Le, *Implementation of a fluorescence-based screening assay identifies histamine H3 receptor antagonists clobenpropit and iodophenpropit as subunit-selective N-methyl-D-aspartate receptor antagonists*. J. Pharmacol. Exp. Ther., 2010. 333(3): p. 650-662.
- [79] Acker, T.M., A. Khatri, K.M. Vance, C. Slabber, J. Bacsa, J.P. Snyder, S.F. Traynelis, and D.C. Liotta, *Structure-activity relationships and pharmacophore model of a noncompetitive pyrazoline containing class of GluN2C/GluN2D selective antagonists*. J. Med. Chem., 2013. 56(16): p. 6434-6456.
- [80] Wang, Q., J.D. Rager, K. Weinstein, P.S. Kardos, G.L. Dobson, J. Li, and I.J. Hidalgo, *Evaluation of the MDR-MDCK cell line as a permeability screen for the blood-brain barrier*. Int. J. Pharm., 2005. 288(2): p. 349-359.
- [81] Frye, S.V., M.C. Johnson, and N.L. Valvano, *Synthesis of 2-aminobenzophenones via rapid halogen-lithium exchange in the presence of a 2-amino-N-methoxy-N-methylbenzamide*. J. Org. Chem., 1991. 56(11): p. 3750-3752.
- [82] Jia, C.-S., Y.-W. Dong, S.-J. Tu, and G.-W. Wang, *Microwave-assisted solvent-free synthesis of substituted 2-quinolones*. Tetrahedron, 2007. 63(4): p. 892-897.
- [83] Draper, J.M., Z. Xia, R.A. Smith, Y. Zhuang, W. Wang, and C.D. Smith, *Discovery and evaluation of inhibitors of human ceramidase*. Mol. Cancer Ther., 2011. 10(11): p. 2052-2061.
- [84] Xu, F., B. Simmons, J. Armstrong, and J. Murry, *Practical preparation of 3, 3-difluoropyrrolidine*. J. Org. Chem., 2005. 70(15): p. 6105-6107.
- [85] Partridge, J.J., S.-J. Shiuey, and M.R. Uskokovic, *Process for the preparation of 24, 24-difluoro-1 α , 25-dihydroxy vitamin D3 and intermediates obtained therefrom*. 1983, Google Patents.
- [86] Abell, A.D., K.B. Morris, and J.C. Litten, *Synthesis and deprotection of [1-(ethoxycarbonyl)-4-[(diphenylmethoxy) carbonyl]-1-methyl-2-oxobutyl] triphenylphosphonium chloride: a key intermediate in the Wittig reaction between a cyclic anhydride and a stabilized ylide*. J. Org. Chem., 1990. 55(18): p. 5217-5221.
- [87] Kendrick, D.A., C. Danzin, and M. Kolb, *2, 2-Difluoro-5-hexyne-1, 4-diamine. A potent enzyme-activated inhibitor of ornithine decarboxylase*. J. Med. Chem., 1989. 32(1): p. 170-173.
- [88] Nicolaou, K., A.A. Estrada, M. Zak, S.H. Lee, and B.S. Safina, *A mild and selective method for the hydrolysis of esters with trimethyltin hydroxide*. Angew. Chem., Int. Ed., 2005. 44(9): p. 1378-1382.
- [89] Strong, K.L., M.P. Epplin, J. Bacsa, C.J. Butch, P.B. Burger, D.S. Menaldino, S.F. Traynelis, and D.C. Liotta, *The Structure-Activity Relationship of a Tetrahydroisoquinoline Class of N-Methyl-d-Aspartate Receptor Modulators that Potentiates GluN2B-Containing N-Methyl-d-Aspartate Receptors*. J. Med. Chem., 2017. 60(13): p. 5556-5585.

- [90] Wiberg, K.B. and D.J. Rush, *Solvent effects on the thioamide rotational barrier: An experimental and theoretical study*. J. Am. Chem. Soc., 2001. 123(9): p. 2038-2046.
- [91] Wiberg, K.B. and P.R. Rablen, *Why does thioformamide have a larger rotational barrier than formamide?* J. Am. Chem. Soc., 1995. 117(8): p. 2201-2209.
- [92] Coppola, G.M., P.J. Kukkola, J.L. Stanton, A.D. Neubert, N. Marcopulos, N.A. Bilci, H. Wang, H.C. Tomaselli, J. Tan, and T.D. Aicher, *Perhydroquinolybenzamides as novel inhibitors of 11 β -hydroxysteroid dehydrogenase type 1*. J. Med. Chem., 2005. 48(21): p. 6696-6712.
- [93] Ojha Lokendra, K., S. Rachana, and B.M. Rani, *Modern drug design with advancement in QSAR: A review*. Int. J. Res. Biosci., 2013. 2(1): p. 1-12.
- [94] Grover, A., M. Grover, and K. Sharma, *A practical overview of quantitative structure-activity relationship*. World J. Pharm. Pharm. Sci., 2015. 5(2): p. 427-437.
- [95] Verma, J., V.M. Khedkar, and E.C. Coutinho, *3D-QSAR in drug design-a review*. Curr. Top. Med. Chem., 2010. 10(1): p. 95-115.
- [96] Luan, F. and M. Cordeiro, *Overview of QSAR modelling in rational drug design*. Recent trends on QSAR in the pharmaceutical perceptions. Sharjah: Bentham Science Publishers, 2012: p. 194-241.
- [97] Nantasenamat, C., C. Isarankura-Na-Ayudhya, T. Naenna, and V. Prachayasittikul, *A practical overview of quantitative structure-activity relationship*. EXCLI J., 2009. 8: p. 74-88.
- [98] Kim, K.H., *Outliers in SAR and QSAR: 2. Is a flexible binding site a possible source of outliers?* J. Comput.-Aided Mol. Des., 2007. 21(8): p. 421-435.
- [99] Lewis, R.A. and D. Wood, *Modern 2D QSAR for drug discovery*. Wiley Interdiscip. Rev.: Comput. Mol. Sci., 2014. 4(6): p. 505-522.
- [100] Ertl, P., B. Rohde, and P. Selzer, *Fast calculation of molecular polar surface area as a sum of fragment-based contributions and its application to the prediction of drug transport properties*. J. Med. Chem., 2000. 43(20): p. 3714-3717.
- [101] Milletti, F., L. Storchi, G. Sforna, and G. Cruciani, *New and original p K a prediction method using grid molecular interaction fields*. J. Chem. Inf. Model., 2007. 47(6): p. 2172-2181.
- [102] Carhart, R.E., D.H. Smith, and R. Venkataraghavan, *Atom pairs as molecular features in structure-activity studies: definition and applications*. J. Chem. Inf. Comput. Sci., 1985. 25(2): p. 64-73.
- [103] Nilakantan, R., N. Bauman, J.S. Dixon, and R. Venkataraghavan, *Topological torsion: a new molecular descriptor for SAR applications. Comparison with other descriptors*. J. Chem. Inf. Comput. Sci., 1987. 27(2): p. 82-85.
- [104] Geladi, P. and B.R. Kowalski, *Partial least-squares regression: a tutorial*. Anal. Chim. Acta, 1986. 185: p. 1-17.
- [105] Clark, M. and R.D. Cramer, *The probability of chance correlation using partial least squares (PLS)*. Mol. Inf., 1993. 12(2): p. 137-145.
- [106] Rosipal, R. and L.J. Trejo, *Kernel partial least squares regression in reproducing kernel hilbert space*. J. Mach. Learn. Res., 2001. 2(Dec): p. 97-123.
- [107] Consonni, V., D. Ballabio, and R. Todeschini, *Comments on the definition of the Q 2 parameter for QSAR validation*. J. Chem. Inf. Model., 2009. 49(7): p. 1669-1678.
- [108] An, Y., W. Sherman, and S.L. Dixon, *Kernel-based partial least squares: application to fingerprint-based QSAR with model visualization*. J. Chem. Inf. Model., 2013.

- 53(9): p. 2312-2321.
- [109] Bennett, K. and M. Embrechts, *An optimization perspective on kernel partial least squares regression*. NATO Sci. Ser. III Comput. Syst. Sci., 2003. 190: p. 227-250.
- [110] Canvas, v. *Schrodinger L.L.C.: New York*. 2012.
- [111] Sastry, M., J.F. Lowrie, S.L. Dixon, and W. Sherman, *Large-scale systematic analysis of 2D fingerprint methods and parameters to improve virtual screening enrichments*. J. Chem. Inf. Model., 2010. 50(5): p. 771-784.
- [112] Duan, J., S.L. Dixon, J.F. Lowrie, and W. Sherman, *Analysis and comparison of 2D fingerprints: insights into database screening performance using eight fingerprint methods*. J. Mol. Graphics Modell., 2010. 29(2): p. 157-170.
- [113] Akamatsu, M., *Current state and perspectives of 3D-QSAR*. Curr. Top. Med. Chem., 2002. 2(12): p. 1381-1394.
- [114] Martin, Y.C., *3D QSAR: current state, scope, and limitations*. Perspect. Drug Discovery Des., 1998. 12: p. 3-23.
- [115] Martin, Y.C., J.L. Kofron, and L.M. Traphagen, *Do structurally similar molecules have similar biological activity?* J. Med. Chem., 2002. 45(19): p. 4350-4358.
- [116] Roy, K., S. Kar, and R.N. Das, *Understanding the basics of QSAR for applications in pharmaceutical sciences and risk assessment*. 2015: Academic press.
- [117] Ghose, A. and V. Viswanadhan, *Combinatorial Library Design and Evaluation: Principles, Software, Tools, and Applications in Drug Discovery*. 2001: CRC Press.
- [118] Bultinck, P., H. De Winter, W. Langenaeker, and J.P. Tollenare, *Computational medicinal chemistry for drug discovery*. 2003: CRC Press.
- [119] Kubinyi, H., G. Folkers, and Y.C. Martin, *3D QSAR in Drug Design: Volume 2: Ligand-Protein Interactions and Molecular Similarity*. Vol. 2. 1998: Springer Science & Business Media.
- [120] Choudhary, M.I., *Frontiers in Drug Design & Discovery*. Vol. 8. 2017: Bentham Science Publishers.
- [121] Lionta, E., G. Spyrou, D. K Vassilatis, and Z. Cournia, *Structure-based virtual screening for drug discovery: principles, applications and recent advances*. Curr. Top. Med. Chem., 2014. 14(16): p. 1923-1938.
- [122] Ferreira, L.G., R.N. dos Santos, G. Oliva, and A.D. Andricopulo, *Molecular docking and structure-based drug design strategies*. Molecules, 2015. 20(7): p. 13384-13421.
- [123] Katsila, T., G.A. Spyroulias, G.P. Patrinos, and M.-T. Matsoukas, *Computational approaches in target identification and drug discovery*. Comput. Struct. Biotechnol. J., 2016. 14: p. 177-184.
- [124] Ul-Haq, Z. and J.D. Madura, *Frontiers in Computational Chemistry: Volume: 3*. Vol. 3. 2017: Bentham Science Publishers.
- [125] Sliwoski, G., S. Kothiwale, J. Meiler, and E.W. Lowe, *Computational methods in drug discovery*. Pharmacol. Rev., 2014. 66(1): p. 334-395.
- [126] *Field-Based QSAR, version 2015-2, Schrödinger, LLC, New York, NY, 2015*.
- [127] Cramer, R.D., D.E. Patterson, and J.D. Bunce, *Comparative molecular field analysis (CoMFA). 1. Effect of shape on binding of steroids to carrier proteins*. J. Am. Chem. Soc., 1988. 110(18): p. 5959-5967.
- [128] Klebe, G., U. Abraham, and T. Mietzner, *Molecular similarity indices in a comparative analysis (CoMSIA) of drug molecules to correlate and predict their*

- biological activity*. J. Med. Chem., 1994. 37(24): p. 4130-4146.
- [129] Klebe, G. and U. Abraham, *Comparative molecular similarity index analysis (CoMSIA) to study hydrogen-bonding properties and to score combinatorial libraries*. J. Comput.-Aided Mol. Des., 1999. 13(1): p. 1-10.
- [130] Acharya, C., A. Coop, J. E Polli, and A. D MacKerell, *Recent advances in ligand-based drug design: relevance and utility of the conformationally sampled pharmacophore approach*. Curr. Comput.-Aided Drug Des., 2011. 7(1): p. 10-22.
- [131] Lipkowitz, K.B. and D.B. Boyd, *Reviews in Computational Chemistry: * Volume 13*. 2000: Wiley Online Library.
- [132] Ghose, A.K., V.N. Viswanadhan, and J.J. Wendoloski, *Prediction of hydrophobic (lipophilic) properties of small organic molecules using fragmental methods: an analysis of ALOGP and CLOGP methods*. J. Phys. Chem. A, 1998. 102(21): p. 3762-3772.
- [133] Muñoz-Gutiérrez, C., D. Cáceres-Rojas, F. Adasme-Carreño, I. Palomo, E. Fuentes, and J. Caballero, *Docking and quantitative structure–activity relationship of bicyclic heteroaromatic pyridazinone and pyrazolone derivatives as phosphodiesterase 3A (PDE3A) inhibitors*. PloS one, 2017. 12(12): p. e0189213.
- [134] Kim, K., *Comparative molecular field analysis (CoMFA)*, in *Molecular similarity in drug design*. 1995, Springer. p. 291-331.
- [135] Kaiser, T.M., S.A. Kell, H. Kusumoto, G. Shaulsky, S. Bhattacharya, M.P. Epplin, K.L. Strong, E.J. Miller, B.D. Cox, and D.S. Menaldino, *The bioactive protein-ligand conformation of GluN2C-selective positive allosteric modulators bound to the NMDA receptor*. Mol. Pharmacol., 2018. 93(2): p. 141-156.
- [136] Cicero, D., G. Barbato, and R. Bazzo, *NMR analysis of molecular flexibility in solution: A new method for the study of complex distributions of rapidly exchanging conformations. Application to a 13-residue peptide with an 8-residue loop*. J. Am. Chem. Soc., 1995. 117(3): p. 1027-1033.
- [137] Norinder, U., *Recent progress in CoMFA methodology and related techniques*. Perspect. Drug Discovery Des., 1998. 12: p. 25-39.
- [138] Han, M.-S., Y.-H. Han, C.-M. Song, and H.-G. Hahn, *The design and synthesis of 1, 4-substituted piperazine derivatives as triple reuptake inhibitors*. Bull. Korean Chem. Soc., 2012. 33(8): p. 2597-2602.
- [139] Horner, K.E. and P.B. Karadakov, *Chemical bonding and aromaticity in furan, pyrrole, and thiophene: a magnetic shielding study*. J. Org. Chem., 2013. 78(16): p. 8037-8043.
- [140] Morris, D.J., A.M. Hayes, and M. Wills, *The “Reverse-Tethered” ruthenium (II) catalyst for asymmetric transfer hydrogenation: Further applications*. J. Org. Chem., 2006. 71(18): p. 7035-7044.
- [141] Gómez-Parra, V., F. Sánchez, and T. Torres, *Carbamates from secondary amines and alkyl chlorides under phase-transfer conditions*. Synthesis, 1985. 1985(03): p. 282-285.
- [142] Carroll, F.I., J.P. Cueva, J.B. Thomas, S.W. Mascarella, and S.P. Runyon, *Arylpiperazine opioid receptor antagonists*. 2016, Google Patents.
- [143] Cianci, C.W., S. Gerritz, S. Kim, D.R. Langley, G. Li, B.C. Pearce, A. Pendri, S. Shi, W. Zhai, and S. Zhu, *Novel piperazine analogs with substituted heteroaryl groups as broad-spectrum influenza antivirals*. 2012, Google Patents.

- [144] Bhatia, P.A., J.F. Daanen, A.A. Hakeem, T. Kolasa, M.A. Matulenko, K.H. Mortell, M.V. Patel, A.O. Stewart, X. Wang, and Z. Xia, *Acetamides and benzamides that are useful in treating sexual dysfunction*. 2009, Google Patents.
- [145] Mahé, O., I. Dez, V. Levacher, and J.F. Brière, *Enantioselective Phase-Transfer Catalysis: Synthesis of Pyrazolines*. *Angew. Chem., Int. Ed.*, 2010. 49(39): p. 7072-7075.
- [146] Barile, E., S.K. De, C.B. Carlson, V. Chen, C. Knutzen, M. Riel-Mehan, L. Yang, R. Dahl, G. Chiang, and M. Pellecchia, *Design, Synthesis, and Structure– Activity Relationships of 3-Ethynyl-1 H-indazoles as Inhibitors of the Phosphatidylinositol 3-Kinase Signaling Pathway*. *J. Med. Chem.*, 2010. 53(23): p. 8368-8375.
- [147] Patel, M.M., B.R. Goyal, S.V. Bhadada, J.S. Bhatt, and A.F. Amin, *Getting into the brain*. *CNS drugs*, 2009. 23(1): p. 35-58.
- [148] Placzek, A.T., S.J. Ferrara, M.D. Hartley, H.S. Sanford-Crane, J.M. Meinig, and T.S. Scanlan, *Sobetirome prodrug esters with enhanced blood–brain barrier permeability*. *Bioorg. Med. Chem.*, 2016. 24(22): p. 5842-5854.
- [149] Meinig, J.M., S.J. Ferrara, T. Banerji, T. Banerji, H.S. Sanford-Crane, D. Bourdette, and T.S. Scanlan, *Targeting fatty-acid amide hydrolase with prodrugs for CNS-selective therapy*. *ACS Chem. Neurosci.*, 2017. 8(11): p. 2468-2476.
- [150] Rousselle, C., P. Clair, J.-M. Lefauconnier, M. Kaczorek, J.-M. Scherrmann, and J. Tamsamani, *New advances in the transport of doxorubicin through the blood-brain barrier by a peptide vector-mediated strategy*. *Mol. Pharmacol.*, 2000. 57(4): p. 679-686.
- [151] Rousselle, C., M. Smirnova, P. Clair, J.-M. Lefauconnier, A. Chavanieu, B. Calas, J.-M. Scherrmann, and J. Tamsamani, *Enhanced delivery of doxorubicin into the brain via a peptide-vector-mediated strategy: saturation kinetics and specificity*. *J. Pharmacol. Exp. Ther.*, 2001. 296(1): p. 124-131.